Cold atmospheric plasma stimulates macrophage killing of bacterial pathogens

Océane Blaise

▶ **To cite this version:**

Océane Blaise. Cold atmospheric plasma stimulates macrophage killing of bacterial pathogens. Cellular Biology. Institut Polytechnique de Paris, 2022. English. NNT : 2022IPPAX121 . tel-04416285

HAL Id: tel-04416285
https://theses.hal.science/tel-04416285

Submitted on 25 Jan 2024

HAL is a multi-disciplinary open access archive for the deposit and dissemination of scientific research documents, whether they are published or not. The documents may come from teaching and research institutions in France or abroad, or from public or private research centers.

L'archive ouverte pluridisciplinaire **HAL**, est destinée au dépôt et à la diffusion de documents scientifiques de niveau recherche, publiés ou non, émanant des établissements d'enseignement et de recherche français ou étrangers, des laboratoires publics ou privés.

INSTITUT POLYTECHNIQUE DE PARIS

NNT : 2022IPPAX121

Thèse de doctorat

Cold atmospheric plasma stimulates macrophage killing of bacterial pathogens

Thèse de doctorat de l'Institut Polytechnique de Paris
préparée à l'École Polytechnique

École doctorale n°626 Ecole Doctorale de l'Institut Polytechnique de Paris (ED IP Paris)
Spécialité de doctorat : Biologie

Thèse présentée et soutenue à Palaiseau, le 01/12/2022, par

Océane Blaise

Composition du Jury :

Pr Colin McGuckin PhD Directeur scientifique, CTIBiotech	Président
Dr Sander Bekeschus PhD, Head of Department Leibniz Institute for Plasma Science and Technology	Rapporteur
Dr Elisa Gomez Perdiguero PhD, HDR, DR Institut Pasteur Development and Stem Cell Biology Department	Rapporteur
Dr Ludovic Tailleux PhD, HDR, DR Institut Pasteur, Department of Microbiology	Examinateur
Pr Colin McGuckin PhD Directeur scientifique, CTIBiotech	Examinateur
Dr Marina-Laurie Trouillas PhD, HDR INSERM UMR-MD 1197	Examinateur
Pr Antoine Rousseau PhD, HDR, DR CNRS UMR7648, LPP Ecole Polytechnique	Directeur de thèse
Pr Sébastien Banzet MD, PhD, HDR INSERM UMR-MD 1197	Co-Directeur de thèse
Dr Nadira Frescaline MD, PhD, HDR Institut Pasteur, Department of Microbiology	Encadrante de thèse

RÉSUMÉ

Le plasma atmosphérique froid stimule l'élimination de bactéries pathogènes par les macrophages.

Les brûlures représentent le quatrième type de traumatisme le plus fréquent à l'échelle mondiale. Entre 7 000 et 10 000 victimes doivent être hospitalisées pour des lésions plus préoccupantes, et 2 000 à 3 000 sont admises dans l'un des 23 centres de traitement des brûlés français. Chez les militaires évoluant sur le terrain, il est estimé que près d'un blessé sur dix est brûlé. La durée d'hospitalisation est d'environ 1 jour pour chaque pourcentage de la surface corporelle totale brûlé.
La prise en charge des patients souffrant de brulures thermiques est un domaine complexe pour les unités de soins avec des millions d'adultes et d'enfants concernés dans le monde entier. Des progrès importants ont été réalisés au cours de la dernière décennie en matière de réanimation, de traitement des plaies ou de reconstruction. Cependant, les patients souffrant de brûlures graves font toujours face à des conséquences invalidantes comme des cicatrices hypertrophiques et surtout un risque élevé d'infections et de septicémie mortelle.
Le plasma, quatrième état de la matière, est obtenu en créant une décharge électrique dans un gaz à basse pression. Il est constitué d'électrons, d'ions, d'atomes et de molécules neutres et produit également des ultraviolets, des rayonnements électromagnétiques et de la chaleur. Ce gaz faiblement ionisé est à température ambiante car seuls les électrons libres sont chauds (>10 000 degrés) mais ils sont trop faibles en densité par rapport aux espèces neutres pour élever la température du gaz.
La médecine plasma, ou l'application thérapeutique des plasmas dans le domaine médical, s'est développée ces dernières années notamment dans le domaine de la cicatrisation cutanée. Lorsque le plasma réagit avec un système biologique, des espèces réactives de l'oxygène et de l'azote (RONS) sont produites et ce sont ces espèces qui sont à l'origine des effets biologiques observés.

Le déroulement de cette thèse s'est effectué autour de trois objectifs principaux. Le premier a consisté à comprendre les mécanismes sous-jacents responsables des effets bénéfiques de CAP lors des infections des plaies *in vitro*, le second à étudier ces effets dans des systèmes biologiques plus complexes, et enfin le dernier objectif a pour but d'étudier l'effet de CAP *in vivo* lors d'une étude pilote.

Dans un premier temps nous nous sommes intéressés à l'effet de CAP sur des cellules clés du système immunitaire : les macrophages. Ce type cellulaire est prédominant dans le cadre d'une plaie cutanée et présente une grande plasticité phénotypique lui conférant plusieurs fonctions. Les macrophages des plaies possèdent des fonctions hétérogènes comme la détection, l'ingestion et la digestion des micro-organismes envahissants aux sites d'infection. Toutefois, les macrophages peuvent présenter un profil pro- ou anti-inflammatoire les rendant cruciaux pour les différentes phases de cicatrisation cutanée à savoir la phase inflammatoire,

prolifératives et de remodelage. Le phénotype pro-inflammatoire intervient dans l'élimination de pathogènes et de débris par la phagocytose tandis que le second est essentiellement impliqué dans la réparation cutanée et interviendra également lors de la phase prolifératives.

L'aptitude des macrophages à éliminer les pathogènes a été étudiée dans le cadre d'infections à *Staphylococcus aureus*. *Staphylococcus aureus* (*S. aureus*) est l'un des principaux pathogènes humains bactériens communs aux infections d'origine communautaire et hospitalière. *S. aureus* est un pathogène opportuniste à Gram positif capable d'envahir les tissus, et lorsqu'il pénètre la circulation sanguine, peut conduite à des infections graves telles que la bactériémie. Il fait partie des principaux pathogènes responsables des infections chez les grands brûlés et présente de multiples mécanismes de résistance aux antibiotiques.

Nos études se sont concentrées sur la capacité des macrophages à éliminer les bactéries lors de la phagocytose. A travers ce processus la cellule internalise la bactérie au sein d'une vacuole, le phagosome, qui va subir un processus de maturation au cours duquel la vacuole va essentiellement s'acidifier, acquérir des enzymes de dégradation et des RONS qui vont permettre l'inactivation du pathogène.

In vitro nous avons démontré que le traitement par CAP engendrait une diminution significative de la charge bactérienne pour deux types de souches de *Staphylococcus aureus* (sensible et résistante à la méthicilline : MSSA, MRSA) lors de leur internalisation par les macrophages. Les RONS étant le principal point commun entre la phagocytose et CAP, nous nous sommes ensuite intéressés à l'évolution de ces espèces au sein des macrophages. Les résultats ont démontré une augmentation significative des RONS après traitement par CAP et une inhibition de cet effet lors d'ajouts d'antioxydant suggérant une médiation par des mécanismes oxydatifs. En outre, nous avons montré que CAP favorise l'association de *S. aureus* avec des vacuoles associées à un marqueur des endosomes tardifs (LAMP-1) dans lesquels les bactéries sont exposées à un pH bas et des hydrolases (cathepsine D). L'ensemble de ces résultats fournit la première preuve que CAP active les mécanismes de défense des macrophages, conduisant finalement à l'élimination bactérienne.

Étant donné l'importance des macrophages pour contenir l'infection, nous avons ensuite étudié l'effet de CAP sur la capacité des macrophages dérivés de la moelle osseuse murine (mBMDM) à tuer *S. aureus*. Nos résultats ont montré que le traitement par CAP à la suite d'une infection par deux souches différentes de *S. aureus* dont USA300 une souche clinique majeure de SARM (*S. aureus* résistant à la méthicilline), conduit à une réduction significative du nombre de bactéries intramacrophagiques sans impacter l'activité prolifératives des macrophages immortalisés et des mBMDMs. Fait intéressant, CAP a entraîné une augmentation significative de la production *de novo* de ROS intracellulaires par les macrophages par rapport au témoin. Suite à la mise en évidence du rôle des RONS intracellulaires dans l'élimination de *S. aureus* nos études se sont orientées sur des études de mécanistique afin de mettre en avant des voies impliquées dans les phénomènes observés.

Le point commun majeur entre la phagocytose effectuée par le macrophage et le dispositif plasma est la génération de ROS ainsi, nous avons abordé l'effet de CAP sur le complexe NOX2, une source majeure de ROS dans les macrophages. La NADPH oxydase ou NOX2 est un complexe enzymatique composé de plusieurs sous-unités (cytosoliques ou membranaires) qui vont venir s'associer sous l'effet de signaux tels que des phosphorylations permettant la formation du complexe actif. Cette forme active va permettre un transfert d'électron et

permettre la génération de superoxide dans la vacuole de dégradation. Afin d'analyser ce complexe nous avons utilisé une approche permettant une inhibition pharmacologique et génétique complémentaires de NOX2. L'ajout de gp91ds-tat et de GSK2795039 (inhibiteurs pharmacologiques de NOX2) aux macrophages, suivi d'une infection bactérienne et d'un traitement par CAP, a ramené les niveaux intracellulaires de ROS au niveau de ceux du contrôle. Fait frappant, l'inhibiteur de NOX2 a abrogé l'effet antibactérien de CAP dans les modèles d'infection 2D. La transfection des macrophages avec des siARNs ciblant le gène *Cybb* codant gp91phox, suivie du traitement par CAP, a entrainé une réduction de la production intracellulaire de ROS et a considérablement augmenté le nombre de bactéries intramacrophagiques vivantes par rapport à l'ARNsi brouillé et aux ARNsi endogènes contrôles. Ensemble, nos résultats indiquent que les effets antibactériens de CAP dépendent du complexe NOX2.

Pour déterminer comment CAP favorise la production de ROS, dépendante de NOX2 dans les macrophages, nous avons quantifié le recrutement de sous-unités NOX2 lors du traitement CAP. Les macrophages ont d'abord été infectés par *S. aureus*, puis traités par CAP pour déterminer si l'exposition à CAP modifie la localisation et l'expression des sous-unités LAMP-1, NOX2 et Rac1. Nos expériences de microscopie confocale ont révélé que bien que le pourcentage de colocalisation totale de Rac1 avec *S. aureus* contenant des vacuoles soit resté inchangé, le niveau de colocalisation avec Rac-GTP a entrainé une augmentation significative pour les macrophages traités par CAP par rapport au témoin. Le traitement par CAP a été associé à un pourcentage plus élevé de colocalisation entre *S. aureus* lié à la vacuole et $gp91^{phox}$, qui coïncidait également avec des niveaux significativement accrus de $p40^{phox}$ phosphorylés et $p47^{phox}$ à 5 h post infection. Nous avons ensuite estimé les niveaux des sous-unités LAMP-1, Rac1 et NOX2 par immunotransfert. Les niveaux de Rac inactif dans les lysats cellulaires entiers extraits des macrophages traités par CAP étaient similaires à ceux du témoin à 5 h post infection. Cependant, les niveaux de Rac1 sous forme GTP-liée active dans les extraits de phagolysosome ont été augmentés lors du traitement par CAP. Le niveau de protéine LAMP 1 a été augmenté dans les lysats de cellules entières et la protéine phagolysosomale en réponse à CAP par rapport au témoin. Le niveau de protéines $gp91^{phox}$ et $p40^{phox}$ a été significativement augmenté dans les lysats de cellules entières en réponse au CAP par rapport au témoin. Les signaux des western blot émis par $gp91^{phox}$ et les protéines $p40^{phox}$ dans la fraction phagolysosomale n'ont pas été soumis à la densitométrie quantitative en raison de l'absence de protéine témoin de charge exprimée de façon constitutive. De plus, Rac1 lié à la GTP (nécessaire à la formation du complexe NOX2 actif) et non la fraction totale de Rac1 a été associé à des phagolysosomes contenant *S. aureus* en réponse au CAP. Ces résultats suggèrent que CAP permet l'association de la forme active du complexe NOX2 en stimulant d'autres voies de régulation plus amont qu'il reste à découvrir.

Afin de d'élucider certains mode d'action de CAP sur des macrophages infectés, nous avons également effectué des analyses transcriptomiques sur des ARNs de macrophages murins (RAW264.7) infectés par *S. aureus*. De façon surprenante aucune différence significative n'a été constatée entre les échantillons traités par CAP et les contrôles. Des analyses complémentaires ont révélé des modifications concernant des gènes impliqués dans les mécanismes infectieux mais dont l'expression allait à l'encontre des éléments précédemment observés et de façon peu homogène. L'expression génétique globale dépend de nombreux

facteurs, notamment le type de cellule, les stimuli environnementaux et le stade de développement. De nombreux gènes sont régulés par l'oxydation à travers le superoxyde, le peroxyde d'hydrogène et divers oxydes d'azote. Ainsi, il sera nécessaire d'obtenir de nouveau échantillons dont l'analyse transcriptomique devrait nous donner des éléments complémentaires concernant NOX2 mais aussi sur la polarisation des macrophages, sur l'effet concernant les mitochondries ou même sur des mutations potentielles. Si le nouvel ensemble de données ne donne une fois de plus aucune différence il est envisageable que les modifications puissent intervenir au niveau protéique ou post traductionnel.

En parallèle de ces essais sur des lignées cellulaires de macrophages murins ou cellules primaires murines nous avons également développé et étudié des modèles de peaux humaines bioimprimées fournis par la startup CtiBiotech. Ces modèles miment les deux principales couches de la peau à savoir le derme et l'épiderme. Ils sont constitués de cellules primaires extraites d'un même donneur suite à une mammoplastie ou abdominoplastie et ne sont pas vascularisés. Les modèles utilisés contiennent des kératinocytes, des fibroblastes et des macrophages primaires mélangés à une bio encre qui permet l'impression de petits modèles dont la structure est pré définie. Une fois les peaux humaines imprimées un processus de maturation a du être effectué pour finir la maturation du derme et de l'épiderme et permettre ainsi la formation de la couche cornée (couche la plus externe de la peau) lors de la mise en contact avec l'air. Cette étape a été réalisée au sein de notre laboratoire de ce fait une nouvelle caractérisation des modèles a dû être effectuée afin de s'assurer de leur bonne constitution. Ainsi de l'histologie et de l'immunomarquage ont été réalisés pour vérifier la structure des modèles, leur viabilité et la présence de protéines clés pour la structure de la peau telles que l'involucrine, la laminine 5, la kératine 14, le collagène IV ou la vimentine qui sont naturellement présents dans une peau humaine saine. L'analyse histologique des modèles 3D de la peau a montré deux composantes distinctes : le derme et l'épiderme avec une couche externe de kératinocytes énucléés qui forment le *stratum corneum* ou couche cornée. De plus, nos résultats ont démontré que la viabilité cellulaire est maintenue jusqu'à 21 jours après l'impression. La reproductibilité des modèles ayant été vérifiée un protocole d'infection a été développé et a entrainé de nouveau marquage pour vérifier la pénétration de *S. aureus* au sein des modèles permettant l'activation des cellules clés telles que les macrophages. Des marquages d'hématoxyline et éosine ont révélé la présence de bactérie dans le derme et l'épiderme de façon reproductible. De plus, la visualisation histologique et immunohistochimique des bactéries intradermiques suggère que *S. aureus* existe en grappes, ce qui est attribué à sa capacité à former des communautés de biofilms. L'inoculation intradermique de modèles 3D avec *S. aureus* a entraîné une infection uniforme et reproductible.

Ayant vérifié la reproductibilité de nos procédures expérimentales nous nous sommes ensuite focalisés sur l'effet de CAP sur les bactéries après leur inoculation au sein des peaux bioimprimées. A la suite de l'inoculation et du traitement par CAP les modèles ont été incubés 24h puis homogénéisés afin d'énumérer les bactéries présentes dans les modèles. Les échantillons de peau ont été scindés en plusieurs groupes infectées non traitées, infectées traitées par hélium (gaz permettant la génération de CAP) et traitées par CAP. Le traitement par hélium était un contrôle important permettant d'estimer un potentiel effet d'éclaboussure lors

de l'application du traitement. Nos résultats ont démontré un effet significatif de CAP sur l'élimination des bactéries au sein des peaux.
En complément des inhibiteurs du complexe enzymatique NOX2 ont été employés afin d'analyser l'importance de NOX2 au sein de ces modèles complexes. Lors de l'ajout des inhibiteurs et traitement par CAP l'effet du CAP est inhibé permettant une augmentation de la charge bactérienne.
En utilisant ces modèles de peaux humaines bioimprimées nous sommes parvenus à obtenir un effet bactéricide du plasma sans effet délétère pour les modèles et à mettre en évidence le rôle de NOX2 dans la propriété antibactérienne du dispositif. Ces expériences ont permis de mettre en avant l'effet direct du plasma avec l'interaction directe des différentes espèces produites sur les bactéries (connu depuis de nombreuses années comme ayant des effets antibactériens) et l'effet indirect de CAP par son action activatrice de NOX2. Dans ce modèle NOX2 peut être activé chez les macrophages mais également chez les fibroblastes, ainsi il sera intéressant de moduler la composition des modèles lors de leur impression afin d'estimer l'importance des différents types cellulaire dans les effets observés.

Afin de se rapprocher de conditions plus physiologiques un modèle murin de brûlure infectées a été développé lors d'une précédente étude. Dans la pratique clinique, les greffes sont utilisées couramment pour couvrir les blessures qui ne guériront probablement pas. Alors que la situation clinique individuelle dicte le type de greffe à placer, les effets perturbateurs d'une infection à *S. aureus* menacent la survie de la greffe quel que soit la technique employée. Ici, nous avons utilisé un modèle reproductible de plaie de brûlure profonde reconstruite avec une greffe de peau allogénique (issue de la queue de l'animal) et inoculée topiquement avec une souche clinique bioluminescente de *S. aureus*.
La plaie infectée a entraîné divers degrés de survie de la greffe selon le traitement appliqué. Les souris ont été divisées en trois groupes : le premier correspondait aux souris infectées traitées par hélium, le second à des souris infectées traitées par CAP et le troisième à des souris infectées traitées à l'aide d'un antibiotique, la mupirocine, couramment utilisé pour lutter contre les infections à *S. aureus in vivo*. Au niveau macroscopique, le traitement placebo a entraîné une perte complète du greffon au quatorzième jour après infection. Les plaies traitées par CAP ou l'antibiotiques topique ont amélioré la survie des greffons après l'infection par rapport au groupe témoin placebo (hélium) apparié dans le temps. Au niveau microscopique, l'évaluation histologique des plaies a montré que les indicateurs de réussite de la greffe de la peau étaient nettement améliorés dans les plaies infectées traitées par CAP par rapport au control. Immédiatement après l'infection, les sous-produits chimioattractifs déclenchent de multiples réponses, y compris l'infiltration de cellules immunitaires au site d'infection. CAP génère une gamme de molécules chimiques (ozone, radicaux hydroxyles, nitrite, nitrate, superoxide) semblables à ceux produits par les phagocytes présents dans les plaies. Nous avons donc émis l'hypothèse que ces molécules biochimiques peuvent agir soit comme des signaux, soit comme des agents chimio attractants pour les cellules immunitaires. Aucune différence statistiquement significative n'a été observée dans le recrutement des cellules immunitaires dans les plaies traitées par CAP par rapport aux témoins appariés dans le temps. Plusieurs antigènes, communément connus pour être exprimés par les leucocytes blessés ont été sondés, y compris CD45 (protéine de surface des cellules détectée sur la plupart des cellules

lymphohématopoïétiques), F4/80 (marqueur de macrophages murine), CD206 (protéine transmembranaire abondante dans les macrophages tissulaires présentant un phénotype de type M2) et Ly6G (exprimé par les neutrophiles). CAP n'a montré aucune influence sur l'ampleur de l'infiltration des cellules immunitaires innées, et il n'a pas modifié les niveaux d'ARNm des macrophages et des chimioattractants neutrophiles établis. Afin d'évaluer le niveau de formation de matrice pendant les phases de prolifération et de remodelage de la guérison, nous avons mesuré l'expression des protéines de matrice dans le tissu de granulation. Trois éléments suggèrent que CAP stimule la formation de matrice extracellulaire (ECM), nécessaire à la restauration fonctionnelle de la peau en tant que barrière protectrice. Tout d'abord, la microscopie de deuxième génération harmonique et la coloration trichrome de Masson ont montré un dépôt significativement plus élevé de collagène fibrillaire dans les plaies traitées par CAP que chez les témoins. Deuxièmement, les principaux marqueurs de l'ECM, comme la laminine et le collagène IV, ont été synthétisés à des niveaux significativement plus élevés à proximité des plaies traitées par CAP que chez les témoins. Troisièmement, la détection d'anticorps spécifiques au collagène indique que CAP a amélioré la synthèse matricielle, sans compromettre le rapport de collagène de type I/III, qui est essentiel pour l'architecture fonctionnelle de la peau. Une coloration de Gram de plaies inoculées avec *S. aureus* et analysées à 7 et 14 jours après infection, a montré des grappes de cocci, généralement intégrées dans le biofilm, et clairement localisées aux compartiments épidermiques, dermiques et hypodermiques de la peau. Moins de bactéries ont été détectées chez les souris traitées par CAP et l'antibiotique par rapport au groupe témoin placebo. L'imagerie bioluminescente en temps réel de *S. aureus* chez des souris vivantes a démontré que le traitement quotidien par CAP réduisait efficacement la charge bactérienne des plaies dès 3 jours après infection par rapport aux plaies témoins appariées dans le temps. Au cours des 14 jours suivant l'infection, les plaies traitées par CAP étaient associées à une charge bactérienne toujours plus faible que le contrôle. Les mesures de bioluminescence ont établi une corrélation positive avec l'analyse quantitative de l'unité formant colonie dénombrée dans les plaies homogénéisées et ont montré une réduction d'au moins 50 % de la charge bactérienne dans les plaies traitées par CAP par rapport aux témoins appariés dans le temps. L'activité anti-staphylococcus du CAP n'a pas compromis l'intégrité de l'ADN de l'hôte, comme l'indique un essai indiquant des dommages à l'ADN des mammifères et la mort des cellules apoptotiques. Ces résultats concordent avec l'analyse de la prolifération des tissus hôtes. CAP n'a aucun effet néfaste sur la prolifération cellulaire *in vivo,* car le nombre de cellules PCNA+ et Ki67+ a augmenté dans les plaies traitées par CAP comparativement au groupe témoin.

Conclusion des deux premiers objectifs de thèse

La fermeture en temps opportun des plaies cutanées est corrélée avec la sensibilité à l'infection, un défi majeur dans le contexte clinique. Ici, nous révélons que le traitement des plaies de brûlures infectées traitées par CAP (I) réduit considérablement la charge de plaie bactérienne, (II) augmente le taux de ré épithélialisation, et (III) stimule la formation d'ECM. De plus, nous élucidons un mécanisme d'action inconnu du traitement par CAP dans lequel il favorise l'activation de NOX2.

Il est raisonnable de supposer que l'organisation et la migration des feuilles stratifiées du néoépiderme ont été améliorées par CAP grâce aux protéines de l'ECM, dont il a été démontré

précédemment qu'elles étaient impliquées dans la ré épithélialisation. Cette hypothèse est fondée dans une première partie sur notre étude actuelle, qui a démontré que CAP augmentait l'expression du collagène pendant la phase de remodelage de la cicatrisation des plaies, et dans une seconde partie, sur nos études précédentes, qui ont montré une expression accrue des protéines de la jonction épidermique pour les plaies traitées par CAP. Des études antérieures sur le transcriptome et de « single cell » des plaies de souris ont révélé que le réapprovisionnement de l'épiderme blessé est régulé par l'activation du gène des cellules souches épidermiques. Dans notre modèle de souris *in vivo*, les gènes de cellules souche ont probablement été activés dans le compartiment épidermique du lit de la plaie du receveur, plutôt que dans la greffe du donneur, qui a été séparée de son apport sanguin. Mis à part l'activation génétique, les déclencheurs physiques sous forme de champ électromagnétique, connus pour être associés à CAP, peuvent avoir polarisé et guidé la migration des cellules épithéliales dans la direction du centre de la plaie. La réparation réussie des tissus, entre autres facteurs, dépend de l'angiogenèse en temps opportun. Des questions demeurent en suspens concernant les signaux qui stimulent l'angiogenèse dans les plaies cutanées traitées par CAP, mais il a déjà été démontré que les stimulateurs angiogéniques, comme l'oxyde nitrique, facilitent les anastomoses vasculaires. L'inflammation de la plaie fait partie intégrante des études de déplétion et témoigne de la théorie selon laquelle les macrophages sont des acteurs essentiels des réponses protectrices de l'hôte. Le consensus actuel est que les macrophages nettoient la plaie des neutrophiles apoptotiques, engloutissant les bactéries et activent la réponse immunitaire adaptative. En plus des fonctions phagocytaires, les macrophages des plaies orchestrent des événements de réparation tissulaire grâce à leur capacité à changer le phénotype. Notre analyse précédente des protéines spécifiques aux macrophages a suggéré que CAP n'avait aucune influence sur les profils temporels des macrophages.

Les mécanismes dépendants de l'oxygène entraînent une production massive de ROS par le phagocyte NADPH oxydase. Cette étude a proposé un mécanisme général pour expliquer l'activité anti-staphylococcale de CAP. Nous avons émis l'hypothèse que CAP génère des éléments qui activent le complexe NOX2, ce qui, à son tour, donne lieu à la production endogène d'oxydants nocifs dérivés de l'hôte avec une activité anti-staphylococcale. Cette hypothèse a été testée dans deux modèles *in vitro* différents d'infection à *S. aureus*, que nous croyons être plus expérimentalement traçable, que le modèle *in vivo*, qui est associé à des limitations, telles que les différences anatomiques spécifiques aux espèces qui existent entre les rongeurs et la peau humaine. Pour cette raison, nous avons eu recours au transfert assisté par ordinateur de composants de la peau humaine, y compris les macrophages, pour reproduire la complexité de la peau humaine. Les modèles tridimensionnels ont fourni un outil reproductible, qui imite la phase aiguë de l'infection staphylococcique de la peau, et a montré que l'ajout exogène d'antagonistes NOX2 inhibait la destruction bactérienne induite par CAP. De plus, l'inhibition pharmacologique et l'inhibition génique de NOX2 ont réduit de façon significative la production de ROS endogènes dérivés de macrophages et ont abrogé les effets antibactériens de CAP. Notre étude précédente a montré que l'addition exogène d'oxydants augmentait la clairance de *S. aureus* par les macrophages, tandis que les antioxydants inhibaient le phénotype antibactérien de CAP. Pris ensemble, ces résultats suggèrent que CAP tue *S. aureus*, soit par l'intermédiaire d'oxydants exogènes dérivés de CAP, soit par stimulation de la destruction

bactérienne endogène dépendante de l'oxygène provenant de l'hôte. Nos résultats indiquent que la phosphorylation de $p40^{phox}$ et $p47^{phox}$ coïncidait avec l'activité anti-*S. aureus* de CAP. De plus, l'association de deux protéines de la membrane phagosomique LAMP-1 et $gp91^{phox}$ a été significativement accrue en réponse au traitement par CAP par rapport au contrôle.
Le Rac1 lié à la GTP (forme active), mais pas le Rac1 total, a été associé à des phagolysosomes contenant *S. aureus* en réponse à CAP. Ces résultats suggèrent que CAP active le NOX2 en déclenchant, des mécanismes effecteurs en amont qu'il reste encore à découvrir. Notre étude récente, a montré que des niveaux accrus de cathepsine protéolytique D intraphagolysosomique étaient associés à CAP par rapport au contrôle. Il y a donc lieu de soupçonner qu'en plus de l'activation directe de l'activité de NOX2, CAP peut également stimuler la formation de « signaux moléculaires » sous forme de dérivés de l'oxygène qui entraînent une régulation électrogénique indirecte des protéases qui tuent les bactéries sans oxydation. Les conséquences d'une exposition à long terme de *S. aureus* au CAP restent à étudier. Il peut être débattu que le traitement répété avec CAP peut activer la transcription des gènes procaryotes codant pour la défense antioxydante staphylococcique et induire une pression sélective pour le phénotype de résistance. Il reste encore beaucoup d'autres questions à régler. Nous savons peu de choses sur les changements qui se produisent dans les transcriptomes eucaryotes et procaryotes en réponse à CAP. Enfin, si l'on reconnaît les limites de CAP et que l'on est réaliste quant à l'endroit, au moment et à la mesure dans lesquels elle peut être utilisée, cette technologie pourrait être bénéfique en conjonction avec l'arsenal d'antimicrobiens actuellement à la disposition du clinicien.

Le dernier objectif de cette thèse visait à se rapprocher de l'étape clinique, le but ultime étant de traiter des modèles de plaies de brûlure infectées plus complexes pour se rapprocher de l'Homme. Pour se faire un dispositif plasma permettant de traiter des surfaces plus étendues a été développé. Une première étape a consisté à effectuer une caractérisation physico-chimique du dispositif *in vitro* pour s'assurer de la sécurité du dispositif. Les caractéristiques ainsi que les résultats précis obtenus dans cette partie ne peuvent pas être décrits dans ce manuscrit néanmoins une plus forte production de peroxyde d'hydrogène et de nitrite a pu être constatée mais n'a engendré aucun effet délétère *in vitro*.
Nos précédents travaux utilisaient des modèles murins cependant ils présentent de multiples limites. Par exemple, les blessures murines guérissent principalement par contraction, et dans une certaine mesure par ré épithélialisation. Les blessures humaines, d'autre part, se contractent en raison de la présence d'actine musculaire α-lisse cytosquelettique, et guérissent principalement par ré épithélialisation. Ainsi, nous avons décidé de mettre en place un modèle grand mammifère plus proche de l'Homme, un modèle porcin, afin d'étudier les avantages potentiels du traitement CAP sur les plaies de brûlure recouverte par une greffe autologue de peau. Le modèle porcin possède certaines propriétés anatomiques et physiologiques similaires à l'homme selon l'âge, le poids et le type de porcs. La peau de porc est caractérisée par une épaisseur cutanée et épidermique proche de celle de l'homme. L'épiderme du porc varie de 30 à 140 µm, ce qui est proche de l'épiderme humain, qui varie de 50 à 120 µm. En outre, le cochon a une peau fermement attachée aux tissus sous-jacents induisant un processus de guérison de la même manière que chez l'Homme. La distribution des vaisseaux sanguins dans le derme, le temps de renouvellement de l'épiderme ou des cheveux sont également proches de ceux de

l'homme. Ainsi nous avons développé une modèle un modèle de brûlure profonde qui est induite à deux endroits sur chaque flanc de l'animal à l'aide d'un dispositif rempli avec de l'eau à 100°C. Une fois la brûlure effectuée l'excision des tissus nécrotiques est effectuée le jour suivant. Durant cette même journée de la peau fine est prélevée sur le dos de l'animal, expansée via une technique de meshage puis fixée sur les plaies. Lors du changement des pansements (toutes les 48h) les plaies seront traitées à l'aide du nouveau dispositif. La procédure durera 14 jours et au dernier jour des prélèvements sanguins, des biopsies de peaux saines et blessées seront effectués pour des analyses complémentaires relatives à l'intensité de la brûlure, l'évolution de la cicatrisation et les potentiels effets mutagènes et génotoxiques du dispositif.
La réalisation de cette étude pilote fournira des indications initiales sur la sécurité du dispositif CAP pour le traitement des brûlures profondes et aidera à optimiser certaines conditions de traitement.
Ainsi, un nouveau dispositif à plasma a été développé pour traiter de plus grandes surfaces et sera utilisé pour la première fois *in vivo* pour une étude pilote sur modèle porcin en octobre 2022.
L'étude pilote sera réalisée en octobre 2022 et impliquera deux porcs. Bien que la petite taille de l'échantillon ne nous permette pas d'effectuer des analyses statistiques sur les mesures de divers paramètres de plaie, le protocole fournira des informations précieuses pour le développement de nos futures études. Nous serons en mesure de voir si le dispositif induit des effets positifs ou négatifs sur la peau, la plaie de brûlure, la greffe de peau et de manière systémique. Ceci peut fournir un aperçu des effets du plasma froid dans le traitement des brûlures étendue et constitue une première étape avant le passage à l'Homme.

Mots clés : Plasmas froids, infections, *S. aureus*, macrophages, NOX2, modeles 3D, étude pilote sur modèle porcin.

ABSTRACT

Cold atmospheric plasma stimulates macrophage killing of bacterial pathogens.

Management of thermal burn-injured patients is a challenging field for care units with millions of adults and children concerned worldwide. Important advances over the past decade have occurred in resuscitation, burn wound management and reconstruction. However, patients with severe burns still face disabling consequences such as hypertrophic scars, high risk of infections and sepsis. Cold atmospheric plasma (CAP) is a partially ionised gas delivering a mixture of reactive oxygen and nitrogen species which favour wound healing and have antimicrobial properties.

This PhD study aimed to understand the underlying mechanisms that are responsible for beneficial effects during wound infections specifically on macrophages immune cells. First, we demonstrated *in vitro* that CAP treatment resulted in a significant decrease in bacterial load for two strains of *Staphylococcus aureus* (methicillin-resistant and sensitive: MSSA, MRSA) during their internalization by macrophages. Then, we showed that the enhancement killing of *S. aureus* by macrophages is mediated by

oxidative mechanisms and that CAP promotes phagosome maturation into acidic degradative vesicle. Second, we reported a positive correlation between antibacterial action of CAP and activation of phagocyte NADPH oxidase (NOX2) machinery in two and three-dimensional models of cutaneous infection.

In addition, to its antimicrobial effects, CAP is a positive regulator of cutaneous wound healing as shown in an *in vivo* murine mouse model infected with *S. aureus*. Finally, the ultimate goal of the project is to treat either uninfected or infected full-thickness burn wounds. Thus, a new plasma device has been developed to treat wounds with large surface area. For the first time, this new prototype will be used in porcine model of full-thickness burn wound reconstructed with partial-thickness allografts. This study demonstrated the therapeutic potential of CAP on infected tissue repair. Investigation on tissue repair are promising, howeverfurther investigations are needed especially on the mutagenicity and genotoxicity of CAP use on animal models with greater similarity to human.

Keywords: Cold atmospheric plasma, infection, *S. aureus*, macrophages, NOX2, three-dimensional models, pig trial.

ACKNOWLEDGMENTS

Au cours de mes trois années de doctorat j'ai eu le privilège d'être intégrée à de nombreuses équipes composées de personnes formidables et bienveillantes. Leur aide, leur écoute et leur soutien ont égayé mes journées et facilité mes recherches.
Ces trois années au laboratoire ont été marquées par l'apparition du Covid, par des moments de creux et de désespoir ou rien ne fonctionnait (fascinants résultats de transcriptomique…) mais aussi par des moments de pur bonheur avec des résultats concluants et prometteurs ! Cette aventure humaine m'a fait énormément évoluée sur le plan personnel et restera gravée dans ma mémoire. Ainsi je souhaite remercier chacune des personnes m'ayant accompagnée dans cette incroyable aventure.

Aux membres du jury,
Je remercie les différents membres d'avoir accepté de faire partie de mon jury. Merci en particulier aux rapporteurs Dr. Elisa Gomez Perdiguero et Dr. Sander Bekeschus.
Merci également au Dr. Ludovic Tailleux, Pr. Colin McGuckin et Dr. Marina Trouillas d'avoir accepté de faire partie des examinateurs de cette thèse.

Je tiens à remercier l'Ecole Polytechnique et la Direction Générale de l'Armement pour le soutien financier de ce projet.

A mes encadrants,
Je tiens à remercier mon directeur de thèse, le Pr Antoine Rousseau, pour m'avoir intégrée au sein du LPP et permis de réaliser ce doctorat. Merci pour ton aide et tes conseils ainsi que pour tes cours sur le plasma. Je suis également reconnaissante pour tes appels skype rassurant pendant la période covid et l'avenir de ma thèse. Je voudrais également remercier le Pr Sébastien Banzet pour sa co-direction durant ma thèse. Merci d'avoir facilité mon intégration au CTSA et d'avoir permis la concrétisation de l'essai porcin. Je tiens également à remercier le Dr. Nadira Frescaline pour sa patience et son encadrement. Merci pour ton soutien pendant la formation à l'expérientation animale et notre essai porcin, que d'émotions. Un grand merci au Pr Olivier Dussurget pour son encadrement au sein de l'Institut Pasteur. Merci d'avoir pris le temps de m'accueillir, de me former, de me conseiller et d'améliorer mes oraux. Merci pour le temps que tu as consacré à mon projet et au projet de façon plus vaste et merci pour ta patience (pas évident lorsque des plaques et les machines disparaissent).

Au laboratoire de physique des plasmas,
Merci à Hang pour m'avoir appris à utiliser l'imprimante 3D et pour tes explications au sujet de mon dispositif. Merci d'avoir répondu à mes interrogations et à mes coups de téléphone lorsque j'étais bloquée. Nos manips étranges sur de la peau de poulet, de cochon et autres extravagances, entrainant de petits fous rire et des mouvements de dégoûts, resteront de bons souvenirs. Un grand merci à Bô pour ta patience et ta gentillesse ainsi que pour ton aide lors de mes premiers pas avec le plasma « the new girl » te remercie ! Un grand merci à Joseph pour le développement du nouveau dispositif plasma. Merci pour ta patience, tes explications, ton

aide pour les manips et pour les déménagements du dispositif au CTSA ou à l'IRBA. Je tiens également à remercier Tarek. Merci de m'avoir aidée à m'intégrer au sein du LPP, pour ton soutien lors des muds race, pour les parties de foot et les pots/BBQ organisés.
Je souhaite remercier l'ensemble du personnel du LPP et sa directrice Dominique Fontaine. Merci à Cherifa Ighoud et Catherine Jegu qui ont réussi à surmonter nos montagnes de commandes parfois complexes. Merci à tous les doctorants et post-doctorants et merci à Garrett Curley pour les discussions en salle café et les parties de foot !

A Pasteur,
Je tiens à remercier le Dr Javier Pizarro-Cerda pour son accueil au sein de l'équipe Yersinia et son investissement dans le projet. Merci à toute l'équipe : Rémi Beau, Sylvie Brémont, Mara Carloni, Christian Demeure, Anne Derbise, Hebert Echenique-Rivera, Pierre Goossens, Pierre Lê-Bury, Marion Lemarignier, Clarisse Leseigneur, Anne-Sophie Le Guern, Julien Madej, Guillem Mas Fiol, Jazmin Meza Torres, et Cyril Savin. Merci à Sylvie pour ton soutien et nos échanges très matinaux ! Une pensée particulière pour Clarisse et nos longues discussions dans ton bureau à me coatcher sur staph, à parler de science, à me remonter le moral ou à échanger longuement sur nos petites bêtes poilues pleines de surprise. Merci à ma co-bureau Marion avec ses cascades à l'animalerie ou ses talents avec les erlens dans l'incubateur ! Nos pauses chococat et moments debriefing me manquent déjà. Force à toi pour la dernière année ! Pierre le jeune, pour les bons moments passés à discuter sur le trajet du retour ou dans l'antichambre. Ironiquement j'ai connu Chopin avant ! Un grand merci à Julien pour ton aide au labo, tes encouragements mais aussi pour tes ravitaillements en chocolat, nos échanges motos ou simplement sur les anecdotes de la vie. Merci à tous pour votre chaleureux accueil et plus particulièrement pour votre gentillesse, votre bienveillance et nos multiples échanges dans l'antichambre.

Au CTSA/IRBA,
Je voudrais remercier Marianne Dedier pour sa bienveillance et ses conseils. Merci pour tes encouragements lors des oraux, nos échanges et ton aide précieuse lors de mes quelques passages à Clamart ! Ta passion pour la reine me fascinera toujours. Merci à Hugo Sugier et Jules Gueguen pour votre bonne humeur et votre humour et nos soutiens mutuels pour cette aventure périlleuse. Merci à toi Hugo de m'avoir accompagnée dans le dédale des blocs opératoire du CTSA, j'ai fini par en sortir ! Merci à Marion Grosbot et Bastien Rival pour votre joie de vivre, votre gentillesse, vos conseils culinaires et surtout pour vos anecdotes sur le pinou. Bastien ton chant est et restera toujours aussi saisissant ! Enfin un grand merci à toute l'équipe : Marina Trouillas, Juliette Peltzer, Dorothée Girard, Muriel Nivet, Marie-Emmanuelle Goriot. C'était un réel plaisir de venir au labo, vous m'avez toujours accueillie chaleureusement même si je n'étais souvent que de passage. Les discussions lors des pauses café ont toujours étaient très divertissantes et amusantes. Un grand merci pour votre soutien, votre sympathie, votre énergie et vos anecdotes plus que croustillantes !

Je tiens à remercier Nicolas Prat, Venetia Cardona, Frédérique Dufour-Gaume, Audrey Bordonne, Florent Montespan, Christophe Boismon, Didier Lici, Fanny Magisson et Mickael Boni. Votre aide pour l'essai porcin ainsi que les nombreux brainstormings ont rendu possible

notre étude ! Merci pour votre partage de connaissance et de locaux, cette aventure restera longtemps gravée dans ma mémoire !

A CTIBiotech,
Un grand merci à l'équipe de CTIBiotech en particulier à Pr Colin McGuckin, Dr Nico Forraz, Clément Millet et Maxime Legues pour m'avoir permis d'utiliser vos modèles aux résultats prometteurs. Merci à Maxime pour ton aide concernant l'organisation et l'optimisation des modèles ainsi que pour le suivi de l'évolution de nos petits.

A mes proches,
Un énorme merci à Constance mon pilier durant ces trois années ! Tu m'as apporté tout ton soutien à la fois scientifique et personnel et je t'en suis très reconnaissante. Ton aide et tes conseils m'ont été très précieux ! D'une relation de travail en est sortie une belle amitié merci encore pour tout !
Merci à Mme Beaufour et Cacat pour votre soutien sans faille et votre positivité !
Je suis reconnaissante envers ma famille sans qui je n'en serais pas là. Merci de m'avoir poussée et soutenue dans les moments difficiles et surtout d'avoir cru en moi. Un grand merci pour les oreilles tendues qui écoutaient les nombreux problèmes rencontrés au labo tout en me conseillant et me rassurant. Merci d'avoir été à l'écoute et d'avoir réussi à me donner le sourire.

Enfin merci à toi Andrew pour avoir embelli mes derniers mois de thèse. Tu as rendu cette dernière ligne droite plus rayonnante et enrichie de ton soutien, tu m'as donné la force de croire en moi et d'atteindre mon objectif !

Table of contents

RÉSUMÉ **2**

ABSTRACT **11**

ACKNOWLEDGMENTS **12**

LIST OF ILLUSTRATIONS **19**

LIST OF TABLES **20**

LIST OF ABBREVIATIONS **21**

Chapter I – State of the art **23**

1. Skin and wound healing complexity **23**

1.1. Structure 23

1.1.1. Epidermis 24

1.1.2. Basement membrane 26

1.1.3. Dermis 27

1.1.4. Hypodermis 28

1.1.5. Antimicrobial defense of the skin 29

1.1.6. Cutaneous microbiota 30

1.2. Wound healing and regeneration 31

1.2.1. Hemostasis 31

1.2.2. Inflammation 31

1.2.3. Proliferation 35

1.2.4. Re-epithelialization 35

1.2.5. Remodeling 36

1.3. Burn wounds 38

1.3.1. Epidemiology 38

1.3.2. Classification 39

1.3.3. Pathophysiology 39

1.3.4. Gold standard treatments and limitations 40

1.3.5. Burn models and perspectives 42

2. Burn wound infections **46**

2.1. Infected burn wounds 46

2.1.1. Burn wound colonization 46

2.1.2. Diagnosis 48

2.1.3. Treatment of burn wound infections 48

2.2. *S. aureus* burn wound infections 50
2.2.1. Epidemiology 50
2.2.2. Antibiotic resistance and treatments 50
3. Key role of macrophages in infected skin wound healing 51
3.1. Vacuole maturation process during phagocytosis 51
3.2. NADPH oxidase 54
3.2.1. Structure 55
3.2.2. Activation of NADPH oxidase, NOX2 56
3.2.3. Functional role 57
3.3. Macrophage interactions with *S. aureus* 58
3.3.1. Defense arsenal of *S. aureus* 58
3.3.2. The role of macrophages in *S. aureus* infections 60
3.3.3. Macrophages strategies to eliminate *S. aureus* infection 61
3.3.4. Therapeutic progress 64
4. Cold atmospheric plasma 65
4.1. Plasma Physics 65
4.2. Genesis of Plasma Medicine 66
4.3. Plasma Medicine 66
4.4. Chemical characterization of CAP 68
4.5. Interactions of CAP with living organisms 69
4.5.1. Importance of RONS for biological systems 69
4.5.2. Impact of CAP on microbes *in vitro* 70
4.6. Interaction of CAP with living tissue: specific focus on the skin 73
4.6.1. Penetration of RONS in tissue models 73
4.6.2. Impact of CAP on the skin surface 74
4.6.3. CAP actions in the depths of the skin 75
4.6.4. CAP in clinic 78

Objectives of the thesis 82

RESULTS 83

Chapter II - CAP treatment enhances endosomal vesicle maturation in RAW264.7 murine cell line during *S. aureus* infection.. 85

Conclusion 101

Chapter III - CAP enhances wound healing and decreases infection through NOX2 activation. 103

Introduction 103

1. Additional results to the study 170

1. Transcriptomic analysis 170
2. Mitochondria involvement in ROS production for *S. aureus* elimination 175

Discussion 177

Conclusion 179

Chapter IV-Development of a homemade CAP device 181

1. Evaluation of the target temperature 181

2. Biological characterization 182

2.1. Hacat cells viability and proliferation 182
2.2. Hacat migration 184
2.3. Conclusion on biological measurements 186

Discussion 186

Conclusion 187

Chapter V - Development of porcine model of full-thickness burn wound reconstructed with autologous skin graft 189

1. Development of the experimental procedure 189

1.1. Justification for the choice of mammalian species 189
1.2. Experimental procedure 190
1.3. Medication and wound management 193
1.4. Examinations and sampling during and after the procedure 195
1.5. Animal welfare during the procedure 196

Discussion 199

Conclusion 200

Discussion and perspectives 202

Conclusion 208

Materials and method of chapter III 211

1.1. Raw264.7 culture conditions 211

1.2. Bacteria culture and preparation 211

1.3. RNA isolation 211

1.4. Quantitative reverse-transcription–PCR 211

1.5. Pharmacological inhibition of ROS activity 212

2.1. Physical characteristics 212

2.1.1. Plasma jet I 212

2.1.2. Jet II plasma device 214

2.2. Chemical characteristics 214

2.2.1. H_2O_2 quantification 214

2.2.2. Measure of NO_x^- 215

2.3. *In vitro* analysis using human cells 215

2.3.1. Hacat culture conditions 215

2.3.2. WST-1 cell proliferation assay 215

2.3.3. CFSE proliferation assay 216

2.3.4. Scratch wound assay 216

Bibliography 217

LIST OF ILLUSTRATIONS

Figure 1: Schematic representation of the human skin structure. 23
Figure 2: Hematoxylin and Eosin-stained microscopic view of the human skin. 25
Figure 3: Typical components found in the basement membrane of the skin. 27
Figure 4:Timeline and approximation of immune cell number arrival to the wound bed. 32
Figure 5: Macrophage phenotype characteristics. 34
Figure 6: Healing trajectory and basic phases of healing of infected wound. 30
Figure 7: Comparison between human, pig, rat and mouse skin. 43
Figure 8: Schematic process of human primary cells extraction for 3D bioprinting. 45
Figure 9: Timeline of common pathogens infections after burn injury. 47
Figure 10: Internalisation of *S. aureus* by professional phagocytes via phagocytosis and phagolysosome maturation. 53
Figure 11: Representation of the NADPH oxidase isoform and their main locations. 55
Figure 12: Activation of the NADPH oxidase NOX2 complex. 57
Figure 13: *S. aureus* mechanisms of subversion of the immune system. 59
Figure 14: Antimicrobial species generated from oxygen and nitrogen. 61
Figure 15: Interaction with *S. aureus*. 63
Figure 16: Physical description of plasmas. 65
Figure 17: Photographs of the fundamental devices used for biomedical applications. 67
Figure 18: Photographs of the CE-certified devices and their treatment area surface. 67
Figure 19: Schematic representation of the reactive species produced by plasma in plasma activated media (PAM) an at different interfaces (Gas-gas/Gas-liquid). 69
Figure 20: SEM micrographs of physical disruption induced by cold plasma on different strains. 71
Figure 21: Assessment of the sequence quality scores of the raw FASTQC data for infected macrophages helium and CAP treated samples. 171
Figure 22: Summary of the Differential Gene Expression (DGE). 172
Figure 23: Summary of the Differential Gene Expression (DGE). 173
Figure 24: Relative mRNA levels of *Cybb, Rac1* and *Rac2* in uninfected and infected macrophages. 174
Figure 25: Relative mRNA levels of pro-inflammatory and NOX2 genes in *S. aureus* Xen36 infected macrophages. 175
Figure 26: Effect of CAP on ROS production in RAW264.7 macrophages and in bactericidal activity in 3D bioprinted human skin. 176
Figure 27: Influence of CAP on Hacat cell viability. 183
Figure 28: Effect of CAP on HaCat proliferation. 184
Figure 29: CAP treatment stimulated HaCat cells migration. 185
Figure 30: Burn induction and treatment of full-thickness burns. 190
Figure 31: Microscopic images of porcine skin stained with H&E. 191
Figure 32: Protective jacket. 192
Figure 33: Example of pig grimace scale applied for the pilot study. 198
Figure 34: Schematic representation of the plasma device used *in vitro*. 214

LIST OF TABLES

Table 1: Growth factors at the wound site..... 33
Table 2: Tissue-engineered epidermal, dermal subsitutes and current surgical techniques for severe burns...... 41
Table 3: Advantages and limits of *in vivo* burn wound models. 44
Table 4: Cold atmospheric plasma applications for chronic wounds. 79
Table 5: Cold atmospheric plasma applications for acute wounds. 80
Table 6: Temperature of pig skin stapled with surgical staples treated with jet II measured with a digital infrared camera...... 182
Table 7: Example of feasible tests on pig blood and organ samples...... 196

LIST OF ABBREVIATIONS

ADSC: **Adipose tissue-derived mesenchymal stem cells**
BM: **Basement membrane**
BMDSC: **Bone marrow-derived mesenchymal stem cell**
CAP: **Cold atmospheric plasma**
CGD: **Chronic granulomatous disease**
DI: **Deionized water**
ECM: **Extracellular matrix**
GEF: **Guanosine exchange facor**
I.M: **Intramuscular**
I.V: **Intravenous**
iNOS: **Inducible nitric oxide synthase**
LDAs: **Lipid-derived aldehydes**
LPS: **Lipopolysaccharide**
LTA: **Lipoteichoic acid**
MMP: **Metalloproteinase**
MPO: **Myeloperoxidase**
mROS: **Mitochondrial ROS**
MRSA: **Methicillin resistant *S. aureus***
MSC: **Mesenchymal stem cell**
MSSA: **Methicillin sensitive *S. aureus***
NO: **Nitric Oxide**

NOX2: **NADPH enzyme**
PAM: **Plasma-activated media**
PCT: **Procalcitonin**
PDGF: **Platelet derived growth factor**
PGN: **Peptidoglycan**
PMN: **Polymorphonuclear cells**
PRR: **Pathogen recognition receptor**
RNS: **Reactive nitrogen species**
RONS: **Reactive oxygen and nitrogen species**
ROS: **Reactive oxygen species**
SIRS: **Systemic inflammatory response syndrome**
SR: **Scavenger receptor**
TBSA: **Total Body Surface Area**
TEWL: **Transepidermal water loss**
TNF: **Tumor necrosis factor**
v-ATPase: **Vacuolar-type proton transporting ATPase**
VEGF: **Vascular endothelial growth factor**

Chapter I.
State of the art

Chapter I – State of the art

1. Skin and wound healing complexity

1.1. Structure

In direct contact with the environment the skin is the largest organ of the body accounting for 15-20% of the total body weight, with a surface area of 1.5-2 m^2. This multifunctional organ provides a life-protective physical barrier against thermal and mechanical aggressions such as friction and against potential pathogens and debris. It allows a constant temperature easily maintained owing to the skin's insulating components (e.g. fatty layer, hair) and its mechanisms for accelerating heat loss (sweat production and a dense superficial microvasculature).
As the outer barrier, the skin is the most challenged organ by a range of external stresses with a thickness depending on the location and the functions[1]. As such, it possesses a complex structure, illustrated in figure 1, and has developed a set of mechanisms to protect itself and to restore tissue integrity when damaged.

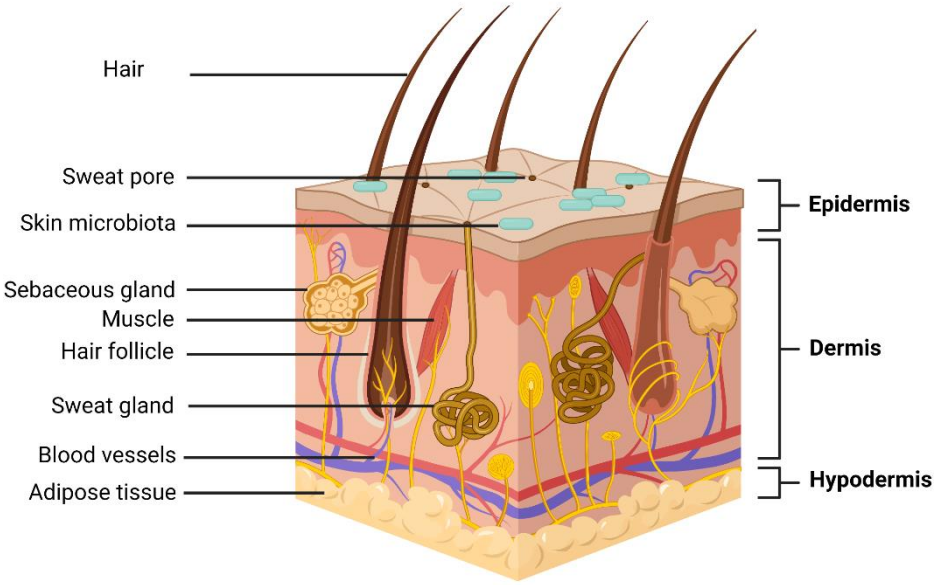

Figure 1: Schematic representation of the human skin structure. The three main layers of the skin are represented: the epidermis, the dermis and the hypodermis. The skin is composed of appendages such as sebaceous glands, sweat glands or hair and skin-specific microbiota. *This illustration was made using biorender.com.*

1.1.1. Epidermis

1.1.1.1. Introduction

The epidermis forms the distinction between the thick and thin skin. It refers to the thickness of the epidermal layer which alone varies from 75 to 150 μm^2 for the thin skin and from 400 to 1400 µm for the thick skin. The total skin thickness, epidermis and dermis, may also vary according to the location on the body: back 4 mm, scalp 1.5 mm thick.
The epidermis is mainly composed of a stratified squamous keratinized epithelium formed of cells called keratinocytes. These cells divide, grow, migrate up, undergo keratinization or cornification and form the protective epidermal and surface layer of the skin. It also contains non-keratinocyte cells as the melanocytes responsible for the skin and hairs pigmentation. Langerhans cells are antigen-presenting cells derived from monocytes. They represent 2%-8% of the cells in epidermis. Langerhans cells bind, process and present antigens to T lymphocytes of the immune system in the same manner as immune dendritic cells in other organs. The epidermis also contains a huge number of CD8+ resident memory T cells second largest population after the blood. Because of these functions, they are implicated in the pathologic mechanisms underlying allergic contact dermatitis or human immunodeficiency virus infection. Finally, Merkel cells are oval-shaped, slow adapting type I mechanoreceptors located in sites of high-tactile sensitivity that are attached to basal keratinocytes by desmosomal junctions. They are found for example in the digits, lips and are sometimes assembled into specialized structures known as tactile discs or touch domes[3]. Light touch to the skin initiates release of neurotransmitters and sensation from that location.

1.1.1.2. Structure and physiology

The ***stratum basale*** is the deepest single layer composed of keratinocytes on a basement membrane separating the dermis from the epidermis (figure 2). The cells are linked to one another by cell junctions called desmosomes and to the underlying basement membrane by hemidesmosomes. The cells of the stratum basale serve as stem cells for the epidermis and so divide continually and mature as they migrate up. Basal keratinocytes are polarized and undergo mitosis. They all produce intermediate keratin filaments that increase in number as the cells move to the top. In addition to the basal stem cells a niche for such cells also occurs in the hair follicle sheaths that are continuous with the epidermis. The human epidermis is renewed every 15-30 days depending on multiple factors such as the age and the region of the body.

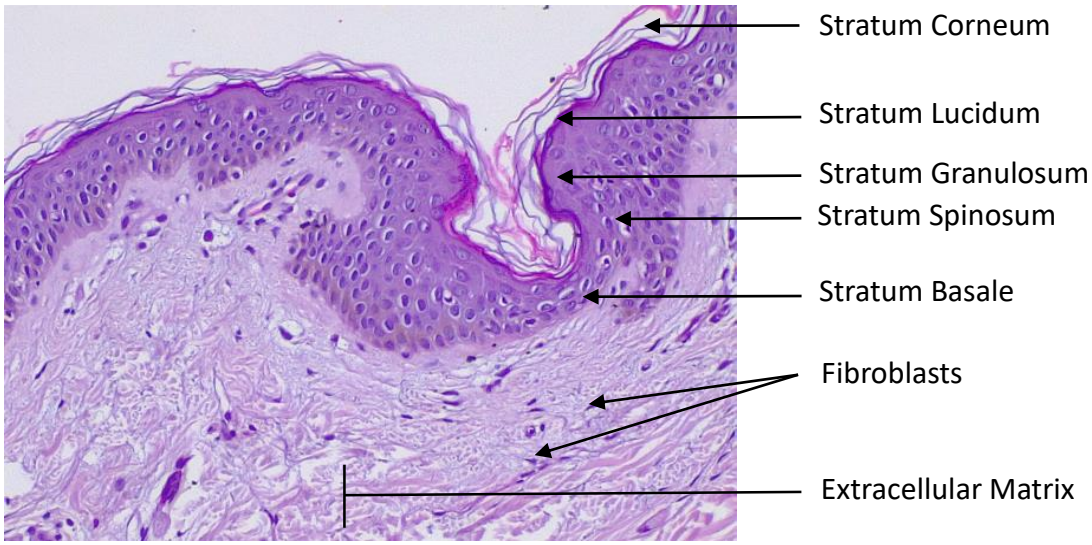

Figure 2: Hematoxylin and Eosin-stained microscopic view of the human skin. The four sublayers of the epidermis are shown: stratum corneum, lucidum, granulosum, spinosum and basale. In the dermis extracellular matrix and fibroblasts are visible. *Adapted from Farcy et al., 2022*[4].

As the keratinocytes are dividing by mitosis, they move upward and form the second layer: the ***stratum spinosum*** (figure 2)**.** It consists generally of polyhedral cells with nucleoli and cytoplasm actively synthesizing keratins. The keratin filaments assemble into microscopically visible bundles called tonofibrils which converge and terminate with desmosomes holding the cell layers together. The cells extend around the tonofibrils leading to the appearance of short "spines" or prickles at the cell surface. The spines represent the localisation where desmosomes are anchored to bundles of intermediate keratin filaments or tonofilaments and to other cells. Theses connections provide cohesion among cells and resistance to the abrasion of the epidermis.

While the cells are maturing they are moving above the *stratum spinosum*, accumulate basophilic keratohyalin granules and form the ***stratum granulosum*** (figure 2). It consists of three to five layers of flattened cells undergoing the terminal differentiation process of keratinization; their cytoplasm is filled with basophilic masses called keratohyaline granules. These secretory granules are not surrounded by a membrane and contain fillagrin masses which induce the aggregation of keratin tonofilaments into tight bundles. This granular layers also include Golgi-derived lamellar granules with many lamellae containing various lipids and glycolipids. The lamellar granules undergo exocytosis producing a lipid-rich, impermeable layer among the last activities of the keratinocytes. These compounds form a major part of the skin's barrier against water loss. Both, keratinization and the production of lipid, have a crucial sealing effect in skin, forming the barrier to penetration by most foreign materials.

The ***stratum lucidum*** (figure 2), present only in thick skin, is a translucent layer of flattened eosinophilic keratinocytes held together by desmosomes. The cells lack nuclei or organelles and the cytoplasm consists almost of packed keratin filaments embedded in an electron-dense matrix.

The last layer of the epidermis is the ***stratum corneum*** (figure 2). It is composed of 15-20 layers of squamous, keratinized cells, called corneocytes, filled with soft keratin filaments. The level of keratin within the different layers of the skin can range from 30% in the basal layer to 80% in the *stratum corneum*. By the end of keratinization, the cells contain amorphous, fibrillary proteins with plasma membranes surrounded by the lipid-rich layer. The lipids released in the intracellular space allow the sealing of corneocytes together and the aggregation of the keratin filaments to form micro fibrils. The keratinized or cornified cells from this layer, called squames, continuously shed at the epidermal surface and are replaced by new cells arising from the deep stratum basale. The epidermis contains neither blood vessels nor lymphatic vessels, is innervated and rests on the demal-epidermal junction, also called basement membrane, which separates it from the dermis.

1.1.2. Basement membrane

The basement membrane (BM), also called-dermal-epidermal junction, forms the interface between the epidermis and the dermis and is synthesized by both basal keratinocytes and dermal fibroblasts. The four main components of the BM are type IV collagen, laminin (LAM), nidogen/entactin and perlecan[4] illustrated in figure 3. Type IV collagen and laminin individually self-assemble into suprastructures and are essential for the BM stability. The BM is a complex structure but can divided into four areas: hemidesmosomes, *lamina lucida*, *lamina densa* and anchoring fibrils.

The first layer corresponds to the junction with the epidermis through an interaction between keratin filaments and ligands of hemidesmosomal transmembrane proteins (COL XVII, a6b4 integrin). Near the epidermis there is the *lamina lucida*, a layer rich in LAM 332[5] and COL XVII.

The *lamina densa* is located in the lower part. It contains perlecan, nidogen and COL IV. Finally, the connection between the BM and the dermis is insured by anchoring fibrils and loops of COL VII which extend to the dermis.

In adult skin two types of LAM are preponderant: LAM-511 (or LAM10) and LAM-332 (or LAM 5). Disorders impacting the components of the BM lead to important diseases such as the junctional epidermolysis bullosa (Herlitz variant) resulting from mutations of LAM-332 gene.

The major functions of the BM are to attach the epidermis and the dermis to each other and provide resistance against shearing forces. Moreover, it serves as a support for the epidermis, determines the polarity of growth, provides developmental signals, and serves as a semipermeable barrier.

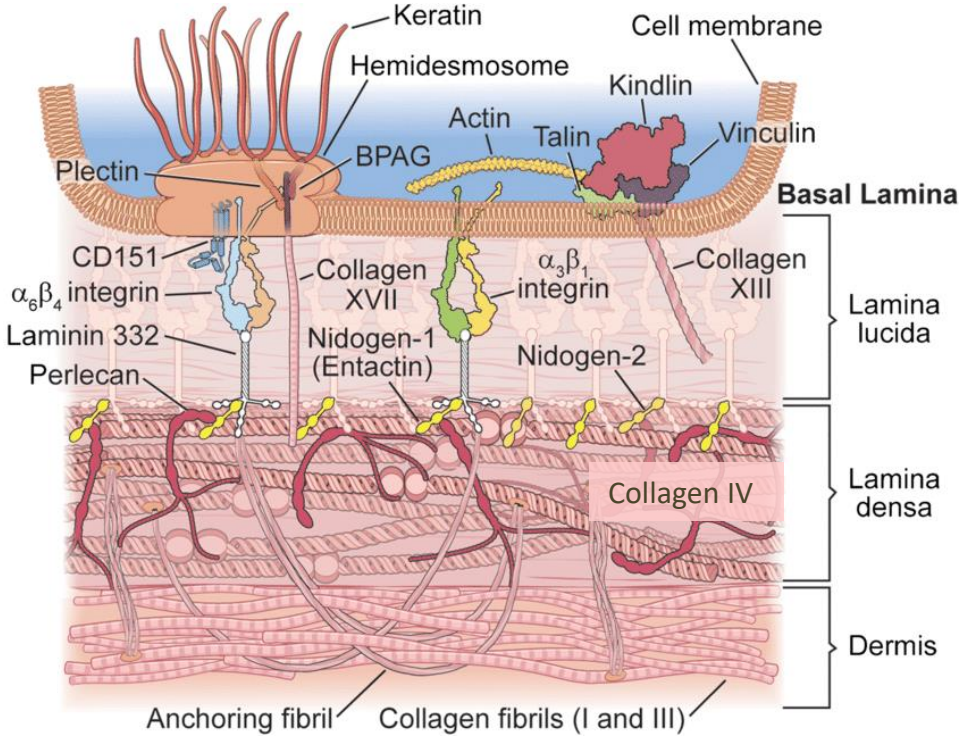

Figure 3: Typical components found in the basement membrane of the skin. Keratinocytes adhere to the basement membrane and the dermis through adhesions that consist of interacting components as hemidesmosome with bullous pemphigoid antigen (BPAG), laminin 332, perlecan, integrin α6β4, anchoring fibrils and other components that vary according to the type and state of the tissue. *Figure adapted from Saikia et al., 2018*[6].

1.1.3. Dermis

Introduction

The dermis is a layer of connective tissue that supports the epidermis and binds it to the hypodermis. The thickness of this tissue depends on the region of the body and reaches its maximum of 4 mm on the back. It is an integrated system of fibrous, filamentous and amorphous extracellular matrix (ECM). The ECM accommodates nerve and vascular networks, epidermal derived appendages (nerves, lymphatic vessels, glands, hair follicles) and contains several resident cell types such as fibroblasts, mast cells or macrophages.
The dermis is vascularized by blood capillaries that help maintaining the skin through the transfer of nutrients and the movement of waste. Bloods enters the skin via small arteries that branch with arterioles and then branch to form capillaries[6]. The deeper vascularization is in contact with hair follicles and sweat glands. The epidermis layer is not vascularized but nutritional capillaries coming from the dermis feed the epidermis.

The dermis is divided into two sublayers: the papillary layer and the reticular layer. The **papillary layer** consists of loose connective tissue with types I and III collagen fibers,

fibroblasts, mast cells, dendritic cells and leukocytes. The **reticular layer** is thicker and consists of dense irregular connective tissue, the ECM, with more fibers and less cells than the papillary layer. In this underlying layer there is also a network of elastic fibers providing elasticity to the skin.
The dermis makes up the majority of the skin, it is between 15-40 times as thick as the epidermis. It provides the pliability and tensile strength of the skin. It protects the body from mechanical injury, contributes to the thermo regulation and includes receptors of sensory stimuli. The epidermis and the dermis interact in order to maintain the properties of both tissues and interacts in repairing and remodelling skin wound.

Key components of the ECM

Fibroblasts are key cells of the dermis, they are involved in the synthesis of the ECM as well as in skin repair processes after injury[7]. Several fibroblasts populations are described based on location and depth in the dermis. Fibroblasts produce the four main classes of ECM components: collagen, elastin, proteoglycans and fibronectin. Elastin and collagen help cells to infiltrate and proliferate in the dermis. Fibroblast also synthesizes proteases to degrade and remodel the ECM[8] and secrete remodelling factors such as matrix metalloproteinase (MMPs). In wound healing, the secretion of collagen fibers by fibroblast favor wound strengthening and contraction by the action of smooth muscles and the alignment of collagen fibers.
Collagens represent around 90% of the dermis protein[2] and are critical for the epidermis dermis adherence. Twenty-seven different collagens are coexisting in the skin and among them collagen VII attaches the basement membrane of the upper dermis while collagen XVII link the basal keratinocytes to the basement membrane[9].
Elastin is also an important fibrous protein of the skin providing its elasticity. Those fibers are stretchable by more than their full resting length. All the dermal material lying outside the cells, except collagen and elastin, is called extrafibrillar matrix. This hydroscopic material is highly active, diverse and organized. It contains proteoglycans, glycoproteins, hyaluronic acid and water. Versican is the most important proteoglycan providing tautness to the skin when it is associated with elastics fibres and hyaluronic acid. Syndecan is a family of proteoglycans involved in different functions as cell adhesion to ECM or coagulation cascades. The ECM contains other multifunctional glycoproteins as laminins, matrilins or tenascins involved in basement membrane, cellular migration and intercellular communication beneficial in a skin healing context.

1.1.4. Hypodermis

Hypodermis or subcutaneous layer is mainly composed of adipocytes that vary in number in different body region. The extensive vascular supply promotes rapid uptake of insulin or drug injected into this tissue. In human skin, the adipose layer is thicker than in other smaller mammals to compensate the absence of fur and it possesses more developed sensory innervations. The adipocytes and connective tissue are responsible for fat storage, internal organ

protection, and insulation[10]. It is also an energetic store for the body due to the presence of fatty acids[11].

1.1.5. Antimicrobial defense of the skin

In addition to the acidic pH human skin produces enzymes and proteins that kill or inhibit the growth of bacterial and fungal cells. Lysozyme, for example, is an enzyme that cleaves peptidoglycan from bacterial walls especially in Gram-positive bacteria (breaks the link between n-acetylmuramic acid and n-acetylglucosamine of the peptidoglycan) and it is also deleterious to Gram-negative bacteria. The lactoferin and calprotectin are two proteins which sequester the metal ions necessary for bacterial growth. Recently research has identified the psoriasin, a small protein, having effective antibacterial activity against *Escherichia coli* (enteric bacteria).

Another major class of antimicrobial compounds secreted by the skin and epithelial surfaces are antimicrobial peptides (AMPs). AMPs are amphipathic peptides that participate in skin defence by disrupting bacterial membranes[12], inhibiting protein and DNA synthesis. In human skin the defensins and the cathelicidin LL-37 are the most studied AMP families. They are produced by a huge variety of skin cells such as keratinocytes, fibroblasts, monocytes or macrophages[13]. Human LL-37 is able to induce differentiation of monocyte-derived dendritic cells, cytokines production and expression of the co-stimulatory molecule CD86. The keratinocytes represent the major source of AMPs in the skin that constitutively express AMPs such as human β-defensin 1 (hBD1) while others are induced when they are exposed to injury or infection (e.g. hBD2-4). Moreover, AMPs are also produced by the commensal bacteria with, for example, *Staphylococcus epidermidis* expressing the phenol-soluble modulin (PSM-)γ. It displays direct antimicrobial activity against *S.aureus* and indirect, by activating pro-inflammatory Toll-like receptor 2 (TLR2) on keratinocytes, thereby enhancing the endogenous production of AMPs[14] and thus, the antimicrobial activity.

The skin also contains immune cells that act as sentinels by sampling environmental antigens. Both myeloid and lymphoid cell subsets are found in the skin. During an injury or tissue infection resident cells and infiltrating cells interact to create a defense network to restore the tissue. Skin-resident myeloid cells as Langerhans cells, dermal dendritic cells, macrophages or mast cells contribute to skin homeostasis and maintain optimal tissue function by phagocytosing debris, pathogens and apoptotic cells. In an inflammatory context myeloid cells immediately produce pro-inflammatory mediators for the activation of cells localy and by infiltration. Lymphoid cells are important in steady state and inflammatory response. For example, αβT lymphocytes induce antiviral state through IFNγ mechanism or γδT lymphocytes produce IL-17 to induce β-defensin expression from keratinocytes.

Despite the fact that human skin is sterile in utero the bacterial colonization begins immediately after birth with the mode of delivery determining the colonization pattern (infants born vaginally or by caesarean section)[15,16] and evolving according the lifestyle of the individual. In the adult, the skin acquires a density of more than 1×10^6 /cm^2 and hundreds of species described[17,18]. The skin microbiota can modulate the expression of innate factors such as interleukin 1α (IL-1α)[19], AMPs, and components of complement[20]. It is now apparent that skin

microbiota is highly specialized to the niches. It not only interacts with the local tissue microenvironment but drives signals at distant organ as well and can influence wound healing[21,22].

1.1.6. Cutaneous microbiota

Being directly in contact with the external environment, the skin is constantly exposed to pathogenic or non-pathogenic microorganisms. It possesses a cutaneous flora composed of millions of bacteria, fungi and viruses. For a long time, it was commonly thought that germs exploiting the host's nutrient resources for their own benefit. It is now accepted that skin microorganisms have an essential role against invading pathogens, stimulation of our immune system and the breakdown of natural products[23,24]. The process of skin microbiota assembly begins during birth then it shifts notably during puberty with a decrease of Firmicutes and an increase of *Corynebacterium* and *Cutibacterium*. In healthy adults the microbial composition was found to be dependent on the skin site associated with fluctuation in moist, dry, sebaceous microenvironment and interpersonal variation. Commonly lipophilic *Propionibacterium* predominantly colonized sebaceous sites and *Staphylococcus* and *Corynebacterium* species are abundant in moist areas[25]. In normal condition this cutaneous flora has a protective function.
On the opposite, an alteration of the microbiota can induce a deregulation of homeostasis and leads to cutaneous diseases (atopic dermatitis, eczema). If the skin suffers damage (cut, burn), opportunistic pathogenic bacteria of the skin, that are normally safe, can induce infection and even sepsis and death. Among the pathogens that break down the physical and chemical barriers of the skin there are those that multiply in extracellular spaces (some bacteria, fungi and parasites) and those that multiply inside the cells (some bacteria or parasites and viruses).

Cutaneous microbiota and immunity

The microbiota also has an impact on the innate and adaptive immune system that promotes tissue integrity and/or repair[26]. It can interact with the complement as well as on the level of IL-1α, an initiator of inflammation[27]. Innate immunity can be influenced for example by the lipoteichoic acids produced by *S. epidermidis* that prevent the inflammatory reaction of keratinocytes through a TLR2-dependent mechanism, on its side *P. acnes* modulates the antimicrobial peptide and chemokine expression of keratinocytes[28]contributing to the recruitment of inflammatory cells to the sites of infection.
The effect on adaptive immunity enhanced the induction or activation of lymphocytes during infection[29]. Tolerance of immune system to commensal germs is dependent on T cells regulators and is acquired from birth[30], and is called "immune homeostasis"[26]. The local regulation is mediated by the ability of microbiota to promote IL-1 production which triggers IL-17 and IFNγ secretion by T cells[27]. Those specific regulations improve the immune response against certain pathogens such as *Leishmania major* or *Candida albicans*[27,31].
In recent years, immunological research has evolved from a lymphoid tissue-centric view of the immune system to the integration of the understanding of the complex tissue microenvironments as a fundamental determinant of immune responses. Better understanding

of microbiota interaction with the skin reveals new potential pathways for therapeutic intervention for patients with deep and chronic wounds.

1.2. Wound healing and regeneration

Evolution has created the skin as a highly adaptive and multifunctional organ that protect the organisms from daily onslaught of chemical, physical and general stresses. Wound healing has been recognized as crucial for health since the beginning of mankind as intact outer sheath is one of the most important feature for organisms. In order to face frequent alterations, the skin has developed a set of complex mechanisms to restore tissue integrity. Skin wound healing is a dynamic and highly regulated process of cellular, humoral and molecular mechanisms that is well coordinated and promotes most wounds closure within two to three weeks if there are no complications (e.g. infection, chronic illness such as diabetes). In healthy people wound closure consists of 4 different steps involving multiple cell types and proteins.

1.2.1. Hemostasis

The first stage of physiological wound healing is to stop blood leakage through the formation of a provisional wound matrix which occurs immediately after injury. The formation of a clot serves as a temporary shield protecting the denuded wound. It consists of platelets embedded in a mesh of fibrin fibers derived from fibrinogen, vitronectin and thrombospondin forming a scaffold structure for the migration of leukocytes, keratinocytes fibroblasts and endothelial cells. This clot is also a reservoir of cytokines and growth factors. In addition of vasoconstriction and vasodilatation phenomenon, the platelets influence the infiltration of leukocytes by the release of chemotactic factors. Indeed, platelets and leukocytes release chemokines, cytokines and growth factors in order to trigger the inflammatory process (IL-1, IL-6, TNF-α), to stimulate the collagen synthesis (TGF-2, TGF-β), activate the formation of myofibroblasts (TGF-β), start angiogenesis (FGF-2, HIF-1α, VEGF-A), and support the reepithelialization process (FGF-2, IGF-1, TGF-α)[32]. The trauma induced on epidermal layer, blood and lymphatic vessels lead to the clearance of the wound bed to remove microorganisms and antigens.

1.2.2. Inflammation

Neutrophils

The signals produced during hemostasis as degranulated platelets and by-products of bacterial degradation initially allow the recruitment of neutrophils to the wound site that are present 2-5 days. They have a crucial role due to their ability in phagocytosis and protease secretion to kill local bacteria and to degrade necrotic tissue. They release mediators as TNF-α and IL-6 (table1) which amplify the inflammatory phase and they release active antimicrobial substances (eicosanoids, cationic peptides, oxygen free radicals) and proteinases (cathepsin G, proteinase

3) to start the debridement[33]. In parallel monocytes arrive within 24 hours in response to chemo-attractants and differentiate locally into macrophages shown in figure 4.

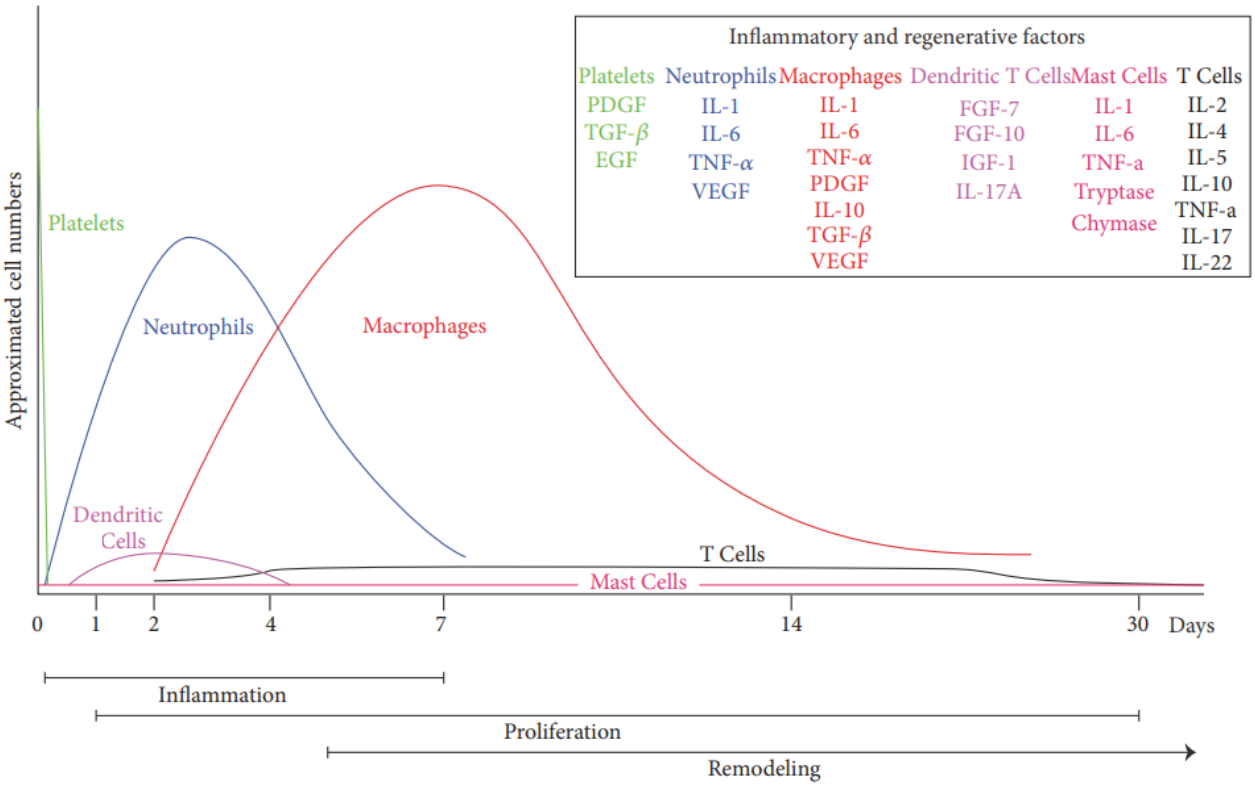

Figure 4: Timeline and approximation of immune cell number arrival to the wound bed. After the wound neutrophils increase and accumulate and start to decline at day 4. Macrophages number increases at day 2 during the inflammation phase, reach their maximum during the proliferation phase and start to decline during the remodeling phase, being the most abundant cell in the wound healing process. Each type of cell secretes pro or anti-inflammatory cytokines, growth factors, enzymes that participate to healing. Approximate time of wound healing phases is illustrated at the bottom of the graphic. *Adapted from* Cañedo-Dorantes et *al.*, 2019 [34].

Macrophages

The infiltration of macrophages increases during the inflammatory stage with a peak at day 2 after injury and their number gradually decreases during maturation but these cells massively remain at later time[35]. The arrival of macrophages into wound bed is changed during the healing process suggesting a diversity of roles of these inflammatory cells in the stages of wound repair. The general functions of macrophages are to help the wound bed clearance by killing microbes through phagocytosis, removing cells and tissue matrix debris and pave the way for angiogenesis and tissue granulation[36]. Once activated macrophages release many growth factors and cytokines at the wound site.

Table 1: Growth factors at the wound site. *Adapted from Martin et al.*, 1997[37]

Growth factor	Source	Target cells and effects
EGF	Platelets	Keratinocyte motogen and mitogen
TGF-α	Macrophages, keratinocytes	
FGFs 1, 2 and 4	Macrophages and damaged endothelial cells	Angiogenic and fibroblast mitogen
PDGF	Platelets, macrophages, keratinocytes	Chemotactic for macrophages, fibroblasts; macrophage activation, fibroblast mitogen, and matrix production
IGF-1	Plasma, platelets	Endothelial cell and fibroblst mitogen
VEGF	Keratinocytes, macrophages	Angiogenesis
TGF β1, β2	Platelets , macrophages	Keratinocyte migration, chemotactic for macrophages and fibroblasts, fibroblast matrix synthesis and remodeling
TGF β3	Macrophages	Antiscarring
IL-1α and β	Neutrophils	Early activators of growth factor expression in macrophages, keratinocytes, and fibroblasts
TNF-α		

They are key cells for wound healing as they are responsible for ending the local inflammation steps as well as the initiation of the following steps of proliferation, angiogenesis, granulation tissue formation, fibroblasts recruitment and the remodeling of the wound[38]. Macrophages are plastic cells that can switch from one phenotype to another[39] during a process called polarization. They acquired specific phenotype and initiate a functional response to the micro-environmental stimuli and signals encountered. Several classes of macrophages have been described in human based on different factors such as the biological activities or cell surface markers. However, two major subpopulations have been described *in vitro*: classically activated (M1) and alternatively activated (M2) macrophages[40] (figure 5). M1 macrophages typically involves Th1 cytokines (IFNγ, TNF-α) or bacterial lipopolysaccharide (LPS) recognition. They secrete a high level of pro-inflammatory cytokines (IL-6, IL-12, IL-23), cyclooxygenase-2 (COX-2) and low levels of IL-10. They have a key role in the removal of pathogens during infection thanks to the activation of the nicotinamide adenine dinucleotide phosphate (NADPH) oxidase enzyme. M1 macrophages have a robust anti-tumoral and anti-microbial activity in tissue regeneration and wound healing. In order to overcome tissue damage, the inflammatory response is inhibited by regulatory mechanisms of the M2 macrophages function the opposite M2 macrophages are anti-inflammatory activated cells. Their polarization is triggered by Th2

cytokines (IL-4, IL-13) and produce anti-inflammatory cytokines (IL-10, TGF-β). The main difference between M1 and M2 cells is that M2 macrophages arginine metabolism is shifted to ornithine and polyamines. The M2-produced ornithine can promote cell proliferation and repair through polyamine and collagen synthesis, fibrosis and other tissue remodeling functions[41]. They are also involved in parasite containment, tumor growth and immunomodulatory functions. In acute wounds, as the tissue begins to repair the macrophages population transitions to one that promotes anti-inflammatory effects (M2), and the migration and proliferation of fibroblasts, keratinocytes and endothelial cells to restore respectively the dermis, the epidermis and the vasculature. Macrophages are also important in vascularization by positioning themselves near newly blood vessels and promoting their stabilization and fusion[42,43]. In the case of chronic wounds the pro inflammatory macrophages persist without differentiating to anti-inflammatory phenotypes, which is thought to contribute to the impairment in tissue repair[44].

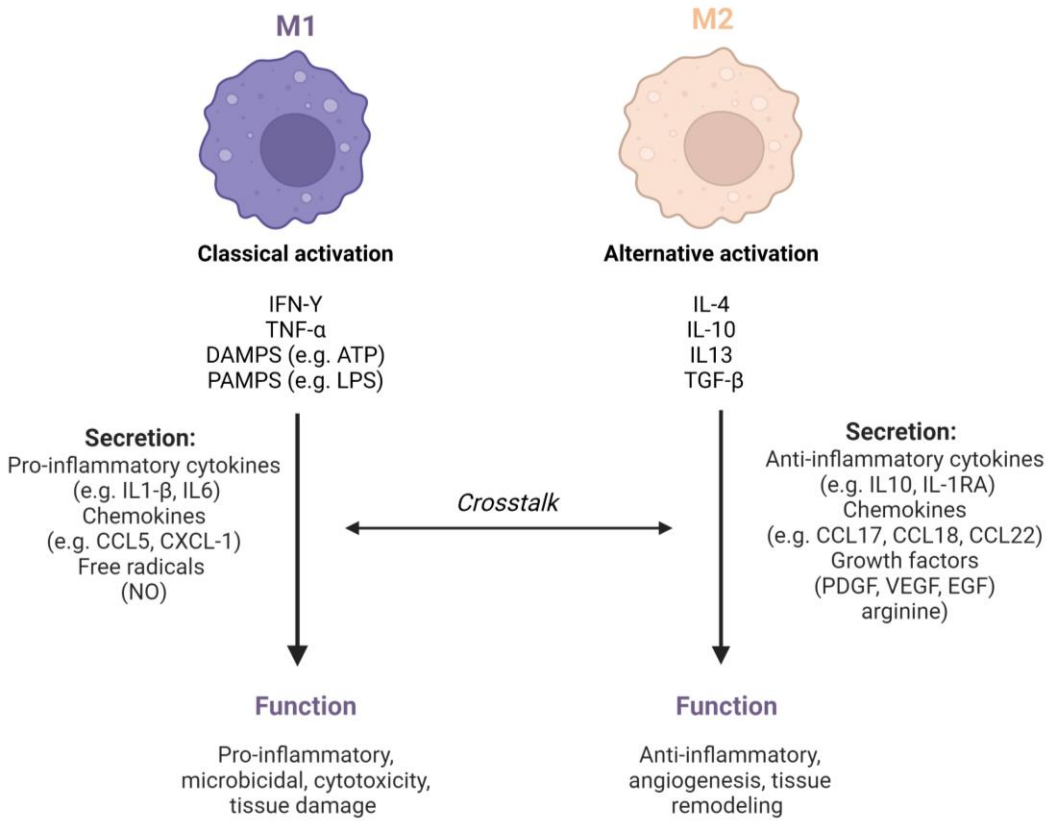

Figure 5: Macrophage phenotype characteristics. Macrophages are differentiated into M1 phenotype in response to stimulation with PAMPs (LPS) and/or cytokines as TNF-α or IFN-γ. The activation of M1 phenotype induce the secretion of pro-inflammatory cytokines, chemokines and free radicals. M1 macrophages mediate inflammatory response, cytotoxicity and tissue damage. Macrophages are polarized into M2 phenotype in response to a stimulation with cytokines and growth factors as IL-4, IL-10 or TGF-β. M2 macrophages promote anti-inflammatory and immune suppressive responses and favor tissue healing[45]. *This illustration was made using biorender.com.*

Thus, both M1 and M2 macrophages are pivotal for healing process. More M1 macrophages are needed to remove debris and kill invading pathogens while the M2 phenotype may have more important role in late phases of wound healing. It has been shown that early depletion of macrophages during the inflammation phase of a surgical wound leads to a reduction of angiogenesis and the formation of granulation tissue together with an alteration of re-epithelialization [46,47]. On the opposite an invalidation of macrophages during the intermediate stage of proliferation causes a hemorrhage in wound and prevents the transition to the maturation and remodeling phase. Finally, depletion of macrophages during the remodeling does not affect the final result[46].

1.2.3. Proliferation

The main focus of this step lies in covering the wound surface and to restore the vascular network. Thus this third step includes different sub-stages as angiogenesis, proliferation and migration of fibroblasts, extracellular matrix synthesis of the dermis and keratinocytes proliferation. The proliferation is characterized by the formation of granulation tissue and results in wound repair. At the same time as immigration of local fibroblasts along the fibrin network and the beginning of re-epithelialization from the edges, neovascularization and angiogenesis are activated by capillary sprouting[48]. The synthesis of collagen and other substances of the new matrix of connective tissue as fibronectin is under the control of cytokines like IFN-γ and TGF-β which will promote wound closure and favor the restoration of the mechanical strength of the wound. Subsequently, the collagen synthesis increases throughout the wound while fibroblast proliferation declines, allowing a balance between synthesis and degradation of the ECM.

1.2.4. Re-epithelialization

Local keratinocytes of the wound edges and epithelial stem cells from hair follicles or sweat glands ensure the re-epithelialization process. It is triggered by multiple cytokines and growth factors as EGF, KGF or IGF-I[32]. An activation of membrane associated kinases leads to an increase in permeability of the membrane to ions leading to a reorganization of intracellular tonofilaments in the direction of migration. Keratinocytes migrate along the fibrin clot in the upper layer of the granulation tissue. The migration is done along a chemotactic gradient established by regulators as IL-1. Simultaneously an active paracrine interaction between keratinocytes, fibroblasts, neutrophils, monocytes-macrophages and other key cells increases the amount of cytokines, growth factors and biomolecules to promote epithelial-mesenchymal interaction between keratinocytes and fibroblasts leading to a stimulation of fibroblasts by keratinocytes to release growth factors that in turn stimulate keratinocytes proliferation[49]. Fibroblasts differentiate into myofibroblasts, allowing collagen deposition and initiating wound contraction. This process persists until cells come into contact.

Angiogenesis/neovascularization

The restoration of the vascular network of the skin is a complex cascade of cellular, molecular and humoral events to reconnect to the nutritive perfusion by forming new blood vessels. After injury local hypoxia stimulates the stabilization of hypoxia inducible factor-1 (HIF-1) in fibroblasts, keratinocytes, macrophages and in vascular endothelial cells leading to the production of angiogenic factors as VEGF, PDGF, or TGF-β1 that trigger neovascularization. The first step is the binding of growth factors to their receptors on the endothelial cells of existing vessels inducing intracellular signaling cascades. Once activated endothelial cells secrete proteolytic enzymes which dissolve the basal lamina. Thus the process of "sprouting" can start meaning that endothelial cells are able to proliferate and migrate into the wound. Endothelial cells also release matrix metalloproteinases at the front of proliferation lysing the surrounding tissue for endothelial proliferation. Then, the initial blood flow completes the angiogenic process once the new arteries and venules are formed and stabilized by the recruitment of pericytes and smooth muscle cells.

Granulation tissue

The development of the granulation tissue is the last step of the proliferation phase which occurs at the same time as the remodeling phase. It replaces the fibrin/fibronectin wound matrix and will produce a scar by maturation[50]. It is so called due to the high amounts of cellular compounds comprising a high density of macrophages, fibroblasts, granulocytes, capillaries and collagen fibers. This tissue is vascularized appearing with a classic redness and a certain fragility to trauma. Fibroblasts are the key cells of the granulation tissue which fulfils different functions as the production of collagen and synthesis of ECM substance (glycosaminoglycans, proteoglycans, hyaluronic acid). The ECM deposition is a major step providing a scaffold for cell adhesion, regulation and organization of the growth, movement and differentiation of the cells within it[50]. Finally, the number of maturing fibroblasts is reduced to myofibroblast and terminated by apoptosis[51].

1.2.5. Remodeling

The third stage of healing consists of remodeling which begins two to three weeks after the lesion and can last for one year or more. During the maturation of the wound the components of the ECM change as collagen III which is replaced by collagen I which is stronger. Later the myofibroblast lead to contractions through their multiple attachment to collagen and promote the reduction of the scar surface[52]. In addition, the wound blood flow declines and the metabolic activity slows down and stops. Thus, a mature wound is characterized as avascular and acellular.

Main stages of wound healing process are represented in figure 6. Wounds are often prone to infections. Bacteria can colonize the wound and form biofilms that can be eliminated efficiently by immune cells or can lead to complications as chronic wounds. Macrophages are key professional phagocytes for the wound bed clearance.

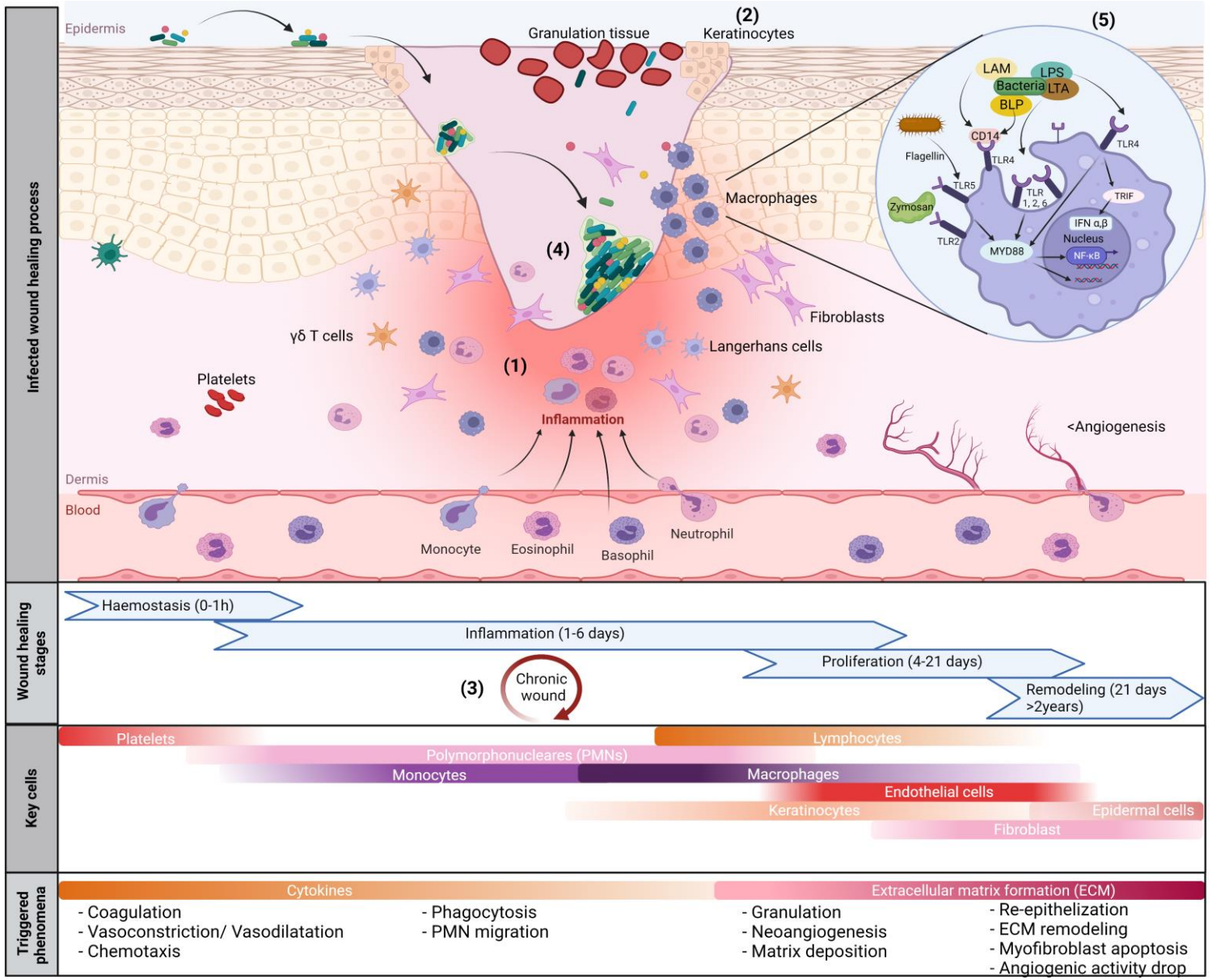
Infected wound healing process
Epidermis
Granulation tissue
(2)
Keratinocytes
(5)
LAM
LPS
Bacteria
LTA
BLP
CD14
TLR4
Flagellin
TLR5
TLR 1, 2, 6
Zymosan
TLR2
MYD88
TRIF
IFN α,β
Nucleus
NF-κB
Macrophages
(4)
Fibroblasts
γδ T cells
Langerhans cells
(1)
Platelets
Inflammation
<Angiogenesis
Dermis
Blood
Monocyte
Eosinophil
Basophil
Neutrophil
Wound healing stages
Haemostasis (0-1h)
Inflammation (1-6 days)
Proliferation (4-21 days)
(3)
Chronic wound
Remodeling (21 days >2years)
Key cells
Platelets
Lymphocytes
Polymorphonucleares (PMNs)
Monocytes
Macrophages
Endothelial cells
Keratinocytes
Epidermal cells
Fibroblast
Triggered phenomena
Cytokines
Extracellular matrix formation (ECM)
- Coagulation
- Vasoconstriction/ Vasodilatation
- Chemotaxis
- Phagocytosis
- PMN migration
- Granulation
- Neoangiogenesis
- Matrix deposition
- Re-epithelization
- ECM remodeling
- Myofibroblast apoptosis
- Angiogenic activity drop

Figure 6: Healing trajectory and basic phases of healing of infected wound.
Normal wound healing consists of several coordinated steps. Haemostasis occurs immediately after the injury and involves vasoconstriction, platelets activation and aggregation and plug formation. During the inflammatory phase neutrophils, macrophages and mast cells are recruited to the site of infection (1) and release proinflammatory cytokines, chemokines, growth factors and remove debris and pathogens from the wound bed. The inflammation decrease activates the proliferation phase inducing wound contraction, angiogenesis, fibroblasts and keratinocytes recruitment (2) for the re-epithelialization process and extracellular matrix deposition. Finally, the remodeling phase corresponds to the conversion of the granulation tissue into mature scar.
In case of a chronic wound (3) the process gets trapped in the inflammation phase. High numbers of inflammatory cells/mediators, wound infection with biofilm formation (4), hypoxia, decrease of cell recruitment and angiogenesis lead to deficient re-epithelialization, growth factor and ECM degradation creating a feed-forward loop preventing wound closure.
The wound bed colonization by pathogens is counteracted by phagocytic cells as macrophages (5). Phagocytic cells recognize Microbe-Associated Molecular Patterns (e.g LPS: lipopolysaccharide, LTA: lipoteichoic acid, BLP: bacteria lipopeptide, LAM: lipoarabinomannan, Zymosan, flagellin) by Pattern Recognition Receptors (e.g TLR). PRRs/MAMPs binding results in signaling cascades that upregulate specific gene expression through signal transduction pathways like NFkB leading to bacterial clearance.
This illustration was made using biorender.com.

1.3. Burn wounds

Thermal injuries represent one of the most devastating and lethal form of trauma that patients can sustain. If the total body surface area reaches 20% this lead to systemic pathology with a persistent pathophysiological stress response and a systemic hypermetabolic-catabolic condition[53]. Despite the fact that many advances have improved the outcomes of burn patients those last few decades an important factor in determining survival of a burn patient is still the wound coverage and healing.

1.3.1. Epidemiology

All burn injuries involve tissue destruction due to energy transfer with electrical, chemical or thermal origins associated to different consequences. For example, flames can cause immediate deep burn, alkaline chemicals cause a colliquative necrosis but acidic burns induce coagulation necrosis. Worldwide burns represent over 11 million people requiring medical care and 180 000 fatalities per year[54,55]. Thermal injuries are the most frequent form of burn comprising 50% of flame burns in adults and 70% of scald burns in children[56]. In France it represents 500 000 victims[57] and 215 deaths/year. Among the 500 000 victims 8 000 need a hospitalization and 30% of them need a specialized burn care unit[57]. Children are the most impacted by severe burns accounting for 25%[58] with a predominance in children aged from 0-4 years. Domestic accidents account for 65-70% of burns requiring hospitalization while occupational accidents

account for 15-20%. Soldiers represent another high-risk population of burn injuries. According to historical data the American army estimated in 2000 that combat burns were higher in the navy (30%), Tank army (25%) and in the air force (25%). Studies also showed that during the Afghan conflicts from 2001 to 2011, 10% of medical evacuations concerned severe burns [59]. In addition combat related burns are also associated with other traumatic injuries in 50% of cases[59].

1.3.2. Classification

The management of burn is based on the Boyer classification. This later is divided into four degrees that can be visually determined. Any burn that does not penetrate the dermis is considered as a superficial burn with a dry and red wound and the barrier is still intact. It causes painful erythema but heal spontaneously after desquamation in 4 to 6 days. Second degree burn is divided into two classes. Superficial partial-thickness of the skin represents a damage of all the epidermis but a part of the dermis. The wound is red with blisters and is wet and painful. The partial thickness burn typically heals within 3 weeks with minimal scarring[60]. The deep partial thickness of the second degree burn corresponds to a damage of the entire epidermis and most part of the dermis. It appears yellow or white and is dry. The vessels and nerves are destroyed so there is a minimal pain. Healing occurs within 3 weeks with large scarring. A burn that completely destroys the dermis and enters the subcutaneous structures is considered to be a full-thickness burn. It appears black/brown and is leathery and dry. It heals with contractures and is longer than 8 weeks and so requires surgical intervention. It extends to muscle, bone or tendon and may require flaps or amputation.

1.3.3. Pathophysiology

Characterization

It exists several pathophysiological models for burn wound evaluation but the most commonly used is Jackson's model described in 1947. Briefly the first zone is the zone of coagulation which presents the maximum damage with reversible tissue loss due to coagulation of the proteins and tissue necrosis. This is surrounded by a zone of stasis, with inflammation and low perfusion[61]. This ischemic zone can progress and become necrotic within the first 48h following burn injury. Outside the zone of stasis is zone of hyperaemia where perfusion increases and tissue is recovered unless there is a sepsis or prolonged hypoperfusion.
Severe burn instantly causes inflammation and produces damage associated molecular patterns (DAMPs) which stimulates the immune system to recruit immune cells[62] as neutrophils. In turn the cells will trigger specific pathways as the immediate activation of nuclear factor κB (NF-κB) that is thought to regulate the induction of inflammatory mediators as tumor necrosis factor (TNF-α)[63] and intercellular adhesion molecule-1 (ICAM-1)[64]. In addition, TNF-α allow the secretion of other proinflammatory mediators as interleukins 1 and 6 (IL1, IL-6) and the apoptosis of various cells in the wound area. The production of proinflammatory mediators by macrophages as prostaglandin E2 are increased through the action of thermal injury. This

immune response can persist up to months and lead to health issues including systemic inflammatory response syndrome (SIRS). SIRS triggers the dilatation of the vascular plexus leading to its permeability and to infiltration of circulating monocytes and lymphocytes inducing fluid leakage.

Oxidative stress

Following burn there is a massive production of ROS which is harmful and involved in inflammation, systemic inflammatory response syndrome, immunosuppression, tissue damage and multiple organ failure[65]. It has been demonstrated that oxygen and nitrogen species (ROS, RNS) could protect the wound against infections,[66,67] however an increase in ROS secretion is also associated with immunosuppression, SIRS, sepsis, tissue damage and organ failure[67]. Thus, wound improvement depends on the balance between expression and elimination of free radicals. Importantly lipid peroxidation of cell membrane polyunsaturated fatty acids with free radicals induces the accumulation of cytotoxic products for example lipid-derived aldehydes (LDAs). Specifics LDAs as the hydroxynonenal[68] or malondialdehyde interact with cell functions (DNA synthesis, enzyme activities) inducing toxicity. Other studies suggest that proinflammatory cytokines (IL-6, TNF-α) or release chemokines lead to a continuous production of ROS conducing to severe cellular injuries[69,70] .

1.3.4. Gold standard treatments and limitations

Traumatic burn represents an exceptional event that requires support by specialized care units, hospitalization is needed for 20% TBSA in children and 30% TBSA in adults. These units include plastic surgeons, anaesthesiologists, nurses but also nutritionists, psychologists and re-educators who work together to ensure the management of the large-burned. Even if today the majority of patients are kept alive, therapeutic limitations remain and result in hospitalization of up to several months. In this section we will focus specifically on the treatment of severe burns and will deliberately avoid the treatment of minor burn (i.e. superficial and superficial partial-thickness).

Early management of large burns first aimed at reducing general hypovolemia and cardio-respiratory shock[71] using different filling techniques (i.e. Parkland method is the most widely used in the world consisting of infusing 4 ml /kg / %TBSA burned from Ringer Lactate to patients within the first 24 hours of hospitalization[72]). In order to limit the spread of burn and necrotic conversion of the stasis zone hydrogels as BurnShield™ or WaterJel™ can be applied to the wound. Nitrate baths may also be used to protect viable tissue from necrosis and to avoid local analgesia[73]. The loss of elasticity of the skin of the burned person can threaten the good oxygenation of the tissues for this purpose incisions can be made according to the strongest axes of tension (trunk, neck, legs). Hypothermia and hypermetabolism are two other consequences of severe burns. As a result, patients are often kept in structures heated to 33°C and provided with adequate nutrition to avoid excessive melting of lean mass; a hypermetabolic patient is estimated to require a daily protein intake of approximately 1.5 g/kg[74]. Finally, in order to avoid the diffusion of DAMPs, PAMPs and lipid toxins, escharrotomy is carried out as

soon as possible to reduce the inflammatory response and necrotic conversion. This practice helps to reduce the circulating levels of IL-6, IL-8, TNF-α and complement. It is accompanied by generalized antibiotic therapy to prevent infections until wound closure[75].

Severe burn is the cause of a phenomenon of inhibition of the spontaneous process of healing and therefore need surgery replacement. Depending on the extent and depth of the burn different options can be considered among autograft, allograft or combined graft. Expanded thin skin autograft remains the "gold standard" of treatment of traumatic burns of which the extent does not exceed 40% of the TBSA. Developed by James Tanner in 1964 this procedure consists in taking healthy skin with a dermatome, perforate it with a mesher and to cover the wounds with it. When the burns extend beyond 50% of TBSA, the donor sites become insufficient to carry out a traditional autograft of thin expanded skin and it is then necessary to use other techniques (Meek or pellet micrografts allow an expansion up to factor 6 or 9) and other processes (examples are shown in table 2). Although current autografts techniques are responsible for significant scarring, they ensure a very good grafting on large surfaces, are not expensive and are easy to set up by the surgeon. It is possible to obtain better aesthetic results by using thick skin grafts, but the donor sites scar harder. Usually these grafts are used in very specific cases, such as face and extremity reconstruction. When the lesions reach 60-70% of TBSA, the use of autografts becomes difficult due to the scarcity of donor sites. Alternative surgical techniques have therefore been developed to treat the serious cases. Currently, there are multiple skin substitutes available on the market, whether they are dermal, epidermal or total, in layer or in spray[76,77]. *In situ* bioprinting is also a new strategy that have already been used to treat experimental burn wounds. This technique appears to improve adhesion between layers, influence epidermal cell proliferation and migration and also to decrease scar formation[78].

Table 2: Tissue-engineered epidermal, dermal subsitutes and current surgical techniques for severe burns.

	Skin substitutes/ culture techniques	Structure	Reference
Epidermal	Cultured epithelial autograft (CEA) *CEA with microskin autograft* *CEA with meshed split thickness autograft* *CEA with split thickness allograft (CUONO's method)*	Confluent autologous keratinocytes	79
	Epicel® (Genzyme biosurgery)	Autologous keratinocytes sheets	80
	Cell Spray (ClinicPerthal Cell Culture)	Non-/cultured keratinocytes (subconfluent cell suspension)	81
Dermal	Laserskin or Vivoderm (Fidia Advanced Biopolymers Srl)	Autologous keratinocytes and fibroblasts, grown on microperforated hyaluronic acid membranes	82
	TransCyte (Smith and Nephew)	Allogeneic human newborn fibroblasts cultured on a nylon mesh (cells non viable at grafting)	83

	AlloDerm®	Allogeneic acellular human dermis (does not allow to cure a 70% burn)	84
	Dermagraft®	Fibroblast cells derived from newborn foreskin tissue seeded onto a biodegradable polyglactin mesh scaffold.	85
	Integra™	Porous matrix of cross-linked bovine type I tendon collagen, shark chondroitin-6-sulfate glycosaminoglycan and a semi-permeable polysiloxane. (does not allow to cure a 70% burn)	86
	Matriderm®	Native (non-cross-linked) collagen matrix supplemented by an elastin hydrolysate. (does not allow to cure a 70% burn)	87
Epidermal and dermal	OrCel™, Forticell Bioscience, Inc.	Collagen sponge with allogeneic fibroblasts and keratinocytes	88
	Apligraf® (Novartis)	Collagen gel with allogeneic fibroblasts and keratinocytes	89

Although the treatment of large burns has undergone a rapid evolution there are still major physical and psychological consequences that often limit the reintegration and quality of life of survivors. In particular, there is a psychological withdrawal of victims and a loss of interest in any social activity[90].

There remain three major therapeutic barriers to the treatment of large burns: (i) long-term deregulation of the patient's immunometabolic status, (ii) random grafting of skin substitutes and latency of scarring, (iii) the appearance of disfiguring and painful hypertrophic scarring. Whether self-healing or skin replacements, the surgical treatment of deep and extensive burns finally promotes the appearance of painful and disfiguring hypertrophic scars that can impact joint mobility and alter the suppleness of the skin. But beyond the hypertrophic scar, sensory dysfunctions experienced by transplant patients are responsible for a significant deterioration in quality of life, with the appearance of itching, paraesthesia, pain or local desensitization.

1.3.5. Burn models and perspectives

1.3.5.1. Experimental models

Despite important advances in burn care, the comprehensive study of burn pathophysiology is necessary for improvements of the current treatment strategies. Severe burns are still painful with psychological and physical consequences which limits the patient recovery. Experimental models have been established to address systemic, cellular, or molecular responses that occur in burn injuries.

In vitro and *in vivo* models are needed, they can respectively provide insights in immediate cell response and can be used for the development of new therapeutics and animal model enable to monitor systemic responses. Thus, animal studies comprise the majority of experimental burn models even if they imperfectly mimic human responses[91].Various models have been described for large and small animals and for humans, but over the last decade rodents, rabbits and pigs have prevailed[92].

Rodents are the most widely used in burn research because of their size, easy maintenance, fast breeding and their lower lab analysis cost. Despite the fact that they share several physiological and pathological features with humans (i.e. cardiovascular, endocrine systems) they have a different skin architecture shown in figure 7.

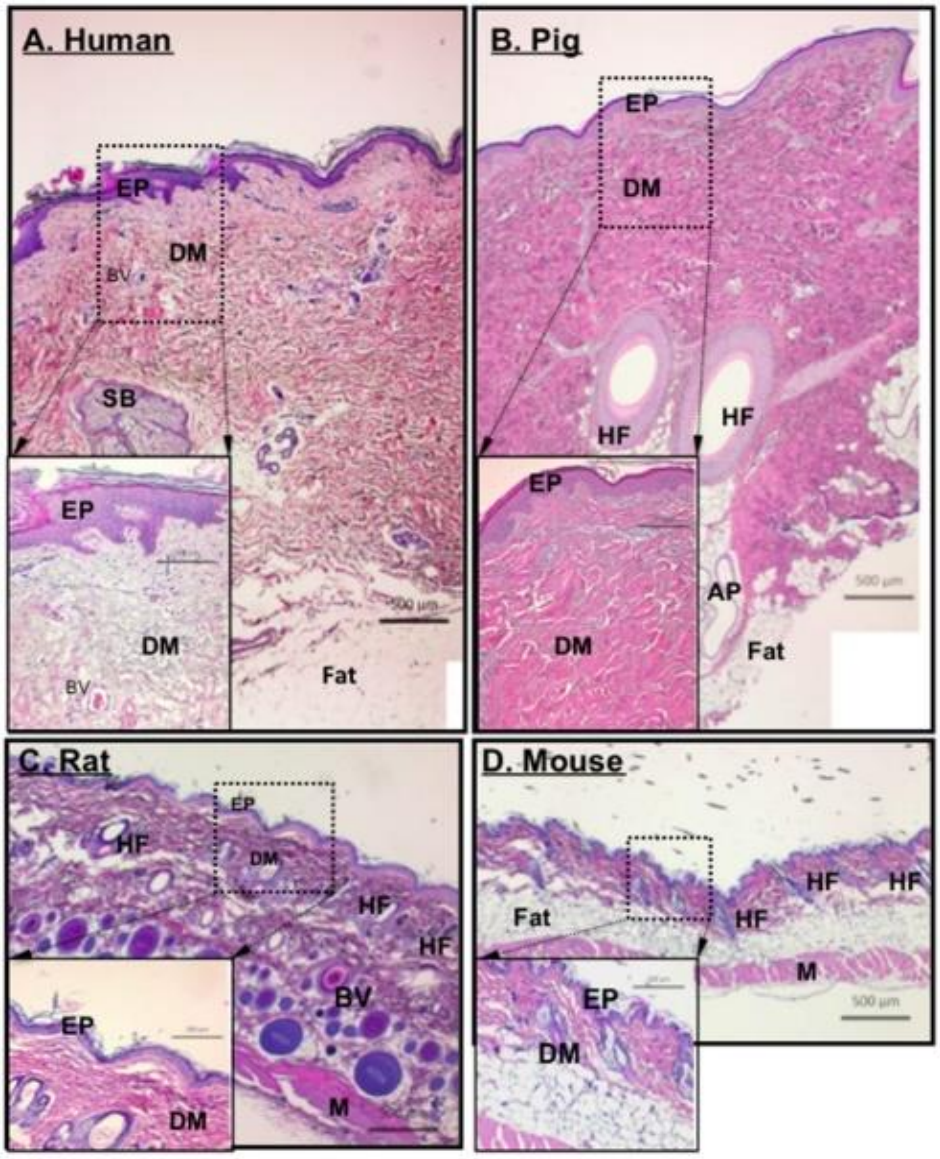

Figure 7: Comparison between human, pig, rat and mouse skin. Sections of paraffin embedded healthy skin from human, pig, rat and mouse with H&E staining. EP, epidermis; DM, dermis; BV, blood vessel; SB, sebaceous gland; HF, hair follicle; AP, apocrine gland; M, muscle. Scale 500 µm. Figure from O'Brien *et al.*, 2014[93].

Rodents have a lack of strong adherence to the underlying structures, a thinner epidermis and dermis and a denser hair coat with a distinct *panniculus carnosus* muscular layer absent in humans[94]. Rodent cutaneous injuries heal mainly through wound contraction instead of healing via re-epithelialization and granulation as in human. Finally, they also present a stronger immune system[95] and so, are less prone to develop sepsis and immunosuppression[96] Table 3. This particular difference may result in important variations in cytokine and chemokine expression. For clinical transposition rodents poorly mimic human process. Larger animals as rabbits and pigs can be used but it is less common due to their high cost and experimental duration even if they share more anatomical and physiological similarities with humans. Commonly, the choice of animals for burn model is mainly based on cost and ethic arguments and further on which species will give the best correlation to human trials.

Table 3: Advantages and limits of *in vivo* burn wound models.

Model	Advantages	Limitations
Rodent	Small size, easy handling, lower cost and morbidity, shorter healing time, physiological similarities as endocrine-musculoskeletal or cardiovascular systems Transgenic knock-in/ knockout mice	Superior immune system, different cytokine profile, differences in skin structures, wound healing by contraction, no hypertrophic scar
Rabbit	Easy handling, similar metabolic and pathological alterations as burn patients, commonly used to study systemic effects of burns	High risk of infection, specific precautions during handling than rodents (more care and sterilized conditions) 10 times more expensive than rodents
Pigs	Anatomical and physiological similarities with humans, the blood vessels distribution or the renewal time of epidermis are close to human, similar cytokines expression	High expense of housing and care, complicated procedure of anaesthesia and analgesia, post-operative care, high risk of sepsis and morbidity

1.3.5.2. 3D human models

As previously mentioned biological questions are traditionally investigated either with animal models or with two –dimensional surfaces. The 2D cultures can use human cells but are non-physiological regarding biophysical properties or cellular organization and animal models are challenging to implement and monitor with human relevance. Thus the biofabrication field has developed cellular constructs that mimic biological processes. These systems incorporate living cells and other biochemical components and are configured into a specific structure used for translational applications such as tissue repair and drug screening[97] illustrated in figure 8.

Within biofabrication there are several enabling technologies and one is bioprinting. The most common and accessible technique is the extrusion bioprinting where the pressure-driven extrusion of a bioink from a printer nozzle is used to print filaments with a user pre-defined design.

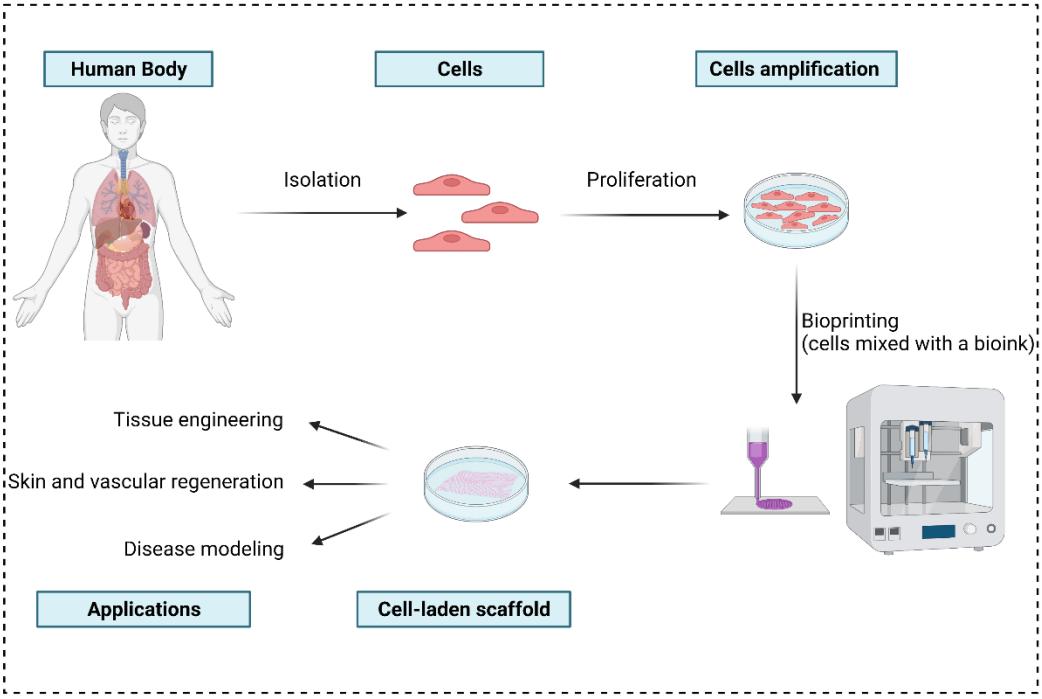

Figure 8: Schematic process of human primary cells extraction for 3D bioprinting. Human cells are isolated, amplified, mixed with a bioink and printed according to a specific scaffold for multiple applications. *This illustration was made using biorender.com.*

This technique allows to study for example biochemical gradients in an angiogenesis context, biophysical morphogenesis or disease models for cancer or fibrosis. Other techniques exist to create such models as lithography or spheroid bioprinting but depend on the biological question. Bioprinting is an advanced technique with a bright future accompanying numerous challenges and problems. It has shown great potential in tissue engineering at its early research stage where many *in vitro* and *in vivo* experiments shown the feasibility. Artificial skin substitutes are bioactive dressings, they cover the wound but also facilitate its function and accelerate healing. This type of skin should have the ability to supply oxygen to the wound bed, maintain moisture, accelerate skin regeneration and may have a protective function against infections[98,99]. Even if it is a promising technology for tissue engineering bioprinting remains an emerging and growing technology with a great potential that cannot replace the actual models but can help the burn wound healing understanding and improving.

1.3.5.3. Perspective for burn treatment

Despite significant progress in burn wound healing urgent need to prevent hypertrophic scarring, blistering or to improve engraftment are needed. The vacuum therapy is an efficient

technique that use pressure below atmospheric pressure. During this kind of therapy, the cells are mechanically stretched which favour the proliferation, increases local blood flow, granulation and epithelization. Encouraging results are also obtained with skin substitutes even if they contain only two cell types (keratinocytes and fibroblasts) which limit the comparison with usual skin autograft. The use of bone marrow-derived stem cells or adipose-derived stem cells (ADSCs) in acute burn is also of interest[100]. ADSCs that are present in the hypodermis can also differentiate in fibroblasts and favour the regeneration of the tissue. Adult mesenchymal stem cells (MSCs) are also delivered to the wound and may help to achieve accelerated healing, and significantly reduced scarring[101]. Their action is associated with a paracrine function and the release of many growth factors , cytokines or extracellular vesicle that are crucial to promote angiogenesis, cells migration and proliferation and importantly for the regulation of the inflammatory phase during healing[102]. Thus, MSCs-based therapy has emerged as a strategy to improve cutaneous wound healing[103]. The importance of the cell-based therapy in support of the graft has been demonstrated for burn wound even if there are still scientific and technical issues that should be solved.
Another challenged for therapeutic management of severe burns is the fight against infections. New bactericidal and antifungal treatment are under research to overcome drug multiresistance and to limit the adverse effect of antibiotics on reepithelialisation.

2. Burn wound infections

2.1. Infected burn wounds

Burn patients faced a myriad of risk factors for infections after thermal injuries. Indeed, sepsis and others invasive infections continue to be the primary reason for death and morbidity after the first 24 h with it being responsible for 51% of the deaths[104,105]. This state induces the rapid death of the patient after the 2 first weeks of admission. In patients with burns of more than 40% TBSA it has been estimated that 75% of mortality is related to infections[106],[107] rather than burn shock and hypovolemia[108]. In order to identify effective treatments to prevent and detect burn wound infection it is crucial to have knowledge about the burn wound colonization. Furthermore, the type and quantity of microorganisms that colonize the wound have an influence on the risk of invasive infections.

2.1.1. Burn wound colonization

After the burn, the wound is initially sterile due to the destruction of the skin flora by the thermal insult. The endogenous flora that was not impacted can invade the wound but the primary mode of colonization remains the environment and the patient's gut or nasopharyngeal tract. As such the nutrient-rich environment and reduced blood supply induce the multiplication of a single bacterium into 10 million bacteria within 24 h to colonize the entire wound bed.
Typically burn wound is initially colonized with Gram-positive bacteria and then antibiotic-susceptible Gram-negative bacteria continue the invasion within a week of the burn injury

(figure 9). The Gram negative bacteria have long been known to cause serious infections in burn patients and are associated with a 50% increase in predicted mortality for patients suffering from bacteraemia compared with those without bacteraemia[109]. If the wound is large and take time to recover and close, and if the patient is colonized and requires treatment with antibiotics other microorganisms as yeasts, fungi and antibiotic-resistant bacteria can be added to bacteria previously mentioned. However, those last few decade antibiotic-resistant bacteria can appear at any time due to their widespread in the environment and that they are responsible not only for nosocomial infections but also for community-acquired infections. Bacteria of major concern include methicillin-resistant *Staphylococcus aureus*, *Streptococcus sp.*, *Escherichia coli*, *Pseudomonas aeruginosa* and *Enterococci sp.* In the military burn center at the Brooke Army Medical Center in Texas researchers have reported that infections were due to *P. aeruginosa* in 15% of the cases, *Acinetobacter spp.* in 53% of the cases and *S. aureus* in 34% of infected burn patients[110]. Those results confirm the fact that the organisms commonly recovered from infected patients in the burn unit are members of the ESKAPE group (*Enterococcus faecium*, *Staphylococcus aureus*, *Klebsiella pneumoniae*, *Acinetobacter baumannii*, Pseudomonas *aeruginosa*, and *Enterobacter* species). This group is the acronym of the pathogens for which it is now crucial to find an innovative therapy because they exhibit multidrug resistance, an arsenal of virulence factors and often counteract the immune system[111].

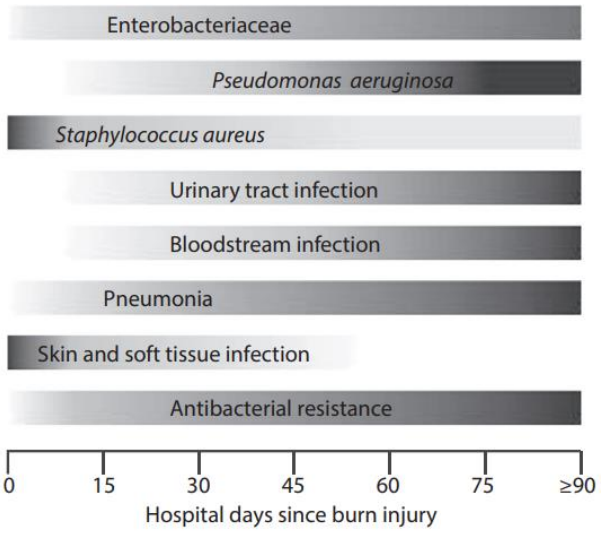

Figure 9: Timeline of common pathogens infections after burn injury. Skin and soft tissue infections occur within the first week of hospitalization with the appearance of *S. aureus*. With a median onset >30 other infections as pneumonia, urinary or bloodstream infections with colonization by *Enterobacteriaceae*, *Pseudomonas aeruginosa* and multidrug resistant bacteria. Figure from Zhou et *al.*, 2019[112].

Other pathogens as yeast and fungi increase in frequency due to the use of topical and systemic antimicrobials. *Candida albicans* is the most common fungus found and is the fourth most common infection in burn wounds[112] from endogenous sources[113]. A majority of fungal infections is due to *C. albicans* but other organisms as *Aspergillus*, *Fusarium*, *Mucor* may also appear.

Viral infections are not common in burn wounds but a reactivation of dormant viruses is possible. The persistent metabolic and inflammatory changes associated with poor wound healing results in immunocompromise states increasing patient susceptibility to viral infections. Herpes simplex and varicella zoster have the highest occurrence in viral burn infections[114] and necessitate a minimum of 10 days of treatment composed of a combination of oral and topical medication.

2.1.2. Diagnosis

The diagnosis of burn wound infection is difficult. Symptoms as pain, fever, hypotension, tachycardia are common after burn trauma and result from the complex cytokine and immune responses. An invasive burn wound infection is characterized by change in colour, exudative drainage, and odor from the wound. An example of invasive burn infection is the Ecthyma gangrenosum caused by *Pseudomonas aeruginosa*. It presents with blue-purple "punched-out" lesions and often causes local thrombosis of the blood vessels. Even if the patient is promptly taken care of, it can progress rapidly to systemic sepsis, shock and possibly death. In 2007 the American Burn Association (ABA) consensus conference met in order to standardize the definitions of infections and sepsis in burn patients. Thus, they defined an invasive burn wound infection as a wound containing greater than 10^5 pathogens per gram of tissue[107]. Some experts recommend to perform routine infection surveillance using swab cultures for excised burns and area of skin too thin to biopsy and biopsy for tissue eschar even if it may not be representative of all pathogens involved. The diagnosis is usually based on clinical examination and quantitative culture but can be confirmed by tissue biopsy for histological analysis that are the gold standard but are not always performed due to labor and costs. Bacterial blood culture is another important aspect for the detection and diagnosis of burn sepsis, however blood culture may take 3 days and even more to produce results and lead to a potential increase in antibiotic resistance. Recent studies have demonstrated that serum procalcitonin (PCT) has an important role in sepsis[115]. This non-hormone active glycoprotein has a concentration lower than 0.1ng/ml in healthy people but the level increases rapidly (in 6-8 h) in patients with systemic bacterial infection and reach a peak at about 24 h. In combination with other indicators this technique may show promising results for invasive infection detection. A systemic antibiotic therapy is often insufficient to control the infections especially if it involves full-thickness burn eschar. Only an excision at the time of diagnosis is an efficient way to proceed.
The compromised local and immune response lead to an increase susceptibility to infections (bacteria, yeast, fungal and viral) and increase virulence from specific pathogenic organisms leading to the development of organ failure. In America over the past decades the most frequent complications faced in burn centers were pneumonia (3.5%), cellulitis (3%) and urinary tract infection[114].

2.1.3. Treatment of burn wound infections

The development of new bactericidal and fungicide formulations (local or systemic) is the subject of intensive research for the treatment of severe burns. The challenges in this area are

twofold: to be both effective against multi-resistant microorganisms, and not to be unfavourable to the process of re-epithelialization. The use of antibiotics is generally carried out, although their effects are often deleterious to the process of re-epithelialization[116].

In the 1940's topical application of antimicrobial agents began with sulfathiazole dressings. Then in 1968 with the discovery of the antimicrobial properties of silver, the silver sulfadiazine dressings became the gold standard treatment[117]. However, recent studies report little effectiveness in preventing wound infection compared to alternate dressings[118] and induce poor eschar penetration and cytotoxicity of silver to keratinocytes and fibroblasts impairing wound healing[118,119]. In addition, Finley *et al.,* 2015[120] report resistance to silver in clinical isolates. New innovative approaches are actively investigated and which generally involve new methods of delivering well-established antibiotics, alternative antimicrobials as synthetic antimicrobial agents as LLKKK18[121].

The wound and full-thickness eschar are poorly perfused, therefore systemic antibiotics have difficulties reaching the tissue and lead to the selection of resistant organisms colonizing the wound[96]. Drug resistant organisms pose a difficult challenge especially MRSA which is the most common resistant organism encountered in burns[122] and will be discussed in the section II b. Gram negative bacteria also present resistance to antibiotics and has seen increasing reliance on the use of old antibiotics. First colistin (polymyxin antiobiotic) was abandoned due to important side effects as neurotoxicity but has been recently re-engineer and redevelop (enhancement of permeability and retention effect) to fight against MDR Gram negative bacteria[123].
In addition to the complexity of treatment of **resistant** bacteria there is also the **persistent** bacteria. Resistant bacteria are defined as the resistance of a heterogeneous population to antibiotics. Antibiotic resistance is identifiable with standard assay and the threat that they impose has been well recognized. However, bacteria surviving antibiotic exposure despite fully susceptible, called antibiotic persistence, is largely underestimated. Persistence is defined as the ability of a bacterial subpopulation to survive to high bactericidal concentrations to which the bacteria are fully susceptible[124]. On the opposite to antibiotic resistance, antibiotic persistence is difficult to measure and therefore can lead to treatment failure. One of the main characteristic of antibiotic persistence is a biphasic killing with a rapid elimination of the susceptible population and a slower elimination of the persiter population requiring longer or higher exposure to antibiotics.

Biofilms are also a limiting factor in combating bacterial wound infection. A biofilm is a complex structure composed of a self-produced biopolymer matrix containing polysaccharides, proteins and DNA originating from the microbes. They are responsible for chronic infections due to the increase tolerance to antibiotics and disinfectant. They can also resist to phagocytosis and other components of the body's defence system. Bacteria can be sensitive to antibiotics, but due to biofilms, antibiotics (topical and systemic) have difficult time reaching encapsulated bacteria. Hence, higher up to 1000 times concentration of antibiotics must be used to see an effect.

Thus, in order to increase antibiotics effects there is a need to improve drug delivery. Full-thickness burn patients have altered physiology which impair antibiotic tissue concentrations conducing to therapeutic failure and to the emergence of resistance. Indeed, physiological changes include fluid balance deregulation, hyperdynamic circulation and organ dysfunctions[125]. New methods with regular monitoring of antibiotics are used and studies demonstrated that delivery of antibiotics through continuous infusion has better effect than in bolus[126].

2.2. *S. aureus* burn wound infections

2.2.1. Epidemiology

Staphylococcus aureus remains one of the most common pathogens isolated from burn patients[127] and is one of the most frequent causes of nosocomial and community-acquired pneumonia, skin and soft-tissue infections or bloodstream infections[128]. This bacteria can lead to severe illness as sepsis or even death through the production of virulence factors (proteinases, collagenases, toxins) promoting tissue invasion[129]. A contributing factor to the high mortality rate of *S. aureus* is increasing antimicrobial resistance. Methicillin-resistant *S. aureus* represents a major burden on health care with studies demonstrated mortality rate greater than 60% and associated with a 2-fold increase in mortality compared to methicillin sensitive *S. aureus* strains[130,131]. According to the Center for Disease Control and Prevention MRSA lead to 323 700 cases and result in 10 600 deaths in 2017 in the United States[132]. On the military medical service MRSA represent a menace for decades. Transmission of MRSA in military settings is elevated in confined spaces as for example on board of seagoing warships. In the US army a study demonstrated a prevalence of 3.5% of MRSA colonization onboard and 49.5% soldiers were colonized with MSSA highlighting the threat posed by *S. aureus*.

2.2.2. Antibiotic resistance and treatments

In the 1940s penicillin resistant strains were detected, they produce penicillinase which cleaves the β-lactam ring of the drug. Two years after the introduction of methicillin to fight against penicillin resistance a methicillin resistant *S. aureus* strain was isolated in Great Britain[133]. The evolution of MRSA is due to the acquisition of the *mecA* gene. This gene codes for a transpeptidase which binds additional penicillin (PBP2a) and reduced affinity to β-lactams and so reducing the efficiency of those antibiotics. This gene gives notably a resistance to methicillin and oxacillin[134]. Despite the fact that methicillin is no longer used the term is still largely used worldwide. In some countries, especially in South America and Japan, more than 50% of *S. aureus* strains are methicillin-resistant, posing a real therapeutic challenge[135]. Thanks to its adaptability this pathogen has the ability to develop resistances to almost all classes of antibiotics, including vancomycin, usually last option against MRSA[136]. Thus, the World Health Organization considered in 2017 *S. aureus* as a high priority in the list of pathogenic bacteria for which there is a crucial need to develop new antibiotics[137].

In most cases of MRSA bacteremia, vancomycin or daptomycin is the recommended treatment[138]. Vancomycin is a glycopeptide that interferes with cross-linking peptidoglycan by binding to the D-alanine-D-alanine ends of the pentapeptides of the cell wall, this molecule is currently the first-line of antibiotic for MRSA bacteremia. Although it is the gold standard treatment it has relatively slow onset of bactericidal activity and doesn't have a good penetration of some tissues[139]. In addition, resistant strains to vancomycin are also beginning to emerge with a modification of D-alanine-D-alanine to D-alanine-D-lactate residues for example, which prevents the binding of vancomycin. US guidelines recommend to use a fixed dose while European guidelines advise to use a dose of vancomycin based on the true plasma concentration. Unfortunately, antibiotic dosage in severe burn is limited by their hyperdynamic state which increases renal clearance of commonly administrated antibiotics[140,141].
Given the limitations of currently approved treatments other therapeutics are being developed. Researchers try to develop vaccines that target one or more *S. aureus* antigens but for the moment the studies have had a minimal success to date[142]. One of the problem of developing such vaccines is probably due to the fact that populations are colonized from birth permanently or transiently, making the action of a vaccine innefficacious because *S. aureus* has a good interaction with humans. Many other studies have evaluated the alternative antimicrobials as ceftaroline, linezolid and quinupristin/dalfopristin but none have been approved yet for the treatment of MRSA bacteremia[138].
As mentioned in the WHO report is a priority for new therapeutics. This is all the more important as the development of new antibiotics by the industry is currently essentially focused on improvement of existing classes of compounds, against which resistances develop very rapidly[143].

3. Key role of macrophages in infected skin wound healing

In all types of injuries macrophages are key cells dampening inflammation to clear the wound bed from potential pathogens and coordinating the tissue repair process. Macrophages are extremely heterogenous and plastic cells. As the wound heals macrophages will follow transitions that are described in a simple way from pro-inflammatory phenotype traditionally referred to as "M1" macrophages to a phenotype that promotes anti-inflammatory effects collectively referred to as "M2" macrophages. Within the wound the complexity of macrophages function is increasingly recognized with adverse effects when they are inappropriately activated. Macrophages subsets, plasticity and their specific effector molecules in wound healing make them cells of choice for the study of new therapeutic tools especially for infections studies.

3.1. Vacuole maturation process during phagocytosis

The key role of macrophages is the elimination of debris or bacteria. In order to have an efficient elimination macrophage must phagocytose the invading bacteria as illustrated in figure 10.

Once the receptors are activated important changes in the membrane remodeling and actin cytoskeleton are triggered. Those specificities, leading to the formation of pseudopods, allow the internalization of the target element inside a membranous organelle called phagosome: the engulfment of the particle begins.

Early phagosome

The nascent phagosome, within 30 min of sealing, becomes a little acidic but not sufficiently to be destructive (pH 6.1-6.5). The pH changes through the different stage of maturation of the phagosome is a very controlled process necessary to allow the activity of the different hydrolases[144]. The low pH allows the disruption of the normal metabolism of most of bacteria and fungi and prevent the use of several essential nutrients[145].
The maturation of the phagosome is modulated by appearance and disappearance of specific membrane proteins. It gains properties of sorting endosomes as revealed by the acquisition of Rab5 and EEA1 (early endosome antigen 1) which promote the fusion of the new phagosome with early endosomes[146]. EEA1 functions as a bridge that links early endosomes to incoming endocytic vesicles and binds to a SNARE (soluble NSF-attachment protein receptor) required for membrane fusion. Rab5 allows also the recruitment of proteins involved in the phagosome maturation including Rab7, an important marker of the late endosome. A small amount of vacuolar ATPase (V-ATPase) is acquired as an important factor for the decrease of the luminal pH. This multimeric protein complex translocates protons (H^+) into the lumen of the phagosome using cytosolic ATP as energy[147]. The maturation is a dynamic process, the addition and removal of material is accomplished by fusion and fission of vesicle and the exchange of material that potentially occurs through the "kiss-and-run" process[148]. This last highlights the fact that endosome and lysosome interact transiently with the phagosome allowing selective exchange by pore fusion.

Late phagosome

After the elimination of proteins that will be recycled or degraded the early phagosome is evolving in late phagosome (between 15-45 min after phagosome sealing). This stage is characterized by the loss of Rab5 and the accumulation of Rab7 and by an acidification of the lumen (pH 5.5-6.0). Rab7 recruits new proteins such as Rab-interacting lysosomal protein (RILP) binding to the dynein-dynactin complex in order to mediate the centripetal movement of late phagosome and lysosomes[149] for the final maturation. New characteristic proteins are also recruited such as lysosomal-associated membrane proteins (LAMPs) that accumulate in the lysosomal membrane. It has been demonstrated that phagosome from LAMP-deficient cells fail to acquire Rab7 and do not fuse with lysosome; this shows the importance of LAMPs family in membrane fusion regulation and so, for maturation.

Maturation into phagolysosome

The maturation culminates with the formation of the phagolysosome around 40 to 60 min after the ingestion which consists in the fusion of the phagosome with the lysosome. Lysosomes

bring various hydrolases (e.g. lysozyme), phospholipase A_2, a ribonuclease and a desoxiribonuclease and also proteases. These enzymes activity is increased by the pronounced acidity of the vacuole, pH 4.5-5.0, resulting from the large V-ATPases present on their membrane.

Apart from the arsenal of antimicrobial agents including antimicrobial proteins, peptides and enzymes, there are also specialized molecules that allow an oxidative attack known as the "oxidative burst".

The oxidative burst done by macrophages, dendritic cells and neutrophils uses oxygenated radicals (ROS: *Reactive Oxygen Species*) and nitrogen radicals (RNS: *Reactive Nitrogen Species*) that are toxic and will damage intracellular components.

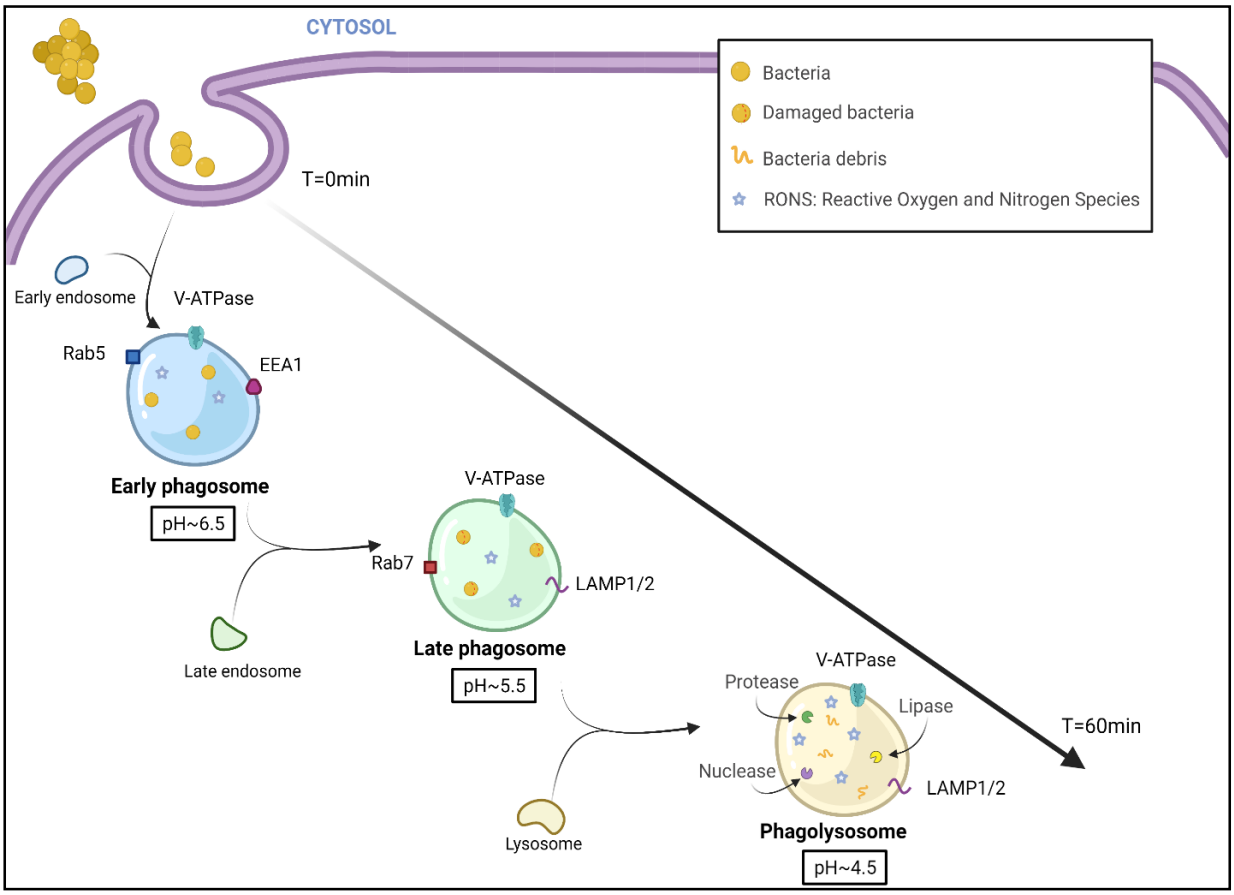

Figure 10: Internalisation of *S. aureus* by professional phagocytes via phagocytosis and phagolysosome maturation. Bacteria are recognized by macrophage and then internalized into a phagosome. The phagosome matures into early phagosome, late phagosome and phagolysosome with the acquisition of specific markers as EEA1, LAMP1/2, or Rab5-7. Through the maturation the pH of the phagosome goes from pH 6.5 to 4.5. The pH modification triggers the activation of specific enzymes as proteases, lipases or nucleases that participate to bacterial elimination. *This illustration was made using biorender.com.*

The generation of reactive nitrogen species requires transcriptional activation of the gene encoding the enzyme inducible Nitric Oxide Synthase (iNOS). The activation of the enzyme leads to the oxidation of L-arginine to give L-citrulline and nitric oxide (NO, a highly effective

antimicrobial agent). When NO is combined with superoxide (O_2^-) produced by another complex, NADPH oxidase (detailed in part 3.2), this lead to the production of peroxinitrite ($ONOO^-$) and toxic S-nitrosothiols.
The ROS and RNS are able to induce oxidation, hydroxylation, chlorination, destruction of iron-sulphur groups in proteins leading to the alteration of microbial molecules. For example, ROS and RNS can oxidize cysteine sulfhydryl present in active sites of many enzymes making them inactive. Those reactive species can also diffuse outside of neutrophils and macrophages and kill extracellular pathogen. In addition, they are important molecules for cell physiology and signalling with an oxidizing role on proteins, lipids and DNA. Long lived species as H_2O_2, can go from one compartment to another but also from one cell to another while other reactive species with a short lifespan cannot (O_3, HOONO).

3.2. NADPH oxidase

The main producers of ROS in many cells are the NOX family of NADPH oxidases also called DUOX (in the presence of peroxidase-like extracellular N-terminal domain). This family of enzymes is widely expressed in eukaryotes cells and is able to reduce molecular oxygen (O_2) to deleterious molecules for pathogens such as superoxide (O_2^-) and, in certain conditions, to hydrogen peroxide (H_2O_2) and hypochlorous acid (HOCL).
NOX/DUOX family and their ROS production have been involved in several functions ranging from host defense to cellular signaling and the regulation of gene expression and are also implicated in tissue repair through the induction of angiogenesis and cell proliferation.
Since the 2000s, seven isoforms of the catalytic core of the NADPH oxidase have been identified in different tissues: NOX1-NOX5 and DUOX1-DUOX2[150] (figure 11).

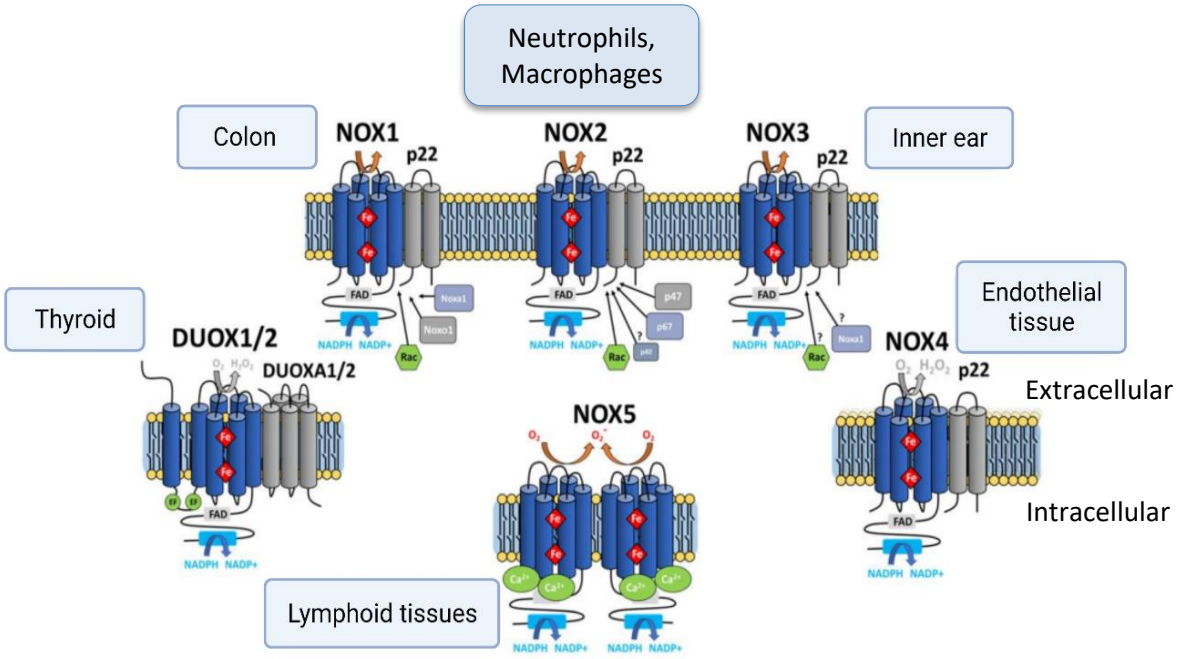

Figure 11: Representation of the NADPH oxidase isoform and their main locations. NOX isoforms have similar structure and enzymatic function but the activation process differs. NOX1 and NOX2 activation needs the phosphorylation of NOXO1 and p47^{phox} respectively and the translocation of multidomain complex as p40^{phox}, p67^{phox} and Rac from the cytosol. As NOX1 and NOX2, NOX3 is p22^{phox}-dependent but its binding to Rac is still unknown. NOX4 is constitutively active. In contrast NOX5, DUOX1 and DUOX2 are calcium-dependent. Activation of these complex induce a reduction of NADPH and a transfer of electrons. NOX1, 2, 3 and 5 are mainly producers of superoxide and NOX4 hydrogen peroxide whereas DUOX1 and 2 produce both. *Adapted from Vermot et al., 2021*[151].

NOX2, the isoform mostly expressed in phagocytes, has been the first to be described and will be of interest in our work. Due to its high level of expression in neutrophils and macrophages NOX2 is commonly referred to as "phagocyte NADPH oxidase". Nonetheless it is important to notice that it is also found in other cells such as in cardiomyocytes, epithelial cells and different types of stem cells.

3.2.1. Structure

The functional NADPH oxidase is composed of six subunits. The transmembrane part of the complex is composed of gp91^{phox} (also known as NOX2) which represents the catalytic core of the enzyme and is directly involved in the electron transport. It is a highly glycosylated protein with a molecular weight of 91 kDa. The second part is p22^{phox}, it has a role in the maturation and the complete stabilization of NOX2 and binds to the stabilizer subunit p47^{phox}.
In order to form an active enzymatic complex cytosolic subunits are needed in particular p47^{phox}, p67^{phox} and p40 ^{phox}. The p47 ^{phox} subunit plays an organizing role, p67^{phox} participates to NOX2 activation (direct interactions) and for p40 ^{phox} its function is less evident and need to be clarified. The activation of the NOX2 complex requires small G proteins, Rac GTPase.

Under the regulation of Guanosine Exchange Factor (GEF) the GTPase alternates between the GDP-bound inactive conformation and the GTP-bound active conformation. In mammals Rac exists in three isoforms Rac1, Rac2 and Rac3[151]. Among phagocytes Rac2 isoform is contained in human neutrophils[152] whereas monocytes and macrophages express both Rac1 and Rac2[153]. During the inactivation state Rac is sequestered into the cytosol by association with the RhoGDI inhibitor protein and under activation there is a dissociation of this complex allowing Rac to insert within the plasma membrane and to interact with $p67^{phox}$, NOX2 ($gp91^{phox}$)[154].

3.2.2. Activation of NADPH oxidase, NOX2

Before NOX2 activation external activators as LPS (lipopolysaccharide) or TNFα (tumor necrosis factor) will induce the "priming" of the enzyme. This results in a pre-activation that will allow a secondary stimulus leading to a faster and enhanced response for bacterial killing. Upon phagocytosis the priming induces phosphorylation of p47 which triggers migration of the complex of cytosolic subunits to the phagosome membrane. There, it associates with the membrane subunits to form the active NOX2 complex as illustrated in figure 12. The cytosolic NADPH is oxidized and electrons are transferred across the membrane to molecular oxygen that are present in the phagosome leading to the production of superoxide anion. Then, this molecule rapidly dismutates to H_2O_2 through the action of superoxide dismutase and rapidly form hypochlorite through myeloperoxidase and chloride anion action.
Multiple signaling cascades are triggered at the onset of phagocytosis, the protein kinase c (PKC) as well as ERK and p38 MAPK phosphorylate all NADPH oxidase subunits for its activation. NOX2 active form is formed even before the phagosome is fully closed, that is less than 1 min. When the complex formation is activated by FcR and complement receptors ROS production goes on for at least 30 min. It has been estimated that macrophages produce 50 µM of O_2^- and 1 to 4 µM of H_2O_2 [155]. This estimation assumes a homogeneity among the phagosome and should be more accurate for *in vitro* measurements, those concentrations were determined using a computer to model the approximate speed of O_2^- by NOX2, the volume of the phagosome, the spontaneous dismutation of H_2O_2 and its diffusion across the phagosome membrane into the cytoplasm[155,156].

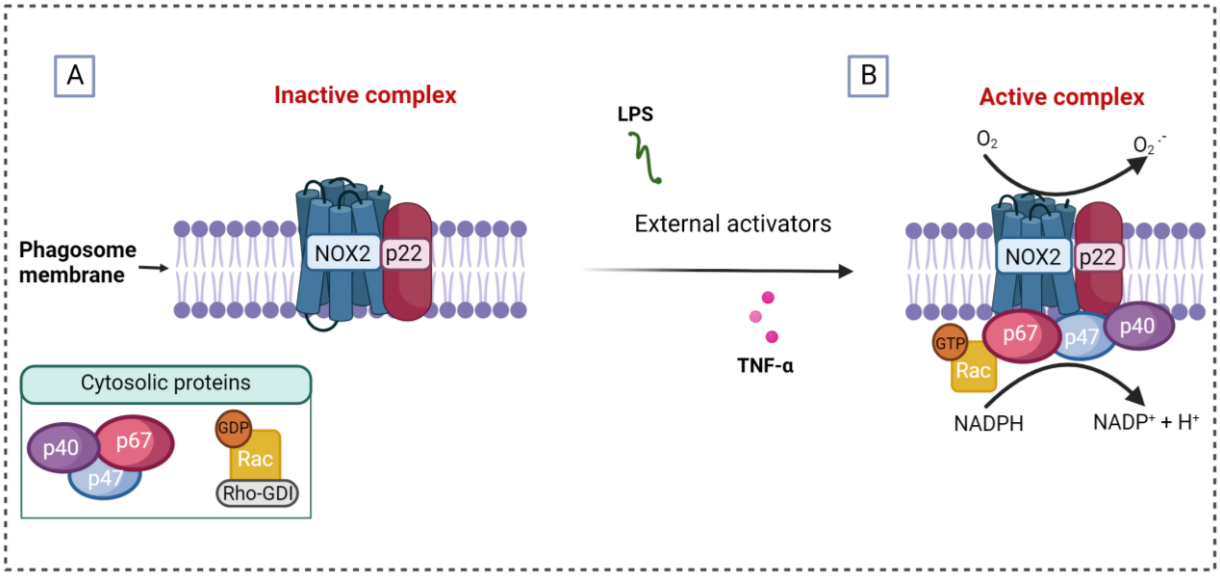

Figure 12: Activation of the NADPH oxidase NOX2 complex.

(A)Membrane subunits (NOX2, $p22^{phox}$) and cytosolic subunits ($p40^{phox}$, $p67^{phox}$, $p47^{phox}$, Rac) of NOX2 enzyme are dissociated making the enzyme inactive.
(B)Under stimuli as LPS or TNF-α the cytosolic protein associate to the one of the phagosome membrane to form the active form of the enzyme. The association lead to the reduction of NADPH into $NADP^+$, H^+ and the formation of superoxide ($O_2^{\cdot-}$). *This illustration was made using biorender.com.*

3.2.3. Functional role

This enzyme is highly expressed in neutrophils and macrophages and is referred to as "phagocyte NADPH oxidase". It can also be found in other cells such as skeletal muscle cells[157], stem cells[158] or endothelial cells[159] but at a lower level. As an enzyme specialized in ROS production NOX2 is involved in a wide range of physiological process and thus has a pleiotropic role.
The importance of NADPH oxidase and its products in pathogen elimination is illustrated by the chronic granulomatous disease (CGD). CGD was firstly described by Johnston RB Jr *et al.*, in *The American Journal of Diseases of Children* (1967), by Baehner and Nathan in *Science* (1967) and by Baehner, R. L. Karnovsky, M.L. in *Science* (1968). However, since 1968, other gene mutations in the NOX2 complex have been identified in humans as a causative factor for CGD. The patients are hypersensitive to fungal and bacterial infections. This hypersensitivity is the result of a failure in the ability of NADPH oxidase subunits to produce oxidizing species. NOX2 complex has a critical role in host defense and it is also the case in murine models. Human but also mice with a mutation in any of the five structural subunits of the NADPH oxidase present a defective production of ROS which lead to chronic infections.
ROS play a key role in immune response but also as messenger in different cellular pathway (cell growth and survival, apoptosis, proliferation and differentiation). In the immune system ROS can act in two different ways against pathogens:

- Direct action: a high level of ROS is cytotoxic due to the damage that are induced on DNA, proteins and lipids[160]. The nucleotides are oxidized which lead to DNA-protein cross-linking and strand rupture[161] but the bacterial death can also be due to the disruption of the iron-sulfur clusters by the impact of ROS on the enzymatic activity[162].
- Indirect action: ROS are able to modify the phagocyte intracellular signaling because the reactive species produced by NOX2 are involved in many immune and inflammatory responses: regulation of the phagosomal pH[163], NETosis, cytokine release or antibacterial autophagy[164].

Interestingly mice deficient in proteases are capable of producing ROS and present the same type recurrent infections that people lacking in NADPH oxidase[165]. The alternative to this hypothesis is that the pH change and the concentration of ions resulting from the NADPH oxidase are mostly implicated in the bactericidal activity. Indeed, the NADPH oxidase produces O_2^- that consume the protons of the phagosomes in order to produce H_2O_2 and lead to the alkalinisation of the pH which stimulates the activation of the proteases (i.e. elastase, cathepsin G) and so, to an indirect action of ROS[166].
However, there are limitations to the inflammatory response. An imbalance in ROS level or in cellular antioxidant capacity can result in an oxidative stress. Clear evidence showed that ROS produced by enzyme as MPO or NOX family may induce tissue injury through a direct or indirect ROS mediated damage of proteins, lipids, nucleic acids leading to chronic inflammation and to neurodegenerative, cardiovascular and metabolic diseases[167,168].

3.3. Macrophage interactions with *S. aureus*

3.3.1. Defense arsenal of *S. aureus*

S. aureus is a Gram positive bacteria aerobic-anaerobic optional allowing it to have a great ability to adapt in various environments and organisms. About a third of the population is colonized permanently and asymptomatically at the mucosa of the anterior pits of the nose. This bacterium is also part of the skin microbiota (hand, armpits, perineum), rectum and vagina[169]. Before the appearance of antibiotics *S. aureus* bacteremia were fatal in 80% of cases[170] but currently the statistics decreased and the percentages of people who die from *S. aureus* infection are between 15-50%[171]. Deaths from nosocomial diseases are mainly due to *S. aureus* bacteremia, but this bacterium is also responsible for a large number of community-acquired infections. *S. aureus* is capable of inducing a wide variety of pathologies as pulmonary infections, meningitis, skin and soft tissue infections or even bone infections. Such a panel shows that the bacterium is particularly well equipped to counter the host's immune response and adapt to the different hostile environments it will encounter during infection[172].
S. aureus is well equipped to adhere to surface, invade or avoid the immune system and cause harmful toxic effects (figure 13).

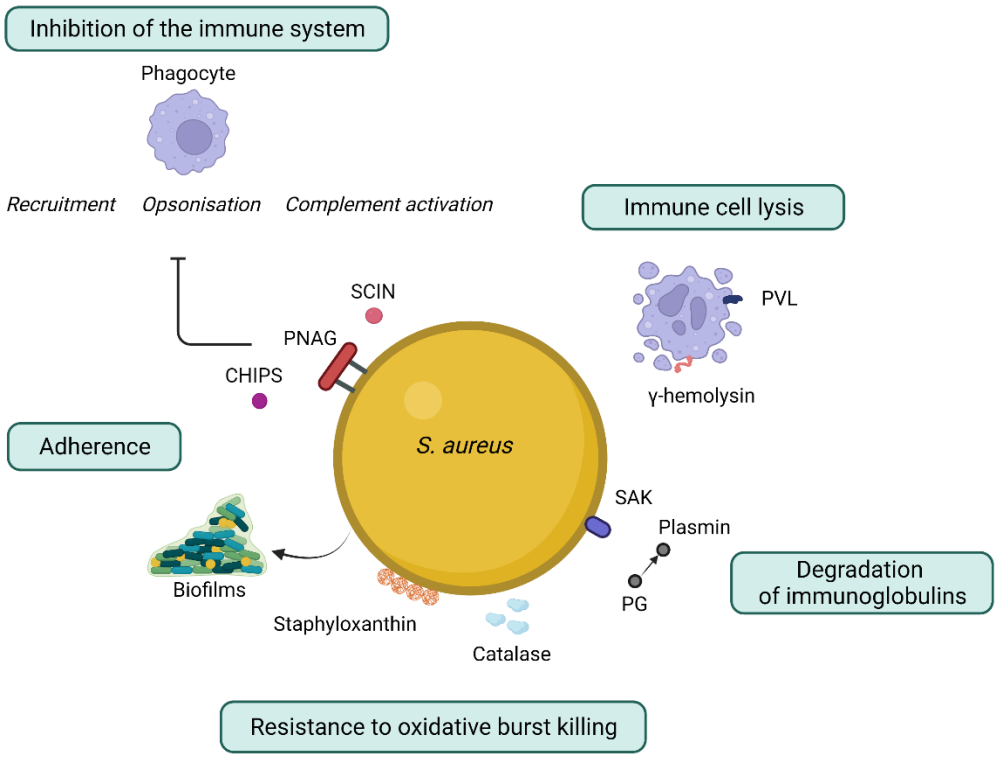

Figure 13: *S. aureus* mechanisms of subversion of the immune system. *S. aureus* inhibits phagocyte recruitment by binding chemotaxis inhibitory protein of staphylococci (CHIPS) to chemokine receptors, prevent opsonisation with poly-N-acetylglucosamine (PNAG) which act to cloak surface bound opsonins of phagocytes. This bacterium can also inhibit the complement activation with the protein Efb binding of soluble C3 and inhibit classic/lectin and alternative C3 convertases by Staphylococcal complement inhibitor (SCIN). *This illustration was made using biorender.com.*

It possesses a plethora of virulence factors responsible for the broad range of infections. The bacterium is able to attach to the host cell surface through the mediation of several adhesins. One major class of adhesins comprises proteins covalently attached to cell peptidoglycans and specifically attached the plasma or extracellular matrix components and are named the microbial surface component recognizing adhesive matrix molecules (MSCRAMMs). The bacterium also secretes toxins that process cytolytic activity that can form β-barrel pores in the plasma membrane leading to intracellular leakage as the α-hemolysin, leukocidin or Panton-Valentin leukocidin. It can also produce proteins which impair the innate and adaptive immune system. Examples of such proteins are the staphylococcal inhibitor (SCIN), chemotaxis inhibitory protein of *S. aureus* (CHIPS) or even the extracellular fibrinogen binding protein (Efb). The enumeration of its arsenal is under the scope of this manuscript but a specific focus will be done on its responses to ROS.

RONS production is essential when bacteria are internalized by phagocytes but *S. aureus* is once again able to resist. It possesses the staphyloxanthin, a carotenoid pigment to which it owes its golden color and which detoxifies ROS[173]. SCIN occupies the active site of MPO preventing the fixation of H_2O_2 its substrate and so inhibits HOCL formation. The bacterium has the ability to dismutate O_2^- and H_2O_2 through the action of superoxide dismutases SodA and

SodM; the catalase KatA will then produce H_2O and O_2. The peroxide regulator (PerR) is a transcriptional regulator which control many antioxidant genes. It modulates the alkylhydroperoxide reductases (AhpC, AhpF) and KatA involved in the resistance to superoxide and H_2O_2 respectively[174]. A deletion of both induce a significant growth decrease enabling *S. aureus* to remove intra or extracellular H_2O_2 which accumulate at toxic levels. The bacterium is capable to take advantage of the host signals. The phagocytosis of *S. aureus* by macrophages lead to the activation of JNK in a TLR2 dependent manner. The activation of the JNK pathway inhibits the superoxide production, impairing the ROS cascade and favoring bacterial survival. On the other hand, TLR2 deficient mouse macrophages were able to kill *S. aureus* more efficiently[175]. The production of lipoic acid is another way to escape the immune system. It is a metabolic cofactor which limits macrophage activation by reducing TLR1 and TLR2 activation by bacterial components[176]. To date many studies were done on neutrophils while macrophages seem to be also of great interest to understand *S. aureus* persistence.

3.3.2. The role of macrophages in *S. aureus* infections

As previously mentioned *S. aureus* is responsible for abscesses formation and a wide range of diseases as bacteremia or endocarditis. In bacteremia murine model there is a transit of extracellular bacteria that are rapidly phagocytosed by liver Kupffer cells (liver-specific macrophages). A major part is killed but a small number can survive intracellularly enabling the progressive formation of abscesses in the liver and can also disseminate to the kidney[177]. In zebrafish model the observation is similar to mice with a loss of macrophages that lead to increased *S. aureus* susceptibility[179]. This type of model allows to show the important role of macrophages; when those cells are depleted in animal infections model as mice model there is an increased bacterial burden and mortality following sepsis[178]. It is now well established that macrophages are key cells for *S. aureus* elimination and recently integrated that phagocytes can also be niches for this bacteria allowing its survival and eventual escape. Despite this, macrophages degrade efficiently most of *S. aureus* with a small proportion surviving[177].
In order to eliminate *S. aureus*, macrophages must first localize the invading bacteria. The phagocyte recruitment is triggered by signals of the host immune system or by the bacteria itself. The recognition of microorganisms is achieved through innate immunity receptors called pathogen recognition receptors (PRRs) that are present at the cell surface. PRRs can recognize staphylococcal molecules as lipoproteins, lipoteichoic acid (LTA), protein A, toxins or peptidoglycan (PGN)[180]. The association of the ligand with the PRRs lead to recruitment and the activation of phagocytes that will produce pro-inflammatory cytokines and chemokines as IL-6, IL-1β or granulocyte-macrophage colony-stimulating factor (GM-CSF)[181]. In an *S. aureus* brain infection in mice it has been demonstrated that the gene expression of multiple pro-inflammatory cytokines (IL-1, TNF-α) and chemokines (CCL9, CXCL13) are upregulated leading to macrophages recruitment. In addition, the production of formylated peptides or specific molecules by *S. aureus* can either act directly as chemoattractant on macrophages[182] or activate the complement cascade leading to the release of C5a, a strong phagocyte chemoattractant[183]. After recruitment of macrophages to the site of infection functional changes appear and the phagocytosis of the pathogen can start. *S. aureus* phagocytosis occurs after the

engagement of multiple receptors on the macrophage surface as scavenger receptors (SRs), complement receptors and Fc receptors.

The elimination of *S. aureus* by macrophages is dependent on the pro or anti-inflammatory immune response. Macrophages actively phagocytose planktonic *S. aureus* but are less quick to eliminate biofilm-associated bacteria. Indeed, researchers demonstrated in a mouse model of catheter-associated biofilm infection that there is a significant reduction of IL-1β, TNF-α, CCL2 and CXCL2 (inflammatory signals respectively responsible for macrophages and neutrophils recruitment) expression during biofilm infection limiting macrophages invasion into biofilm *in vivo*[184]. Another study showed that in an intradermal infection in burned mice *S. aureus* dermal infection requires M1 macrophages whereas the presence of M2 phenotype was related to uncontrolled bacterial spread[185].

This was extended to keratinocytes where *S. aureus* biofilms present a lesser inflammatory response than with planktonic bacteria[186] all these elements lead to the conclusion that macrophages polarization induce a different response to *S. aureus* invasion promoting pro- or anti-inflammatory responses[187].

3.3.3. Macrophages strategies to eliminate *S. aureus* infection

In order to fight against such a complex bacterium, macrophages possess a powerful degradative process. As previously mentioned macrophages have the NADPH oxidase (NOX2) enzymatic complex. It catalyzes and converts the superoxide anion (O_2^-) into different ROS which are toxic depending on their concentration. The production of ROS is important for bacterial clearance and is the key process used by macrophages and neutrophils. Even if superoxide is able to efficiently destroy bacteria it is extremely volatile and degrades rapidly into hydrogen peroxide (H_2O_2) or interacts with nitric oxide (NO) to form peroxinitrite ($ONOO^-$) (figure 14).

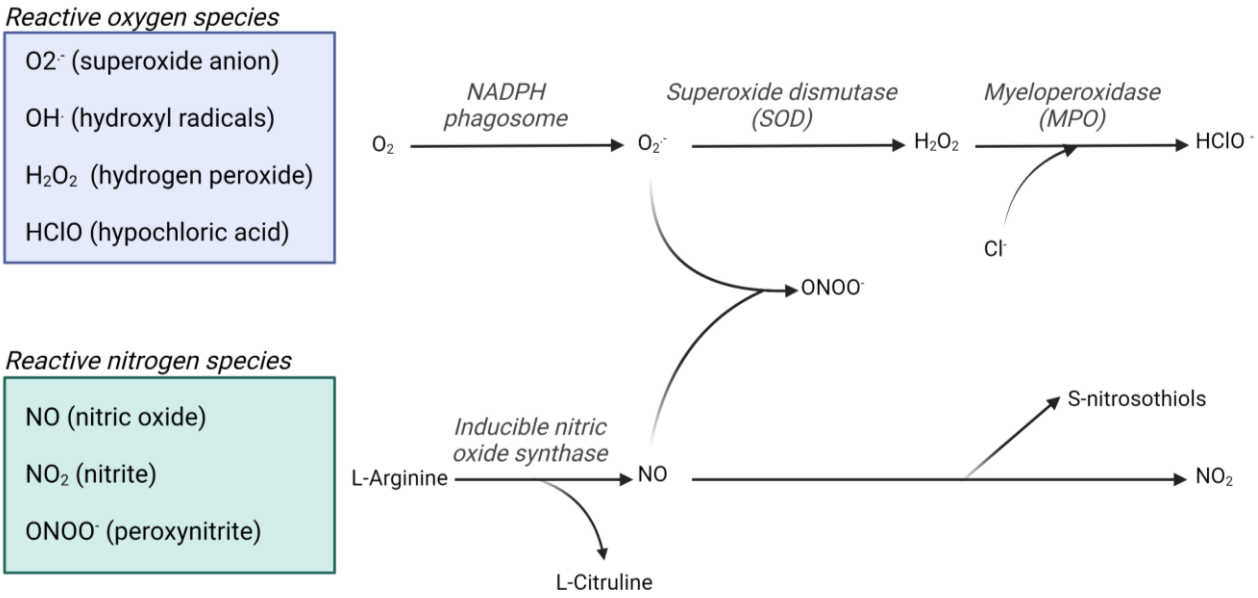

Figure 14: Antimicrobial species generated from oxygen and nitrogen. *This illustration was made using biorender.com.*

H_2O_2 is the product of O_2^- dismutation and is thus generated continuously within the phagosome. However, H_2O_2 reacts poorly with most biological molecules and therefore the levels are below the concentration required for bacterial killing *in vitro*[188]. In addition, *S. aureus* is a catalase positive bacterium and can inactivate H_2O_2. Among the different reactions that occur the Fenton reaction is able to form hydroxyl radicals (OH^-) by the interaction between H_2O_2 and O_2^- and the iron or catalytic metals present in the phagolysosome[189,190]. The OH^- seems to be the strongest oxidant produced with a high reduction potential suggesting a good microbicidal activity[191]. One of the main reaction is also the production of hypochlorous acid (HOCl) generated through metabolism of H_2O_2 by myeloperoxidase (MPO). This process is abundant in neutrophils but other phagocytes as macrophages express it. HOCl is a potent antimicrobial ROS *in vitro* and can be a molecule of interest to NOX2 mediated killing of *S. aureus*. Nonetheless data obtained with MPO-deficient patients are in contradiction with this fact. MPO deficiency is frequent but not related with a detectable increase in frequency of bacterial infections in contrast with the recurrent infections in chronic granulomatous disease (CGD) patients[192]. Those latter have mutations in one of the subunits of NOX2, resulting in inability to produce ROS making them more susceptible to *S. aureus* infections. There is also a production of RNS inside macrophages. Nitric oxide (NO) radicals are catalased by inducible nitric oxide synthase (iNOS) that is only expressed following a stimulation with IFNγ the key cytokine for iNOS induction in macrophages[193]. However, iNOS seems to be less active in comparison to NOX2 for *S. aureus* infections. Mice deficient in iNOS do not have a significant increase of intracellular *S. aureus* while NOX2 deficient mice have a significant increased burden and higher mortality[194,195] highlighting NOX2 importance against *S. aureus*.

ROS are also produced by mitochondria (mROS) and studies demonstrated that mROS acts within macrophages[196,197]. *S. aureus* infected macrophages triggered stress of endoplasmic reticulum that will induce the production of mROS which are delivered to the bacterial-containing phagosome by mitochondria-derived vesicles[197]. In this study they demonstrated that IRE1α (endoplasmic stress sensor) lead to mROS production and specifically H_2O_2 upon MRSA infection. Thus mitochondrial redox capacity enhances macrophage antimicrobial function through mROS delivery. In addition, mitochondria favor the acidification of the phagosome through the increase of mROS and caspase 1 activation following mitochondria association with the membrane of *S. aureus*-containing macrophage phagosomes. However, *S. aureus* is capable to counteract this phenomenon by the secretion of alpha-hemolysin[198] and is able to prevent the recruitment of mitochondria to the phagosome membrane in a caspase-11-dependent manner[199].

Another key mechanism for *S. aureus* elimination is the phagosome acidification as previously described in section III.a. Commonly a low pH of 4.5 reduces the bacterial growth and thus should affect *S. aureus* even if its lethal pH is as low as 2. Furthermore, the acidification induces the activation of specific enzymes as the cathepsin D an essential lysosomal acid hydrolase which participates actively in bacterial degradation[200] (figure 15). The acidification results from the influx of protons (H^+) that penetrate the phagosome through the vacuolar-type proton transporting ATPase (v-ATPase) present in the phagosome membrane. v-ATPase induces a reduction of the pH to 6 and 4.5 for endosome and lysosome respectively[201]. As the phagosome mature the proton permeability is decreased to maintain the acidification and thus the low pH[202].

In the literature it is reported that in *S. aureus* infected RAW264.7 cells the phagosomal pH is around 5 12 hours post infection[203] and in murine peritoneal macrophages it is reduced to 5.7 to 6 within 6 to 8 min of infection associated with v-ATPase activity[204]. Once again *S. aureus* can adapt to the acidic phagosome and recent studies even suggest that exposure to acidification may promote intracellular bacterial survival. *S. aureus* can survive and replicate in mature phagosomes[205] in murine and human cells and the inhibition of the acidification induce only a small drop in bacterial survival. Other studies demonstrated that macrophages with phagosome containing *S. aureus* do not acidify correctly this was notably shown in THP-1 cells infected with *S. aureus* and the main explanation was that the reduction of the acidification may precede bacterial evasion[206].

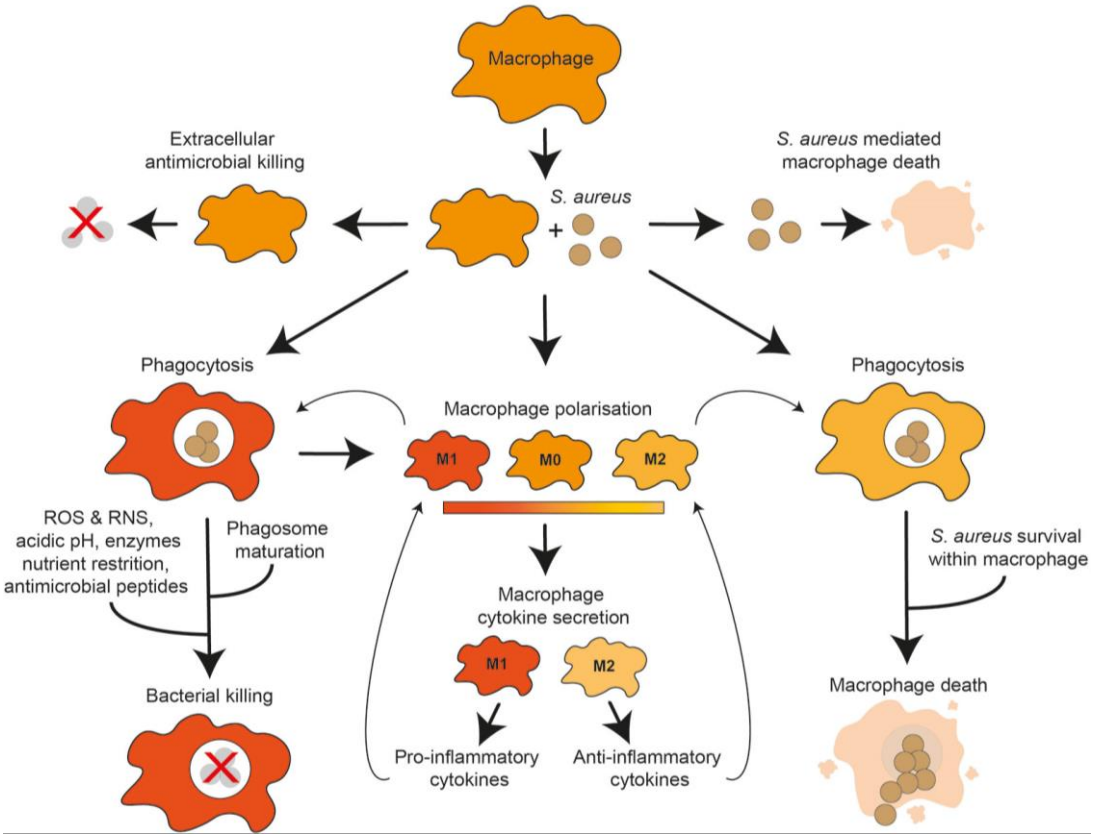

Figure 15: Interaction with *S. aureus*. Macrophages exert extracellular killing and also intracellular killing via phagocytosis. *S. aureus* influences macrophages polarization and thus modulates a pro or anti-inflammatory response inducing a modification in cytokine secretion. *S. aureus* is also capable to kill macrophages extracellularly with its set of virulence factor. In addition, this bacterium is able to resist to the mechanisms of destruction of macrophages to survive within vacuoles, to proliferate causing macrophage death and leading to its escape and spread. Pidwill et *al.*, 2021[207].

Related to acidification mature phagosome contain hydrolytic enzymes as proteases, lipases, phosphatases that have an optimal efficiency in an acidic environment. Cathepsins, for example, are proteases found in the lysosomal compartment which are highly expressed in macrophages. This enzyme has been shown to participate to *S. aureus* engulfment and killing with cathpesin

L and K favouring non-oxidative killing and IL-6 production respectively[208]. However, *S. aureus* possess an arsenal of strategies to overcome the efficiency of enzymes. For example, the lysozyme is an enzyme that cleaves the peptidoglycan but in *S. aureus* there is an acetylation of PGN by O-acetyltransferase (OatA) which prevent the cleavage. In addition of hydrolytic enzymes macrophages defense consists also to the use of antimicrobial peptides. Calprotectin is able to sequesters metal ions to reduce their bioavailability and thus inhibit growth of *S. aureus* in a mouse abscess model for example[209]. Cathelicidins opsonize bacteria to enhance *S. aureus* phagocytosis by macrophages *in vitro*[210]. Interestingly *S. aureus* killing by macrophages with LL-37 endocytosis is associated with an increase ROS production and lysosomal fusion[211]. This manuscript is focused on ROS interaction with macrophages and *S. aureus* thus the other mechanisms of macrophages to fight against *S. aureus* as macrophages extracellular traps are not going to be described.

3.3.4. Therapeutic progress

S. aureus has acquired a wide range of resistance to antibiotics making it more complicated to treat with a strong limitation to therapeutic options. Antibiotics used to treat *S. aureus* and especially MRSA are often expensive and especially less and less effective with important costs. The urgency of the situation leads in 2017 the World Health Organization to class *S. aureus* as a priority in the list of pathogenic bacteria for which it is crucial to find new treatments[137]. In addition, the report on antibiotic resistance of 2016 for the British government (Review on Antimicrobial resistance – Final report and Recommendations 2016, chaired by Jim O'Neill) warned that if no new antibiotic molecule is developed antibiotic resistance will become the leading cause of death in the world before cancers with nearly 10 million deaths per year from 2050.

Thus, innovative strategies are under progress. Most of the antibiotics cannot access the intraphagocytic niche[212] thus new therapeutic try to deliver components intracellularly. The methods include the development of intracellular antimicrobials, nanogels that will specifically target macrophages with bacterial enzymes to free vancomycin[213], and other nanoparticles that will active targeting of macrophages to induce endocytosis, releasing singlet oxygen to kill intracellular *S. aureus*[214]. Regarding the development of new antibiotics, it is less optimistic. Antibiotic development is long and expensive. Currently for only 30-40 new antibiotics in the clinical trial phase compared to 4000 new anti-cancer drug candidates[215]. The portfolio of pharmaceutical industries is currently very limited and consists mainly in improving the compounds already existing.

In the present topic focusing on the role of infected macrophages and bacterial wound infection the use of cold atmospheric plasma seems to be a promising strategy.

4. Cold atmospheric plasma

4.1. Plasma Physics

In biology the term plasma refers to the non-cellular fluid component of blood, but in physical sciences it corresponds to an ionized gas. It refers to as the fourth state of matter distinct from the solid, liquid and gaseous phases and represents more than 99% of the visible matter in the universe (figure 16). Plasmas are visible as natural phenomena like northern lights or lightening in thunderstorms and from a cosmological point of view they can be found as stars, the sun and even stellar winds. It is also a technology commonly used in energy saving lamp, air and water purification and also for space propulsion.

This specific state consists of positive and negative ions and neutral particles. Plasmas contain the same density of positive and negative charge particles and thus are globally neutral. When a significant amount of energy (i.e. thermal, radiative sources, electrical discharge) is applied to a gas atom the electrons can escape from atoms or molecules allowing ions to move freely and more electrons and ions are produced due to collisions induced by the acceleration of the particles in the electric field. This process is called "ionization" and depending on the degree of ionization η there are different type of plasma: cold (η<0.01%), thermal (η ~1-50%) and hot (100%). In hot plasmas (stars, fusion reactors such as tokamaks…), the media is fully ionized and contains only charged particles. In thermal plasmas (electric arcs, lightnings…), the neutral particle temperature T_n is close to the electron temperature T_e, such a plasma is classified as an equilibrium plasma and can reach several thousand Kelvin. Cold or non-thermal plasmas are produced when the T_n is much lower than the T_e in those conditions it is classified as a non-equilibrium plasma and the temperature is close to the room temperature. In term of medical use, "cold" means temperatures close to ambient temperature at the target site during plasma treatment[216].

The plasmas thus produce, generate a highly reactive mixture of species that has interesting properties in multiple fields and especially in biology[217].

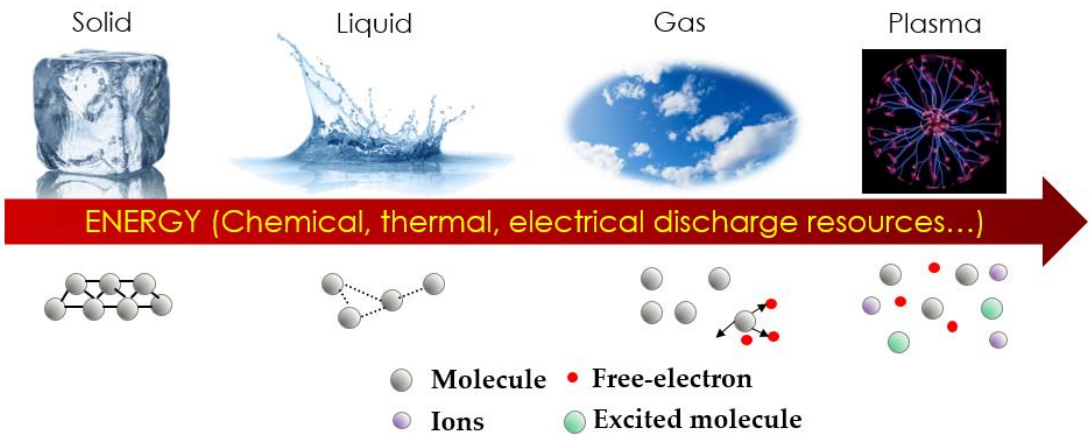

Figure 16: Physical description of plasmas.

4.2. Genesis of Plasma Medicine

In 1879 Sir William Crookes established the fundamentals of plasma science by ionizing a gas through the application of high voltage. Since this discovery it has been used in many spheres over the past few decades involving either low pressure plasmas or hot plasmas with important thermal effects. The US National Aeronautics and Space Administration, NASA, investigates the implication of low-pressure oxygen plasma for the destruction of biological matter for space applications. This technology was also used in the mid-1990s in experiments to inactivate bacteria[218]. The results of those studies raised the interest of the Physics and Electronics Directory of the US Air Force Office of Scientific Research (AFOSR) leading to the development of a specific program with mains objectives: the **disinfection** and **treatment** of soldier's wound as well as the **sterilization** and **decontamination** of biotic and abiotic surfaces. In addition, since its discovery multiple studies showed that nonthermal plasma can interact with prokaryotic and eukaryotic cells and living tissues to induce biological outcomes. Thus, in the mid 2000s, the potential of the plasma led to the formation of a global research community called "plasma medicine" involving many laboratories that investigate the biomedical applications of plasma, pushing the field forward those last few decades.

4.3. Plasma Medicine

Plasma medicine is a multidisciplinary field at the interface between physics, chemistry, biology and medicine which investigate the use of "plasma technology in the treatment of living cells, tissues and organs"[219]. In medical sciences cold plasmas are developed for a wide range of applications such as cancers[220], dental decays[221], treatment of chronic wounds[222], and dermatological applications[223]. There are also important implications for biotechnologies for health to investigate the enhancement of cell transfection[224], stem cell differentiation[225] and tissue regeneration[226]. A wide range of plasma sources are described in the literature and differ in their plasma generation mechanism, source geometry, working gas[227] (figure 17). Research activities in medicine are mainly focused on two fundamental concepts of CAP devices: dielectric barrier discharges (DBD) and plasma jets working at atmospheric pressure. DBD systems are characterized by plasma ignition in a gap between two electrods insulated by a dielectric limiting the current and preventing the formation of an arc. For biological applications, the target is generally connected to the ground. Thus, cells or living tissues are part of the discharge electrode configuration and the target is exposed to the electric field necessary for plasma generation and is in direct contact with the plasma. In the case of a plasma jet, the plasma is ignited inside a capillary flown by a noble gas. The electrode setup for the generation of the plasma for medical applications is often located around or in the tube and generally in a pen-like device. The plasma propagates along the gas and is brought in direct contact with the target. Most of plasma jet devices are using noble gases (helium, argon) but they can also be mixed with small amounts of molecular gases (oxygen, nitrogen).

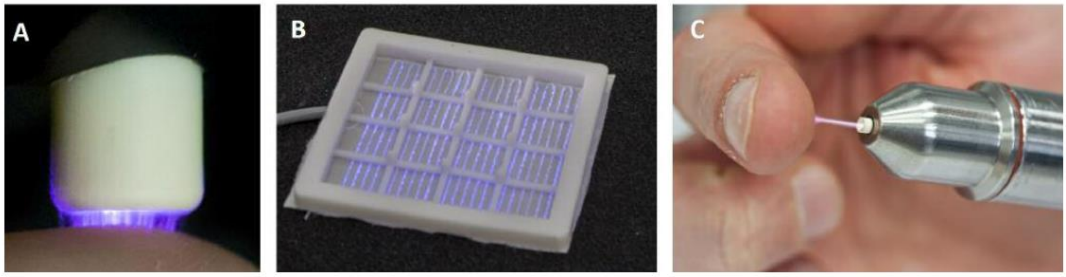

Figure 17: Photographs of the fundamental devices used for biomedical applications. Volume and surface DBD (A, B) and plasma jets (C). Figure from Woedtke et *al.*, 2013.

A few number of sources are CE certified and commercialized for medical use, they have been extensively optimized to ensure safety for tissue applications[228,216]. Among the three sources there are the DBD device PlasmaDerm® VU-2010 (CINOGY Technologies GmbH), the atmospheric plasma jet (APPJ) kINPen® MED (INP Greifswald/neoplas tools GmbH) and the SteriPlas (Adtec Ltd., London, United Kingdom) illustrated in figure 18. Those devices are medical product used to treat chronic wounds in humans but also to decrease the microbial load (SteriPlas) and have good efficacy and tolerability. The kINPen® Med and the SteriPlas cover a small surface around 1 cm^2 and 12 cm^2 with an important variation of cost from 28 900 and 70 000 euros respectively. The PlasmaDerm® VU-2010 covers a larger surface 27.5 cm^2 with a cost of 2500 euros but requires a contact with the area to be treated.
Currently, the plasma technology has shown promising results especially for the treatment of skin alterations including atopic eczema[229], itch, wound healing and scar treatment[230]. Although these results are encouraging, additional studies are needed to assess the potential risk of CAP under different conditions, intensities and frequencies of use.

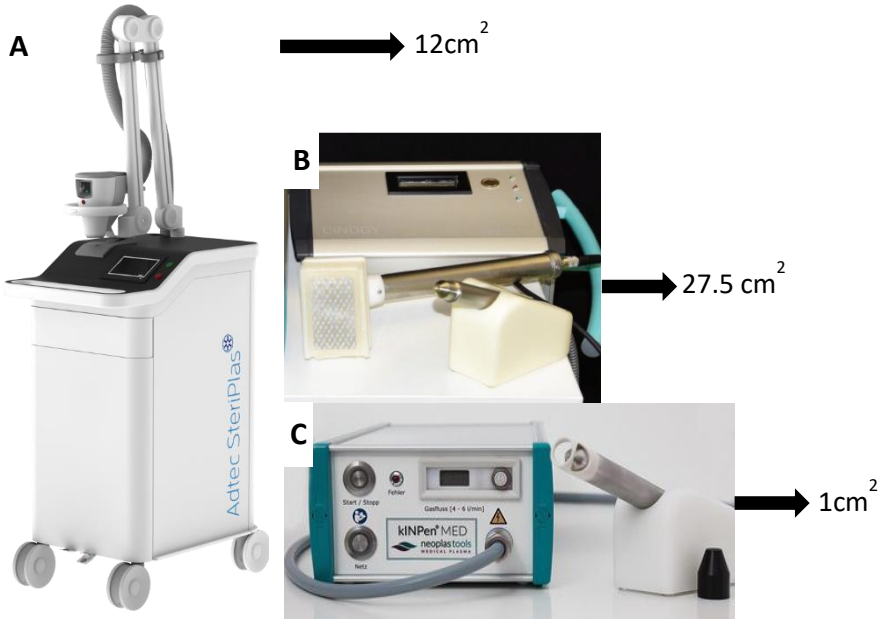

Figure 18: Photographs of the CE-certified devices and their treatment area surface. Adtec SteriPlas (A), PlasmaDerm® VU-2010 (B), kINPen® MED (C). *Adapted from Bernhardt et al., 2019[224]; Schönebeck et al., 2018[232,233]*.

4.4. Chemical characterization of CAP

CAP is a complex mixture that emits electromagnetic radiation, UV radiation and visible light, it contains excited gas molecules, ions (positively and negatively charged), free electrons, radicals and the most important for biomedical applications seems to be reactive oxygen/nitrogen species (ROS/RNS).

When the gas is ionized to plasma the charged species react with the matter with which they enter in contact and so meet different interfaces. In the case of Plasmajets, RONS are produced by interaction between the noble gas plasma exiting the capillary and the ambient air. Despite the fact that plasma is sustained with a noble gas it mixes with the air, air molecules such as O_2, N_2 and H_2O can also dissociate and react forming new different reactive charged and neutral species (figure 19). CAP can also interact directly with a solid or liquid target. In the case of a solid the reactive species may modify the physical characteristics of the surface by changing the charge or ablating the external layer of the surface (i.e. wettability). When it enters in contact with a liquid this interaction occurs through photons and electric fields, reactive species flux and through other processes. The plasma-liquid interface is a complex domain in which it is difficult to determine exactly the species engaged. The type of media (for culture cell)/liquid is also important and change the nature of the produced species.

Once the RONS are generated in the atmosphere they diffuse and are solubilized in the liquid medium. Some species are directly produced from water vapour entering in contact with CAP as it is the case for hydrogen peroxide (H_2O_2) and/ or are produced directly in liquid phase. Among the RONS produced by CAP at significant levels there are single delta oxygen ($O_2\Delta$), nitrite (NO_2^-), nitrate (NO_3^-), ozone (O_3), superoxide anion ($O2^{\cdot-}$), hydroxide radicals ($OH^{\cdot}$) and hydrogen peroxide (H_2O_2). All those species have different life time and two types of molecules can be distinguished: long live species and short live species.

The short-lived species comprise singlet oxygen (O_2), peroxynitrite ($ONOO^-$), ozone (O_3), hypochlorite anion (ClO^-) that have seconds lifetime in biological media. Due to their short lifetime those species can have a short diffusion distance, for example $OH^{\cdot}$ is calculated to have 10^{-9}s with a diffusion distance of 0.009 µm within mammalian cells[231] which can result from its high reactivity. On the opposite there are long-lived species as hydrogen peroxide (H_2O_2), nitrite (NO_2^-) or nitrate (NO_3^-) that can persist in the media and can still be measured several hours[232] after plasma treatment.

In order to detect the plasma-generated RONS in aqueous solution multiple techniques are used such as electron spin resonance (ESR) or the liquid chromatography mass spectrometry (LC-MS)[232,233]. However due to the reactivity of the species and their interaction it is a challenge to fully characterize the plasma.

In plasma-medicine it is possible to treat biological samples in two different ways:

- Direct treatment of the target with the ionized gas.
- Indirect treatment consisting in treating the aqueous media that will be then applied to the biological target.

In the case of a pre-treatment of the media the studies are more focused on the impact of long-lived species (ozone, nitrate). Nevertheless, the plasma activated media (PAM) may have an impact after several days on the long-lived species that can produce secondary radicals, short-lived species[234]. For example, during photolysis H_2O_2 is converted by UV into $OH^{\cdot}$. Moreover,

when plasma reactive species encounter biologically active targets it creates an even more complex environment with feedback loops and with invariably unmeasured and even unknown variables playing key roles.

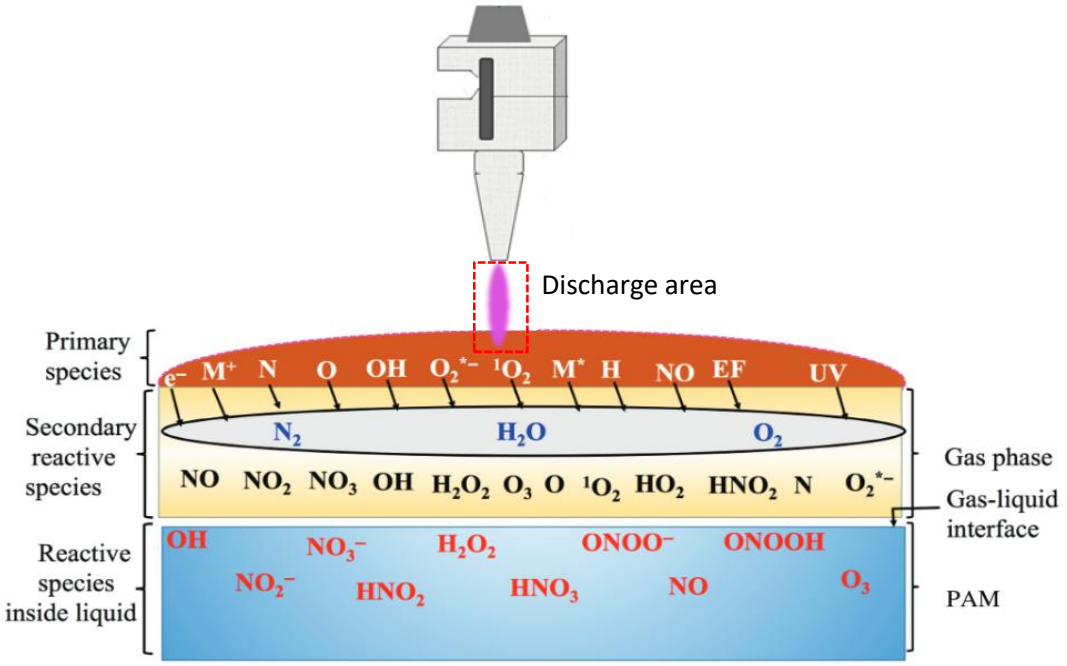

Figure 19: Schematic representation of the reactive species produced by plasma in plasma activated media (PAM) an at different interfaces (Gas-gas/Gas-liquid). *Adapted from Kaushik et* al.*, 2018*[235].

4.5. Interactions of CAP with living organisms

4.5.1. Importance of RONS for biological systems

In order to understand better the involvement of plasma in biology it is crucial to explain the important role of RONS within living systems. Historically RONS were thought to be deleterious species for the organism often associated with mutations and free-radical aging[236]. Current thought now focuses on their role with the conviction that actions and characteristics of reactive species are woven into all inter- and intracellular signalling networks with a chemical balance between the different parts.

A key point for RONS cell-signaling network is that they are able to form covalent bonds. This macromolecular interaction can be mediated by shape, charge, hydrophobicity and so forth that can lead to formation or bond rupture. This may induce changes in protein shape leading in transcription and translation that result in the formation of new proteins or other cellular outcomes.

H_2O_2 seems to be one of the most important molecules among the ROS[237]. An example is the production of H_2O_2 from the conversion of O_2^- through the enzymes NOX of the oxidative burst (part 3.2). This newly formed molecule once in the cytosol reacts with enzymes to transform

them into their oxidized states promoting for example the phosphorylation of proteins with tyrosine (which can inactivate it). Apart from H_2O_2, the RNS "NO" changes dramatically the biochemistry of the environment. The main product combination between O_2^- and NO is the peroxynitrite anion ($ONOO^-$), a very reactive ROS that may kill bacteria at low concentrations[238] and so playing a key role in immune system. One of the multiple actions of RONS is also to released second messengers in the cytosol that will oxidize thiol (-SH) or thiolate groups on specific proteins. The oxidation leads to a modification of their cellular function by the alteration of the conformational and/or the enzymatic properties of the protein. Obviously this description has been limited to a few examples but the number of pathways that are known to be regulated by RONS is large and many of them are still unknown. An important list of molecules regulated by RONS (phosphatases, translation regulators, ions channels) is still growing with different mode of action ranging from regulation of cell motility, secretion, respiration, gene expression to senescence control. The question of the ability of RONS to diffuse as well as their lifetime is also important not only for cell-signaling mechanisms but also for any plasma-biomedical purposes.

4.5.2. Impact of CAP on microbes *in vitro*

The technologies using cold atmospheric plasma to inactivate or kill bacteria has been widely used for several years in particular for food preservation and decontamination but also for medical sterilization. However, the mechanisms involved for these different uses have not yet been elucidated and many assumptions are made.

Investigations about the impact of the plasma stream on the external structure of bacteria have been done. Laroussi et *al.*, demonstrate that with the use of plasma generated by a DBD there are substantial damages induced in *Escherichia coli* but not in *bacillus subtilis*. The difference observed between the two bacteria could be explained by a different structure of the cell wall[239]: Gram negative bacteria (ex: *E. coli*) have a cell wall composed of two cell membranes and a thin peptidoglycan layer whereas Gram positive bacteria (ex: *B. subtilis*) have a thick peptidoglycan layer and cell membrane[240]. The authors suggested that the damages observed for *E. coli* can result from the electrostatic rupture of the outer membrane.

Nevertheless, contradictory results on the visible impact of CAP on bacteria can be found with the example of the research of Lunov et *al.*, 2016 which demonstrate deleterious impacts of their own devices on both Gram negative/positive bacteria in a dose dependant manner (relative to time and voltage exposure)[241]. Additionally Han et *al.*, demonstrate that *S. aureus* was mainly inactivated by intracellular damage and *E. coli* by cell leakage and a low level of DNA damage[242] which show a deeper difference between Gram negative and positive bacteria due to their structure.

The bactericidal effect of plasmas drew the attention of researcher on the impact of CAP on antibiotic resistant strains such as methicillin-resistant *Staphylococcus aureus* (MRSA). A five-log reduction in the number of MRSA was shown even with lower energy values (0.12 kJ/cm²) but higher energy values (0.35 kJ /cm²) were needed for more degradation of the resistance gene *mecA* [243].

According to literature multiple research demonstrate that there are different scenarios depending on the bacteria strains, the structure of the cellular envelope, the microbial growth phase[244], the environment of the microbe but also the parameters of the plasma device. However some authors agree that CAP induce bacteria surface damages and demonstrate it by using scanning electronic microscopy (SEM) studies confirming contribution of physical mechanisms[245,246] (figure 20).

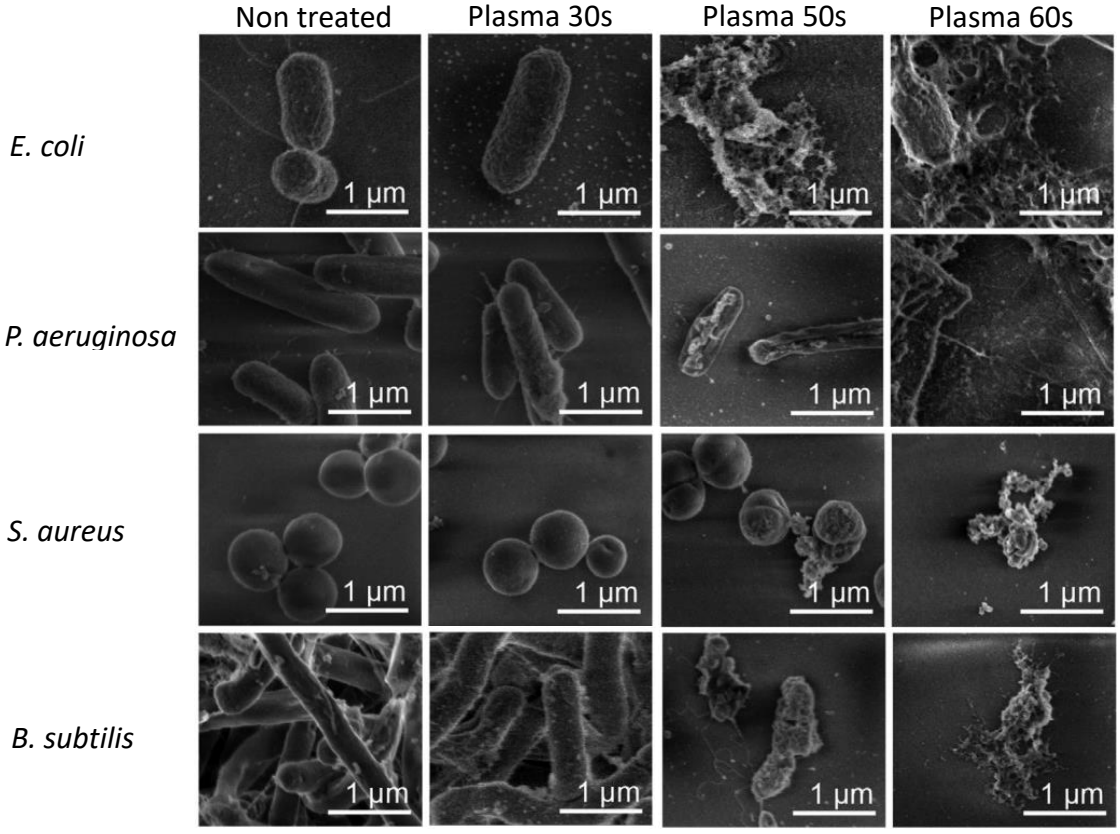

Figure 20: SEM micrographs of physical disruption induced by cold plasma on different strains. Non-treated (control), plasma treatment at different time point (30 s, 50 s and 60 s) on *Escherichia coli*, *Pseudomonas aeruginosa*, *Staphylococcus aureus* and *Bacillus subtilis*. *Adapted from Lunov et al., 2016[244].*

The impact of plasma on the intracellular components seems to be less disparate. The first important point before describing processes is that CAP has an impact on the cellular membrane as explained before. This property is a known process especially used as an electroporation technique which consist to expose to an external pulsed electric field the membrane that transiently becomes permeable for multiple species such as ions or hydrophilic drugs[247] and can facilitate the penetration of plasmid DNA for example. Thus CAP is able to change the membrane integrity through interactions with proteins and the formation of pores but also to change the cell membrane potential[248]. The disturbance of the potential is at the origin of alterations of the proton-motive force which consequently lead to abnormal ATP synthesis and impairment of cell metabolism and division[249]. CAP can induce the release of nucleic acids

from the cells and has a direct effect on DNA, generally it is believed that it is the result of both UV and reactive compounds of plasma[250] . In the cell the plasma-induced RONS oxidize proteins by the generation of hydroperoxyde groups in their structure[251]. This form strong intramolecular crosslinks with the nucleic acids, called DNA-protein crosslinks (DPCs), that are responsible for hard-to-repair damages. Studies suggest that the reactive species that are able to penetrate the cell could cause the degradation of proteins by the destruction of hydrogen, sulphide and peptides bonds by the compounds of plasma. Hosseinzadeh Colagar et *al.* analysed the impact of cold plasma on protein degradation and they demonstrated on *E. coli* samples that the concentration of protein with a molecular mass below 25 kDa increased after argon plasma treatment[252]. These results led them to think that the large proteins (50-90 kDa) are the first to be destroyed by the treatment. Other studies have supplemented these observations explaining that CAP has an impact on the three dimensional structure (primary, secondary, tertiary) of the protein that lead to a decline in the enzymatic activity of the cells[253]. Interestingly, CAP does not always induce the death of the microorganism but can reduce its metabolism leading to a cell that does not undergo cell division and become viable but not cultivable (VBNC)[254] also called spores; in the study the cells were not resuscitated but their metabolic activity was detected through the cellular mRNA.

Multiple studies have worked on the impact of CAP on spores which are resistant structures that have acquired the possibility to survive in adverse environmental conditions and are a permanent source of contamination[244]. It is a scourge for pharmaceutical industries but also for medicine due to their resistance to disinfectants, chemical sterilants and thermal inactivation. As for the vegetative form, spores are sensitive to CAP with change in the spore size, leakage of the cytoplasm and membrane disruption[255]. Among the forms of resistance of bacteria there are also biofilms. Microbial biofilms are a community of aggregated bacteria embedded in a self-produced matrix of extracellular polymeric substances (EPS). These communities exhibit higher resistance to external factors (antibiotics, temperature, pH) thanks to the composition of the EPS (polysaccharides, lipids, proteins, nucleic acids) and thus they are a real challenge for medicine. The effect of CAP on biofilms is dependent on the thickness of the structure and the species of biofilm-forming microorganisms. Once again several reports demonstrate the sensitivity of biofilms to CAP however a longer exposure to plasma is needed for a full inactivation in comparison to planktonic cells[253,256]. Mai-Prochnow et *al.* have compared the reduction of Gram positive and negative biofilms. The virtual reduction of the bacteria in the Gram negative biofilm was observed after 1min treatment in comparison with Gram positive biofilm where a 10 min CAP resulted in <1 log reduction[257].

The same kind of results as the bactericidal effect of CAP on planktonic bacteria were obtained on yeasts and also on viruses[258]. To conclude, the reactive species of CAP have a deleterious effect on bacteria with damage on the extracellular matrix, cell wall, cellular membrane and internal cell structures. For this reason, CAP technology is already used industrially for the decontamination of medical devices, food, waste-water or even indoor air treatment. Many investigations are focused on the effect of CAP on bacteria but the precise molecular mechanisms on microbial organisms are still unclarified and raised doubt especially for the safety of the sterilization method[254].

4.6. Interaction of CAP with living tissue: specific focus on the skin

Although the skin is a complex protective structure against external aggressions it is not a sealed barrier. The organ exchanges and interacts with the external environment and can let different molecules penetrate the skin in three ways: intracellularly (through the cells), intercellularly (space between the cells or the skin pores) and via the transappendageal way (through the glands and hair follicles)[259].

4.6.1. Penetration of RONS in tissue models

One of the key question in plasma medicine relates to the extent of penetration of RONS into tissue, it is an important point in order to understand: what is the mode of action of CAP? What are the reactive species involved in the different element observed? What are the safe doses for biomedical applications?
Thus, investigators used various tissue models *in vitro* as well as tissues *ex situ* to try to provide some answers or hypothesis but the variability between the devices must be taken into account and make comparisons often difficult.
In 2016 Oh et *al.*, measured the concentrations of RONS using a UV-Vis spectrophotometer as well as chemical reporters for hydrogen peroxide and nitrite delivered in deionized water present in a homemade model: an agarose film covered a volume of deionized water contained in a quartz cuvette and the RONS that penetrate this model[260] were measured. They found that direct helium treatment caused a deoxygenation of the DI water whereas CAP treatment through the agarose film induce an oxygenation of the DI water. They also demonstrate that the RONS delivered to DI water were kept being delivered for up to 25 min after removal of the plasma. Oh and collaborators concluded that in the example of an open wound CAP treatment may lead to hypoxia (reduction in dissolved oxygen) while CAP through tissue may provide oxygenation of biological fluids[261].
A first step to model the penetration of RONS through tissue was an experiment using a gelatin matrix target with embedded phospholipids vesicles which contained a self-quenched dye (resulting in a clear fluorescence switch-on upon vesicle destruction). The results of this study demonstrate that the RONS delivery into the vesicles does not induce the rupture of the vesicle membrane[262]. A second study using a gelatin gel, a derivative of collagen, showed that the spatial surface distribution and penetration depth of CAP RONS were similar to the pattern observed for vesicle destruction: they reported that H_2O_2 (in particular) penetrated the tissue model for up to 1.5mm thickness of gelatin film[263]. In order to produce more realistic conditions Duan et *al.* used pig muscle slices of different thickness placed above PBS solution and different CAP treatment (with a helium/oxygen mixture)[264]. The results demonstrate that most of O_3, OH and H_2O_2 were consumed by the tissue and can't penetrate 500 µm thick real tissue (pig muscle). On the opposite the measurement of NO_2^- and NO_3^- revealed that more than 80% of them can penetrate a tissue slice of 500 µm. Another very recent study from Duan et *al.*[265] used a mice skin model and once again it was shown that nitrite and nitrate penetrate easily but not O_3, OH and H_2O_2. Interestingly they demonstrated that RONS penetration was enhanced when the

stratum corneum of the skin is removed highlighting the fact that the treatment of wounded skin versus healthy skin may be different in link with RONS penetration.
Those models are simple organic skin mimics that have been used to quantify and measure the diffusion kinetics of the RONS after CAP treatment but they permit to have an idea of the molecules that diffuse into biological tissues. Indeed, in real life the physiochemical barriers of the skin can modify and even slow down the diffusion and neutralize most of the reactive species. The exact quantification of RONS passing through the tissue, even by using a real skin, can be altered by the nature of the media used to collect and analyse them[266]. Small molecules such as nitric oxide passively diffuse through the cell membrane; some others molecules can pass through channel proteins. The water channel aquaporins for example[267,268], were shown to facilitate the diffusion of H_2O_2 produced by CAP treatment[269,270]. As previously mentioned the lipid peroxidation induced by CAP can also generate transient pores on the membrane and participate to RONS penetration. In addition the electric field applied during the treatment contribute to destabilize the cell membrane and so, to the pore formation[271,272]. Recently sophisticated 3D models have been developed with models of mammary glands[273] and extracellular matrix[274,275] but also 3D skin which can contain immune[276] cells maybe future plasma medicine research should adopt them to get closer to reality.

4.6.2. Impact of CAP on the skin surface

The outer layer of the skin, the *stratum corneum*, provide an "acidic mantle" that confers it a pH ranging from 4 to 6. This acidic mantle is generated through endogenous factors (ex: sebaceous and sweat glands) but also exogenous ones such as the bacteria that make up the skin microbiota as explained before, and so, a healthy epidermis is relatively acidic. In plasma research it has been demonstrated that in addition to their oxidizing effects, the RONS generated by CAP induce an acidification of the treated target[277]. The pH drop can be attributed to acidic species such as the reactive species resulting from the nitric oxide precursor that generate nitric (HNO_3) and nitrous (HNO_2) acids in solution[278] in concentrations proportional to the CAP time exposure. The pH quickly decreases, around few minutes, and tends to stabilize at pH values between 3.5 and 2.5 due to the transient formation of HONO/ONO^- buffer and the generation of nitrous acid. In correlation with those elements CAP exposure is able to lower the pH of biological tissues. Indeed investigations showed that pork skin sebum and human lipids can be rapidly acidified by CAP treatment[279] and this was also confirmed by clinical trials on intact human skin[280,281]. In an acute skin wound a physiological acidification enhanced the proteases activity and stimulate fibroblast proliferation[282], thus the lower pH is also able to stimulate and accelerate skin renewing.
Thanks to this property CAP contribute to have healthy conditions for the skin. However even if higher skin pH induces pathologies, very acidic pH can burn the external layer of the tissue and so CAP exposure and parameters have to be controlled [281]. This parameter is still used for chemical peel or chemexfoliation to force skin renewal to fight against the sign of ageing.
Cold plasma treatments can modify skin hydration and can have a double effect. CAP is able to modify and destabilize the skin barrier and to desiccate the external layer of the epidermis (i.e. the *stratum corneum*). In 2011 Fluhr et *al.* did a clinical trial using the "Kinpen 09" to study

its impact on physiological parameters of the skin such as water loss, temperature and the evolution of beta-carotene. After the treatment the water concentration was reduced in the different cell layers down to a depth of ~24 µm. The major reduction where an average of 30% reduction of the original water and was detectable down to a depth of 25 µm. However, in the deeper parts of the SC the water content did not change. The evaporation of the water could not result from an increase of skin-surface temperature (Kinpen 09 induce a plasma between 30-43°C) because for each volunteer the surface temperature only increased by 1.8°C which is clinically irrelevant (from 28.4 to 30.2°C)[283]. During the clinical trial volunteers reported a mild sensation of pain comparable to a superficial needle puncture during plasma application and a temporarily mild erythema which normalized within a short period of time. This study showed skin physiology parameters that are modified under CAP but without damaging the skin or skin functions.

CAP is known to deposit charges on surfaces and interestingly the skin treatment induces a higher attraction of water molecules. Indeed, skin wettability is a determinant factor for skin protection but also for molecule absorption as well as transdermal drug delivery. Ahtanasopoulos et *al.* study demonstrated that chemical reactivity of human *stratum corneum* to plasma leads to hydrophilic skin surface[284] which is highly relevant especially for health applications.

4.6.3. CAP actions in the depths of the skin

4.6.3.1. Impact on the cell proliferation

The maintenance of healthy skin requires the continual proliferation and differentiation capacity of the keratinocytes to keep the epidermis turnover which is around 6 to 8 weeks in human adults. The active growth of epidermal cells is essential for fast wound healing but also for healthy skin tissue. The keratinocytes receive most of the nutrients needed for their development through dermal fibroblasts and thus, they are also key cells. Fibroblasts regulate and promote re-epithelialization in facilitating the migration and differentiation of keratinocytes and the formation of the dermo-epidermal junction. The positive effect of CAP on keratinocytes and fibroblasts has been demonstrated on cell lines *in vitro*. Short exposure to a CAP device (30s helium-DBD) is able to stimulate HaCaT human keratinocytes and MRC5 fibroblasts cell lines proliferation and motility[285]. Such a stimulation involved a decreased in the gap-junction protein activity and changes in the adherent junctions and cytoskeletal dynamics with E-cadherin and integrins down-regulation but on the opposite it triggers the activation of β-catenin-mediated proliferative signal[286]. β-catenin is a key factor in the Wnt signaling pathways and acts as a transcriptional regulator that promotes the expression of cell proliferation genes (ex: cyclin D1, c-MYC)[287] and so may participate actively to the positive effect of CAP on cells. Others studies using HaCaT cell lines confirmed the impact of CAP on keratinocytes. In addition to the decrease of E-cadherin previously shown, it has been demonstrated a simultaneously increased β1-integrin expression and a decrease of EGFR expression after CAP exposure[288]. Moreover, after CAP treatment the keratinocytes present an increased level of ROS which induce cell adaptation mechanisms after several weeks of redox challenge[289].

Schmidt et *al.* have identified more than 260 genes that are differently expressed in HaCaT under CAP exposure including genes coding for cytokines, growth factors and antioxidant enzymes. Strikingly the HSP-27 cell protective heat-shock protein involved in cell development and differentiation was strongly up regulated[289]. They found a lot of genes that are up-regulated and particularly after 6 hours compared to 3 or 24 hours, interestingly the incubation time seems to be more relevant than the treatment time. In 2019, investigators highlighted that the p53 cascade is a major pathway of cold plasma cell interactions in keratinocytes[290] with an impact related to the voltage used for the desired application (cancer or wound healing). A recent study demonstrated the existence of a cross talk between CAP treated fibroblasts and keratinocytes[291] by focusing on the HIPPO pathway. This signaling pathway regulates cellular proliferation, organ size, and survival in highly conserved mammals[292]. In 2020, Shome et *al*. have evidenced that a co-cultured model of these cells with an exposure to plasma initiated a higher HIPPO pathway activity and that the transcriptional coactivator of this pathway (YAP: Yes-associated protein) was significantly up-regulated. This HIPPO pathway seems important for the field of skin scaring by CAP. In the study the authors presumed that two downstream target genes of YAP, CTGF (Connective Tissue Growth Factor) and Cyr61 (Cysteine-rich angiogenic protein 61) secretion from fibroblasts, activate keratinocytes via paracrine signaling and they demonstrate that HaCaT lines had greater mobility after exposure to recombinant CTGF and Cyr61 secretion even in the absence of CAP treated fibroblasts.

In order to better understand the action of CAP *in vivo* the effect of plasma was investigated in mouse models. Schmidt et *al.* have demonstrated in human intact skin explants[293] that CAP increased the proliferation of the *stratum basale* keratinocytes. Interestingly short treatments were shown to increase the proliferation of dermal fibroblast[294] whereas few minutes treatments exert a toxic effect[295]. The deleterious effect of longer exposure is maybe due to their location in the skin. Indeed, they are in the deep dermis and so fibroblasts are less equipped to endure an external oxidative stress.

4.6.3.2. Impact of CAP on skin oxygenation and vascularization

The oxygenation is a necessary process for proper cellular metabolism. However, application of plasma can cause a deoxygenation of its target as it is the case for treated liquid[296]. But, contrary to the *in vitro* results, *in vivo* studies revealed the enhancement of the underneath tissues oxygenation[296] on mouse skin and an increase of the post capillary oxygen saturation in human skin[280,297]. One of the possible hypothesis explaining this fact is the induction of a local vasodilatation through the application of warm (30 to 40°C) which lead to an increase of tissue oxygenation; this vasodilatation can also result from the $NO^{\cdot}$ directly or indirectly produced through CAP application as it is a vasodilator molecule. Skin oxygenation is directly related to the vascularization; a healthy skin possesses a well-organized vascular network. An insufficient vascularization results in impaired wound healing in patients with diabetes or systemic sclerosis.

Established *in vitro* models with endothelial cells are used to investigate the influence of CAP on angiogenesis. To determine the angiogenic activity different parameters are measured such as the ability of endothelial cells to proliferate, migrate, to form tubes or the level of pro-

angiogenic factors that they produce. Several research teams have already demonstrated that CAP enhanced the proliferation of porcine endothelial cells for example a 30s treatment with an air-DBD increased endothelial cells proliferation and induce the release of the fibroblast growth factor-2 (FGF2)[298]. Following these studies more complex experiments have been developed to prove the tube formation of endothelial cells[299,300]. Arnujan et *al.* found the enhancement of tube formation using primary porcine aortic endothelial cells and they reported that hydroxyl radicals and hydrogen peroxides seem to be responsible for the observation[301]. Even in more complex models using the in-ovo chick embryo chorioallantoic membrane assay (CAM assay) the formation of new micro-vessels was stimulated[302].

However, Karghatgi et *al.* proved that FGF-2 was responsible for angiogenesis whereas Arjunan et *al.* and Arndt et *al.* showed that ROS are probably the mains actors. Hydrogen peroxide and NO appear to be the two main molecules essentially involved. $NO^{\cdot}$ can act as a pro- or anti-angiogenic factor depending on its concentration[303,304] and H_2O_2 stimulates angiogenesis by the induction of iNOS[305] *in vitro* but high concentrations have anti-angiogenic actions and thus can be used in cancer therapy[306]. Indeed, ROS and RNS are pro-angionenic factors as growths factors (i.e. VEGF, EGF, TGF) and cytokines (i.e. IL-1, 6,8; TNF). Non-toxic concentrations of ROS are known to increase transcription factors[307], to stimulate the growth of endothelial cells and particularly O_2^- and H_2O_2 are involved in neovascularisation. NO has also the ability to increase the synthesis of collagen IV and activate cells adhesion. Indeed, type IV collagen is a major basement membrane component of blood cells. The assembly of collagen IV orchestrates the organization of the vascular basement membrane which is required for endothelial cell adhesion to the ECM. Thus collagen cleavage is regulated during angiogenesis to promote endothelial sprouting and lumen formation during vessel maturation. Duchesne et *al.* first demonstrated that during CAP treatment there is an increase of the endogenous NO production *in vitro* but also *in vivo* to go further in their discovery a murine model of a burn wound has been developed[308]. Using this model, they showed that plasma-generated RONS increase the expression of the endothelial nitric oxide synthase (eNOS). Finally, they showed an increase of the NO production by the enzyme eNOS which, combined with the stimulated production of proangiogenic factors, led to the acceleration of wound closure[309]. In addition to the elements previously mentioned more and more data demonstrate the activation and the importance of the NRF2 pathway under CAP treatment. This transcription factor activates cellular rescue pathways against oxidative injury but also against inflammation and apoptosis. It is known to play a key role in cellular defence against imbalance in redox homeostasis. Schmidt et *al.* demonstrated that CAP prepares cells against exogenic stresses and increases their resilience against oxidative species through the NRF2 pathway[293]. Possibly the NRF2 activation maintains transcriptional noise to counterbalance with the oxidative stress of plasma treatment. This adaptation of cells allows a cell-cell communication via paracrine mechanisms to generate a benefit also for the more distant cells.

The enhancement of angiogenesis can also result from the activation of keratinocytes. Indeed, *In vivo* endothelial cells are not directly exposed to CAP so the increase of angiogenesis could be induced through paracrine mechanisms mediated by keratinocytes that are directly exposed[299,310].

4.6.3.3. CAP involvement in the immune system activation

As previously mentioned, CAP can have a bactericidal effect but can also stimulate immune cells. A nanosecond pulsed CAP treatment activates macrophages and improves wound healing[311]. CAP can also modulate phorbol 12-myristate 13-acetate-induced differentiation of U937 human monocytes to macrophages[312]. Researchers shown that CAP treatment increased calreticulin level on the cancer cells, and trigger the expression of damage-associated molecular pattern signals to locally stimulate immune cells[313,314]. Arndt et *al.* showed an up regulation of β-defensins in keratinocytes, an antimicrobial peptide active against bacteria, fungi and viruses. This fact is particularly interesting since β-defensins concentration decreases in burn wound. In cutaneous healing process, polymorphonuclear cells (PMNs) play a central role in the first inflammatory response after injury and infection. Yet little is known about the CAP impact on PMNs which are the first responders and are responsible for effective wound healing. Thus a recent study of Kupke et *al.* investigated this topic and demonstrated that CAP activates PMNs. In addition, those human cells shown an increased or decreased migration depending on the CAP treatment time the same tendency was observed for ROS production and cell stimulation. No impact on neutrophil extracellular traps (NET) formation or viability has been demonstrated[315]. In the same line for PMNs other studies demonstrated that CAP increases heme oxygenase 1 (HMOX1) and IL8 in monocytes highlighting that CAP may promote the first line of defense after a wound[316].

4.6.4. CAP in clinic

4.6.4.1. CAP on chronic and acute wounds

The initial clinical trial in 2007 for plasma device use was for rejuvenation procedures[317]. Then, CAP for regenerative medicine aimed at accelerating chronic and acute wound healing by alleviating bacterial infections. The antimicrobials effects of CAP was shown in 1990s and thus was used to help bacterial clearance in wounds as bacteria significantly slow the healing process[318].

The first randomized pilot study was done by Isbary et *al.*, 2010, authors demonstrated that CAP significantly reduced infections without side effects on microbial infection mitigation in chronic ulcer wounds[319]. In a second study the same authors reported that two-minute CAP treatments efficiently reduced microbial load and improved chronic ulcer healing[320]. In these studies, different types of ulcers were analyzed (venous, arterial, diabetic ulcers) and a significant reduction of the bacterial load was shown independently of the bacterial type. This type of chronic wounds is common especially the venous ulcers that affect 2% of the population but reduction and cure is complex and requires long-term care[321]. In addition, 15% of patients with ulcers never heals and 71% have complicated remission[322]. The complexity of chronic wound healing is mainly due to bacterial infection and the multiple strains present that have developed resistance to conventional antibacterial treatment[323]. CAP benefits were shown in different types of ulcers with promising results table 4.

Table 4: Cold atmospheric plasma applications for chronic wounds.

Wound	Plasma device	Main results	Exposure time
Chonic leg ulcers[319]	MicroPlaSter plasma	Increase wound healing, decrease of the bacterial load	5 min/day
Chronic ulcers[324]	MicroPlaSter alpha and beta		2 min/day
Chronic venous leg ulcer[325]	PlasmaDerm® VU-2012 DBD device	Strong antimicrobial effect, rapid wound size reduction	45s/cm^2 (max 11min)/3x per week/ 8 weeks
Pyoderma gangrenosum[326]	Plasma jet device with variable electrode types	Gradual healing of wound	>5min until all area was not irradiated/ every second day / 6 and 8 times
Venous ulcer[327]	MicroPlaSter α/β Torch	Greater reduction in width and length, wound healing aceleration	Daily (average of 7 treatments), 3-7min
Diabetic foot ulcer[328]	kINPen Med Jet	Acceleration of wound healing No significant difference in reduction of infection and microbial load	5xdaily, then 3x every second day, 30s/cm^2
Diabetic foot ulcer[329]	Plasma jet	After 3 weeks the wound size is significantly reduced, decrease of the bacterial load	3x week for 3 weeks, 5min

In addition, to beneficial effects in chronic wound CAP is also promising for acute wounds. CAP proved its efficiency in wound healing essentially due to increased cutaneous microcirculation, monocyte stimulation, keratinocytes and fibroblasts proliferation[330,331]. Among studies one involved patients with different size of lower extremity skin transplants with two groups: one receiving a placebo and the other treated by CAP. Results demonstrated a better healing for the CAP treated group from the second day after CAP application[332]. Gao et *al.*, investigated the effect of CAP on two traumatic wounds of the lower extremities. The first patient used mupirocin and glucocorticoid ointments with non sterile hot water to clean the wound leading to eczema in the wound and exudation and crusting. The second patient had left pretibial/ wound with no wound resolution after 2 months of antibiotics use. For the first patient 20 min CAP treatment every second day ceased wound exudation and wound healing was visible after three consecutive treatments rounds. The second patient had complete wound healing after three consecutive rounds of CAP[333]. Most of CAP application for acute wound healing are listed in table 5.

Table 5: Cold atmospheric plasma applications for acute wounds. *Adapted from Brany et al., 2020*

Wound	Plasma device	Main results	Exposure time
Traumatic wound[326]	Plasma jet with variable electrode types	Stop wound exudation, complete wound healing after three treatment procedures	20 min for the entire wound/ every two day/ 3 repetition of treatment
Burn wound[334]	Plasma jet/He	Decrease in pain and itching, increase re-epithelization	3min/ 2 times with 16 h between 1st and 2nd applications
CO_2 laser skin lesion[335]	kINPen® MED plasma jet/Ar	No side effect, improve scar recovery	3-10 s/3 days
Wounds at the donor skin graft sites[332]	Plasma jet/Ar	Rapid healing of skin graft donor sites	Daily 2 min/7 days
Dog bite wound[336]	KinPEN®VET plasma jet/Ar	Antimicrobial effects	<2 min of exposition

4.6.4.2. CAP safety and clinical trials

CAP treatment demonstrates efficiency in different fields especially in oncology or dermatology and also shows interesting antimicrobial properties. Its activity could be due to the RONS that are produced including NO, H_2O_2 or $O2^{\cdot-}$. However, its rapid mode of action in particular against bacteria involves among others lipid peroxidation, oxidative DNA damages and acidification that might be harmful on skin human cells. Therefore, the safety of CAP therapy for the human host must be carefully investigated.

Many studies investigated the safety of CAP *in vitro* and *in vivo*. Different animal models were used as mice, rabbits[337] or pigs[338] for which the skin is close to the human one. In the pig study performed by Dobrynin *et al.* researchers demonstrated that with two types of plasma devices (direct non thermal dielectric barrier discharge and indirect thermal spark discharge) CAP treatment is safe *in vivo* on intact and wounded skin. The safety was shown with doses several times higher than the ones required for inactivation of bacteria. They reported that toxic effects of CAP are related to the increase of the skin temperature which is dependent on the frequency of the discharge and the treatment time. Impact of CAP on mutagenicity is also of interest, *in vivo* and *in vitro* studies showed no increase of mutations[339,340] and the viability of skin cells was not impacted[341]. Experiments performed on skin cells in the context of cutaneous wound revealed that CAP did not induce apoptosis, cell viability *in vitro* and cell proliferation *in vivo* was not modified under applied conditions in keratinocytes[341]. Several cytotoxic studies were performed and did not show any detrimental effect of CAP in the host, however it was not performed over a long period of time. Schmidt *et al.* performed analysis one year after fourteen consecutive treatments on murine full-thickness ear wound with the kINPen device. They concluded that the skin tissue healed similarly to the control and that kINPen device was safe to use due to an absence of tumor and malignant tissue formation. In addition, the level of

cytokines and immune cells was normal indicating a physiological immune regulation without pathological or excessive inflammation[342].

The first clinical study aimed at showing the bacterial elimination and safety of CAP devices in chronic human wounds was published in 2010[319]. Isbary *et al.* shown that a 2 min argon device CAP treatment is a safe, painless and effective technique against bacteria[324]. Using the Kinpen 09 researchers also demonstrated the effect of CAP on skin physiology. They investigated the impact on epidermal barrier function, *stratum corneum*, hydration, surface temperature and irritation on seven healthy volunteers before and after plasma treatment[343]. They demonstrated that CAP leads to a decrease in beta-carotene particularly in the *stratum corneum*, slight increase of the skin temperature of 1.74°C (clinically irrelevant), increase of transepidermal water loss (TEWL), and a slight increase in skin redness. The superficial damages are in accordance with the reported enhanced penetration of topically applied substances after CAP treatment of the skin[344]. Nonetheless, the different modifications are not changed to an extent that would lead to damage to the skin or skin functions and are safe in regard to skin physiology under clinical applications. Then research revealed that CAP may accelerate healing of chronic and acute wounds[327]. A pilot study on treatment of chronic leg venous ulcers shown a reduction of 50% of the wound size in the CAP treated group[325]. Acute wound was also investigated with the example of a series of case-reports for which four sterile laser skin lesions were induced in five volunteers. Those acute wounds were treated with the kINPenMED (neoplas tools GmbH, Greifswald, Germany) with different timing (10 s, three times 10 s or 30 s) or left untreated. CAP treatment induced an early wound healing as well as 6 or 12 months after treatment[345]. A study using the MicroPlaSter β (Adtec Plasma Technology Co.Ldt., Hiroshima, Japan/London, U.K) demonstrated a significantly improved wound healing on skin graft donor sites[332]. However a meta-analysis published in 2019 of the different review and publication statistically concluded that CAP treatment based on the included studies has no significant effect on ulcers healing and reduction of bacterial bioburden[346]. This paper included 9 randomized controlled trials and cohort studies and demonstrated that even if the treatment is safe it is ineffective for wound size reduction and the bacterial log decrease is too low in comparison to other treatment modalities such as antibiotics.
Due to the vast range of plasma devices and operating parameters the term “dose” in plasma medicine is not well defined and so is controversial. Identification of optimal treatment modalities for the panel of CAP application is one of the main challenges to be solved for future clinical trials. Thus, other studies are needed in particular to determine the long term effect of CAP.

Objectives of the thesis

Despite improvements achieved in severe burn wound management those last few decades, issues of grafting and skin scarring persist. In addition, infections remain one of the main causes of death in burn units aggravated by the development of multi-resistant bacterium to formerly effective antibiotics. Since the development of plasma technology in the 19th it appears to be an innovative therapy mainly due to the reactive oxygen and nitrogen species produced.

Since the beginning of plasma application in dermatology CAP beneficial properties in wound healing were demonstrated promoting tissue re-epithelialisation and angiogenesis. Its use in burn wound field is recent, raising new questions: Will it have the same positive effects on a full-thickness burn as on a superficial burn wound? Will it allow better engraftment? Is its use not likely to cause cytotoxic, mutagenic or genotoxic effects in short or long term treatments or with repetitive applications? All these questions are worthy of interest but advances in the field of plasma medicine do not provide answers yet.
CAP is also an innovative technology against bacteria, its antimicrobial properties were demonstrated for surface, food and medical device decontamination but also for superficial wound disinfection or cutaneous diseases related to bacteria. Those promising results encourage studies on the bactericidal effects of plasma *in vivo* rising new questions on the interaction between bacteria and cells, the possible acquisition of resistance genes after CAP treatment and more particularly the effect of CAP on healthy cells surrounded an infection. However, as seen in the previous sections the lack of standardization among the devices, device parameters and protocols of plasma applications prevents comparisons often giving opposite results for the same experimental question.

CAP presents a promising therapy with multiple perspectives. In our work we are focused on an infected burn wound context. In our previous studies we demonstrated the efficiency of our plasma jet on skin engraftment and wound healing and preliminary data were obtained for its antimicrobial properties. Thus, the objective of my thesis was to investigate the pathways that can be triggered by CAP and responsible for its positive properties.

This study was focused on macrophages. This cell type was chosen because macrophages are involved in the three phases of wound healing: the inflammatory, proliferative and remodelling phase. They are essentially involved in bacterial clearance during inflammation through the process of phagocytosis.
The aim of my PhD was twofold: to determine if plasma has an impact on macrophage activity and to investigate if this activity is related to the positive effects previously observed from a macroscopic point of view during *Staphylococcus aureus* infection.

First, we investigated the impact of CAP on macrophage bactericidal activity during *S. aureus* infection trying to determine if it is mediated by oxidative mechanisms. Second, we focused on NADPH oxidase complex enzyme (NOX2) in cellular and three-dimensional models of cutaneous infection. In parallel, we also studied the impact of the plasma in an *in vivo* murine mouse model of burn wound infected with *S. aureus*. The final goal of the project was to characterize the effect of the new plasma device in biological models of wound healing. The objective was to design a device and enable the treatment of wounds with extensive surface area and to use it for the first time in a pilot study of a full-thickness burn wound reconstructed with autologous split-thickness allograft.

RESULTS

Chapter II.

CAP treatment enhances endosomal vesicle maturation in RAW264.7 murine cell line during *S. aureus* infection.

Chapter II - CAP treatment enhances endosomal vesicle maturation in RAW264.7 murine cell line during *S. aureus* infection.

In burn wounds, bacterial infections are a leading cause of death[347]. Patients with extensive burns are susceptible to opportunistic pathogens as *S. aureus* due to the open wound and the compromised immune system. During an infection monocytes reach the wound bed and differentiate into macrophages. Appart from their crucial role in wound healing phases those professional phagocytes are able to engulf microorganisms and trigger responses leading to microbial death. Among the responses macrophages induce the oxidative burst leading to the production of RONS (H_2O_2, $O2^{\cdot-}$, $ONOO^-$) that have a direct or indirect effect on bacteria viability. Macrophages are particularly of interest due to their role of effectors of tissue homeostasis, inflammation and host defence.
Despite the multiple efficient topical and systemic antimicrobials used to reduce bacterial colonization of burn wounds more and more healthcare-associated infections are caused by drug resistant pathogens[348]. New treatment strategies are urgently needed to fight antibiotic resistant bacteria. *In vitro* and *in vivo* studies in plasma medicine demonstrate the efficiency of cold atmospheric plasma on bacteria[349] and cells, skin wound infections[350], wound repair[351] or chronic wounds[352]. Those studies shown an improvement of wound healing by CAP related to its antimicrobial activity, cellular proliferation and migration and microcirculation[353]. Studies on plasma-treated cell-line derived macrophages shown a higher migratory activity[354], cytokine release[316] and elevated TNF-α[355] *in vitro*.

In this work we tried to understand the phenomenon that are involved in the decrease of bacteria viabily under CAP treatment. It is well established that CAP generates RONS that may have an important role in host immune response which lead to a decrease in bacteria survival. However, the precise mode of action inducing this effect is still unclear. In this work we hypothesized that CAP bactericidal properties in a wound healing context may be due to macrophages stimulation and particularly to an activation of their phagocytosis properties. During our preliminary experiments we noticed that the number of engulfed bacteria was not modified between helium and CAP conditions. Knowing this we assumed an indirect effect of CAP inside the cells thus we investigated CAP role on *S. aureus* internalisation inside macrophages phagosomes.

AMERICAN SOCIETY FOR MICROBIOLOGY | mSphere®

RESEARCH ARTICLE

Cold Atmospheric Plasma Promotes Killing of *Staphylococcus aureus* by Macrophages

Constance Duchesne,[a,b*] Nadira Frescaline,[a,b] Océane Blaise,[a,b] Jean-Jacques Lataillade,[a] Sébastien Banzet,[a] Olivier Dussurget,[c,d] Antoine Rousseau[b]

[a]Institut de Recherche Biomédicale des Armées, INSERM UMRS-MD 1197, Centre de Transfusion Sanguine des Armées, Clamart, France
[b]Laboratoire de physique des plasmas, École Polytechnique, Sorbonne Université, CNRS, Palaiseau, France
[c]Institut Pasteur, Unité de Recherche Yersinia, Département de Microbiologie, Paris, France
[d]Université de Paris, Sorbonne Paris Cité, Paris, France

Constance Duchesne and Nadira Frescaline contributed equally to this work. Author order was agreed based on the substantial work on the draft article.

ABSTRACT Macrophages are important immune cells that are involved in the elimination of microbial pathogens. Following host invasion, macrophages are recruited to the site of infection, where they launch antimicrobial defense mechanisms. Effective microbial clearance by macrophages depends on phagocytosis and phagolysosomal killing mediated by oxidative burst, acidification, and degradative enzymes. However, some pathogenic microorganisms, including some drug-resistant bacteria, have evolved sophisticated mechanisms to prevent phagocytosis or escape intracellular degradation. Cold atmospheric plasma (CAP) is an emerging technology with promising bactericidal effects. Here, we investigated the effect of CAP on *Staphylococcus aureus* phagocytosis by RAW 264.7 macrophage-like cells. We demonstrate that CAP treatment increases intracellular concentrations of reactive oxygen species (ROS) and nitric oxide and promotes the elimination of both antibiotic-sensitive and antibiotic-resistant *S. aureus* by RAW264.7 cells. This effect was inhibited by antioxidants indicating that the bactericidal effect of CAP was mediated by oxidative killing of intracellular bacteria. Furthermore, we show that CAP promotes the association of *S. aureus* to lysosomal-associated membrane protein 1 (LAMP-1)-positive phagosomes, in which bacteria are exposed to low pH and cathepsin D hydrolase. Taken together, our results provide the first evidence that CAP activates defense mechanisms of macrophages, ultimately leading to bacterial elimination.

IMPORTANCE *Staphylococcus aureus* is the most frequent cause of skin and soft tissue infections. Treatment failures are increasingly common due to antibiotic resistance and the emergence of resistant strains. Macrophages participate in the first line of immune defense and are critical for coordinated defense against pathogenic bacteria. However, *S. aureus* has evolved sophisticated mechanisms to escape macrophage killing. In the quest to identify novel antimicrobial therapeutic approaches, we investigated the activity of cold atmospheric plasma (CAP) on macrophages infected with *S. aureus*. Here, we show that CAP treatment promotes macrophage ability to eliminate internalized bacteria. Importantly, CAP could trigger killing of both antibiotic-sensitive and antibiotic-resistant strains of *S. aureus*. While CAP did not affect the internalization capacity of macrophages, it increased oxidative-dependent bactericidal activity and promoted the formation of degradative phagosomes. Our study shows that CAP has beneficial effects on macrophage defense mechanisms and may potentially be useful in adjuvant antimicrobial therapies.

KEYWORDS plasma jet, reactive oxygen species, reactive nitrogen species, staphylococci, phagosome maturation, LAMP-1, cathepsin D, *Staphylococcus aureus*, phagocyte, phagosome

Citation Duchesne C, Frescaline N, Blaise O, Lataillade J-J, Banzet S, Dussurget O, Rousseau A. 2021. Cold atmospheric plasma promotes killing of *Staphylococcus aureus* by macrophages. mSphere 6:e00217-21. https://doi.org/10.1128/mSphere.00217-21.

Editor Paul Dunman, University of Rochester

Copyright © 2021 Duchesne et al. This is an open-access article distributed under the terms of the Creative Commons Attribution 4.0 International license.

Address correspondence to Constance Duchesne, constance.duchesne@lpp.polytechnique.fr, or Olivier Dussurget, olivier.dussurget@pasteur.fr.

* Present address: Constance Duchesne, L'Oréal Research & Innovation, Aulnay-sous-Bois, France.

Received 5 March 2021
Accepted 20 May 2021
Published

ID: Amit.Kumar1Time: 23:39I Path: //mumnasprod/home$/joshis$/SM-MSPH210181

Macrophages are key components of the innate immune system. Along with neutrophils, they are in the first line of immune defense against infectious agents. In contrast to short-lived neutrophils, tissue macrophages are long-lived migratory cells that perform an array of immune surveillance functions and are equipped to recognize, phagocytose, and destroy microbial pathogens by oxidative and nonoxidative mechanisms (1–3). Pathogen recognition by phagocytic receptors triggers signaling cascades, leading to microbial uptake and formation of the early phagosome. Newly formed phagosomes are not initially microbicidal; a succession of fusion events between an intermediary phagosome and lysosomes results in the formation of mature phagolysosomes. During maturation, the phagosome gains microbicidal activity with progressive acidification and acquisition and activation of multiple antimicrobial components such as lactoferrin, NADPH oxidase, lysozyme, lipases, and proteases (including cathepsins) (4). This dynamic process is characterized by the appearance and disappearance of membrane proteins through successive fusion and fission between phagosomes and early endosomes, late endosomes, and, finally, lysosomes. New phagosomes rapidly acquire early endosome proteins such as early endocytic antigen 1 (EEA1) and the small GTPase Rab5. Further phagosome maturation leads to progressive loss of Rab5, recruitment of Rab7 mediating fusion with late endosomes, and acquisition of lysosomal-associated membrane proteins (LAMPs) (5).

Despite the potency of macrophage antimicrobial arsenal, some pathogenic bacteria have developed strategies to preclude pathogen degradation (6). For instance, some intracellular pathogens prevent phagosome-lysosome fusion, while others modify the intraphagosomal environment or escape into the cytosol (7). Increasing evidence suggests that *Staphylococcus aureus*, an important human pathogen that causes a wide range of clinical infections (8), has evolved mechanisms to evade intracellular defense mechanisms that may lead to replication within macrophages (9). Infected macrophages may form reservoirs that lead to bacterial persistence and cause recurrence of infection (10). Furthermore, *S. aureus* is notorious for its ability to become resistant to antibiotics, which poses a great challenge for infection control by limiting treatment options (11, 12).

Cold atmospheric plasma (CAP) refers to partially ionized gases that are globally neutral, since the density of positively charged species is equivalent to that of the negatively charged species. CAP is produced by electrical discharge in a neutral gas (see Fig. S1 in the supplemental material). Due to their high reactivity and temperature close to room temperature, cold plasmas are appropriate for biological applications (13). Cold plasmas are known to produce thermal radiation, reactive radicals, ions and electrons, visible light, UV radiation, and electromagnetic fields. Their interactions with ambient air lead to the production of reactive species that can induce multiple biological effects. Chemical species produced at significant concentrations include reactive oxygen and nitrogen species (RONS) such as ozone, superoxide anion, and hydrogen peroxide, and nitrogen oxides (NO), including nitrite, nitrate and nitric oxide (Fig. S1). Previous studies showed that low CAP energy deposition has stimulating effects on the proliferation and migration of cells, whereas high-energy deposition induces lethal effects that are studied for cancer treatment (14–16). We recently reported that treatment with CAP promotes cutaneous tissue repair (14). In addition to its prohealing properties, CAP has previously been shown to have antimicrobial properties (17–23). The mode of action of CAP is not completely understood; however, it is reasonable to speculate that RONS, which are generated by CAP, may have an important role in enhancing host immune response, leading to reduced survival of pathogenic bacteria. Thus, we hypothesized that CAP could stimulate elimination of bacteria by macrophages. In this study, we demonstrate that CAP treatment is associated with enhanced killing of both methicillin-sensitive *S. aureus* (MSSA) and methicillin-resistant *S. aureus* (MRSA) strains following phagocytosis by macrophages. This effect is mediated by oxidative mechanisms, since antioxidants inhibit CAP-dependent bactericidal activity of macrophages. Furthermore, CAP treatment promotes phagosome maturation into a

ID: Amit.Kumar1Time: 23:39I Path: //mumnasprod/home$/joshis$/SM-MSPH210181

degradative vesicle. Our study uncovers the ability of CAP to enhance phagosomal defense mechanisms in infected macrophages.

RESULTS

CAP treatment is associated with increased intracellular levels of reactive oxygen species and NO in macrophages. To investigate if CAP could modulate macrophage defenses, we measured the intracellular RONS levels upon CAP treatment of RAW264.7 cells infected or not with *S. aureus*. We first determined the levels of intracellular reactive oxygen species (ROS) by measuring 2,7-dichlorodihydrofluorescein diacetate (DCFH-DA) fluorescence in macrophages following CAP treatment. CAP induced a significant increase in intracellular ROS levels in both infected and noninfected macrophages compared to those in untreated macrophages ($P < 0.05$ and $P < 0.01$, respectively; one-way analysis of variance [ANOVA] followed by Dunn's posttest; $n = 9$) (Fig. 1A). As expected, ROS levels did not increase when cells were incubated with antioxidant *N*-acetyl cysteine (NAC) prior to CAP treatment (one-way ANOVA followed by Dunn's posttest; $n = 3$) (Fig. 1B). Higher levels of intracellular ROS were also detected upon 8 μM H_2O_2 treatment compared to those in untreated macrophages, which corresponds to the concentration of H_2O_2 produced by the CAP treatment under our experimental conditions ($P < 0.05$; one-way ANOVA followed by Dunn's posttest; $n = 3$) (Fig. 1B). Interestingly, ROS levels were lower than those upon CAP treatment, unless a much higher concentration of H_2O_2 was used (Fig. S2A). We next determined the levels of nitrogen oxides (NO) by measuring 4-amino-5-methylamino-2′,7′-diacetate fluorescein (DAF-FM DA) fluorescence in macrophages following CAP treatment. The levels of intracellular NO were significantly higher in macrophages treated by CAP than those in untreated macrophages, irrespective of *S. aureus* infection ($P < 0.05$; one-way ANOVA followed by Dunn's posttest; $n = 9$) (Fig. 1C). As expected, NO levels were also increased in macrophages treated with the NO donor *S*-nitroso-*N*-acetyl-DL-penicillamine (SNAP) (see Fig. S2B) in the supplemental material. To determine if CAP treatment was toxic to cells, we measured the apoptosis and the viability of RAW264.7 macrophages. We first evaluated apoptosis levels of macrophages by terminal deoxynucleotidyltransferase-mediated dUTP-biotin nick end labeling (TUNEL) assay upon CAP treatment. Untreated macrophages and CAP treated-macrophages showed similarly low levels of apoptosis by TUNEL staining (Student's *t* test; $n = 3$) (Fig. 1D and E). In contrast, DNase I treatment, as expected, led to massive DNA damage (Fig. 1D). We next determined cellular viability using the WST-1 assay at 24 and 48 h after CAP treatment. Untreated macrophages and macrophages treated with CAP for 30 s had similar viabilities at both time points (Mann-Whitney U test; $n = 6$) (Fig. 1F). Increasing the treatment duration to 90 or 180 s did not lead to any significant increase in cell mortality. Together, our results indicate that macrophage intracellular ROS and NO levels are increased upon CAP treatment without any significant cellular toxicity.

CAP treatment increases *S. aureus* killing by macrophages in an ROS-dependent manner. Having demonstrated that CAP affects macrophage defenses, we next investigated if CAP could increase the bactericidal activity of macrophages. A gentamicin protection assay was used to evaluate the impact of CAP treatment on phagocytosis and intracellular bacterial survival. Phagocytosis of *S. aureus* by RAW264.7 macrophages was very efficient at 37°C (Fig. 2A), while it was expectedly blocked at 4°C (see Fig. S3 in the supplemental material), irrespective of treatment. The percentage of internalized bacteria was similar in CAP-treated and untreated macrophages at 1 h postinfection (Fig. 2A). Thus, CAP treatment does not significantly influence the capacity of macrophages to internalize *S. aureus*. However, the number of viable intracellular bacteria was significantly lower in CAP-treated macrophages than those in untreated macrophages at 2, 5, and 7 h postinfection (h p.i.) ($P < 0.05$ at 2 h p.i. and $P < 0.01$ at 5 and 7 h p.i.; 2-way ANOVA followed by Tukey's posttest; $n = 4$) (Fig. 2B; see also Fig. S4 in the supplemental material). We next wondered if CAP could also enhance killing by macrophages of an antibiotic-resistant strain of *S. aureus*, the MRSA strain USA300. The percentage of intracellular bacteria was lower in macrophages treated by CAP than

ID: Amit.Kumar1Time: 23:39I Path: //mumnasprod/home$/joshis$/SM-MSPH210181

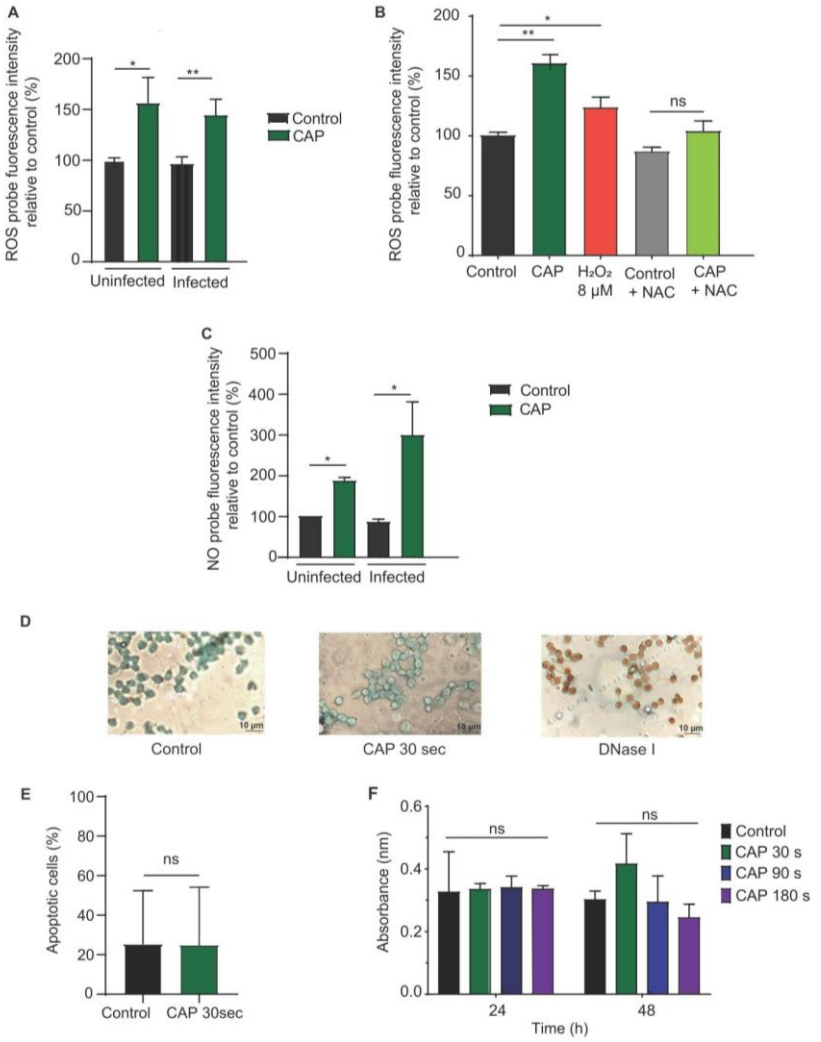

FIG 1 Cold atmospheric plasma (CAP) treatment increases the levels of reactive oxygen species (ROS) and nitrogen oxides (NO) in macrophages without altering their viability. (A to C) RAW 264.7 macrophages were left uninfected or were infected with *Staphylococcus aureus* Xen36 for 1 h, and nonengulfed bacteria were killed using gentamicin for a 30-min period before treatment with CAP. (A) RAW-264.7 macrophages were incubated with 20 μM fluorogenic 2,7-dichlorodihydrofluorescein diacetate (DCFH-DA) to quantify intracellular ROS. Relative fluorescence of cells untreated (control) or treated with CAP for 30 s was measured 45 min after treatment. Data are mean ± standard error of the mean (SEM) (*, $P < 0.05$; **, $P < 0.01$, ns, nonsignificant; one-way analysis of variance [ANOVA] followed by Dunn's posttest; $n = 9$). (B) RAW-264.7 macrophages were incubated with 20 μM DCFH-DA for 45 min to quantify intracellular ROS. Relative fluorescence of uninfected cells treated with 8 μM H_2O_2, or with CAP for 30 s, with or without 1 mM *N*-acetyl cysteine (NAC), was measured using a fluorescence microplate reader. Data are mean ± SEM (*, $P < 0.05$; **, $P < 0.01$, ns, nonsignificant; one-way ANOVA followed by Dunn's posttest; $n = 3$). (C) RAW-264.7 macrophages were incubated with 5 mM fluorescent 4-amino-5-methylamino-2′,7′-diacetate fluorescein (DAF-FM DA) for 1 h to quantify the level of intracellular NO. Relative fluorescence of cells untreated (control) and cells treated with CAP for 30 s was measured by flow cytometry. Data are mean ± SEM (*, $P < 0.05$, ns, nonsignificant; one-way ANOVA followed by Dunn's posttest; $n = 9$). (D) Representative images of terminal deoxynucleotidyltransferase-mediated dUTP-biotin nick end labeling (TUNEL) staining of RAW 264.7 cells left untreated (control), 24 h after CAP treatment for 30 s or after treatment with 1 μg/μL DNase I, used as a positive control. Brown nuclear staining with 3,3′-diaminobenzidine (DAB) indicates DNA damage. DNA was counterstained with methyl green. (E) Quantitative detection of apoptosis by TUNEL assay at 24 h posttreatment. Data are mean ± SEM (Student's *t* test; $n = 3$; ns, nonsignificant). (F) Analysis of cellular viability using the WST-1 assay on RAW 264.7 cells left untreated (control), or at 24 and 48 h after CAP treatment for 30, 90, or 180 s. Data are mean ± SEM (Mann-Whitney U test; $n = 6$; ns, nonsignificant).

ID: Amit.Kumar1Time: 23:39I Path: //mumnasprod/home$/joshis$/SM-MSPH210181

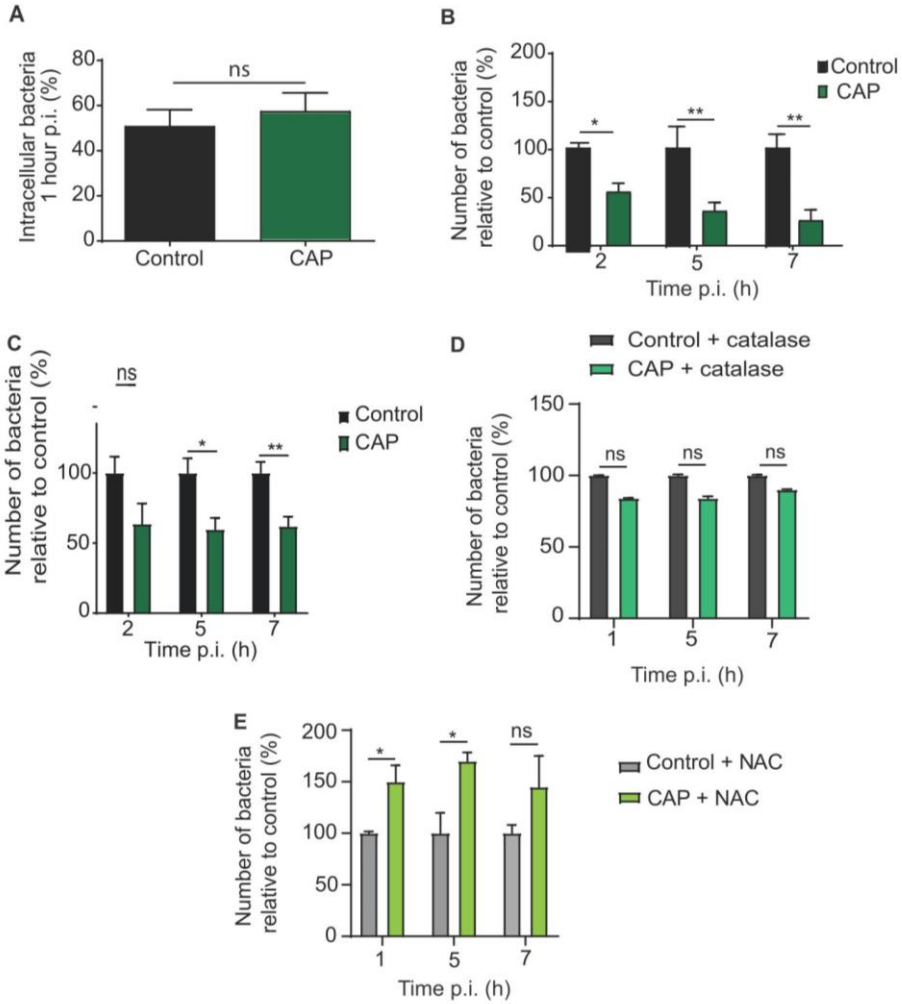

FIG 2 CAP treatment promotes elimination of *S. aureus* in macrophages. RAW 264.7 macrophages were treated with CAP or left untreated (control) in 24-well plates at a voltage of 32 kV, a gap of 5 mm, and a helium mass flow of 500 sccm. After incubation overnight, cells were infected with *S. aureus* Xen36 or USA300 strains. (A) Relative number of *S. aureus* Xen36 contained in macrophages 1 h postinfection, corresponding to the ratio of the number of internalized bacteria to the total number of bacteria used to infect cells. (B) Number of *S. aureus* Xen36 bacteria contained in macrophages at 2, 5, and 7 h postinfection (h p.i.) after CAP treatment relative to the number of bacteria contained in untreated macrophages (*, $P < 0.05$; **, $P < 0.01$; ****; $P < 0.0001$, CAP versus control; 2-way ANOVA followed by Tukey's posttest). Three independent experiments were performed with 4 to 6 replicates per conditions. (C) Number of *S. aureus* USA300 bacteria contained in macrophages at 2, 5, and 7 h postinfection after CAP treatment relative to the number of bacteria contained in untreated macrophages (*, $P < 0.05$; **, $P < 0.01$, CAP versus control; 2-way ANOVA followed by Tukey's posttest; $n = 3$). (D) Number of *S. aureus* Xen36 bacteria contained in macrophages at 1, 5, and 7 h postinfection after CAP treatment relative to the number of bacteria contained in untreated macrophages in the presence of 0.1 mg/ml catalase. (E) Number of *S. aureus* Xen36 bacteria contained in macrophages at 1, 5, and 7 h postinfection after CAP treatment relative to the number of bacteria contained in untreated macrophages in the presence of 1 mM NAC (*, $P < 0.05$, CAP plus NAC versus NAC only; 2-way ANOVA followed by Tukey's posttest; $n = 5$).

that in untreated macrophages ($P < 0.05$ at 5 h p.i. and $P < 0.01$ at 7 h p.i.; 2-way ANOVA followed by a Tukey's posttest; $n = 3$) (Fig. 2C). Thus, CAP treatment promotes killing of both MSSA and MRSA strains by macrophages. These effects were not due to enhanced gentamicin permeability following CAP treatment because the intracellular concentration of gentamicin was similar in macrophages treated with CAP and in untreated cells (see Fig. S5 in the supplemental material). Additionally, intracellular gentamicin concentration stayed under its MIC for *S. aureus* Xen36 (i.e., 8 μg/ml),

ID: Amit.Kumar1Time: 23:39I Path: //mumnasprod/home$/joshis$/SM-MSPH210181

irrespective of treatment, even when the protection assay was performed with 50 μg/ml of gentamicin (Fig. S5). Furthermore, CAP treatment did not increase cell death or proliferation, as the number of macrophages did not differ between conditions (Fig. 1D to F). Along these lines, levels of macrophage cell surface and intracellular markers, including those of growth factors and cytokines, remained unchanged in response to CAP treatment (see Fig. S6A and S6B in the supplemental material). Since we observed a link between CAP treatment and ROS production by macrophages, we next investigated the role of oxidative defenses in CAP-dependent killing of *S. aureus*. Bacterial survival was quantified in macrophages treated or not with CAP and in the presence of catalase and NAC. Catalase inhibited the effect of CAP on bacterial killing, and the combination of CAP and NAC even increased the number of bacteria ($P < 0.05$; 2-way ANOVA followed by Tukey's posttest; $n = 5$) (Fig. 2D and E). It is of note that direct CAP treatment of *S. aureus* can also induce the death of bacteria in an ROS-dependent manner ($P < 0.01$; one-way ANOVA followed by Dunn's posttest; $n = 6$ to 9) (see Fig. S7A and B in the supplemental material). Together, our results show that CAP increases the bactericidal activity of macrophages in an ROS-dependent manner, without affecting their capacity to internalize bacteria.

CAP treatment is associated with increased numbers of acidic, LAMP-1-, and cathepsin D-positive vesicles in macrophages infected with *S. aureus*. Having established that CAP stimulates bactericidal activity of macrophages by oxidative mechanisms, we next wondered whether CAP had additional effects on macrophage defense mechanisms and analyzed the phagosomal maturation upon CAP treatment of macrophages infected with *S. aureus*. Bacteria and markers of early (EEA1 and Rab5) and late (LAMP-1 and cathepsin D) phagosomes were detected by immunofluorescence at 20 min, 1 h, and 6 h postinfection. After 20 min of infection, *S. aureus* was detected in EEA1-positive phagosomes (Fig. 3A) and in Rab5-positive phagosomes (Fig. 3B) of both CAP-treated and untreated macrophages. At that time point, more than 70% of *S. aureus*-containing phagosomes were positive for EEA1 and Rab5, while only ~10% were positive for LAMP-1 (Table 1). As expected, the percentage of bacteria associated with early phagosomal markers decreased with time (Table 1). CAP treatment did not lead to any significant change in the number of early phagosomes associated with *S. aureus* (Mann-Whitney *t* test) (Table 1). The number of bacteria associated with late phagosomal markers progressively increased over time (Table 1). By 1 h postinfection, the number of LAMP-1-positive phagosome containing bacteria increased to 25%. At 6 h postinfection, the percentage of LAMP-1-positive *S. aureus*-containing phagosomes reached 36% in untreated macrophages (Table 1). Strikingly, the number of LAMP-1-positive phagosomes containing bacteria was higher in macrophages treated with CAP than that in untreated macrophages (Fig. 4). The percentage of phagosomes showing an association between *S. aureus* and LAMP-1 increased to 46% upon CAP treatment ($P < 0.05$, Mann-Whitney *t* test) (Table 1). To confirm that CAP modulated late stages of phagosome maturation, we next imaged and quantified the association of the lysosomal enzyme cathepsin D with phagosomes containing *S. aureus*. At 1 h after infection, a third of the phagosomes were positive for cathepsin D, irrespective of CAP treatment (Table 1). After 6 h of infection, *S. aureus* was also detected in cathepsin D-positive phagosomes of both CAP-treated and untreated macrophages (Fig. 5). However, the percentage of *S. aureus*-containing phagosomes that were positive for cathepsin D was higher in CAP-treated macrophages than that in untreated macrophages, i.e., 53 and 43%, respectively ($P < 0.01$, Mann-Whitney *t* test) (Table 1). Interestingly, *S. aureus* localized to cathepsin D-positive acidic phagosomes (Fig. 5), and phagosomal acidification was promoted by CAP treatment ($P < 0.001$, Mann-Whitney *t* test) (Table 1). To confirm our quantification based on microscopic observations, we determined the levels of markers on phagosomes isolated from infected macrophages upon CAP treatment. To verify the purity of isolated phagosomes, known cellular organelle markers were probed. Nuclear matrix protein p84 was mostly detected in the nuclear fraction, and the ubiquitous GAPDH was detected in all fractions, while LAMP-1 and cathepsin D were clearly only present in the phagosomal fraction (Fig. 6A). Western blot analysis demonstrated that CAP treatment

ID: Amit.Kumar1Time: 23:39I Path: //mumnasprod/home$/joshis$/SM-MSPH210181

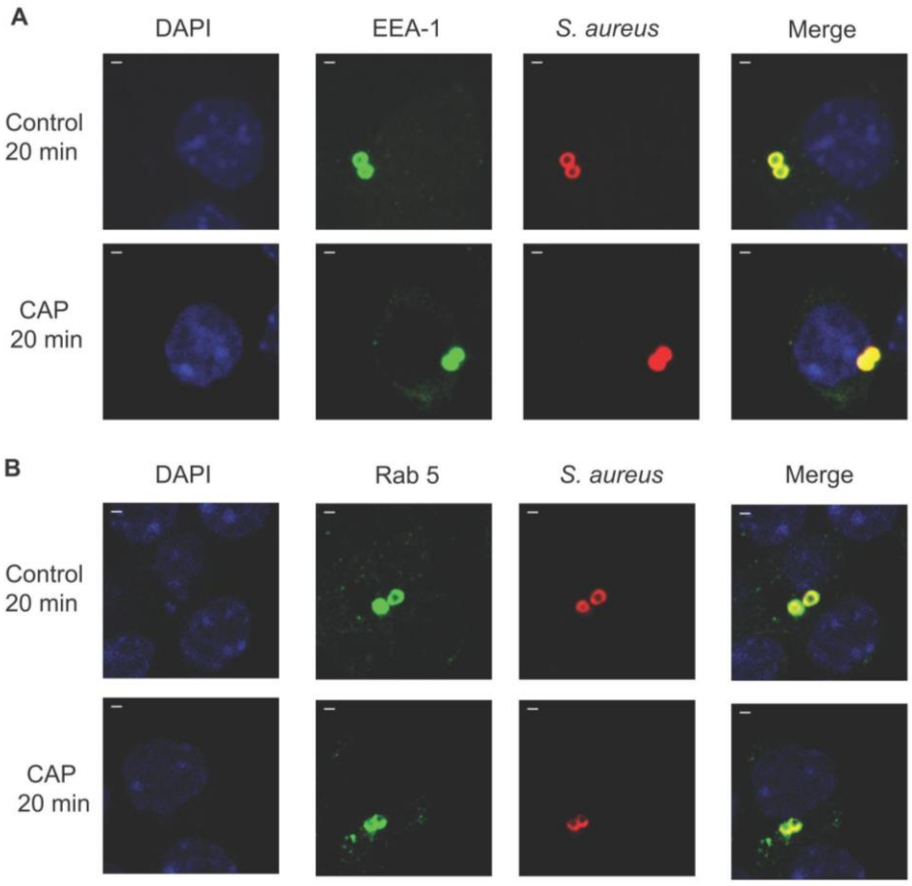

FIG 3 CAP treatment does not influence the acquisition of early phagosomal markers in macrophages infected with *S. aureus*. CAP-treated or untreated RAW-264.7 macrophages were infected with *S. aureus* Xen36 (multiplicity of infection [MOI] = 10), and markers of early phagosomes were analyzed by immunofluorescence at 20 min postinfection. (A) Representative confocal images of EEA-1 staining. EEA-1 (green), bacteria (red), nucleus (blue), EEA-1/bacteria colocalization (yellow). DAPI, 4′,6-diamidino-2-phenylindole. (B) Representative confocal images of Rab5 staining. Rab5 (green), bacteria (red), nucleus (blue), Rab5/bacteria colocalization (yellow). Bar, 5 μm.

significantly increased the levels of both LAMP-1 and cathepsin D in the 60 to 40% fractions of *S. aureus*-infected macrophages by 6 h postinfection ($P < 0.05$, Student's t test; $n = 3$) (Fig. 6B). Together, these results suggest that CAP treatment promotes the formation of degradative organelles upon phagocytosis of *S. aureus*.

TABLE 1 Percentage of colocalization of *S. aureus* Xen36 bacteria with phagosome markers in RAW 264.7 cells untreated (control) and treated with CAP

	Colocalization % at time p.i.[a]:					
	20 min		1 h		6 h	
Phagosome marker	Control	CAP	Control	CAP	Control	CAP
EEA-1	79.8 ± 1.8	77.5 ± 1.3	48.3 ± 3.8	45.9 ± 3.4	26.2 ± 2.9	30.7 ± 2.6
Rab5	72.0 ± 1.5	70.4 ± 1.1	51.4 ± 2.1	50.4 ± 2.2	16.0 ± 0.6	16.1 ± 0.8
LAMP-1	12.1 ± 1.4	10.6 ± 0.7	25.1 ± 1.7	29.5 ± 3.4	36.0 ± 2.8	46.5 ± 2.5[b]
Cathepsin D	ND	ND	36.6 ± 5.7	31.6 ± 3.4	43.8 ± 1.5	53.6 ± 1.4[c]
Lysotracker	ND	ND	37.5 ± 5.2	28.7 ± 4.3	44.3 ± 2.7	61.1 ± 2.2[c]

[a]Mean value ± standard error of the mean (SEM). ND, not determined; p.i., postinfection.
[b]$P < 0.05$; Mann-Whitney t test.
[c]$P < 0.001$; Mann-Whitney t test.

ID: Amit.Kumar1Time: 23:39I Path: //mumnasprod/home$/joshis$/SM-MSPH210181

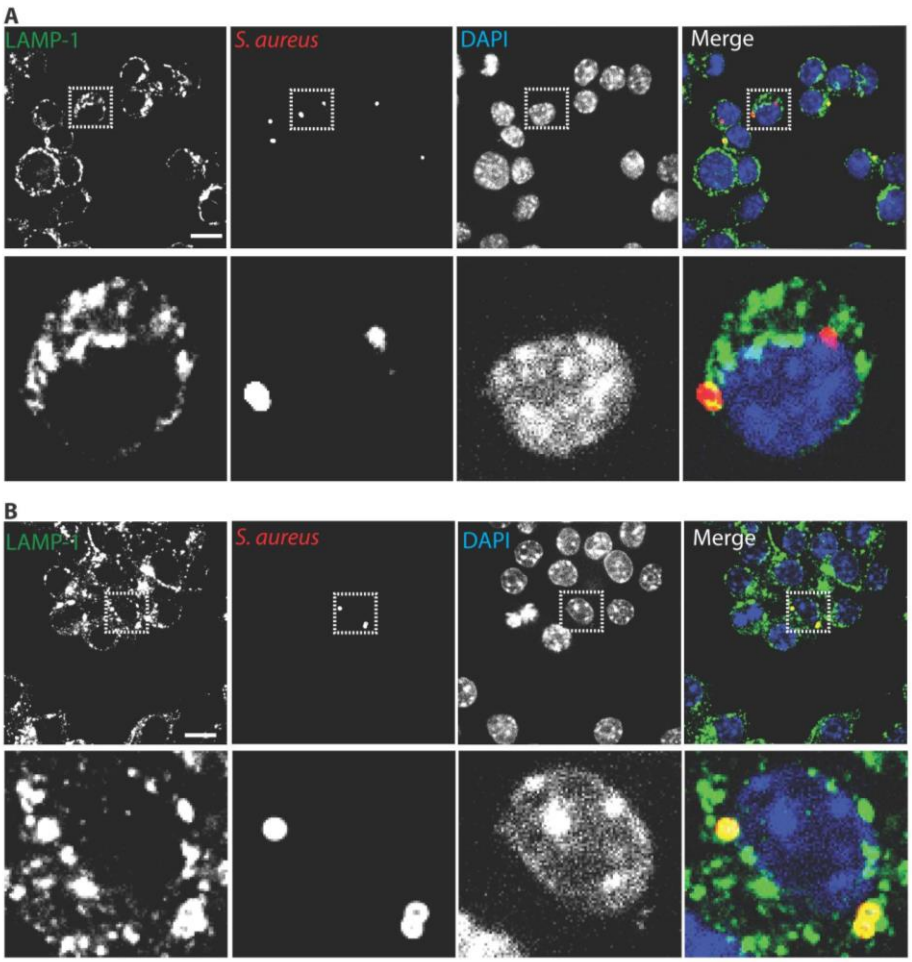

FIG 4 CAP treatment promotes the recruitment of LAMP-1, a late phagosomal marker, in macrophages infected with *S. aureus*. CAP-treated and untreated RAW-264.7 cells were infected with *S. aureus* Xen36 (MOI = 10), and LAMP-1 recruitment was analyzed by immunofluorescence at 6 h postinfection. Representative confocal images of LAMP-1 staining in untreated RAW-264.7 cells (A) and in CAP-treated RAW-264.7 cells (B). LAMP-1 (green), bacteria (red), nucleus (blue), LAMP-1/bacteria colocalization (yellow). Upper panels are ×63 magnification; bar, 20 μm. Lower panels represent enlarged views of the boxed regions.

DISCUSSION

The ability of some pathogenic bacteria to escape immune defense mechanisms and the emergence of multidrug resistance pose a significant threat to human health (24). Unprecedented global spread of antibiotic-resistant bacteria, coupled with a low number of preclinical and clinical antibacterial drugs in the pipeline, highlights the urgent need for the development of pathogen-specific and adjunctive antimicrobial approaches (25). *S. aureus* has been listed by the World Health Organization in the ESKAPE (*Enterococcus faecium*, *Staphylococcus aureus*, *Klebsiella pneumoniae*, *Acinetobacter baumannii*, *Pseudomonas aeruginosa*, and *Enterobacter* species) group of bacteria against which new therapeutics are urgently required (26). *S. aureus* displays an arsenal of virulence factors that allow it to persist intracellularly within macrophages by impairing host cell defenses such as phagosomal acidification, phagosome maturation, and cathepsin D activation (27). In this study, we investigated the effect of CAP on the phagocytic activity of RAW 264.7 macrophages infected with *S. aureus*. While CAP treatment did not influence the ability of macrophages to engulf bacteria, it significantly increased the bactericidal activity of infected macrophages. Interestingly, killing of both MSSA and MRSA strains was

ID: Amit.Kumar1Time: 23:39I Path: //mumnasprod/home$/joshis$/SM-MSPH210181

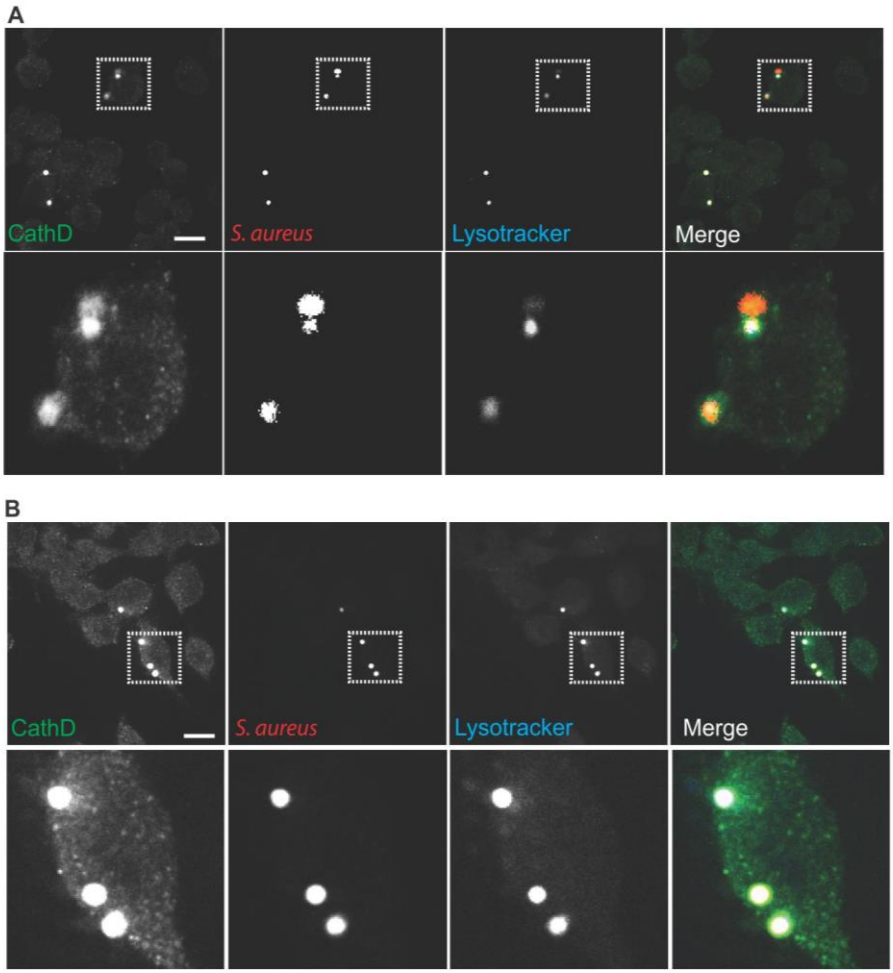

FIG 5 CAP treatment is associated with recruitment of cathepsin D and with phagosome acidification in macrophages infected with *S. aureus*. CAP-treated and untreated RAW-264.7 cells were infected with *S. aureus* Xen36 (MOI = 10). Cathepsin D recruitment and phagosomal acidification were analyzed by immunofluorescence at 6 h postinfection. Representative images of cathepsin D staining and LysoTracker signal in untreated RAW-264.7 cells (A) and in CAP-treated RAW-264.7 cells (B). Cathepsin D (green), LysoTracker (blue), bacteria (red), cathepsin D/bacteria colocalization (yellow), cathepsin D/LysoTracker/bacteria colocalization (white). Upper panels are ×63 magnification; bar, 20 μm. Lower panels represent enlarged views of the boxed regions.

increased by CAP. This finding is significant because the clinical MRSA strain USA300 that was used in this study is highly virulent and has been shown to survive in macrophages by perturbing phagolysosome formation (28). Given that CAP has previously been shown to induce changes in cellular membrane permeability (29, 30), we wondered if the increase in bacterial killing could be due to elevated intracellular gentamicin concentration induced by CAP. This hypothesis was refuted by our data, which clearly demonstrated that CAP did not change the intracellular concentration of gentamicin, which remained at subinhibitory levels. Our results suggest that the increased bacterial killing associated with CAP was not due to changes in cellular viability either.

CAP is a source of a wide variety of potentially bactericidal ROS, such as hydrogen peroxide, superoxide, hydroxyl radicals, and ozone, and of reactive nitrogen species (RNS), including nitrite, nitrate and NO (31). Likewise, phagocyte activation results in the production of intracellular ROS derived from NADPH oxidase (NOX2) and of RNS, which are generated as a result of enzymatic activity of inducible nitric oxide synthase (iNOS/NOS2) (32). Robust production of RONS is critical for the elimination of microbial

ID: Amit.Kumar1Time: 23:39I Path: //mumnasprod/home$/joshis$/SM-MSPH210181

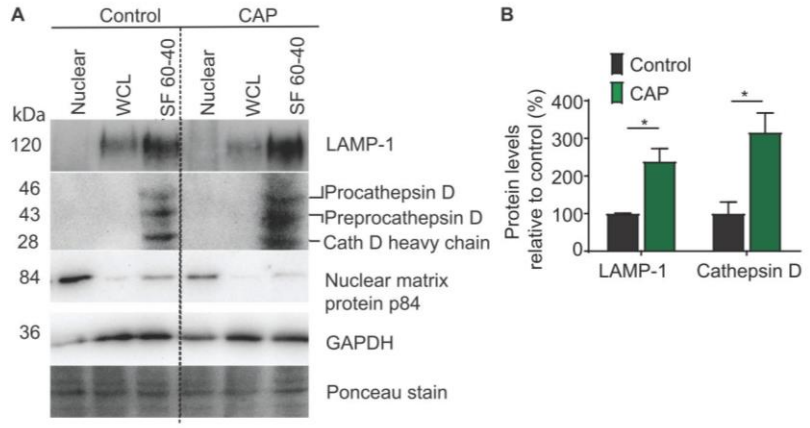

FIG 6 CAP treatment increases the levels of phagosomal LAMP-1 and cathepsin D in macrophages infected with *S. aureus*. Untreated (control) and CAP-treated RAW 264.7 cells were infected with *S. aureus* Xen36 (MOI = 10) and submitted to subcellular fractionation at 6 h postinfection. (A) Western blot analysis of nuclear fraction, whole-cell lysate (WCL), and subcellular fraction 60 to 40% (SF 60-40) of control (left) and CAP-treated (right) cells upon sucrose gradient ultracentrifugation. The same amount of total protein (40 μg) was analyzed for each fraction. Samples were immunoblotted with anti-LAMP-1, anti-cathepsin D, anti-nuclear matrix protein p84, and anti-GAPDH antibodies. Ponceau staining of polyvinylidene difluoride (PVDF) blotting membrane was used as a loading control. LAMP-1, lysosomal-associated membrane protein 1; GADPH, glyceraldehyde 3-phosphate dehydrogenase. (B) Relative levels of LAMP-1 and cathepsin D in SF 60-40 of *S. aureus*-infected RAW 264.7 cells. Values are means ± SEM of three replicates (*, $P < 0.05$, Student's *t* test; $n = 3$).

pathogens (33–39). Thus, we hypothesized that oxidative mechanisms could contribute to bacterial killing by macrophages treated with CAP. We demonstrated that the action of CAP was ROS dependent because dismutation of hydrogen peroxide by catalase and ROS scavenging by NAC inhibited CAP-dependent bacterial killing by macrophages. NAC even promoted *S. aureus* survival after CAP treatment, possibly through redox control of cellular defense components and/or bacterial factors. Moreover, CAP treatment rapidly increased intracellular ROS concentration in macrophages. Upon CAP treatment, bacterial killing by macrophages could rely on both endogenous and exogenous ROS (40). However, in our experimental design, macrophages were treated 24 h before the infection. This design does not support a direct bactericidal role for CAP-generated exogenous ROS, and it can reasonably be hypothesized that macrophage endogenous ROS were increased upon CAP treatment, leading to increased bactericidal effects. We also demonstrated that the intracellular concentration of NO in macrophages increases immediately after CAP treatment. NO possesses important immunologic functions (41–43) and reacts with superoxide anion ($O_2^{\cdot -}$) to produce peroxynitrite, a powerful oxidant capable of inactivating intramacrophagic microorganisms (44). Thus, the capacity of CAP to rapidly deliver and promote formation of both ROS and RNS in macrophages possibly contributes to overcoming bacterial immune escape strategies and to controlling infection. The composition of CAP is complex, and its physical components (e.g., UV and electromagnetic fields) may have a biological activity independently of and/or in synergy with its chemical components. When exposed to CAP, bacteria can, for instance, be altered by UV radiation and electromagnetic fields (45–47). In macrophages, NADPH oxidase generates $O_2^{\cdot -}$ through electron transfer from cytosolic NADPH to oxygen, producing electron current (48). Therefore, it is reasonable to hypothesize that electric fields generated by CAP contribute to the modulation and activation of the phagocyte NADPH oxidase complex.

Oxidative killing in macrophages occurs in a dynamic process of maturation of the phagosome. During phagosomal maturation, macrophages also eliminate phagocytosed microbes by nonoxidative mechanisms, such as acidification and proteolytic degradation along phagosome maturation pathways (5). We hypothesized that CAP could modulate

ID: Amit.Kumar1Time: 23:39I Path: //mumnasprod/home$/joshis$/SM-MSPH210181

the phagosome maturation of infected macrophages. CAP treatment did not affect the early stages of phagosome maturation. Indeed, EEA-1- and Rab5-positive compartments progressed to LAMP-1-positive compartments with rapid loss of both EEA1 and Rab5 in late phagosomes by 6 h postinfection, independently of CAP treatment. In contrast, CAP promoted association of LAMP-1 and cathepsin D with phagosomes containing *S. aureus*. These results suggest that CAP treatment favors the maturation of phagosomes into phagolysosomes. The colocalization of *S. aureus* and cathepsin D at 6 h postinfection occurred in acidic phagosomes, which promote the activity of hydrolases. Furthermore, the localization of *S. aureus* within acidic phagosomes was significantly increased upon CAP treatment. The molecular mechanisms underlying the effect of CAP on phagosome maturation remain to be determined. CAP could possibly promote phagosomal maturation through upregulation of intracellular ROS production, as has recently been shown for bioactive lipid lysophosphatidylcholine (49). In conclusion, we have shown here that CAP enhances macrophage defense mechanisms upon *S. aureus* infection. As the capacity of *S. aureus* to survive intracellularly contributes to its pathogenicity, CAP is an attractive adjuvant therapeutic candidate that could be used in the health care setting to control staphylococcal infections.

MATERIALS AND METHODS

Cold atmospheric plasma. CAP was generated using a device that we previously described (15). Briefly, CAP was generated in a dielectric polylactic acid (PLA) capillary flown with helium and using a high-voltage electrode surrounding the capillary. CAP was propagated from the source to the target in the form of a single-channel plasma jet. RONS are formed at the output of the capillary when plasma interacts with ambient air. High voltage was set to 32 kV, and helium mass flow was set to 500 sccm, leading to a power of 80 ± 10 W. Production of long-lived species in liquid exposed to CAP increased proportionally with treatment time. The concentrations of H_2O_2, NO_2^-, and NO_3^- that corresponded to a 30-s CAP treatment were 8, 1.2, and 0.5 μM, respectively.

Bacteria and growth conditions. *S. aureus* Xen36, an MSSA strain derived from a clinical isolate of a bacteremic patient, was obtained from PerkinElmer (Villebon-sur-Yvette, France). *S. aureus* USA300, a highly virulent MRSA strain involved in multiple outbreaks in healthy individuals, was obtained from ATCC (reference BAA-1717). Bacteria were grown aerobically at 37°C in brain heart infusion (BHI) broth (BD Biosciences, San Jose, CA) with shaking at 200 rpm or on BHI agar plates.

Cell line and culture conditions. The murine macrophage-like cell line RAW 264.7 (ATCC, Molsheim, France) was grown in RPMI medium (Gibco, Paisley, PA) supplemented with 4 mM GlutaMax and 1 mM sodium pyruvate (Thermo Fisher Scientific, Waltham, MA) and 10% fetal bovine serum (BioWest, Nuaillé, France) at 37°C in 10% CO_2 atmosphere.

Quantification of ROS levels in macrophages. RAW 264.7 cells were seeded onto 24-well plates at a density of 10^5 cells per well. RAW 264.7 cells were left uninfected or were infected with *S. aureus* Xen36 at a multiplicity of infection (MOI) of 10:1 for 1 h. Cells were incubated in 20 μg/ml gentamicin-containing medium for 30 min before treatment with CAP to kill extracellular bacteria. They were then incubated with the cell-permeant fluorogenic ROS probe DCFH-DA (Sigma-Aldrich Ltd., Dublin, Ireland) at a final concentration of 20 μM for 5 min at 37°C. Cells were treated with CAP or H_2O_2 (Sigma-Aldrich, St. Louis, MO) at a concentration corresponding to the one produced by our CAP treatment conditions (8 μM). CAP treatment was performed in culture medium or in culture medium supplemented with 1 mM NAC (Sigma-Aldrich, St. Louis, MO). After 45 min of incubation, cells were resuspended in phosphate-buffered saline (PBS). The suspension was transferred into a 96-well microplate, and fluorescence was measured using a Synergy HT multimode microplate reader (BioTek Instruments, Winooski, VT) at excitation and emission wavelengths of 485 nm and 525 nm, respectively.

Quantification of NO levels in macrophages. RAW 264.7 cells were seeded onto 24-well plates at a density of 10^5 cells per well. RAW 264.7 cells were left uninfected or were infected with *S. aureus* Xen36 (MOI = 10) for 1 h. Cells were incubated in 20 μg/ml gentamicin-containing medium for 30 min before treatment with CAP to kill extracellular bacteria. They were then incubated with the cell-permeant fluorescent NO probe DAF-FM DA (Sigma, Saint-Quentin-Fallavier, France) at a final concentration of 5 mM for 5 min at 37°C before treatment. A solution of the NO donor SNAP (Sigma-Aldrich, St. Louis, MO) at 45 μM was used as a positive control. After 1 h of incubation at 37°C, cells were resuspended in PBS, and fluorescence was measured by flow cytometry at 500 nm (CytoFlex S; Beckmann-Coulter, Villepinte, France).

Quantification of bacteria survival in macrophages. RAW 264.7 cells were seeded onto 24-well plates at a density of 10^5 cells per well. Cells were treated with CAP for 30 s in fresh culture medium or were left untreated, then incubated at 37°C overnight. For inhibition assays, 1 mM NAC (Sigma-Aldrich, St. Louis, MO) or 0.1 mg/ml catalase (Sigma-Aldrich, St. Louis, MO) were added to the culture medium before CAP treatment. Cells were infected with *S. aureus* at an MOI of 10:1 and incubated for 1 h at 37°C to allow phagocytosis or at 4°C to block phagocytosis. To eliminate extracellular bacteria, cells were incubated in 20 μg/ml gentamicin-containing medium. Infected cells were lysed at 1, 2, 5, and 7 h

ID: Amit.Kumar1Time: 23:39I Path: //mumnasprod/home$/joshis$/SM-MSPH210181

postinfection with 0.2% Triton X-100 for 5 min, and dilution series were plated onto BHI agar for enumeration of intracellular bacteria and quantification of bacterial CFU.

Quantification of intracellular gentamicin. RAW 264.7 cells were seeded onto 24-well plates at a density of 10^5 cells per well. Cells were then treated with CAP for 30 s in fresh culture medium or left untreated (control), then incubated at 37°C overnight. Cells were infected with *S. aureus* at an MOI of 10:1 and incubated at 37°C for 1 h to allow phagocytosis. Cells were incubated in 0, 5, 20, or 50 μg/ml gentamicin-containing culture medium. After 0, 3, and 6 h of incubation, cells were lysed and gentamicin concentration determined using a gentamicin enzyme-limited immunosorbent assay (ELISA) kit (Creative Diagnostics, Shirley, NY) according to the instructions of the suppliers.

Quantification of cellular viability and proliferation. Cellular viability was determined using the stable tetrazolium salt WST-1 reagent (Sigma-Aldrich, St. Louis, MO), which is cleaved to soluble formazan by cellular mitochondrial dehydrogenases. RAW 264.7 cells were treated with CAP for 30 s, and the WST-1 assay was conducted according to the manufacturer's instructions at 24 h and 48 h posttreatment. Absorbance was measured using a microplate reader (Labsystems, Finland) at 450 nm.

TUNEL assay. A TUNEL assay (Sigma-Aldrich, St. Louis, MO) was conducted to detect apoptotic cells undergoing extensive DNA degradation. RAW 264.7 cells were treated with CAP for 30 s and incubated for 24 h before TUNEL staining according to the manufacturer's instructions. DNase I (Sigma-Aldrich, Saint-Louis, MO) at 1 μg/μl in 1× Tris-buffered saline (TBS)/1 mM $MgSO_4$ was used as a positive control. At the end of the assay, coverslips were mounted on microscope slides and analyzed using an inverted microscope (Eclipse TE2000-U; Nikon, Tokyo, Japan) equipped with a high-resolution digital camera (ORCA-ER; Hamamatsu Photonics, Tokyo, Japan). Images were analyzed by manual counting of labeled cells. For each point, at least 100 *S. aureus*-containing vacuoles were counted and scored for the presence or absence of markers. Ten fields of microscopic view per well were captured and averaged. Three independent experiments were performed with 3 replicates per experiment.

Antibodies. Goat anti-EEA1 (catalog no. ab206860), rat monoclonal anti-LAMP-1 (catalog no. ab25245), mouse monoclonal anti-nuclear matrix protein p84 (catalog no. ab487), and rabbit anti-*Staphylococcus aureus* (catalog no. ab20920) antibodies were obtained from Abcam (Cambridge, UK). Goat anti-cathepsin D (catalog no. STJ140018) and goat anti-Rab5b (catalog no. STJ140061) antibodies were purchased from St John's Laboratory (London, UK). Donkey anti-goat IgG (H+L) cross-adsorbed Alexa 488 (catalog no. A-11055), goat anti-rat IgG (H+L) cross-adsorbed Alexa 488 (catalog no. A110006), and goat anti-rabbit IgG (H+L) highly cross-adsorbed Alexa 488 (catalog no. A-11034) secondary antibodies were purchased from Invitrogen (Thermo Fisher Scientific). Goat anti-rabbit IgG (H+L) Cy3 and goat anti-rabbit IgG (H+L) C5 antibodies were purchased from Jackson ImmunoResearch Europe Ltd. (Cambridge, UK). For Western blotting, mouse monoclonal anti-LAMP-1 (catalog no. 611043) were purchased from BD sciences (San Jose, CA), mouse monoclonal anti-GAPDH, (catalog no. 60004-1) was purchased from Proteintech (Manchester, UK), nuclear matrix protein p84 (catalog no. ab487) was purchased from Abcam (Cambridge, UK), mouse anti-rabbit horseradish peroxidase (HRP; catalog no. SC-2357), goat anti-mouse IgG HRP (catalog no. SC-2005), and mouse anti-goat IgG HRP (catalog no. SC-2354) were purchased from Santa Cruz Biotechnology (Santa Cruz, CA). For flow cytometry, rat monoclonal anti-mouse CD80 fluorescein isothiocyanate (FITC; catalog no. 13365564), anti-mouseCD86 phycoerythrin (PE)-cyanine 7 (catalog no. 15598436), anti-mouse CD206 PE (catalog no. 16360604), anti-mouse CD163 allophycocyanin (APC; catalog no. 16380684), anti-mouse transforming growth factor beta (TGF-β; catalog no. 15558676), anti-mouse interleukin 10 (IL-10) FITC (catalog no. 15298349), anti-mouse tumor necrosis factor alpha (TNF-α) PE (catalog no. 15259319), and IL-1β anti-mouse APC (catalog no. 15350830) and the corresponding IgG isotype were purchased from Thermo Fisher Scientific.

Flow cytometry. RAW 264.7 cells were seeded onto 24-well culture plates at 5×10^5 cells per well. After 24 h, cells were treated with brefeldin A (5 μg/ml) to increase intracellular staining. Cells were harvested at 1 h, 6 h, and 24 h after treatment and washed twice with cold phosphate-buffered saline (PBS). For surface staining, cells were incubated with 20 μl of FITC-conjugated anti-CD80, PE-conjugated anti-CD206, APC-conjugated anti-CD86, PE-Cy7-conjugated anti-CD167, or isotype-matched controls for 20 min on ice. For cytokine staining, cells were incubated with 20 μl of FITC-conjugated anti-IL-10, PE-conjugated anti-TNF-α, APC-conjugated anti-IL-1-β PE-Cy7-conjugated anti-TGF-β, or isotype-matched controls for 20 min on ice. Then, stained cells were suspended in cold buffer and analyzed by flow cytometry (CytoFlex; Beckman Coulter, Villepinte, France).

Fluorescence microscopy. RAW 264.7 cells were seeded onto glass coverslips at a density of 10^5 cell/cm^2. Cells were either treated with CAP for 30 s or left untreated, then incubated at 37°C overnight. Cells were then infected with *S. aureus* Xen36 at an MOI of 10:1. Three different time points were studied. One group of cells were fixed for 15 min with 4% paraformaldehyde (PFA; Electron Microscopy Sciences, Hatfield, PA) at 20 min postinfection. The second group of cells were incubated in culture medium containing 20 μg/ml of gentamicin at 30 min postinfection and fixed with 4% PFA at 1 or 6 h postinfection. Fixed cells were permeabilized with 0.1% Triton TX-100 (Sigma-Aldrich, Saint-Louis, MO) and blocked with 5% goat serum (Sigma-Aldrich, Saint-Louis, MO). Cells were then incubated with primary antibodies for 1 h, and then with fluorophore-tagged secondary antibodies for 1 h. Finally, 1 μM 4′,6-diamidino-2-phenylindole (DAPI) was added to cells for 15 min. Samples were mounted on glass coverslips and observed with a Zeiss Axio Observer Z1 confocal microscope (Zeiss, Oberkochen, Germany). Analyses were performed with CellProfiler software (50). For each point, at least 100 *S. aureus*-containing phagosomes were counted and scored for the presence or absence of markers. Results were expressed as the mean percentage of marker colocalization on *S. aureus*-containing phagosomes plus or minus the standard error of the mean (SEM). To study acidic compartments, LysoTracker Red DND-99 (Fisher Scientific, Illkirch, France) was added along with bacteria. The LysoTracker Red DND-99 was used

ID: Amit.Kumar1Time: 23:39I Path: //mumnasprod/home$/joshis$/SM-MSPH210181

concomitantly with a cathepsin D marker to quantify phagosomal acidification. The anti-*S. aureus* antibody enables the detection of both dead and living bacteria.

Cell fractionation. RAW 264.7 cells were fractionated according to a previously described protocol (51). Briefly, cells were washed and resuspended in PBS-bovine serum albumin (BSA) 0.5%, and then centrifuged at 300 × *g* for 5 min. PBS-BSA 0.5% was exchanged for homogenization buffer (8% sucrose in imidazole 3 mM, $MgCl_2$ 1 mM supplemented with EGTA 0.5 mM, gelatin 0.5%, and Complete protease inhibitors [Roche, Mannheim, Germany]) and cells were centrifuged at 300 × *g* for 10 min. Cells were then resuspended and mechanically disrupted in homogenization buffer using a 25-gauge 5/8 needle. After centrifugation at 2,000 × *g* for 15 min, the postnuclear fraction was collected, brought to 40%, sucrose and loaded on top of a 60% sucrose cushion. A discontinuous 60/40%, 40/30%, 30/20%, and 20/8% sucrose gradient was prepared and ultracentrifuged at 100,000 × *g* for 1 h. The recovered fractions were adjusted to a final concentration of 10% sucrose.

Immunoblotting. Cellular and subcellular extracts from RAW2 264.7 cells were lysed in ice-cold radioimmunoprecipitation assay (RIPA) buffer (Cell Signaling Technology, Beverly, MA) supplemented with Complete protease inhibitors (Roche). The lysate was centrifuged at 15,000 × *g* for 10 min at 4°C, and the supernatant was assayed for protein content. Protein content was quantified using a Pierce BCA bicinchoninic acid (BCA) quantification kit (Thermo Fisher Scientific, Rockford, IL) according to the manufacturer's instructions. Total protein was prepared in Laemmli buffer (Bio-Rad Laboratories, Hercules, CA), and 40 μg of protein was subjected to SDS-PAGE separation and immunoblotting. Following protein electrotransfer, a polyvinylidene difluoride (PVDF) membrane (Immun-Blot; Bio-Rad Laboratories) was incubated in Ponceau S staining solution for 5 to 10 min at room temperature. An image of the Ponceau-stained membrane was captured. Membranes were incubated with primary antibodies directed against LAMP-1 (1:100 dilution), cathepsin D antibody (1:200 dilution), GAPDH (1:2,000 dilution), and nuclear matrix protein p84 (1:500 dilution), and revealed with secondary antibodies (1:2,000 dilution). Chemiluminescent detection was performed using the Clarity Western ECL substrate (Bio-Rad Laboratories). Chemiluminescence signals were acquired using the ChemiDoc X-ray spectrometry plus (XRS+) system and Image Lab software (Bio-Rad Laboratories). Signal intensity was determined by densitometry to calculate relative levels of protein.

Statistical analysis. Statistical analysis was performed using Prism 6.04 software (GraphPad Software, San Diego, CA). For a two-group comparison, a nonparametric Mann-Whitney U test was used. For a comparison of more than two groups, a nonparametric Kruskall-Wallis test (one-way ANOVA) was used. In this case, multiple comparisons were done with Dunn's test. When two variables were studied, a two-way ANOVA was used with Tukey's multiple-comparison posttest to compare replicate means. In this case, it was assumed that the distribution of the sample was normal. Data were expressed as mean values ± SEM, and *P* values lower than 0.05 (*), 0.01 (**), or 0.001 (***) were considered to be statistically significant.

SUPPLEMENTAL MATERIAL

Supplemental material is available online only.

FIG S1, EPS file, 1.4 MB.

FIG S2, EPS file, 1.5 MB.

FIG S3, EPS file, 1.7 MB.

FIG S4, EPS file, 1.2 MB.

FIG S5, EPS file, 1.3 MB.

FIG S6, EPS file, 1.6 MB.

FIG S7, EPS file, 2 MB.

ACKNOWLEDGMENTS

We are grateful to Pascale Cossart and Javier Pizarro-Cerda for sharing equipment and useful discussions. We thank Michael Connor for providing insight and sharing expertise in confocal microscopy and data analysis.

This work was supported by La Direction Générale de L'Armement and by L'École polytechnique, Institut Pasteur, and Université de Paris. The *Yersinia* Research Unit is a member of the Laboratory of Excellence Integrative Biology of Emerging Infectious Diseases (ANR-LBX-62-IBEID).

We declare that we have no conflicts of interest.

REFERENCES

1. Kinchen JM, Ravichandran KS. 2008. Phagosome maturation: going through the acid test. Nat Rev Mol Cell Biol 9:781–795. https://doi.org/10.1038/nrm2515.
2. Murray PJ, Wynn TA. 2011. Protective and pathogenic functions of macrophage subsets. Nat Rev Immunol 11:723–737. https://doi.org/10.1038/nri3073.

ID: Amit.Kumar1Time: 23:39I Path: //mumnasprod/home$/joshis$/SM-MSPH210181

3. Geissmann F, Manz MG, Jung S, Sieweke MH, Merad M, Ley K. 2010. Development of monocytes, macrophages, and dendritic cells. Science 327:656–661. https://doi.org/10.1126/science.1178331.
4. Pauwels AM, Trost M, Beyaert R, Hoffmann E. 2017. Patterns, receptors, and signals: regulation of phagosome maturation. Trends Immunol 38:407–422. https://doi.org/10.1016/j.it.2017.03.006.
5. Levin R, Grinstein S, Canton J. 2016. The life cycle of phagosomes: formation, maturation, and resolution. Immunol Rev 273:156–179. https://doi.org/10.1111/imr.12439.
6. Kaufmann SHE, Dorhoi A. 2016. Molecular determinants in phagocyte-bacteria interactions. Immunity 44:476–491. https://doi.org/10.1016/j.immuni.2016.02.014.
7. Hybiske K, Stephens RS. 2008. Exit strategies of intracellular pathogens. Nat Rev Microbiol 6:99–110. https://doi.org/10.1038/nrmicro1821.
8. Tong SY, Davis JS, Eichenberger E, Holland TL, Fowler VG, Jr. 2015. *Staphylococcus aureus* infections: epidemiology, pathophysiology, clinical manifestations, and management. Clin Microbiol Rev 28:603–661. https://doi.org/10.1128/CMR.00134-14.
9. Horn J, Stelzner K, Rudel T, Fraunholz M. 2018. Inside job: *Staphylococcus aureus* host-pathogen interactions. Int J Med Microbiol 308:607–624. https://doi.org/10.1016/j.ijmm.2017.11.009.
10. Dey S, Bishayi B. 2015. Killing of *Staphylococcus aureus* in murine macrophages by chloroquine used alone and in combination with ciprofloxacin or azithromycin. J Inflamm Res 8:29–47. https://doi.org/10.2147/JIR.S76045.
11. Foster TJ. 2017. Antibiotic resistance in *Staphylococcus aureus*: current status and future prospects. FEMS Microbiol Rev 41:430–449. https://doi.org/10.1093/femsre/fux007.
12. Klevens RM, Morrison MA, Nadle J, Petit S, Gershman K, Ray S, Harrison LH, Lynfield R, Dumyati G, Townes JM, Craig AS, Zell ER, Fosheim GE, McDougal LK, Carey RB, Fridkin SK, Active Bacterial Core surveillance (ABCs) MRSA Investigators. 2007. Invasive methicillin-resistant *Staphylococcus aureus* infections in the United States. JAMA 298:1763–1771. https://doi.org/10.1001/jama.298.15.1763.
13. Park G. 2012. Atmospheric-pressure plasma sources for biomedical applications. Plasma Sources Sci Technol 21:043001. https://doi.org/10.1088/0963-0252/21/4/043001.
14. Duchesne C, Banzet S, Lataillade JJ, Rousseau A, Frescaline N. 2019. Cold atmospheric plasma modulates endothelial nitric oxide synthase signalling and enhances burn wound neovascularisation. J Pathol 249:368–380. https://doi.org/10.1002/path.5323.
15. Duchesne C, Frescaline N, Lataillade J-J, Rousseau A. 2018. Comparative study between direct and indirect treatment with cold atmospheric plasma on *in vitro* and *in vivo* models of wound healing. Plasma Med 8:379–401. https://doi.org/10.1615/PlasmaMed.2019028659.
16. Frescaline N, Duchesne C, Favier M, Onifarasoaniaina R, Guilbert T, Uzan G, Banzet S, Rousseau A, Lataillade J-J. 2020. Physical plasma therapy accelerates wound re-epithelialisation and enhances extracellular matrix formation in cutaneous skin grafts. J Pathol 252:451–464. https://doi.org/10.1002/path.5546.
17. Weltmann KD, Kindel E, von Woedtke T, Hähnel M, Stieber M, Brandenburg R. 2010. Atmospheric-pressure plasma sources: prospective tools for plasma medicine. Pure Appl Chem 82:1223–1237. https://doi.org/10.1351/PAC-CON-09-10-35.
18. Mohd MN, Lee BK, Yap SS, Thong KL, Yap SL. 2016. Cold plasma inactivation of chronic wound bacteria. Arch Biochem Biophys 605:76–85. https://doi.org/10.1016/j.abb.2016.03.033.
19. Boekema B, Vlig M, Guijt D, Hijnen K, Hofmann S, Smits P, Sobota A, van Veldhuizen EM, Bruggeman P, Middelkoop E. 2016. A new flexible DBD device for treating infected wounds: *in vitro* and *ex vivo* evaluation and comparison with a RF argon plasma jet. J Phys D: Appl Phys 49:e044001. https://doi.org/10.1088/0022-3727/49/4/044001.
20. Wiegand C, Fink S, Hipler UC, Beier O, Horn K, Pfuch A, Schimanski A, Grunler B. 2017. Cold atmospheric pressure plasmas exhibit antimicrobial properties against critical bacteria and yeast species. J Wound Care 26:462–468. https://doi.org/10.12968/jowc.2017.26.8.462.
21. Ermolaeva SA, Varfolomeev AF, Chernukha MY, Yurov DS, Vasiliev MM, Kaminskaya AA, Moisenovich MM, Romanova JM, Murashev AN, Selezneva II, Shimizu T, Sysolyatina EV, Shaginyan IA, Petrov OF, Mayevsky EI, Fortov VE, Morfill GE, Naroditsky BS, Gintsburg AL. 2011. Bactericidal effects of non-thermal argon plasma *in vitro*, in biofilms and in the animal model of infected wounds. J Med Microbiol 60:75–83. https://doi.org/10.1099/jmm.0.020263-0.
22. Yu Y, Tan M, Chen H, Wu Z, Xu L, Li J, Cao J, Yang Y, Xiao X, Lian X, Lu X, Tu Y. 2011. Non-thermal plasma suppresses bacterial colonization on skin wound and promotes wound healing in mice. J Huazhong Univ Sci Technol [Med Sci] 31:390–394. https://doi.org/10.1007/s11596-011-0387-2.
23. von Woedtke T, Schmidt A, Bekeschus S, Wende K, Weltmann KD. 2019. Plasma medicine: a field of applied redox biology. In Vivo 33:1011–1026. https://doi.org/10.21873/invivo.11570.
24. Jee Y, Carlson J, Rafai E, Musonda K, Huong TTG, Daza P, Sattayawuthipong W, Yoon T. 2018. Antimicrobial resistance: a threat to global health. Lancet Infect Dis 18:939–940. https://doi.org/10.1016/S1473-3099(18)30471-7.
25. Theuretzbacher U, Outterson K, Engel A, Karlen A. 2020. The global preclinical antibacterial pipeline. Nat Rev Microbiol 18:275–285. https://doi.org/10.1038/s41579-019-0288-0.
26. Tacconelli E, Carrara E, Savoldi A, Harbarth S, Mendelson M, Monnet DL, Pulcini C, Kahlmeter G, Kluytmans J, Carmeli Y, Ouellette M, Outterson K, Patel J, Cavaleri M, Cox EM, Houchens CR, Grayson ML, Hansen P, Singh N, Theuretzbacher U, Magrini N, WHO Pathogens Priority List Working Group. 2018. Discovery, research, and development of new antibiotics: the WHO priority list of antibiotic-resistant bacteria and tuberculosis. Lancet Infect Dis 18:318–327. https://doi.org/10.1016/S1473-3099(17)30753-3.
27. Jubrail J, Morris P, Bewley MA, Stoneham S, Johnston SA, Foster SJ, Peden AA, Read RC, Marriott HM, Dockrell DH. 2016. Inability to sustain intraphagolysosomal killing of *Staphylococcus aureus* predisposes to bacterial persistence in macrophages. Cell Microbiol 18:80–96. https://doi.org/10.1111/cmi.12485.
28. Tranchemontagne ZR, Camire RB, O'Donnell VJ, Baugh J, Burkholder KM. 2016. *Staphylococcus aureus* strain USA300 perturbs acquisition of lysosomal enzymes and requires phagosomal acidification for survival inside macrophages. Infect Immun 84:241–253. https://doi.org/10.1128/IAI.00704-15.
29. Connolly RJ, Lopez GA, Hoff AM, Jaroszeski MJ. 2010. Characterization of plasma mediated molecular delivery to cells *in vitro*. Int J Pharm 389:53–57. https://doi.org/10.1016/j.ijpharm.2010.01.016.
30. Xu D, Wang B, Xu Y, Chen Z, Cui Q, Yang Y, Chen H, Kong M. 2016. Intracellular ROS mediates gas plasma-facilitated cellular transfection in 2D and 3D cultures. Sci Rep 6:27872. https://doi.org/10.1038/srep27872.
31. Dobrynin D, Fridman G, Friedman G, Fridman AA. 2009. Physical and biological mechanisms of direct plasma interaction with living tissue. New J Phys 11:115020. https://doi.org/10.1088/1367-2630/11/11/115020.
32. Buvelot H, Posfay-Barbe KM, Linder P, Schrenzel J, Krause KH. 2017. *Staphylococcus aureus*, phagocyte NADPH oxidase and chronic granulomatous disease. FEMS Microbiol Rev 41:139–157. https://doi.org/10.1093/femsre/fuw042.
33. van Sorge NM, Beasley FC, Gusarov I, Gonzalez DJ, von Kockritz-Blickwede M, Anik S, Borkowski AW, Dorrestein PC, Nudler E, Nizet V. 2013. Methicillin-resistant *Staphylococcus aureus* bacterial nitric-oxide synthase affects antibiotic sensitivity and skin abscess development. J Biol Chem 288:6417–6426. https://doi.org/10.1074/jbc.M112.448738.
34. Dinauer MC, Deck MB, Unanue ER. 1997. Mice lacking reduced nicotinamide adenine dinucleotide phosphate oxidase activity show increased susceptibility to early infection with *Listeria monocytogenes*. J Immunol 158:5581–5583.
35. Nathan C, Shiloh MU. 2000. Reactive oxygen and nitrogen intermediates in the relationship between mammalian hosts and microbial pathogens. Proc Natl Acad Sci U S A 97:8841–8848. https://doi.org/10.1073/pnas.97.16.8841.
36. Laubach VE, Shesely EG, Smithies O, Sherman PA. 1995. Mice lacking inducible nitric oxide synthase are not resistant to lipopolysaccharide-induced death. Proc Natl Acad Sci U S A 92:10688–10692. https://doi.org/10.1073/pnas.92.23.10688.
37. MacMicking JD, Nathan C, Hom G, Chartrain N, Fletcher DS, Trumbauer M, Stevens K, Xie QW, Sokol K, Hutchinson N. 1995. Altered responses to bacterial infection and endotoxic shock in mice lacking inducible nitric oxide synthase. Cell 81:641–650. https://doi.org/10.1016/0092-8674(95)90085-3.
38. Murray HW, Nathan CF. 1999. Macrophage microbicidal mechanisms in vivo: reactive nitrogen versus oxygen intermediates in the killing of intracellular visceral *Leishmania donovani*. J Exp Med 189:741–746. https://doi.org/10.1084/jem.189.4.741.
39. Wei XQ, Charles IG, Smith A, Ure J, Feng GJ, Huang FP, Xu D, Muller W, Moncada S, Liew FY. 1995. Altered immune responses in mice lacking inducible nitric oxide synthase. Nature 375:408–411. https://doi.org/10.1038/375408a0.
40. Tan HY, Wang N, Li S, Hong M, Wang X, Feng Y. 2016. The reactive oxygen species in macrophage polarization: reflecting its dual role in progression and treatment of human diseases. Oxid Med Cell Longev 2016:2795090. https://doi.org/10.1155/2016/2795090.

ID: Amit.Kumar1Time: 23:39I Path: //mumnasprod/home$/joshis$/SM-MSPH210181

41. Schairer DO, Chouake JS, Nosanchuk JD, Friedman AJ. 2012. The potential for nitric oxide releasing therapies as antimicrobial therapies. Virulence 3:271–279. https://doi.org/10.4161/viru.20328.
42. Adler BL, Friedman AJ. 2015. Nitric oxide therapy for dermatologic disease. Future Sci OA 1:FSO37. https://doi.org/10.4155/fso.15.37.
43. Del Rosso JQ, Kircik LH. 2017. Spotlight on the use of nitric oxide in dermatology: what is it? What does it do? Can it become an important addition to the therapeutic armamentarium for skin disease? J Drugs Dermatol 16:s4–s10.
44. Prolo C, Alvarez MN, Radi R. 2014. Peroxynitrite, a potent macrophage-derived oxidizing cytotoxin to combat invading pathogens. Biofactors 40:215–225. https://doi.org/10.1002/biof.1150.
45. Laroussi M, Leipold F. 2004. Evaluation of the roles of reactive species, heat, and UV radiation in the inactivation of bacterial cells by air plasmas at atmospheric pressure. Int J Mass Spectrom 233:81–86. https://doi.org/10.1016/j.ijms.2003.11.016.
46. Freebairn D, Linton D, Harkin-Jones E, Jones DS, Gilmore BF, Gorman SP. 2013. Electrical methods of controlling bacterial adhesion and biofilm on device surfaces. Expert Rev Med Devices 10:85–103. https://doi.org/10.1586/erd.12.70.
47. Daeschlein G, Napp M, von Podewils S, Lutze S, Emmert S, Lange A, Klare I, Haase H, Gümbel D, von Woedtke T, Jünger M. 2014. *In vitro* susceptibility of multidrug resistant skin and wound pathogens against low temperature atmospheric pressure plasma jet (APPJ) and dielectric barrier discharge plasma (DBD). Plasma Process Polym 11:175–183. https://doi.org/10.1002/ppap.201300070.
48. Petheo GL, Demaurex N. 2005. Voltage- and NADPH-dependence of electron currents generated by the phagocytic NADPH oxidase. Biochem J 388:485–491. https://doi.org/10.1042/BJ20041889.
49. Lee HJ, Hong WG, Woo Y, Ahn JH, Ko HJ, Kim H, Moon S, Hahn TW, Jung YM, Song DK, Jung YJ. 2020. Lysophosphatidylcholine enhances bactericidal activity by promoting phagosome maturation via the activation of the NF-kB pathway during *Salmonella* infection in mouse macrophages. Mol Cells 43:989–1001. https://doi.org/10.14348/molcells.2020.0030.
50. Wahlby C, Kamentsky L, Liu ZH, Riklin-Raviv T, Conery AL, O'Rourke EJ, Sokolnicki KL, Visvikis O, Ljosa V, Irazoqui JE, Golland P, Ruvkun G, Ausubel FM, Carpenter AE. 2012. An image analysis toolbox for high-throughput *C. elegans* assays. Nat Methods 9:714–716. https://doi.org/10.1038/nmeth.1984.
51. Pizarro-Cerda J, Jonquieres R, Gouin E, Vandekerckhove J, Garin J, Cossart P. 2002. Distinct protein patterns associated with *Listeria monocytogenes* InlA- or InlB-phagosomes. Cell Microbiol 4:101–115. https://doi.org/10.1046/j.1462-5822.2002.00169.x.

ID: **Amit.Kumar1**Time: 23:39I Path: //mumnasprod/home$/joshis$/SM-MSPH210181

Conclusion

In this study we demonstrated the impact of CAP on phagosome maturation. CAP was shown to improve intracellular RONS levels, to promote *S. aureus* killing and increase the expression of markers of phagolysosome maturation. The increase in the levels of RONS needs further investigations. It can be the consequence of RONS generated by CAP that penetrate the cells. Exogenous RONS could be triggering a succession of cascades that can induce activation of specific complex or organelles which will in turn produce reactions leading to endogenous reactive species production. It is also possible that macrophages are polarized into an M1 phenotype after the oxidative storm.

In our experimental design, macrophages are treated 24 h before the infection which does not support a direct effect of CAP-generated ROS on infected macrophages but preliminary activation of cells. As the cells are treated in culture media that are composed of vitamins, minerals and other molecules it is also possible that new reactive species are formed specifically in response to the liquid composition and also favour cells activation. Indeed, plasma activated media (PAM) are also the subject of promising studies for their biological functions in living tissue sterilization, blood coagulation or even for the destruction of cancer cells[356].

In plasma medicine it is now well established that CAP induces direct bactericidal effect but its direct or indirect effects on cells are still unclear. As we succeed to demonstrate an indirect effect of CAP on macrophage phagosome maturation our next investigation will focus on the underlying mechanistic using a procedure that get closer to real conditions with an infection followed by CAP treatment.

Chapter III.

CAP enhances wound healing and decrease infection through NOX2 activation.

Chapter III - CAP enhances wound healing and decreases infection through NOX2 activation

Introduction

Oxidative stress is considered to be a powerful tool, which enables the immune system to fight against pathogens. The reactive species produced during internalization and phagocytosis of bacteria are necessary for eradication and allow an oxidation of the target. ROS are constantly produced in the electron-transport chain during respiration and by several constitutively active oxidases. They can also be produced by the NADPH oxidase complex (NOX2) during the oxidative burst, and are thus critical for antimicrobial host defense.
Since the discovery of NOX family in 2000 it is assumed that all the cells of our body produce superoxide in a regulated manner. Short living cells such as neutrophils have a high expression of NOX2 and use a range of highly reactive species to eliminate pathogens. On the other hand, long-lived phagocytes such as macrophages express NOX2 at lower levels than neutrophils, but produce higher amount of reactive species in comparison to other cells such as endothelial cells. It has also been demonstrated that circulating and resident tissue macrophages use oxidants for both intra and intercellular signaling purposes[357]. One of the molecule of interest is hydrogen peroxide (H_2O_2), which isderived from superoxide by dismutation that can be spontaneous or mediated by enzyme such as the superoxide dismutase. Under physiological conditions H_2O_2 in the intracellular space is regulated between 1-100 nM, hundreds of times lower than extracellular concentrations.
Macrophages are among the first-line phagocytes to respond to pathogens invasion. Currently it is well established that NOX2 is critical for neutrophil-mediated host defense, but its role in macrophages is less known. However, NOX2 dysfunction have been implicated in several pathogeneses such as Crohn's-like inflammatory bowel disease and more interestingly in chronic granulomatous disease triggering chronic infections in patients.

H_2O_2 or $O_2^{\cdot -}$ are among others reactive species commonly produced on one side by macrophages and particularly by NOX2 complex of phagosome and on the other side by CAP. Previously we demonstrated that CAP favor phagosome maturation during macrophages infection which is probably correlated to an increase of intracellular RONS. Knowing this we hypothesized that CAP could increase indirectly ROS levels inside phagosome for longer time point and that it can be due to a modulation of NOX2 complex activation.
The aim of this study was first to investigate if CAP induces the same bactericidal effect as *in vitro* studies in a burn wound mouse model under an infectious context. Then as macrophages are key cells in burn wound healing phases and for wound clearance we investigated the precise mechanism that can be related to the observed phenomenon *in vitro* in 2D and 3D cultures.

Physical plasma accelerates wound healing and subdues bacterial infection via *de novo* generation of oxygen derivatives in NOX2-dependent manner

Océane Blaise[1,2,7], Constance Duchesne[1,2,7], Marie-Anne Nahori[3], Michael G. Connor[4], Melanie A. Hamon[4], Javier Pizarro-Cerda[1], Jean-Jacques Lataillade[5], Colin McGuckin[6], Antoine Rousseau[2], Sébastien Banzet[5], Olivier Dussurget[1,8], Nadira Frescaline[1,8]

1 Institut Pasteur, Université Paris Cité, CNRS UMR6047, Unité de Recherche *Yersinia*, Paris, France. **2** École Polytechnique, Sorbonne Université, Université Paris Saclay, CNRS UMR7648, Laboratoire de Physique des Plasmas, Palaiseau, France. **3** Institut Pasteur, Université Paris Cité, CNRS UMR6047, Unité des Toxines Bactériennes, Paris, France. **4** Institut Pasteur, Université Paris Cité, Unité Chromatine et Infection, Paris, France. **5** Institut de Recherche Biomédicale des Armées, INSERM UMRS-MD 1197, Centre de Transfusion sanguine des Armées, Clamart, France. **6** CTIBiotech, Meyzieu, France.

7 contributed equally to the work

8 jointly supervised the work

Corresponding authors: Prof. Olivier Dussurget (olivier.dussurget@pasteur.fr) and Dr. Nadira Frescaline (nadira.frescaline@pasteur.fr).

Keywords: antimicrobial therapy, cold atmospheric plasma, skin, burn, graft, staphylococci, MRSA, macrophage, phagocyte NADPH oxidase, ROS

Abstract

Antimicrobial resistance renders conventional antibiotic therapy unsuccessful. Cold atmospheric plasma (CAP) is an unconventional alternative to topical antibiotics. Antibacterial effects of CAP in clinically infected human wounds are remarkable, however molecular mechanisms driving this process remain enigmatic.

Here, we show that CAP activates the phagocyte NADPH oxidase complex NOX2 – a critical enzymatic effector of innate immune defense. An increase in intracellular reactive oxygen species (ROS) is induced by CAP but subdued by NOX2 inhibitors. Genetic and pharmacological inhibitions of NOX2 in macrophages and in a three-dimensional model of human skin infected with *Staphylococcus aureus*, show a significant reduction in intracellular oxidants and increased bacterial survival upon CAP treatment. We further show that CAP triggers activation of the small GTPase Rac1 and phosphorylation of $p40^{phox}$ and $p47^{phox}$ required for NOX2 complex assembly and respiratory burst of infected macrophages. In addition to its antibacterial effects, we show that CAP is a positive regulator of cutaneous wound healing. Murine wounds infected with *S. aureus* are characterized by significant acceleration of wound closure, increased rate of re-epithelialisation and extracellular matrix formation in response to CAP treatment.

Thus, we reveal a previously unreported host-derived molecular defence mechanism triggered by CAP that leads to increased bacterial killing without compromising the proliferative activity of the host. CAP technology opens new therapeutic perspectives and adds a powerful weapon to existing antibacterial arsenal available to the clinician.

Visual abstract

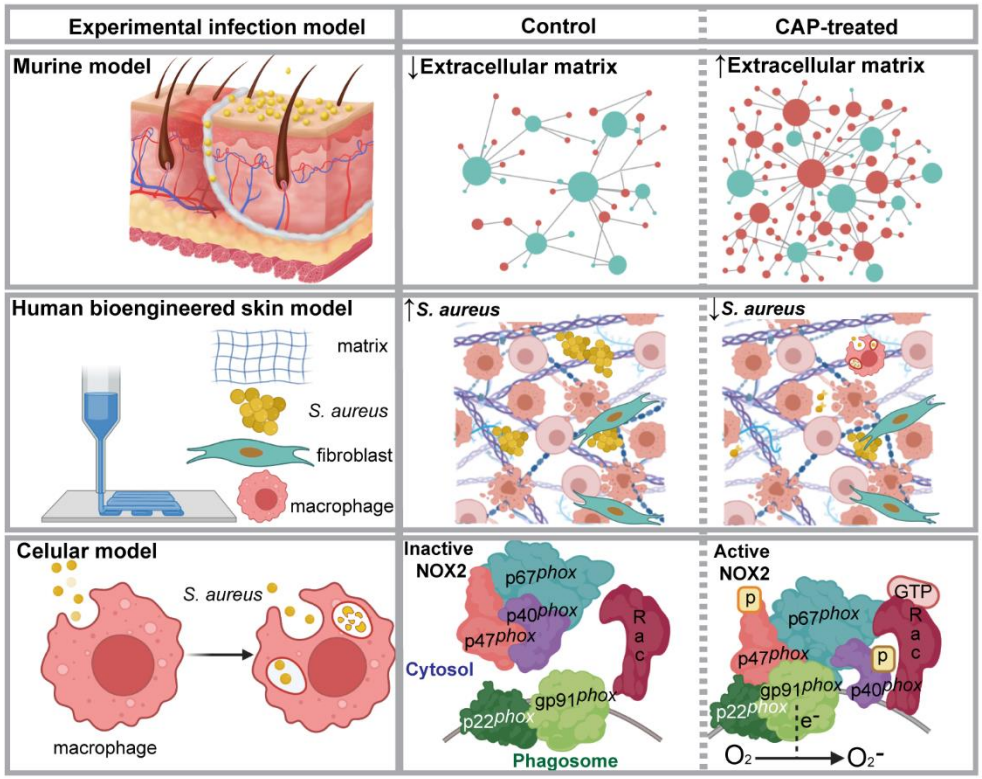

Introduction

Cutaneous wound repair is a complex physiological process aimed at restoration of skin homeostasis. Bacterial wound infection is a common complication, which compromises the wound healing by damaging the epidermal and dermal cell lineages. Contextual pathogens, such as *Staphylococcus aureus* are known to act either as an asymptomatic commensal or pathogenic coloniser of wounds, particularly in the context of extensive breach of protective skin barrier.[1-5] Local multiplication of *S. aureus* within the cutaneous wound may lead to its dissemination via the bloodstream from the primary focus of infection to distant sites giving rise to potentially life-threatening systemic complications.[2,6]

Complex epithelial-immune cell communication,[3,7] triggered by bacterial by-products and other cues, results in activation of skin resident[8] and blood-derived macrophages recruited to the site of wound infection.[9] Killing of *S. aureus* by macrophages is mediated by several mechanisms, including the concerted actions of reactive oxygen species (ROS) produced upon activation of NOX2 and respiratory burst.[10,11] The phagocyte NADPH oxidase (NOX2) is a multicomponent enzyme,[12] composed of catalytic subunit gp91^{phox}, transmembrane protein p22^{phox}, cytosolic subunits p40^{phox}, p47^{phox}, p67^{phox} and small GTPase Rac.[1,10] NOX2 catalyses the production of superoxide (O_2^-),[10,11] which is then converted to other downstream ROS, including hydrogen peroxide (H_2O_2), hypochloric acid (HOCl), and hydroxyl radical (·HO).[10,11] Molecular on–off switches such as post-translational modifications of NOX2 components, including phosphorylation of p47^{phox} and p40^{phox}, translocation of cytosolic p47^{phox}, p67^{phox} and p40^{phox} to the phagocytic cup on the endosomal membrane,[11] and recruitment of GTP-Rac to p67^{phox} lead to assembly of the enzymatic complex. Once assembled, the active complex generates superoxides by transporting electrons from cytoplasmic NADPH to phagosomal oxygen. The crucial antimicrobial role of ROS production by phagocytes is highlighted by aberrations in

NOX2 signalling in patients with chronic granulomatous disease, resulting in impaired killing of pathogens. [13-15]

Emerging antimicrobial resistance is a global public health threat. Among fatality attributable to antimicrobial resistance, more than 100,000 deaths were caused by methicillin-resistant *S. aureus* (MRSA) in 2019.[16] Design and development of alternative in addition to conventional antibiotics are thus urgently needed.[17] Cold atmospheric plasma (CAP) is a promising technology used to fight disease-causing pathogens in the context of infected cutaneous wounds.[18-20] CAP produces photons, UV radiation, electromagnetic field, electrons, ions and neutral radicals, such as reactive oxygen and nitrogen species (RONS).[19,21-23] CAP is generated by applying electrical energy to a conductive gas, which becomes ionized.[24] Typical degree of ionization is low: $n_e/(n_n + n_e) < 10^{-5}$, where n_n and n_e are the neutral gas and electron densities, respectively.[24] The effects of weak ionization of the gas jet on a liquid[24] is thought to generate aqueous-based antimicrobial formulations comprising a rich mixture of oxidants such as O_2^-, NO, H_2O_2, O_3, NO_2^- and NO_3^-.[23,25,26] Desirable features of cold plasma jet include simplicity, portability, low cost generation of biologically active and biodegradable 'green chemicals', which, in low concentrations are nontoxic to host tissues.[18,27,28] Here, we elucidate a previously unknown antimicrobial mechanism of CAP, which recruits and activates the NOX2 complex that kills bacteria by *de novo* generation of oxygen derivatives.

Results

Treatment with CAP promotes healing of infected skin burn wound by stimulating extracellular matrix formation

To mimic bacterial infection in a cutaneous wound, we adapted a model that we previously used to study the effect of CAP on skin graft integration.[25,27,29] In the clinical practice, skin grafts are used routinely to provide coverage for wounds unlikely to heal by secondary intentions. While individual clinical situation dictates the type of graft to be placed, disruptive effects of *S. aureus* infection threaten graft survival regardless of the type. Here, we used a reproducible model of burn wound reconstructed with allogeneic skin graft and inoculated with *S. aureus* (Figure 1a). Staphylococcal wound infection resulted in varying degrees of graft survival depending on the applied treatment (Figure 1b). On macroscopic level, placebo treatment resulted in complete loss of graft by 14 d. p. i. (Figure 1b). Wounds treated with either CAP (Supplementary Video 1) or topical antibiotics (ABX) improved graft survival following infection compared to time-matched placebo control (Figure 1b). On microscopic level, histological wound assessment showed that indicators of successful skin engraftment were markedly improved in infected wounds treated with CAP compared to placebo control (Figure 1c-f). Immediately after the infection, bacterial by-products, damage signals and chemoattractants trigger multiple responses, including the infiltration of immune cells to the site of infection. CAP generates a range of chemical molecules (Supplementary Figure 1) similar to those produced by wound phagocytes.[7] We, therefore, hypothesized that these biochemical molecules may act either as signals or chemoattractants to immune cells. No statistically significant difference was observed in immune cell recruitment in wounds treated with CAP compared to time-matched control. Several antigens, commonly known to be expressed by wound leukocytes were probed, including CD45 (cell-surface protein detected on most lymphohematopoietic cells[30,31]), F4/80 (marker of murine macrophages[32]), CD206

(transmembrane protein abundant in tissue macrophages displaying an M2-like phenotype[33]) and Ly6G (expressed by neutrophils[34]). CAP showed no influence on the magnitude of innate immune cell infiltrate (Extended Figure 1), neither did it change the mRNA levels of established macrophage and neutrophil chemoattractants (Extended Figure 1c). To assess the level of matrix formation during proliferative and remodelling phases of healing, we measured the expression of matrix proteins within granulation tissue (Figure 2). Three lines of evidence suggest that CAP stimulates the formation of ECM, which is necessary for the functional restoration of the skin as a protective barrier. First, second harmonic generation microscopy and Masson's trichrome staining showed a significantly increased deposition of fibrillar collagen in wounds treated with CAP compared to control (Figure 2a-c). Second, key markers of ECM, such as laminin and collagen IV were synthesized in significantly higher levels in the vicinity of wounds treated with CAP compared to control (Figure 2f, g and Supplementary Figure 2b). Third, collagen-specific antibody detection indicated that CAP enhanced matrix synthesis, without compromising the ratio of collagen type I/III, which is essential for functional skin architecture (Figure 2d, e and Supplementary Figure 2a).

The net effect of CAP leads to resolution of wound infection at a rate comparable to anti-staphylococcal antibiotic

A Gram stain of wound lesions inoculated with *S. aureus* and analysed at 7 and 14 d. p. i., showed clusters of cocci, typically embedded in biofilm, and clearly localized to epidermal, dermal and hypodermal compartments of the skin (Figure 3a). Fewer bacteria were detected in mice treated with CAP and ABX compared to placebo control. Real time bioluminescent imaging (BLI) of *S. aureus* in living mice, demonstrated that daily treatment with CAP effectively reduced bacterial wound burden as early as 3 d. p. i. compared to time-matched control wounds (Figure 3b and d). Over the course of 14 days following infection, CAP-treated

wounds were associated with consistently lower bacterial wound burden than control (Figure 3c-d). BLI measurements positively correlated with quantitative analysis of CFU enumerated in homogenized wounds and showed at least a 50% reduction in bacterial burden in wounds treated with CAP compared to time-matched control (Figure 3c). Anti-staphylococcal activity of CAP did not compromise the host DNA integrity as indicated by an assay indicative of mammalian DNA damage and apoptotic cell death (Figure 3e). These results are consistent with the analysis of host tissue proliferation. CAP has no detrimental effect on cellular proliferation *in vivo* as the number of $PCNA^+$ and $Ki67^+$ cells were increased in wounds treated with CAP compared to control (Figure 3f-h and Supplementary Figure 3).

CAP inactivates *S. aureus* in a three-dimensional (3D) model of cutaneous infection

To recapitulate staphylococcal wound infection in a human skin model, we bioengineered 3D models of macrophage-laden human skin equivalents (Figure 4a and Extended Figure 2a). Histological analysis of 3D models of skin showed two distinct components: dermis and epidermis with an outermost layer of enucleated keratinocytes that form the *stratum corneum* (Figure 4b and Extended Figure 2). The epidermal compartment of 3D printed skin expresses epidermal markers including keratin 14 and 1, which are typically present in healthy human skin. Positive immunostaining for involucrin and laminin 5 (Extended Data 2b-c) suggests that 3D models express key markers of functional dermal-epidermal junction. Our results demonstrated that cellular viability is maintained up to 21 days post-printing (Extended Figures 2d-e). Histological and immunohistochemical visualization of intradermal bacteria, suggested that *S. aureus* existed in clusters, which is attributed to its capacity to form biofilm communities (Figure 4c). Intradermal inoculation of 3D models with *S. aureus* resulted in consistent and reproducible infection (Figure 4d). Treatment with CAP resulted in significant reduction in the number of live intradermal bacteria (Figure 4d) in 3D skin models.

Anti-staphylococcal activity of CAP is NOX2 dependent

Wound macrophages represent a diverse population of immune cells with heterogeneous functions including detection, ingestion and digestion of invading microorganisms at sites of infection.[8,9] Staphylococcal skin infection drives monocytopoiesis, whereby bone marrow promonocytes are mobilized, and consecutively recruited from the circulation into infected tissues.[35,36] Given the importance of macrophages in containing infection, we next investigated the effect of CAP on the ability of murine bone marrow-derived macrophages (mBMDM) to kill *S. aureus*. Our results showed that treatment with CAP following infection with two different strains of *S. aureus*, including USA300, a major MRSA strain that spread globally in both community and healthcare settings, leads to a significantly reduced number of intramacrophagic bacteria without comprising the proliferative activity of both immortalized macrophages (Figure 5a and b) and mBMDM (Extended Figure 3d and e). Interestingly, CAP induced a significant increase in the *de novo* production of intracellular ROS by macrophages compared to control (Figure 5c). We next addressed the effect of CAP on NOX2, a major source of ROS in macrophages, using complementary pharmacological and genetic inhibition approaches. Addition of gp91ds-tat and GSK2795039 (pharmacological inhibitors of NOX2) to macrophages, followed by bacterial infection and treatment with CAP, brought the intracellular levels of ROS down to the control level (Figure 5c and Extended Figure 3a). Strikingly, NOX2 inhibitor abrogated the antibacterial effect of CAP in both 2D and 3D models of infection (Figure 5d and Extended Figure 3b, c). Macrophage transfection with siRNA targeting the *Cybb* gene encoding gp91^{phox} (Figure 5e), followed by CAP treatment, reduced intracellular ROS production (Extended Figure 3f), significantly increased the number of live intramacrophagic bacteria compared to scrambled siRNA (Figure 5f) and endogenous control siRNA (Extended Figure 3g). Together, our results indicate that CAP antibacterial effects rely on NOX2.

CAP facilitates the switch to GTP-bound active form of Rac1

To determine how CAP promotes NOX2 dependent production of ROS in macrophages, we quantified the recruitment of NOX2 subunits upon CAP treatment. Macrophages were firstly infected with *S. aureus*, and then treated with CAP to determine whether exposure to CAP alters LAMP-1, NOX2 subunits and Rac1 localization and expression. Our confocal microscopy experiments revealed that although the percentage of total Rac1 colocalization with *S. aureus*-containing vacuoles remained unchanged, the level of colocalization with Rac-GTP was significantly increased in macrophages treated with CAP compared to control (Figure 6a-g and Supplementary Figure 4a-b). Treatment with CAP was associated with a higher percentage of colocalisation between vacuole-bound *S. aureus* and catalytic gp91^{phox}, which also coincided with significantly increased levels of phosphorylated p40^{phox} and p47^{phox} at 5 h. p. i. (Figure 6e, Extended Data Figure 4 and Supplementary Figure 4c-d). We next estimated the levels of LAMP-1, Rac1 and NOX2 subunits by immunoblotting. The levels of inactive Rac in whole cell lysates extracted from CAP-treated macrophages was similar to that of control at 5 h. p. i. (Extended Data Figure 4e). However, the levels of active GTP-bound form of Rac1 in phagolysosome extracts were increased upon CAP treatment (Figure 6g). The level of LAMP-1 protein was increased in both whole cell lysates (Extended Data Figure 4e) and phagolysosomal protein (Figure 6f) in response to CAP compared to control. The level of gp91^{phox} and p40^{phox} proteins was significantly increased in the whole cell lysates in response to CAP compared to control (Extended Data Figure 4e). Western blot signal emitted by gp91^{phox} and p40^{phox} proteins in the phagolysosomal fraction was not subjected to quantitative densitometry due to the lack of constitutively expressed loading control protein (Figure 6f).

Discussion

Timely closure of cutaneous wounds is correlated with susceptibility to infection - a major challenge within the clinical setting.[6,37,38] Here, we reveal that treatment of infected burn wounds with CAP (i) significantly reduces bacterial wound burden, (ii) increases the rate of re-epithelialisation, and (iii) stimulates ECM formation. Additionally, we elucidate a so far unknown mechanism of action of CAP treatment in which it promotes NOX2 activation.

It is reasonable to speculate that organisation and migration of stratified sheets of the neoepidermis was enhanced by CAP through ECM proteins, previously shown to be involved in re-epithelialization.[39,40] This hypothesis is based in one part, on our present study, which demonstrated that CAP enhanced the expression of collagens during the remodelling phase of wound healing, and in another part, on our previous studies, which showed enhanced expression of dermal-epidermal junction proteins in wounds treated with CAP.[27] Previous mouse wound transcriptome and single cell-studies revealed that replenishment of injured epidermis is regulated by epidermal stem cell gene activation.[39] In our *in vivo* mouse model, the stem cell genes were probably activated in the epidermal compartment of the recipient wound bed, rather than within the donor graft, which was separated from its blood supply. Apart from gene activation, physical triggers in the form of electromagnetic field, known to be associated with CAP,[41] may have polarized and guided epithelial cell migration in the direction of the wound centre.[42]

Successful tissue repair, among other factors, depends on timely angiogenesis.[38] Open questions remain regarding the signals that stimulate angiogenesis in cutaneous wounds treated with CAP, but angiogenic stimulators, such as nitric oxide, were previously shown to facilitate vascular anastomoses.[25] Wound inflammation is integral, and depletion studies are a testimony to the theory that macrophages are vital players of host-protective responses.[43] The current consensus, is that macrophages clear the wound of apoptotic neutrophils, engulf extracellular

bacteria and activate adaptive immune response.[8,11] Apart from phagocytic functions, wound macrophages orchestrate tissue repair events through their capacity to change phenotype.[9,44] Our previous analysis of macrophage-specific proteins[22] suggested that CAP had no influence on temporal profiles of macrophages.[7]

Oxygen-dependent mechanisms result in massive ROS production by the phagocyte NADPH oxidase.[12] This study proposed a general mechanism to explain anti-staphylococcal activity of CAP. We hypothesized that CAP generates cues that activate NOX2, which, in turn, results in endogenous host-derived production of noxious oxidants with known anti-staphylococcal activity.[10] This hypothesis was tested in two different *in vitro* models of *S. aureus* infection, which we believe to be more experimentally tractable, than the *in vivo* model, which is associated with limitations, such as species-specific anatomical differences that exist between rodent and human skin.[44] For this reason, we resorted to computer-aided transfer of human skin components, including macrophages, to reproduce human skin complexity. Three-dimensional models provided a reproducible tool, which mimicked the acute phase of staphylococcal skin infection, and showed that exogenous addition of NOX2 antagonists inhibited bacterial killing capacity of CAP. Furthermore, gene silencing and pharmacological inhibition of NOX2 significantly reduced macrophage-derived endogenous ROS production and abrogated antibacterial effects of CAP. Our previous study[22] showed that exogenous addition of oxidants enhanced *S. aureus* clearance by macrophages, whereas antioxidants inhibited antibacterial phenotype of CAP. Taken together, these results suggest that CAP kills *S. aureus*, either via exogenous CAP-derived oxidants or by stimulation of endogenous host-derived oxygen-dependent bacterial killing.

Our results indicate that phosphorylation of $p40^{phox}$ and $p47^{phox}$ coincided with anti-*S. aureus* activity of CAP. In addition, association of two phagosomal membrane proteins LAMP-1 and $gp91^{phox}$ was significantly increased in response to CAP treatment compared to placebo control.

GTP-bound Rac1 (active), but not total Rac1 was associated with *S. aureus*-containing phagolysosomes in response to CAP. These results suggest that CAP activates NOX2 by triggering, yet to be discovered, upstream effector mechanisms. In the light of the evidence provided in this article, we suggest a model depicting the effect of CAP on NOX2 activation and activation of enzymatic subunits (Supplementary Figure 5).

Previously discovered mechanisms demonstrated the existence of a link between the formation of superoxide and the activation of proteases in phagocytic vacuole.[45] Our recent study, showed that increased levels of intraphagolysosomal proteolytic cathepsin D were associated with CAP compared to placebo.[22] Thus, there is a reason to suspect that apart from direct activation of NOX2 activity, CAP may also stimulate the formation of "molecular signals" in the form of oxygen derivatives that result in indirect electrogenic[19,45] regulation of proteases that perform non-oxidative killing of bacteria.

The consequence of long-term exposure of *S. aureus* to CAP remains to be investigated. It may be debated that repeated treatment with CAP may activate the transcription of prokaryotic genes encoding for staphylococcal antioxidant defence and induce selective pressure for the resistance phenotype. Many other open questions remain to be addressed. We know little about changes that occur in eukaryotic and prokaryotic transcriptomes in response to CAP. RNA sequencing should provide an insight into transcriptional landscape under homeostatic and non-homeostatic conditions. Finally, if one recognizes the limitations of CAP and is realistic about where, when and to what extent it may be used, this technology may be beneficial in conjunction with antimicrobial arsenal currently available to the clinician.

Acknowledgements

This work was supported by La Direction Générale de L'Armement, l'Agence de l'Innovation de Défense, École Polytechnique, Université Paris Cité and Institut Pasteur, Paris. We thank

Professor Pascale Cossart (Institut Pasteur, Paris) for providing research equipment necessary for the conduct of the project and helpful discussions. The *Yersinia* Research Unit is a member of the Laboratory of Excellence Integrative Biology of Emerging Infectious Diseases (ANR-LBX-62-IBEID). M.G.C. is supported by the Pasteur Foundation Fellowship. We thank our colleagues Maryline Favier and Rachel Onifarasoaniaina (Institut Cochin, Paris) for histological sample preparation and Dr Thomas Guilbert (Institut Cochin, Paris) for excellent expertise in two-photon and second harmonic generation microscopy. The authors thank Dr Bruno Honnorat (Leibniz Institute for Plasma Science and Technology, Greifswald, Germany) for in-depth discussions related to plasma physics and chemistry. The authors acknowledge Maxime Lègues, Clément Milet and Nico Forraz (CTIBiotech, Lyon) for their expertise in biofabrication of 3D skin models and helpful discussions.

Competing interests

Professor Colin McGuckin is the President and Chief Scientific Officer of CTIBiotech, Lyon, France.

Author contributions

NF and OD conceived, designed the experiments and interpreted the data. OB and CD carried out experiments, acquired and analysed data. M-AN contributed substantially to the acquisition and analysis of live *in vivo* bioluminescent imaging. CMG contributed substantially to design, analysis and interpretation of data related to bioengineered human skin models. MGC created modular pipelines and contributed substantially to interpretation of confocal microscopy data. SB, J-JL, JP-C, MAH and AR contributed substantially to design of experiments and critical revision of the manuscript for its important intellectual content. NF and OD wrote the

manuscript. All authors substantively revised the manuscript, approved the final submitted version, and agreed to be personally accountable for all aspects of the work.

Materials and methods

Cold atmospheric plasma

Helium gas was used to produce plasma as previously described.[25,27] The plasma source consisted of a dielectric polylactic acid capillary surrounded by a high-voltage electrode, through which flows helium gas. CAP was propagated from the source to the target in a single channel plasma jet. Voltage was set to 24 kV during *in vivo* and 32 kV *in vitro* experiments. Helium mass flow was regulated by mass flow controller and set to 500 sccm. The gap between CAP nozzle and the target was set to 4-6 mm. The duration of treatment in all experiments was 2 minutes. The operating power value is estimated to be 90 ±10 mW.

Bacterial strain and culture conditions

The bioluminescent *Staphylococcus aureus* Xen36 strain (PerkinElmer, Waltham, Massachusetts, USA) was used in this study. This MSSA strain was derived from a clinical isolate of bacteremic patient and has been genetically engineered to express a stable copy of the modified *Photorhabdus luminescens luxABCDE* operon at a single integration site on a native plasmid. A highly virulent MRSA strain, *Staphylococcus aureus* USA300, was obtained from ATCC (reference BAA-1717). Bacteria were grown aerobically, as previously described,[22] in brain heart infusion (BHI) broth (BD Biosciences, San Jose, CA) with shaking at 200 rpm at 37°C or on BHI agar plates. Overnight cultures were collected or diluted 1:50 in fresh BHI and grown at 37 °C until exponential phase (optical density at 600 nm (OD_{600}) of 1.0). OD_{600} values

were measured using a Biochrom Libra S22 spectrophotometer (Biochrom Ltd., Cambridge, UK).

In vivo mouse model

All experiments were approved by the Institut Pasteur Animal Ethics Committee (approval number APAFIS#15346-2018053111431668 v1) following European and French Code of Practice for the Care and the Use of Animals for Scientific Purposes (Council Directive 86/609/EEC). Six-weeks-old (20-25 g), inbred, immunocompetent hairless female Crl:SKH1-Hr^{hr} mice (Charles River Laboratories, Germany) were divided into three groups of five to twelve animals per group. Intraperitoneal injection of ketamine (100 µg/g) and xylazine (10 µg/g) was administered to induce general anaesthesia, and subcutaneous injection of lidocaine (5 µg/g) was administered to induce local anaesthesia. Buprenorphine (0.05 µg/g) was administered subcutaneously, and paracetamol (3 mg/ml) was added to drinking water to control intra and post-operative pain. A 79-mm^2 burn wound was created on the dorsal surface using a brass block as previously described.[22,25] Twenty-four hours after the wound induction, necrotic tissue was excised to fascia and reconstructed with a full-thickness allogenic skin graft secured with a Leukosan surgical adhesive (BSN medical, Hamburg, Germany). *S. aureus* Xen 36 overnight cultures were diluted in BHI and bacteria were grown to an optical density at 600 nm (OD_{600}) of 1. Bacterial cultures were centrifuged at 3,500 × *g* for 15 min and washed three times in PBS. Following skin grafting, mice were infected topically with 1×10^8 bacteria diluted in 50 µl of PBS supplemented with $CaCO_3$ (50 mg/mL). Serial dilutions of the inoculum were plated to control the number of bacteria inoculated. Wounds were treated once daily with either (i) placebo control (topical treatment with inert, helium gas), (ii) topical treatment with CAP (2 min, 24 kV) or (iii) topical application of 200 µl of mupirocin at 2% w/v (Bactroban, GlaxoSmithKline, Middlesex, UK). Low-adherent paraffin gauze (Adaptic, North Yorkshire,

UK) wound dressing and Micropore™ Surgical Tape (3M, Cergy-Pontoise, France) were changed daily. BLI was performed on alternate days to assess bacterial wound burden in living animals. Bacterial wound burden was assessed by measuring bioluminescent signal in anesthetised animals using IVIS Spectrum Imaging system and Living Image 4.5.5 software (Perken Elmer, Boston, MA, USA). Two wound biopsies were collected at 3, 7 and 14 d. p. i. using a sterile 6 mm biopsy punch (Acuderm Inc. FL, USA). The first wound biopsy was homogenized, serially diluted on BHI plates and grown over 24 h at 37°C. Colonies were counted to assess bacterial load per biopsy. The second wound biopsy was bisected with one half fixed in 10% buffered formalin and processed for histology and immunohistochemistry. The other half was fast frozen in liquid nitrogen for RNA extraction, MPO and NAG quantitation.

Histology, immunohistochemistry and image analysis

Histological sections (4 μm thickness) were prepared from formalin-fixed and paraffin-embedded tissue, which were stained with Haematoxylin and Eosin (H&E) or subjected to immunohistochemistry using a Leica Bond III stainer (Leica Biosystems, Nanterre, France). Primary antibodies were applied and incubated for 1 h. Detection was performed by species-specific horseradish peroxidase (HRP) or alkaline phosphatase (AP)-conjugated secondary antibodies. Sections were reacted with one of two substrates: (i) for HRP,3,3'-diaminobenzidine (DAB) with Bond enhancer (AR9432, Leica Biosystems, Wetzlar, Germany), which produced a brown to black colour or (ii) for AP, Bond Polymer Refine Red (DS9390, Leica Biosystems, Wetzlar, Germany), which yielded a bright red colour. For identification of non-specific binding and other experimental artefacts, negative controls were used. These consisted of omission of primary antibodies with a non-immune immunoglobulin of the same isotype and concentration as the primary antibody or incubation with antibody diluent. All control sections

showed negligible staining. The list of antibodies and dilution factors is provided in Supplementary Table 1. Stained sections were scanned using a Lamina instrument (Perkin Elmer, Waltham, MA, USA), visualised with the CaseViewer digital microscope application (3Dhistech, Budapest, Hungary), and analysed with ImageJ software.

Histological wound assessment

Histological samples were randomised using a computer-based random number generator. Histological slide assessment and data acquisition were performed by two assessors. Only one of the two assessors was formally blinded. Histological slides stained with H&E were evaluated for the microscopic wound length. The public domain software ImageJ was used to determine the microscopic wound length by drawing a straight line between the dermal wound margins. To estimate the degree of re-epithelialisation (% of the original wound), the area of the wound that was covered with neo-epidermis was expressed as a percentage of the entire wound, as described previously.[25,27]

Quantification of immunohistochemical staining was by colour deconvolution as described previously.[46,47] A total of six microscopic fields of view were used for the immunohistochemical data analysis. Out of the six microscopic images, two represented the region around the left border of the wound lesion, two additional images included the graft region, and the two remaining images included the area around the right border of the wound. Both the epidermal and dermal regions were assessed. Control average was normalized to 1. For each time point, the value of integrated density (arbitrary units) is shown relative to the value of the integrated density in control.

Gram stain

Sections (4 µm) of formalin-fixed paraffin embedded tissue were de-waxed and taken through a decreasing series of graded alcohols to water. Gram stain was performed using a Gram Stain Kit (Sigma-Aldrich, St Louis, MO, USA) to visualise *S. aureus* in tissue sections according to the manufacturer's instructions. *S. aureus* are stained in blue and the remaining biological tissue is visible in varying shades of magenta.

Masson's trichrome and May Grunwald-Giemsa staining

For histological assessment of collagen deposition in the dermis, trichrome staining was performed using a Masson Trichrome Staining Kit according to the manufacturer's instructions (Sigma-Aldrich, St Louis, MO, USA). May Grunwald-Giemsa staining was performed on formalin-fixed and paraffin-embedded sections to visualise cellular components of human bioengineered skin (Sigma-Aldrich, St Louis, MO, USA).

Multiphoton microscopy

Multiphoton inverted stand Leica SP5 microscope (Leica Microsystems Gmbh, Wetzlar, Germany) was used to assess mouse wounds as previously described.[27] A Ti:Sapphire Chameleon Ultra (Coherent, Saclay, France) with a center wavelength at 810 nm was used as the laser source to generate second harmonic and two-photon excited fluorescence signals (TPEF). The laser beam was circularly polarized and equipped with a Leica Microsystems HCX IRAPO 25x/0.95 W objective, which was used to collect and excite second harmonic generation (SHG) and TPEF. Signals were detected in epi-collection through a 405/15-nm and a 525/50 bandpass filters respectively, by NDD PMT detectors (Leica Microsystems, Wetzlar, Germany). LAS software (Leica Microsystems, Wetzlar, Germany) was used for laser scanning control and image acquisition.

Collagen second harmonic generation index

SHG and TPEF images were acquired using detectors with a constant voltage supply and constant laser excitation power allowing direct comparison of SHG intensity values. Analyses were performed using homemade Image J routine (http://imagej.nih.gov/ij/). Two fixed thresholds were chosen to distinguish biological material from the background signal (TPEF images) and specific collagen fibers were imaged with SHG images. Collagen SHG score was then established by comparing the area occupied by the collagen relative to the sample surface. TPEF (green) and SHG (magenta) images were pseudocoloured and overlaid for publication using Image J.

TUNEL assay and DNase I treatment

The Calbiochem® TdT-FragEL™ DNA Fragmentation Detection Kit was purchased from Sigma-Aldrich (Saint-Quentin Fallavier, France). Formalin-embedded samples of mouse skin tissue were sectioned (4 µm) and placed on a glass slide pre-coated with Biobond tissue section adhesive (vWR International, Radnor, PA, USA). Skin tissue sections were treated according to the manufacturer's protocol. Briefly, all sections were deparaffinised by immersion in HistoClear (Euromedex, Souffelweyersheim, France) and hydrated by transferring the slides through a graduated ethanol series to 1× Tris-buffered saline (TBS) solution. Specimens were stripped of proteins by incubation with 100 µl of 20 µg/ml proteinase K per section. A positive control was generated by using deparaffinised sections of mouse skin that were initially incubated with 20 µg/ml proteinase K, and then treated with 1 µg/µl DNase I (Sigma-Aldrich, Saint-Quentin Fallavier, France) in 1 × TBS/1 mM $MgSO_4$. Terminal deoxynucleotidyl transferase (TdT) binds to exposed 3′-OH ends of DNA fragments generated in response to apoptotic signals and catalyses the addition of fluorescein-labelled and unlabelled deoxynucleotides. When excited, fluorescein generates an intense signal at the site of DNA

fragmentation of apoptotic cells. DAPI staining was used to visualise normal and apoptotic cells. TUNEL-stained sections were scanned using a Lamina instrument (Perkin Elmer, Waltham, MA, USA), and analysed with the CaseViewer digital microscope application (3DHISTECH).

Biofabrication of three-dimensional human skin

Primary human keratinocytes and dermal fibroblasts were isolated from male and female adult skin through enzymatic dissociation. The skin specimens were sampled by a surgeon during sessions of elective abdominoplasty or reduction mammoplasty. The study was conducted in accordance with the 1975 Declaration of Helsinki. Informed written consent was obtained from all donors. All protocols were reviewed by relevant committees of "Le Ministère de l'Enseignement supérieur, de la Recherche et de l'Innovation" under approval number AC-2018-3243 and DC-2018-3242 and were performed in accordance with national laws and guidelines for the collection, use and storage of human tissue. Keratinocytes were cultured in EpiLife medium (Gibco Paisley, PA, USA) supplemented with Human Keratinocytes Growth Supplement (Gibco Paisley, PA, USA). Fibroblasts were cultured in RPMI 1640 Medium (Gibco Paisley, PA, USA) supplemented with 15% FetalClone III (GE Healthcare Bio-Sciences, Uppsala, Sweden). All cells were used at passages 2-3. Peripheral blood mononuclear cells (PBMC) were isolated from buffy coat using Ficoll (GE Healthcare Bio-Sciences, Uppsala, Sweden). $CD14^+$ monocytes were isolated by magnetic selection (Miltenyi Biotech, Bergish Gladbach, Germany) and differentiated using M1-Macrophage Generation medium DXF (PromoCell GmbH, Heidelberg, Germany). Three-dimensional modelling computer software, including open-source 3D printing toolbox (Slic3r https://slic3r.org/) and SketchUp (Trimle Inc., Sunnyvale, CA, USA), were used to design the pattern of 3D structures. Computer-aided transfer of prescribed organization was performed through deposition of

bioink formulation (CTIBiotech, Lyon, France) containing single-cell suspensions. Three dimensional skin models were built through the layering of printed filaments with the assistance of a BIO X^{TM} bioprinter (CELLINK, Gothenburg, Sweden). Following bioprinting, skin models were cultured for 21 days. During this period, 3D models were cultured in medium (CTIBiotech, Lyon, France), which aided dermal maturation, epidermis differentiation, air-liquid interphase cornification. Each sample measured 1 cm (length) x 1 cm (width) x 200 µm (depth). Cellular viability was controlled at day 21 after bioprinting with an alamarBlue™ Cell Viability Reagent (Life Technologies Corporation, Eugene, OR, USA) and Invitrogen™ LIVE/DEAD™ Viability/Cytotoxicity Kit for mammalian cells (Life Technologies Corporation, Eugene, OR, USA). Staining was performed according to manufacturer's instructions. Fluorescence was visualized with a fluorescence microscope (Leica, DMLB or Nikon Eclipse-Ti) linked to a digital camera (Leica DFC420C or Nikon Digital Sight R1) and recorded with image acquisition software (LAS Version 3 or Nis-Elements Br).

Infection of bioengineered three-dimensional human skin

At day 21 after bioprinting, 3D bioengineered skin was inoculated by injecting a total of 1 x 10^8 of *S. aureus* Xen36 bacteria diluted in 50 µl of PBS. To maximize the even distribution, the intradermal inoculum was administered through five entry points (10 µl at 12, 3, 6 and 9 o'clock plus one in the centre). Serial dilutions of the inoculum were plated to control the number of bacteria inoculated. Each model was treated for the duration of 2 min with either placebo control (helium) or CAP at 1 and 4 h. p. i. All skin models were collected at 24 h. p. i. and homogenized in 2 ml of 1 x PBS. Homogenized skin was serially diluted, plated onto BHI plates and grown overnight at 37°C. CFU were enumerated to assess bacterial load. CFU average in control group was normalized to 1.

Cells and culture conditions

Murine macrophage-like cell line RAW 264.7 (ATCC®, Molsheim, France) was grown in DMEM high glucose supplement pyruvate (Gibco Paisley, PA, USA) and 10% foetal calf serum (BioWest, Nuaillé, France) at 37°C in 5% CO_2.

Primary BMDMs were obtained from female C57BL/6J WT mice. BMDMs were grown in complete medium containing Roswell Park Memorial Institute (RPMI) 1640 Medium (Gibco Paisley, PA, USA) supplemented with 10% foetal calf serum (BioWest, Nuaillé, France), 2 mM glutamine (Gibco Paisley, PA, USA), 1 mM sodium pyruvate (Gibco Paisley, PA, USA), 10 mM HEPES (Sigma-Aldrich, MO, USA), 50 µM β-mercaptoethanol, 100 U ml^{-1} penicillin/streptomycin (Gibco Paisley, PA, USA) and 25 ng/ml mouse M-CSF (Miltenyi Biotec GmbH, Bergisch Gladbach, Germany).

Bacterial infection of macrophages

RAW 264.7 cells were seeded onto a 24-well plate at a density of 10^5 cells per well. Cells were infected with *S. aureus* (MOI of 10), and incubated for 20 min at 37°C. The samples were incubated for another 30 min, but this time with gentamicin-containing medium at 20 µg/ml (Sigma-Aldrich, MO, USA) to kill extracellular bacteria. After a washing step, complete medium was added and macrophages were treated either with placebo control (inert helium gas) or CAP for 2 min. Infected cells were lysed at 0, 2 and 5 h post infection with 0.1% Triton X-100. For enumeration of intracellular bacteria, dilution series of lysed macrophages were plated onto BHI agar.

Primary BMDMs were plated at 5 x 10^5 cells/ml onto a 92 x 16 mm petri dish and cultured in the presence of complete medium. At day 5, medium was replaced with fresh complete medium. At day 7, cells were washed and seeded onto a 24-well plate at a density of 10^5 cells per well. Cells were cultured in complete medium without antibiotics and incubated for 24 h before

bacterial challenge. For infection of BMDMs, bacteria were grown in BHI overnight, then regrown to exponential phase and added to the cells at a MOI of 10, centrifuged at 900 g for 1 min and incubated at 37 °C for 20 min. To follow a synchronized population of bacteria, extracellular bacteria were killed through incubation of BMDM in RPMI containing 20 μg mL^{-1} gentamicin (Sigma-Aldrich, MO, USA) for 30 min. To compare the intracellular growth profiles of control and CAP-treated macrophages, the samples were then either lysed immediately, to measure the initial number of intracellular bacteria, or replaced with fresh media containing gentamicin (20 μg mL^{-1}), thus permitting the invaded bacteria to replicate for 2 or 5 h. p. i. For enumeration of intracellular bacteria, infected cells were lysed with 0.1% Triton X-100 for 5 min and dilution series were plated onto BHI agar. The number of living intracellular bacteria was monitored by counting CFU. The initial number of intracellular bacteria (0 h. p. i.) was averaged was normalized to 100. The data reported are the means and standard error of means of triplicate determinations and are representative of at least three experiments.

Cell proliferation assay

Cellular proliferation was determined using tetrazolium salt WST-1 reagent (Roche Applied Science, Rotkreuz, Switzerland), which is cleaved to soluble formazan by cellular mitochondrial dehydrogenases. Infected RAW 264.7 and BMDM were treated with either placebo control or CAP and supernatants were collected from cultured macrophages at 0, 2 and 5 h. p. i. Colorimetric assay (WST-1 based) for the quantification of cell proliferation was performed using the 96-well-plate format according to the manufacturer's instructions. Absorbance was measured using a microplate reader (GloMax® Discover Microplate reader, Promega, MI, USA) at 555 nm.

ROS measurement

RAW 264.7 cells were seeded onto 24-well plates at a density of 10^5 cells per well. Cells were infected with *S. aureus* at a MOI 10:1, gently centrifuged and incubated for 20 min at 37°C to synchronize phagocytosis. The extracellular bacteria were eliminated by the addition 20 µg/ml gentamicin-containing medium and incubation for 30 min. Cells were treated by placebo control (helium) or CAP for 2 min. Fluorescent ROS probe (Sigma-Aldrich, MO, USA) was added and incubated for 30 min at 37°C. Fluorescence was measured using a microplate reader (GloMax® Discover Microplate reader, Promega, MI, USA) at 640 nm.

Pharmacological inhibition of NOX2

RAW 264.7 cells and bioengineered human skin were pre-incubated with two different NOX2 inhibitors: (i) GSK2795039 (MedChemExpress, NJ, USA) at 30 and 50 µM respectively, and (ii) gp91 ds-tat (Anaspec, CA, USA) at 50 and 100 µM respectively. Following a 30-min incubation with GSK2795039 and gp91 ds-tat, samples were treated either with placebo control (helium) or CAP.

Transfection of small interfering RNAs (siRNAs)

RAW 264.7 cells were transfected with non-targeting negative control small interfering RNA (siRNA) (ON-TARGETplus Non-Targeting Control Pool, Dharmacon, CO, USA) or endogenous positive control siRNA (ON-TARGETplus GAPD Control Pool, Dharmacon, CO, USA) at final concentration of 25 nM. ON-TARGETplus Mouse *Cybb* siRNA (Dharmacon, CO, USA) was transfected at 50 nM final concentration using DharmaFECT™ transfection Reagent (Dharmacon, CO, USA). Transfection of negative control, positive control and target siRNA was performed in serum-free medium in triplicates according to manufacturer's instructions. mRNA extraction and cell viability analysis were performed at 24 h after

transfection. Samples with target mRNA knockdown of > 80% and cell viability > 80% were used for subsequent experimentation.

RNA isolation

RNA isolation from RAW 264.7 cells was carried out using TRIzol Reagent (Thermofisher Scientific, Waltham, MA, USA) and RNeasy Mini Extraction Kit (Qiagen, Courtaboeuf, France) as described by the manufacturer. Total RNA was isolated from mouse wounds, which were homogenised in TRIzol™ Reagent (Thermofisher Scientific, Waltham, MA, USA) using GentleMACS M-tubes (Miltenyi Biotec, Bergisch Gladbach, Germany) and gentle MACS™ dissociator (Miltenyi Biotec, Bergisch Gladbach, Germany). After homogenizing the sample with TRIzol™ Reagent, chloroform was added. RNA was precipitated with isopropanol, washed to remove impurities, and then resuspended for use in downstream applications. DNA elimination was performed using Invitrogen™Ambion™TURBO DNA-free kit (Invitrogen Life Technologies Corporation, Oregon, USA). Total RNA concentration was quantified using Nanodrop 2000 (ThermoScientific, Waltham, MA, USA) or Qubit® RNA BR Assay Kit (Invitrogen Life Technologies Corporation, Oregon, USA). The RNA quality was determined by analysing the proportion between 28S to 18S ribosomal RNA electropherogram peak using an Agilent RNA 6000 Nano Kit and Agilent 2100 Bioanalyzer (Agilent Technologies, Waldbronn, Germany). Samples with a RNA integrity number >8 were used for cDNA synthesis.

Quantitative reverse-transcription–PCR

cDNA was synthesized from 1 μg of RNA using reverse Transcriptase Core Kit (Eurogentec, Seraing, Belgium). Quantitative reverse-transcription–PCR (qRT–PCR) was performed using a QuantiTect SYBR Green PCR Kit (Qiagen, Courtaboeuf, France) and C1000 CFX384 Touch

Real-Time PCR System (Bio-Rad Laboratories, Hercules, California, USA). Gene expression assays were performed with primer sequences purchased from Qiagen (Qiagen, Courtaboeuf, France). The list of primer is provided in Supplementary Table 2. Housekeeping control gene was used to normalize the amounts of cDNA within each sample. Differences were calculated using the Ct and comparative Ct methods for relative quantification. The relative level of gene expression was normalized with a housekeeping gene and used as a reference to calculate the relative level of gene expression according to the following formula: 2-ΔΔCt, where-ΔΔCt=Δ Ct gene - Δ Ct Average where Δ Ct gene = Ct gene - Ct Hprt1 and Δ Ct Average = Average Δ Ct control. For all biological replicates, 2 technical replicates were performed. All samples were evaluated in at least three independent experiments.

Fluorescence microscopy

Eight-mm round glass coverslips (Electron Microscopy Sciences, Hatfield, PA, USA) were sterilized, coated with poly-l-lysine (Sigma-Aldrich, MO, USA) and placed into the wells of a 24-well plate. RAW 264.7 cells were seeded onto coverslips at a density of 10^5 cells/cm^2, incubated in complete medium without antibiotics at 37°C overnight, and infected with *S. aureus* Xen36 at MOI of 10. Infected RAW 264.7 cells were incubated in antibiotic-free culture medium for 30 min, after which the medium was supplemented with 20 µg/ml of gentamicin to ensure the killing of extracellular bacteria. At 5 h. p. i., all samples were washed in PBS, fixed in 4% paraformaldehyde (Electron Microscopy Sciences, Hatfield, USA) in PBS for 60 minutes and washed in 0.5% bovine serum albumin in PBS. Paraformaldehyde-fixed cells were permeabilised with 0.1% Triton X-100 in PBS for 4 minutes. Cells were blocked with 5% goat serum (Sigma-Aldrich, Saint-Louis, MO, USA) in PBS for 30 minutes, incubated with primary antibody diluted in 0.5% BSA in PBS for 60 minutes, and then washed with 0.5% BSA in PBS. Cells were incubated with the appropriate fluorophore-tagged secondary antibodies for 60

minutes, washed with 0.5% BSA in PBS. The list with antibody names and dilution factors is provided in Supplementary Table 1. Coverslips were mounted in VECTASHIELD HardSet Antifade Mounting Medium with DAPI (Vector Laboratories, Burlingame, CA, USA) on glass slides. Cell imaging was performed with an inverted Eclipse TiE Nikon microscope equipped with a CSU-X1 spinning disk confocal scanning unit (Yokogawa, Ishikawa, Japan) and with an Evolve 512 Delta EMCCD Camera (Photometrics, AZ, USA). Images were acquired with a x100 1.4 numerical aperture oil objective and MetaMorph software (Molecular Devices, CA, USA). Images were converted to 8 bit images using ImageJ software, and then exported as .tif files. Analyses were performed with an open source CellProfiler 4.1.3. (https://cellprofiler.org/) software.[48] Briefly, the pipeline segmented channel intensity using 'IdentifyPrimaryObjects' module followed by 'MeasureImageIntensity'. Next, colocalization was pre-formed with the 'MeasureColocalization' module for each channel within the identified objects (Bacteria, Cell, Protein target of interest) with a minimum threshold of 15. The correlation overlap was then classified to the Bacteria or Cell regions using 'ClassifyObjects' module. The data of the colocalisation analysis are expressed as the values for 50-100 *S. aureus*-containing phagosomes, which were counted and scored for the presence or absence of markers. All samples were evaluated in triplicate and in at least three independent experiments. Results were expressed as the mean percentage of marker colocalisation on *S. aureus*-containing phagosomes ± SEM.

Cell fractionation

RAW 264.7 cells were fractionated according to the protocol previously described.[49] Briefly, cells were washed and resuspended in 0.5% BSA diluted in PBS, and centrifuged at 300 g for 5 minutes. Cells were next resuspended in homogenization buffer (8% sucrose in imidazole 3 mM MgCl2 1 mM supplemented with EGTA 0.5 mM, gelatine 0.5%, Complete™ protease and

phosphatase inhibitors (Roche, Mannheim, Germany)) and centrifuged at 300 g for 10 minutes. Mechanical disruption of cells was performed in homogenization buffer using a 25G 5/8 needle. Following centrifugation at 2000 g for 15 minutes, the post-nuclear fraction was collected, brought to 40% sucrose and gently layered on top of 60% sucrose in an open-top transparent tube (Beckman Coulter GmbH, Krefeld, Germany). A 60/40%, 40/30%, 30/20%, and 20/8% sucrose gradient was prepared and ultra-centrifugation was performed using a SW 41 Ti Swinging-Bucket Rotor (Beckman Coulter, Villepinte, France) at 100,000 g for 1 hour. The recovered fractions were adjusted at a final concentration of 10% sucrose. To precipitate protein, one volume of 100% (w/v) trichloroacetic acid was added to 4 volumes of the sample, and incubated for 10 min at 4 °C. After centrifugation at 14000 g for 5 min the supernatant was removed and the pellet was washed twice with cold acetone. The pellets were heated to 95 °C for 5–10 min and the dried pellets were resuspended in 50 µl of 1% SDS. The protein concentration was assessed using the Qubit™ Protein Assay (Life Technologies Corporation, Oregon, USA). The samples and standards were read with the Qubit™ Flex Fluorometer (Life Technologies Corporation, Oregon, USA).

SDS-Polyacrylamide Gel Electrophoresis (SDS-PAGE), immunoprecipitation and immunoblotting

RAW2 264.7 cells were lysed in ice-cold RIPA buffer (Cell Signaling Technology, Beverly, MA, USA) supplemented with Complete™ protease and phosphatase inhibitors (Roche, Mannheim, Germany). The lysate was centrifuged at 15000 × g for 10 min at 4 °C, and the supernatant was assayed for protein content. Protein content was quantified using QubitTM Protein Assay (Life Technologies Corporation, Oregon, USA) and QubitTM Flex Fluorometer (Life Technologies Corporation, Oregon, USA) according to the manufacturer's instructions. Total protein was prepared in 4× Laemmli buffer (Bio-Rad Laboratories, Hercules, CA, USA)

and 80 mM DTT. For immunoprecipitation, protein was incubated with 5 mg of antibody bound to Invitrogen Dynabeads™ Protein G (Thermo Fisher Scientific, Vilnius, Lithuania) for 2 h at 4°C with constant mixing. Tubes containing Dynabeads™ Protein G/antibody/antigen complex were washed three times with 1 × PBS and placed on a MagnaRack™ (Thermo Fisher Scientific, Waltham, MA, USA) magnetic separation rack to remove the supernatant between each wash. Antibody and the bound proteins were solubilised in NuPAGE™ LDS Sample Buffer and NuPAGE™ Sample Reducing Agent (Invitrogen, CA, USA). Protein was resolved on a 4%–20% Mini-PROTEAN TGX Stain-Free Protein Gel (Bio-Rad Laboratories, Hercules, CA, USA). Forty µg of protein was subject to SDS-PAGE separation and immunoblotting. Following protein electrotransfer, Immun-Blot® PVDF (Bio-Rad Laboratories, Hercules, CA, USA) membrane was blocked for 1 h at RT in 1X TBS containing 5% (w/v) BSA. Proteins were detected by incubation with primary antibodies in blocking solution overnight at 4 °C. Following three 5 min washes of TBS with 0.1% Tween-20, membranes were incubated in the appropriate dilution of horseradish peroxidase conjugated, species-specific secondary antibodies diluted in 5% blocking solution for 1 h at RT. Chemiluminescent detection was performed using the Clarity Western ECL Substrate (Bio-Rad Laboratories, Hercules, CA, USA). Chemiluminescence signals were acquired using the ChemiDoc XRS+ System and Image Lab Software (Bio-Rad Laboratories, Hercules, CA, USA). Signal intensity was determined by densitometry and fold changes in protein levels was calculated from this data. Uncropped western blots are displayed in Supplementary Fig. 6. The list with antibody names and dilution factors is provided in Supplementary Table 1.

Statistical analysis.

Statistical analysis was performed using GraphPad Prism 9 software (GraphPad Inc, San Diego, CA, USA) and statistical tests are reported in figure legends. Data normality was tested by

D'Agostino-Pearson test, and appropriate parametric or non-parametric tests were performed. *In vivo* experiments were performed on age and sex-matched mice. Prior power calculations were performed to predetermine the sample size using an open-access software (https://shade.pasteur.fr/) and based on previous experience with similar wound healing models. Blinded assessment of experimental outcomes was not always applicable; however, it was used whenever possible. Unless stated otherwise, the data of the *in vitro* experiment analyses is reported as mean ± s.e.m. of the values for repeated conditions in separate wells and are representative of at least three experiments performed. Each biological replicate had at least two technical replicates. The number of biological replicates is indicated in the figure legends. *P* values less than 0.05 (*), 0.01 (**), or 0.001 (***) were considered as statistically significant.

Figure 1.

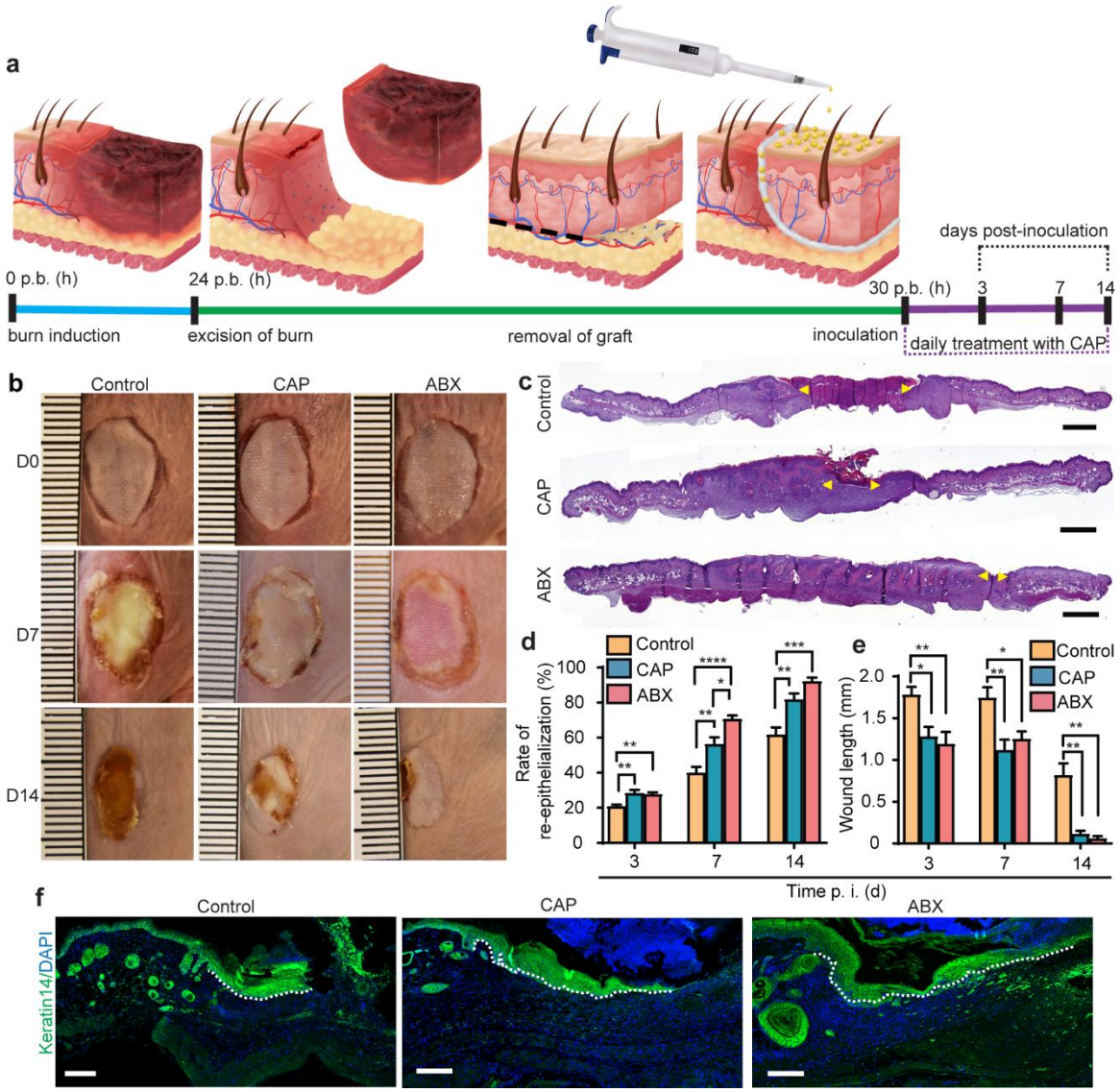

Figure 1. Infected burn wounds treated with cold atmospheric plasma heal faster than placebo controls. (a) Experimental outline of the *in vivo* mouse wound healing assay. Burn wounds were grafted, inoculated with *S. aureus*, and treated either with control, CAP or mupirocine (ABX). **(b)** Representative images of grafted mouse burn wounds from two independent experiments. Scale, 1 mm. **(c)** Overview images of H&E-stained wounds at 14 d. p. i. Yellow arrows indicate the margins of the microscopic wound length. Scale, 1000 µm. **(d)** The rate of wound re-epithelialization at 3, 7 and 14 d. p. i. Per order in the bar graph, n = 12, 14, 9 for control, n = 11, 10, 5 for CAP and n = 11, 10, 5 for ABX groups, *P < 0.05, **P < 0.01, ***P < 0.001, ****P < 0.0001 *versus* control. One-way ANOVA with Tukey's multiple

comparison post-hoc test. **(e)** Graphical representation of microscopic wound length. n = 12, 14, 9 for control, n = 11, 10, 5 for CAP and n = 11, 10, 5 for ABX groups, *P < 0.05, **P < 0.01 *versus* control. One-way ANOVA with Tukey's multiple comparison post-hoc test. Data represent mean ± s.e.m from two independent experiments. **(f)** Representative images of wounds (7 d. p. i.) immunolabeled with epidermal marker keratin 14 (green). Dotted line demarcates the advancing epidermal tongue (neo-epidermis). Scale bars, 100 µm. p. b. (h), post-burn (hours); CAP, cold atmospheric plasma; ABX, antibiotics; d. p. i., days post-inoculation; time p. i. (d), time post-inoculation (days).

Figure 2.

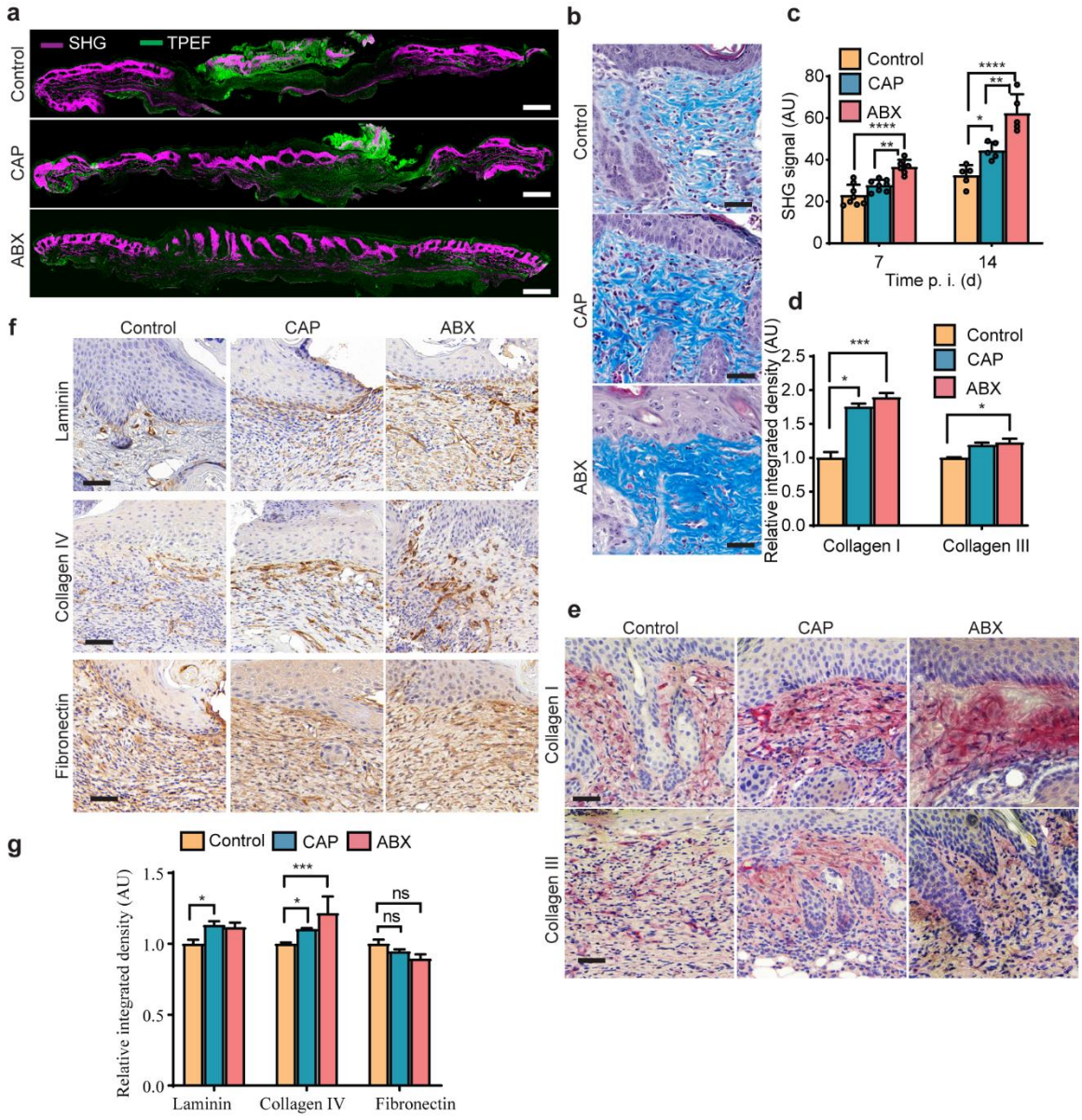

Figure 2. Extracellular matrix proteins are upregulated *in vivo* in response to cold atmospheric plasma. (a) Two photon microscopy images of wound sections (14 d. p. i.). Scale bar 1 mm. **(b)** Masson's trichrome (14 d. p. i.) staining. Scale bar 20 µm. **(c)** SHG signal in mouse wounds (7 and 14 d. p. i.). *n* = 8 for control, *n* = 8 for CAP and *n* = 6 for ABX for day 7; *n* = 5 for control, *n* = 5 for CAP and *n* = 5 for ABX for day 14. **P* < 0.05, ** *P* <0.01, **** *P* <0.0001 *versus* control. One-way ANOVA with Tukey's multiple comparison post-hoc test. **(d)** Quantitative microdensitometric evaluation and **(e)** representative images of wound sections

stained for collagen I and III (7 d. p. i.). *n* = 7 for control, *n* = 7 for CAP and *n* = 7 of ABX, **P* < 0.05, *****P* < 0.0001 *versus* control. Scale bar 25 µm. **(f)** Representative images and **(g)** quantitative evaluation of laminin, collagen IV and fibronectin (7 d. p. i.). *n* = 8 for control, *n* = 8 for CAP and *n* = 8 of ABX, **P* < 0.05, ***P* < 0.01, *** *P* <0.001 *versus* control. Scale bar 50 µm. One-way ANOVA non-parametric Kruskal–Wallis with Dunn's multiple comparison post-hoc test was used in **(d)** and **(g)**. Results in **(c)**, **(d)**, and **(g)** are reported as mean ± s.e.m.; AU arbitrary units; CAP cold atmospheric plasma; ABX antibiotics; SHG second harmonic generation; TPEF two-photon excited fluorescence; time p. i. (d), time post-inoculation (days).

Figure 3.

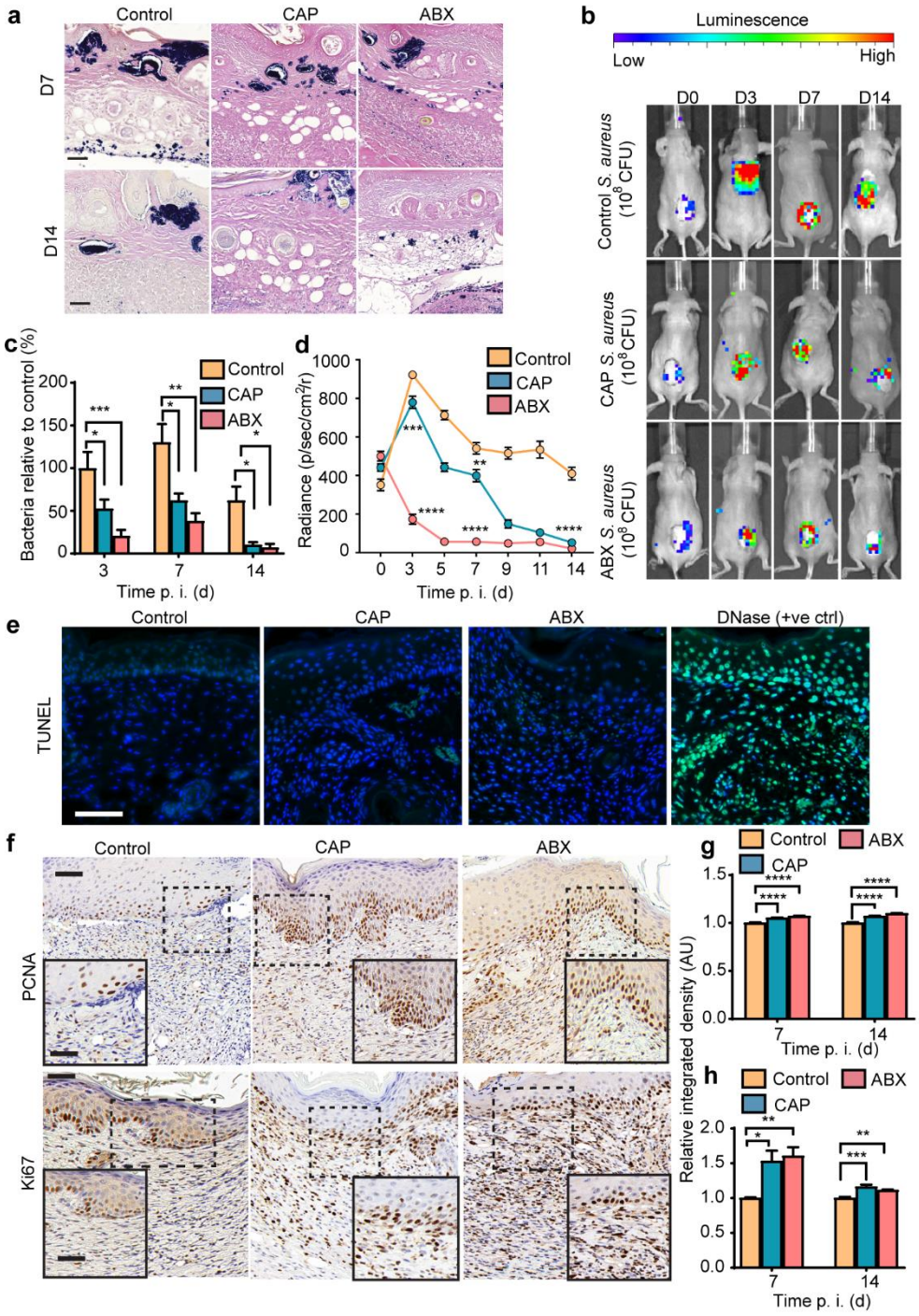

Figure 3. Reduced bacterial wound burden and enhanced cellular proliferation coincide with CAP treatment. (a) Wound sections stained with Gram stain. Scale bar 20 µm. **(b)** Real-time monitoring of *S. aureus* Xen 36 *in vivo*. **(c)** Bacterial wound burden by CFU enumeration. The number of CFU is shown relative to the number of CFU detected in control wounds at 3 d.

p. i. **(d)** Quantification of *S. aureus* Xen 36 bioluminescence signal. **(e)** TUNEL staining (7 d. p. i.). Apoptotic cells are green; DAPI is blue. Scale bar 20 µm. **(f)** Representative images (7 d. p. i.) and **(g)** quantitative evaluation of PCNA (mitotic marker) and **(h)** Ki67 (proliferation marker) in mouse wounds. Enlarged views of the boxed regions are shown in the insets. Scale bar 50 µm; inset 20 µm. In **(c), (d), (g)** and **(h)** $n = 11$ for control, $n = 10$ for CAP and $n = 10$ for ABX for day 3 and 7; $n = 5$ for control, $n = 5$ for CAP and $n = 5$ for ABX for day 14. $^{*}P < 0.05$, $^{**}P < 0.01$, $^{***}P < 0.001$ *versus* control. One-way ANOVA with Tukey's multiple comparison post-hoc test was used in **(c), (d), (g)** and **(h)**. Results in **(c), (d), (g)** are expressed as mean ± s.e.m. of two independent experiments. CFU colony forming units; ctrl control; CAP cold atmospheric plasma; time p. i. (d) time post-inoculation (days).

Figure 4.

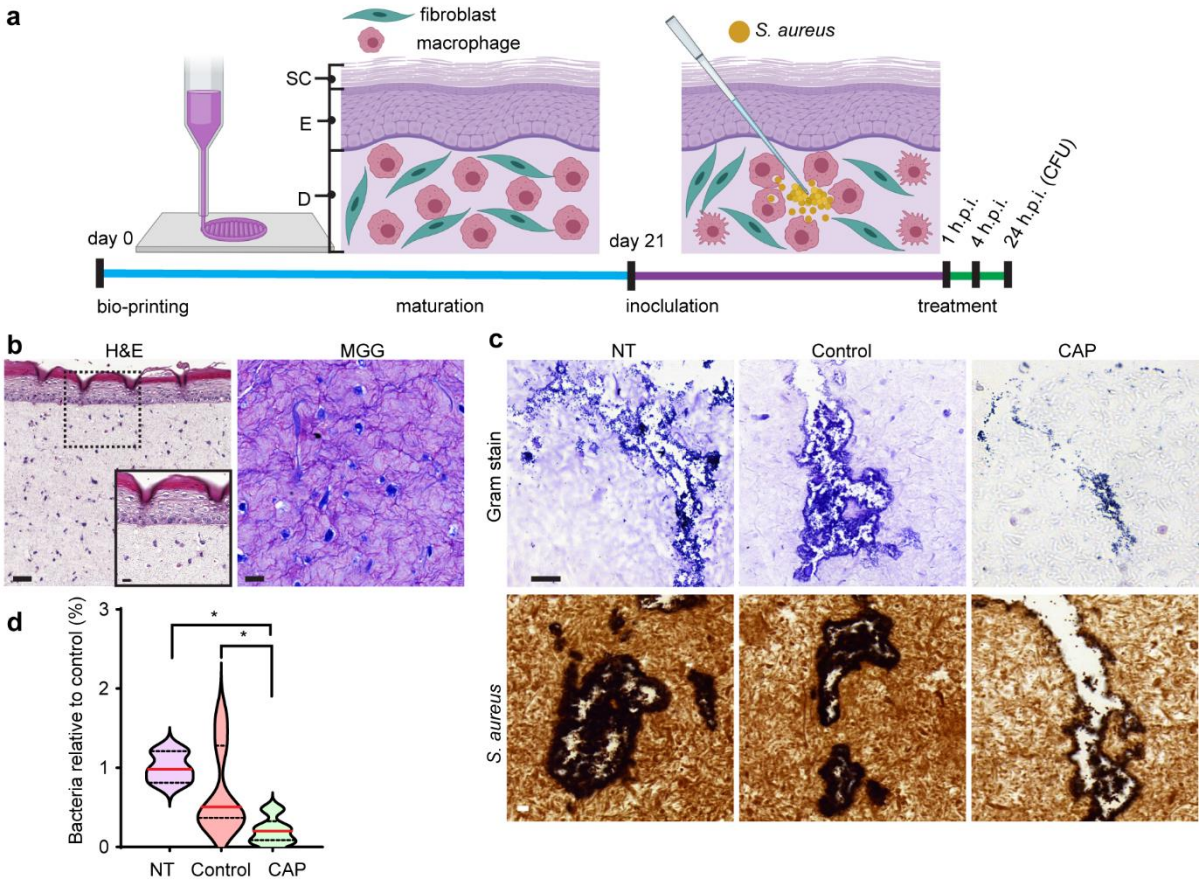

Figure 4. Treatment with CAP facilitates bacterial clearance in a 3D model of human staphylococcal wound infection. (a) Schematic representation of experimental timeline. Using bioink with suitable rheological behaviour, 3D bioprinting of human skin equivalent was performed. Following maturation steps, bioengineered skin was wounded using a pipette and intradermal inoculation was performed with 1×10^8 CFU. **(b)** Microscopic images of bioengineered human skin collected at 24 h. p. i. and stained with either H&E (left) or MGG (right). Enlarged view of the boxed region is shown in the inset. Scale bar: H&E (large) 100 µm; inset 20 µm; MGG-stained image 20 µm. **(c)** Bioengineered human skin was wounded, inoculated with *S. aureus*, and processed for microscopic visualisation of intradermal bacteria. Representative images of Gram stain (upper panel) and immunohistochemical staining using

anti-*S. aureus* antibodies (lower panel). Scale bar 20 µm. **(d)** Violin plot with mean denoted in red. *In vitro* wounds were infected and analysed for the number of living bacteria by counting CFU at 24 h. p. i. CFU average in NT group was normalized to 1 and compared to two other experimental conditions. $n = 3$ for NT, $n = 7$ for control and $n = 10$ for CAP. $^{*}P < 0.05$ *versus* NT. One-way ANOVA non-parametric Kruskal–Wallis with Dunn's multiple comparison post-hoc test. Results are expressed as mean ± s.e.m. of three independent experiments. SC *stratum corneum*, E epidermis, D dermis, h. p. i. hours post inoculation; H&E hematoxylin and eosin; MGG May Grunwald-Giemsa; NT no treatment, CFU colony forming units; CAP cold atmospheric plasma.

Figure 5.

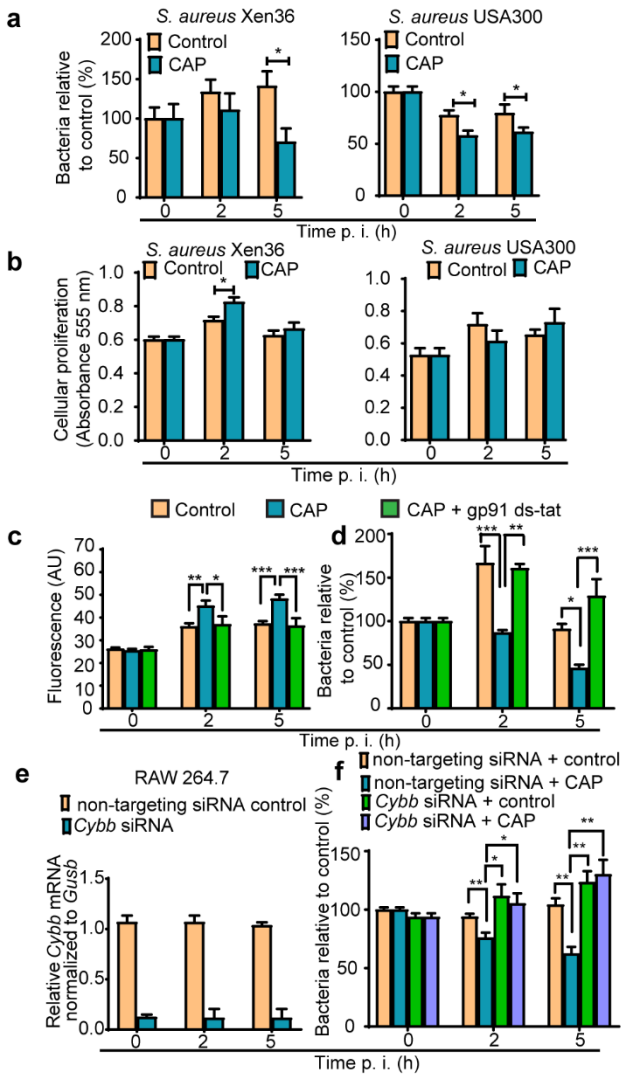

Figure 5. NOX2 inhibition and *Cybb* knockdown downregulate ROS production in macrophages and abrogate anti-staphylococcal activity of CAP. (a) RAW264.7 macrophages were infected with *S. aureus* Xen 36 (left) and *S. aureus* USA300 (right). Cells were lysed at 0, 2, and 5 h. p. i., and released bacteria were counted by CFU enumeration. **(b)** The effect of CAP treatment on cellular proliferation of RAW264.7 macrophages infected with *S. aureus* Xen 36 (left) and *S. aureus* USA300 (right) was determined. **(c-d)** RAW264.7 macrophages were pre-treated with gp91 ds-tat (NOX2 antagonist), infected with *S. aureus* Xen 36 and exposed to CAP. **(c)** ROS production and **(d)** the number of living bacteria was monitored by counting CFU. **(e)** RAW264.7 were transfected with either non-targeting siRNA or *Cybb* siRNA and analysed for *Cybb* mRNA expression by RTqPCR. **(f)** RAW264.7 were transfected with siRNA and infected with *S. aureus* Xen 36. The number of living bacteria was monitored by counting CFU. In **(a), (d)** and **(f)** time zero average was normalized to 100. For each time point and for each strain, the number of CFU is shown relative to the number of CFU at time zero. Values are expressed as mean ± s.e.m. of three independent experiments with at least 6 biological replicates in each condition. For **a** and **b** significance was determined by

Mann–Whitney U test, and **c-f** by one-way ANOVA with Tukey's multiple comparison post-hoc test, *$P < 0.05$, **$P < 0.01$, ***$P \leq 0.001$. of at least three independent experiments.

Figure 6.

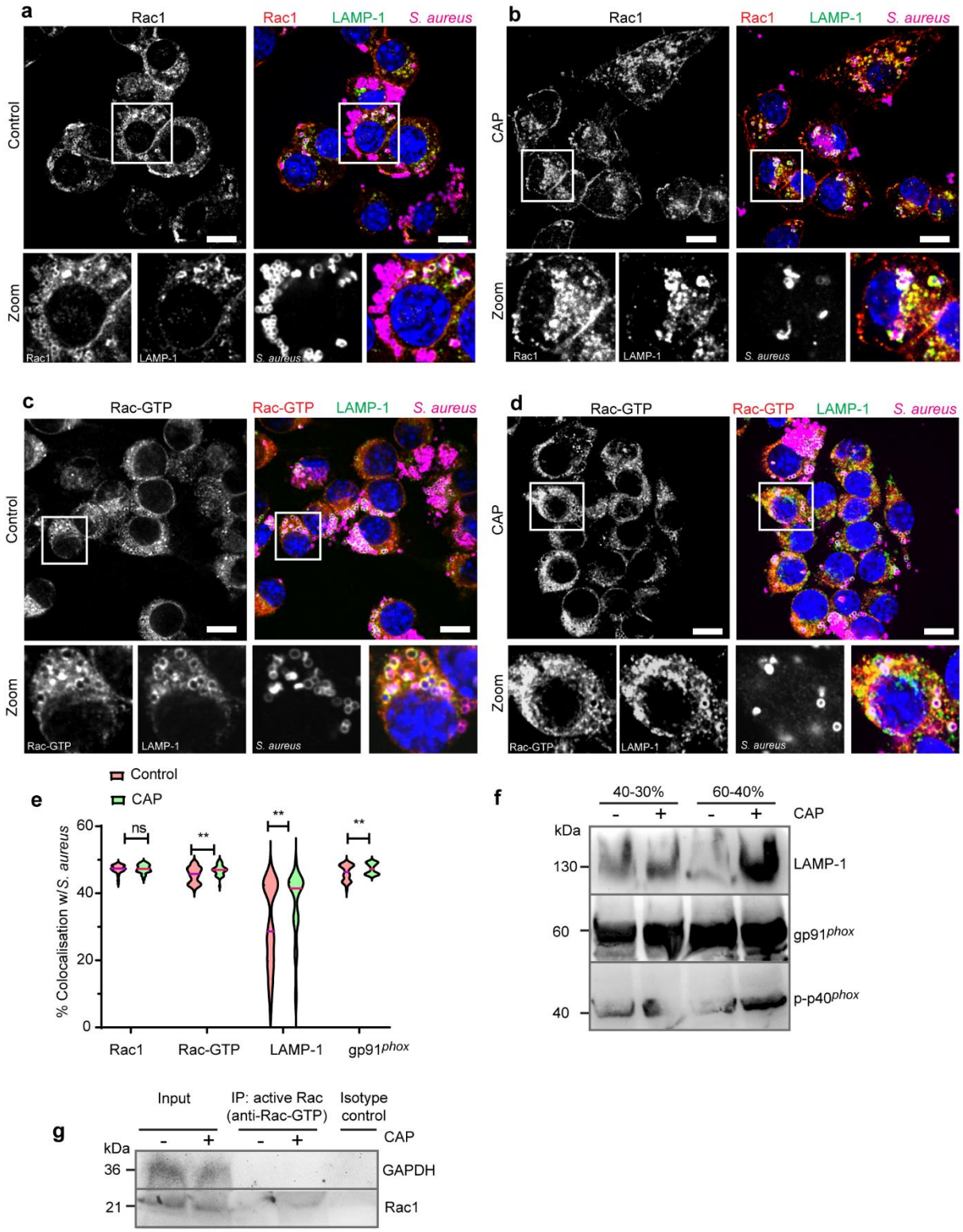

Figure 6. Cold atmospheric plasma activates Rac1. (a-d) RAW264.7 macrophages were inoculated with *S. aureus* (MOI = 10; 5 h. p. i.). Representative confocal microscopy images.

Scale bar 10 µm. Zoomed in views of the boxed regions are indicated. **(e)** *S. aureus*-containing vacuole localisation with Rac1 (total), Rac-GTP (active form), LAMP-1, and gp91^{phox} was calculated at 5 h. p. i. Median is indicated by a solid (magenta) line. Values are expressed as mean ± s.e.m. of three independent experiments. Mann-Whitney U test; $^{**}P \leq 0.01$; ns, not significant. (n = 3 biological replicates; 50-60 cells per group). **(f)** RAW264.7 macrophages were infected with *S. aureus* (MOI of 10) and collected at 5 h. p. i. Subcellular fraction (40-30% or 60 to 40%) of cells were immunoblotted with LAMP-1, gp91^{phox} and p-p40^{phox}. **(g)** Subcellular fraction (60-40%) from RAW264.7 macrophages infected with *S. aureus* (MOI of 10) were collected at 5 h. p. i. and incubated with antibodies to Rac-GTP (IgM) bound to magnetic protein-G beads. Precipitates were analysed by immunoblotting. IP, immunoprecipitate; WCL, whole cell lysate.

Extended Data Video 1. Weakly ionized helium gas jet. Video imaging of the single-channel helium gas jet used in the present study to produce cold atmospheric plasma. The violet-tinted plasma jet is ejected from the nozzle. The jet (or excited glow discharge) is made up of short and long-lived reactive oxygen and nitrogen species, excited states and charged particles such as electrons and ions. The plasma jet was operated at a 0.50-slm gas flow rate (slm, standard litres per minute) and a 50-Hz repetition frequency. The voltage was set to 24 kV. The video image demonstrates the interaction between the plasma jet and cell culture medium inside a 24-well plate.

Extended Data Figure 1.

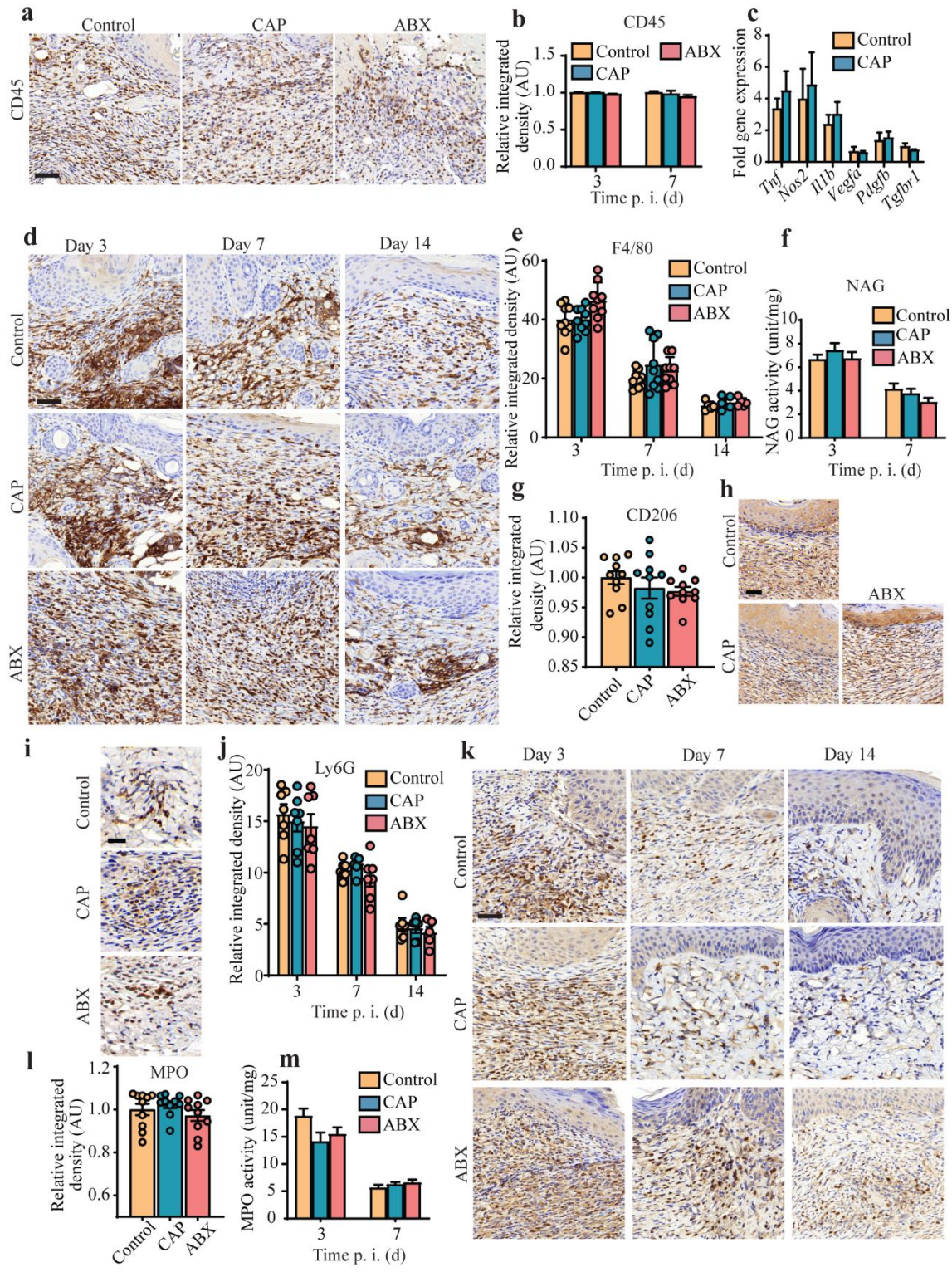

Extended Data Figure 1. Cold atmospheric plasma exerts no changes to immune cell infiltration *in vivo*. (a) Images (7 d. p. i.), and **(b)** quantification of CD45 staining. *n* = 11 for control, *n* = 11 for CAP and *n* = 11 of ABX. Scale bar 50 µm. **(c)** Gene expression in wounds

determined by RTqPCR and normalised to *Hprt1*. *n* = 11 for control, *n* = 11 for CAP. **(d)** Images, and **(e)** quantification of F4/80 staining. *n* > 5 for control, *n* >5 for CAP and *n* > 5 of ABX. Scale bar 50 µm. **(f)** NAG in wounds. *n* = 6 for control, *n* = 6 for CAP and *n* = 6 of ABX. **(g)** quantification of CD206 (7 d. p. i.) and **(h)** CD206 images. *n* = 11 for control, *n* = 11 for CAP and *n* = 11 of ABX. Scale bar 50 µm. **(i)** Images, and **(l)** quantification of MPO (3 d. p. i.). *n* = 11 for control, *n* = 11 for CAP and *n* = 11 of ABX. Scale bar 20 µm. **(j)** Quantification of Ly6G and **(k)** Ly6G images. *n* > 5 for control, *n* >5 for CAP and *n* > 5 of ABX. Scale bar 50 µm. **(m)** MPO in wounds. *n* = 6 for control, *n* = 6 for CAP and *n* = 6 of ABX. Results in all graphs are reported as mean ± s.e.m.; One-way ANOVA non-parametric Kruskal–Wallis with Dunn's multiple comparison post-hoc test was used in **(b), (e)**, **(f)**, **(j)** and **(m)**. Two-tailed unpaired Student's t-test Two-tailed unpaired Student's t-test (control *versus* treatment) in **(c)**, **(g)**, and **(l)**. AU arbitrary units; NAG N-Acetylglucosaminidase; MPO myeloperoxidase.

Extended Data Figure 2.

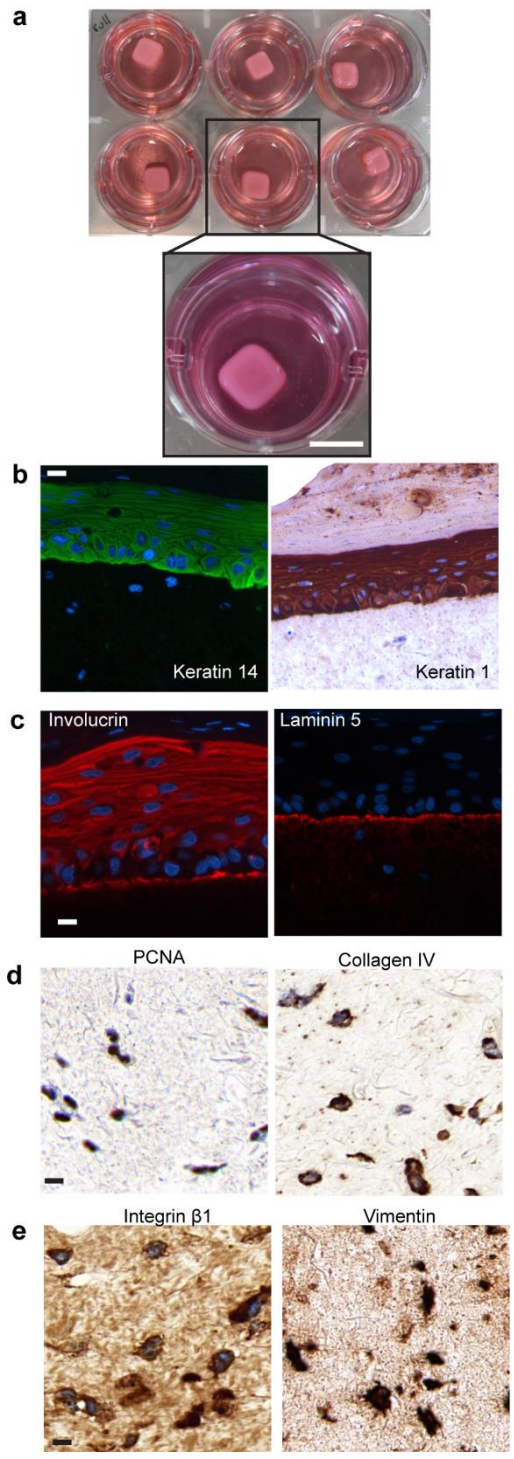

Extended Data Figure 2. Bioengineered human skin expresses essential markers of human epidermal and dermal components. (a) Representative image of bioengineered human skin cultured in a 6-well plate. Scale bar 1 cm. Following dermal maturation, epidermal differentiation, and air-liquid interface cornification, 3D models were fixed in paraformaldehyde, and analysed for the expression of markers of epidermis, dermal-epidermal junction and dermis. Three-dimensional models were stained with: **(b)** anti-keratin 14 and anti-keratin 1; **(c)** anti-involucrin and anti-laminin 5, (d) anti-PCNA and anti-collagen IV; (e) anti-integrin β1 and anti-vimentin antibodies. Representative images of immunofluorescent and immunohistochemistry analysis is shown. Scale bar 20 µm.

Extended Data Figure 3.

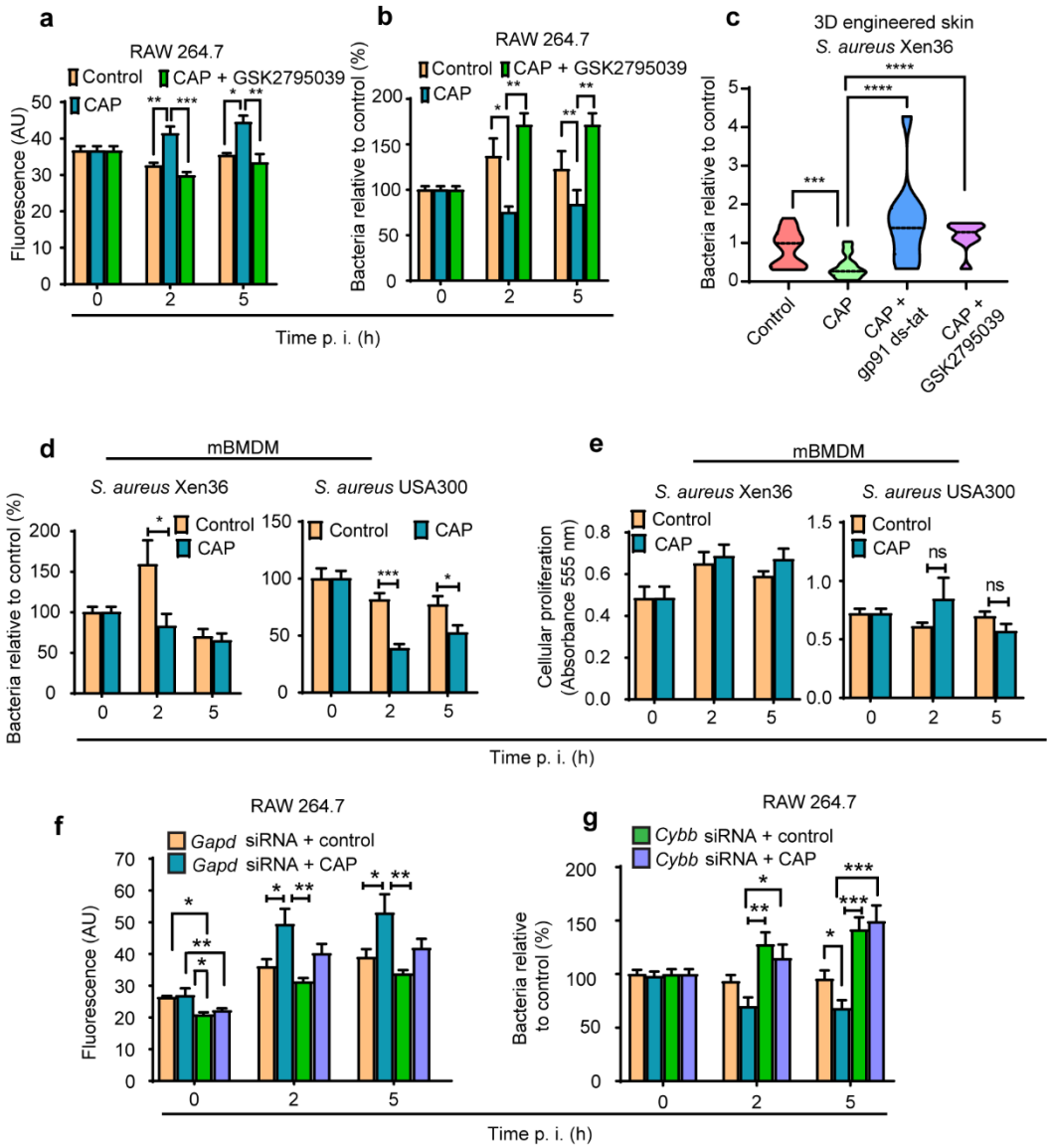

Extended Data Figure 3. Addition of NOX2 inhibitors downregulated *S. aureus* killing in 2D and 3D *in vitro* models of bacterial infection. (a) ROS production and **(b)** the number of living bacteria was monitored by counting CFU in RAW264. **(c)** Three-dimensional skin was inoculated with *S. aureus*. The number of living bacteria was determined by counting CFU at 24 h. p. i. CFU average in control group was normalized to 1. n = 9 for control, n = 12 for control, n = 10 for CAP+gp91 ds-tat, n= 10 CAP + GSK2795039. Values are expressed as mean ± s.e.m. of three independent experiments. Two-tailed unpaired Student's t-test. *$P < 0.05$, **$P < 0.01$, ***$P \leq 0.001$, ****$P \leq 0.0001$. **(d)** mBMDM were inoculated with *S. aureus*, and

released intracellular bacteria were counted by CFU enumeration. **(e)** Cellular proliferation of mBMDM infected with *S. aureus*. **(f-g)** RAW264.7 macrophages were transfected with either endogenous control siRNA (*Gapd*) or *Cybb* siRNA. After successful transfection, cells were infected with *S. aureus* Xen 36 and exposed to CAP. **(f)** ROS production and **(g)** the number of living bacteria was monitored by counting CFU in RAW264. In (**a), (b)**, and **(d-g)** values are expressed as mean ± s.e.m. of three independent experiments with at least six biological replicates. Significance was determined by one-way ANOVA with Tukey's multiple comparison post-hoc test, $*P < 0.05$, $**P < 0.01$, $***P \leq 0.001$, *versus* control. In **(b), (d),** and **(g)** time zero average was normalized to 100. For each time point, the number of CFU is shown relative to the number of CFU at time zero.

Extended Data Figure 4.

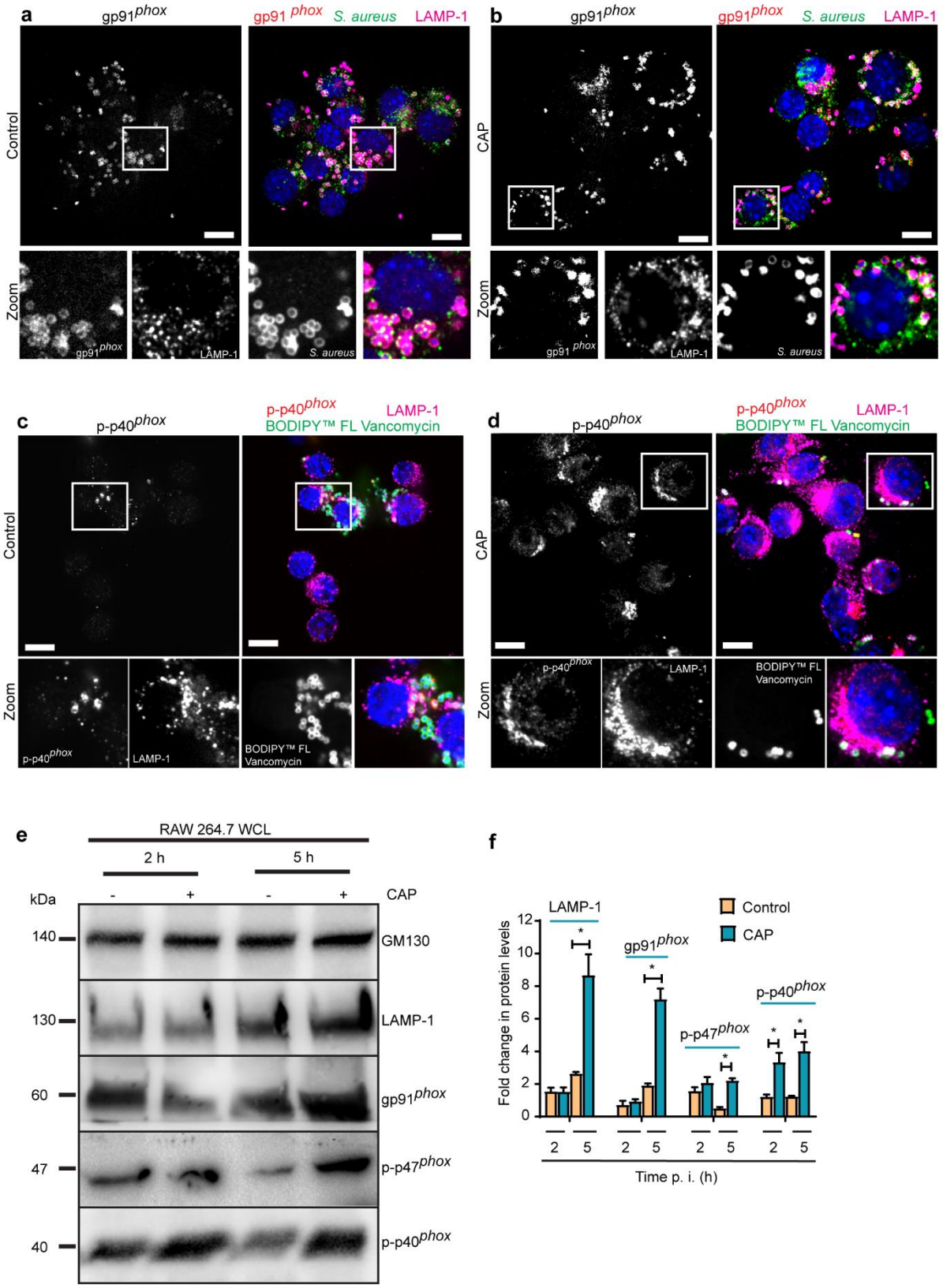

Extended Data Figure 4. Cold atmospheric plasma upregulates protein levels of key NOX2 components. (a-d) RAW264.7 macrophages were inoculated with *S. aureus* (MOI = 10) and fixed with PFA at 5 h. p. i. Representative confocal microscopy images. **(a-b)** The different colours indicate the following: gp91^{phox} (red), *S. aureus* (green), LAMP-1 (magenta), and DAPI (blue). **(c-d)** The different colours indicate the following: p-p40^{phox} (red), LAMP-1 (magenta), BODIPY^{TM} FL Vancomycin-positive *S. aureus* (green), and DAPI (blue). Scale bar 10 µm. Zoomed in views of the boxed regions are indicated. **(e)** RAW264.7 were infected with *S. aureus* (MOI of 10) and collected at 5 h. p. i. Whole cell lysate extracts were immunoblotted with gp91^{phox}, p-p47^{phox}, p-p40^{phox}, total Rac, and LAMP-1. GM130 was used as a loading control. **(f)** Bar graph showing the fold change in protein levels. Values are means ± s.e.m. of three independent experiments with at least three biological replicates in each condition. Two-tailed unpaired Student's t-test (control *versus* treatment). *$P < 0.05$. WCL, whole cell lysate; PFA paraformaldehyde; CAP cold atmospheric plasma.

Supplementary Figure 1.

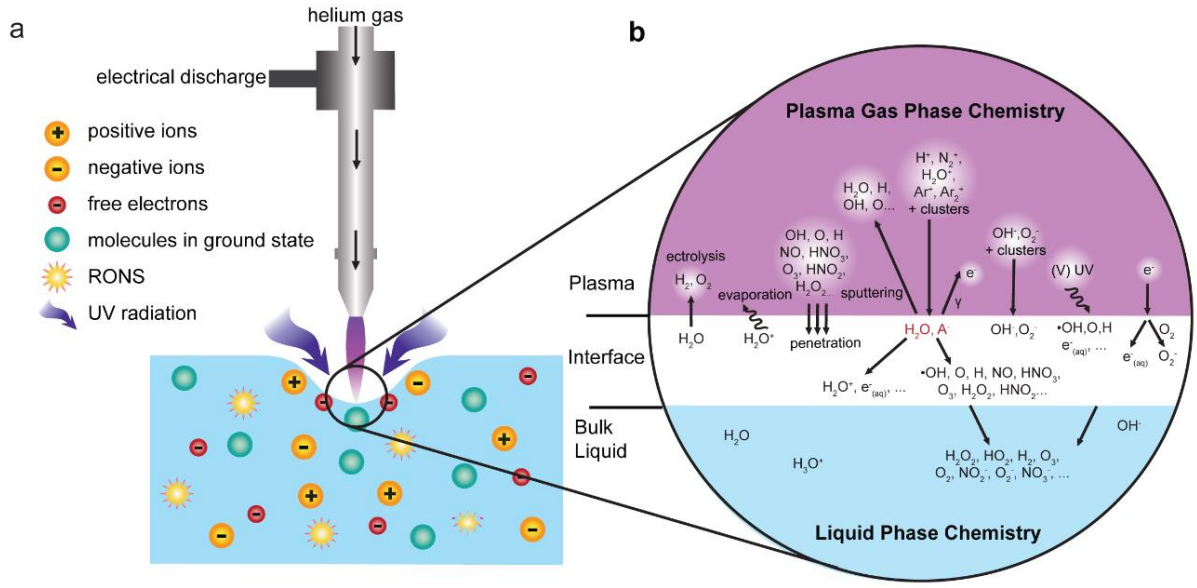

Supplementary Figure 1. Schematic representation of major physical and chemical processes occurring at the plasma–liquid interface. **(a)** Experimental setup of a device designed to produce weakly ionized gas or cold atmospheric plasma (CAP). The plasma jet device is set up vertically with the pure helium gas flowing downwards. Helium is propagated through a capillary tube at a constant rate. Electrical discharge is applied to helium via a high voltage generator. A visible plume of violet-tinted plasma is visible at the inferior end of the capillary tube where plasma interacts with the surrounding air and target liquid. The plasma jet operates under atmospheric pressure and ambient air. Direct contact of plasma with liquids leads to generation of short and long-lived reactive oxygen and nitrogen species (RONS). Plasma is also a source of electric field, ultra-violet radiation and charged particles (e.g. ions and free electrons). **(b)** The biological effects of plasma can be attributed to the synergistic effects of ultra-violet radiation, electric fields and RONS. Plasma is a form of advanced oxidation technology, which involves the breakdown of organic and inorganic compounds. The gas phase chemistry (top, purple) is different from the liquid phase chemistry (bottom, blue). The interface (middle, white) is the region between the plasma plume and liquid target. A broad range of short and long-lived species are produced at the interphase. Different species have

different penetration depths depending on their chemical lifetimes. The short-lived oxygen species, such as superoxide radical (O_2^-) and hydroxyl radical ($^{\bullet}OH$) produced at the interface, may undergo reactions to form long-lived RONS including H_2O_2 either near or within the target liquid. Plasma-generated long-lived species may accumulate within the interphase and undergo subsequent hydration or solvation before entering the target liquid via poorly understood molecular transport processes. These reactions may lead to production of RONS such as O_2^-, NO_2^-, NO_3^-, O_3 and $ONOO^-$. At the interface, plasma induces evaporation of water, thus creating a source of water molecules that can be dissociated by UV photons that are generated by the CAP jet, into hydroxyl radical (•OH). In aqueous solution, short-lived and highly reactive hydroxyl radicals generate longer-lived but less reactive molecules such as H_2O_2 and NO_2^-. NO_2^- nitrite. NO_3^- , nitrate. UV, ultraviolet. NO, nitric oxide. NO_2, nitrogen dioxide. O_3, ozone. RONS, reactive oxygen and nitrogen species. (b) Adapted from Bruggeman *et al.*[26]

Supplementary Figure 2.

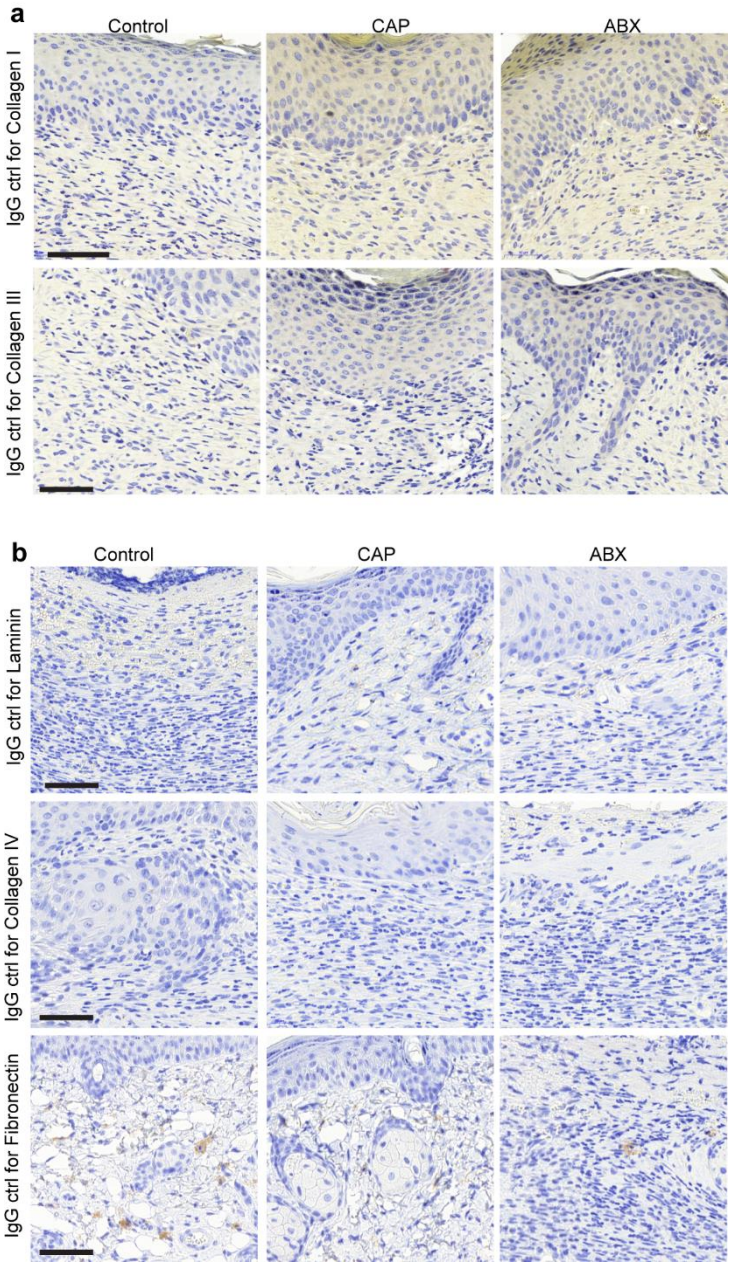

Supplementary Figure 2. **Negative isotype control resulted in negligible background staining**. **(a-b)** Mouse wound sections (7 d. p. i.) were stained with IgG antibodies raised in rabbits. **(a)** Representative images of immunohistochemistry staining (negative test for antibody specificity of the staining presented in **Fig. 2e**). Scale bar 50 µm. **(b)** Representative images of isotype control staining to test for antibody specificity presented in **Fig. 2f**). Scale bar 20 µm. Note that IgG isotype control staining in **(a)** and **(b)** is associated with negligible non-specific

background signal. Ctrl control; CAP cold atmospheric plasma; ABX antibiotics; d. p. i. days post-infection.

Supplementary Figure 3.

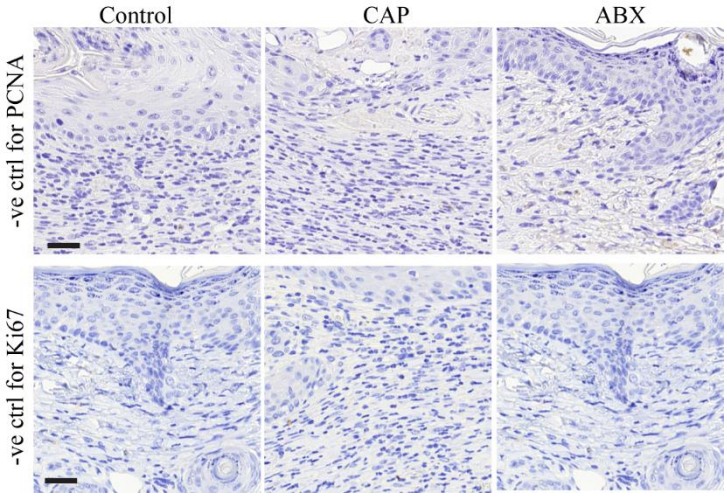

Supplementary Figure 3. **Negative control staining confirmed specificity of antibodies against PCNA and Ki67**. Representative immunohistochemistry images of negative control staining. Mouse wound sections (7 d. p. i.) were processed in a similar manner as the sections presented in **Fig. 3f**. Primary antibodies were substituted with PBS. Negative control was associated with negligible staining. Scale bar 20 µm. Ctrl control; CAP cold atmospheric plasma; ABX antibiotics; PCNA proliferating cell nuclear antigen; d. p. i. days post-infection.

Supplementary Figure 4.

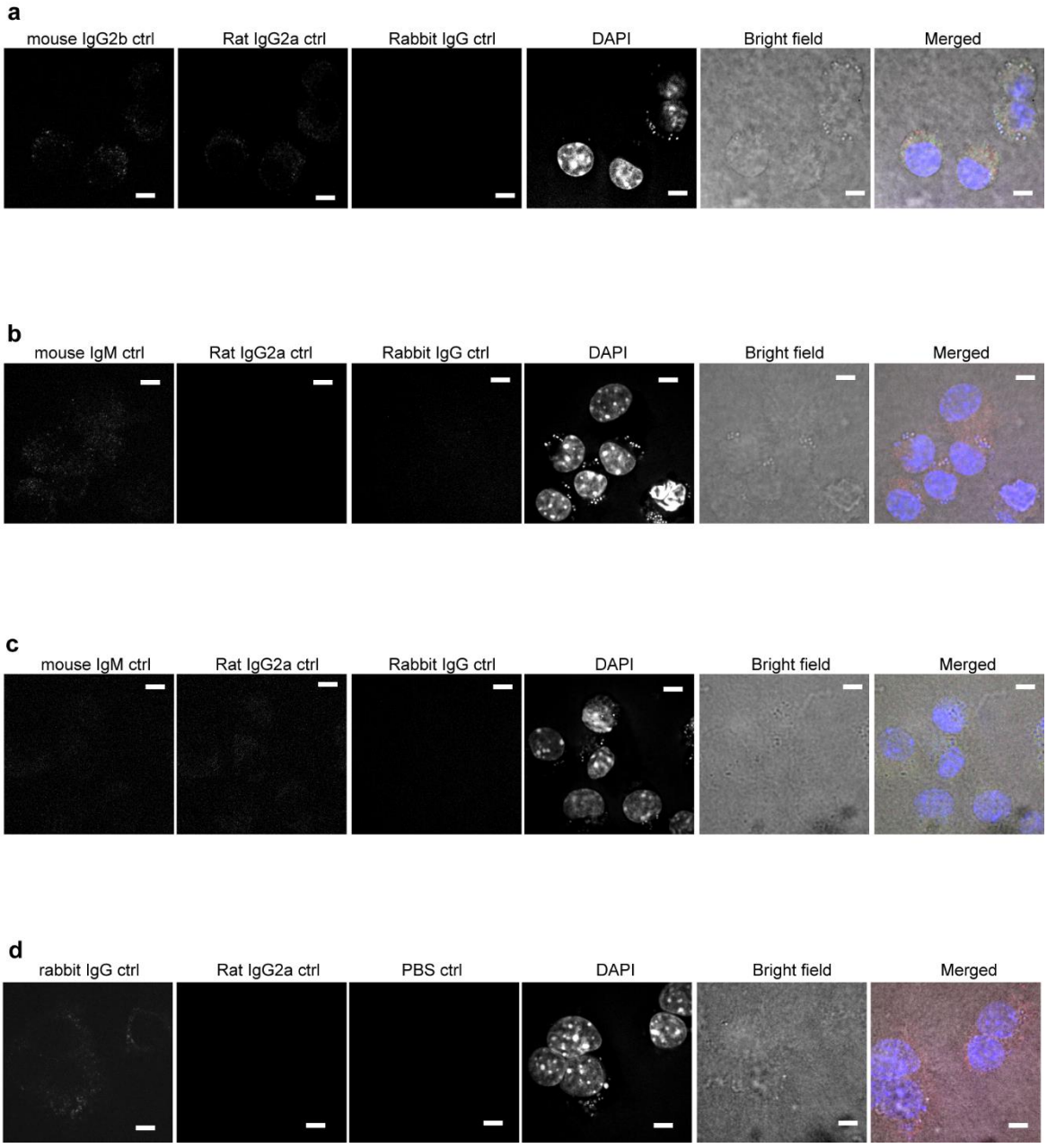

Supplementary Figure 4. Omission of primary antibodies and substitution with species and isotype specific antibodies demonstrates specificity of primary antibodies. (a-d) RAW264.7 macrophages were grown on coverslips, inoculated with *S. aureus* Xen 36 (MOI of 10) and fixed with 4% paraformaldehyde at 5 h. p. i. Cells were immunostained for species and isotype specific antibodies and imaged with confocal microscope. Scale bar 10 µm. **(a)** The

different colours indicate the following: mouse IgG2b (red), rat IgG2a (green), rabbit IgG (magenta), and DAPI (blue). Negative isotype test to control for antibody specificity presented in **Fig. 6a** and **b**. **(b - c)** The different colours indicate the following: mouse IgM (red), rat IgG2a (green), rabbit IgG (magenta), and DAPI (blue). Negative isotype test to control for antibody specificity presented in **Fig. 6b-c** and **Ext. Fig. 4a-b**. **(d)** Isotype control for antibodies used in **Ext. Fig. 4c-d.** The different colours indicate the following: rabbit IgG (red), rat IgG2a (magenta), PBS control (green), and DAPI (blue). Note that all isotype control images show negligible positive staining. PBS phosphate-buffered saline.

Supplementary Figure 5.

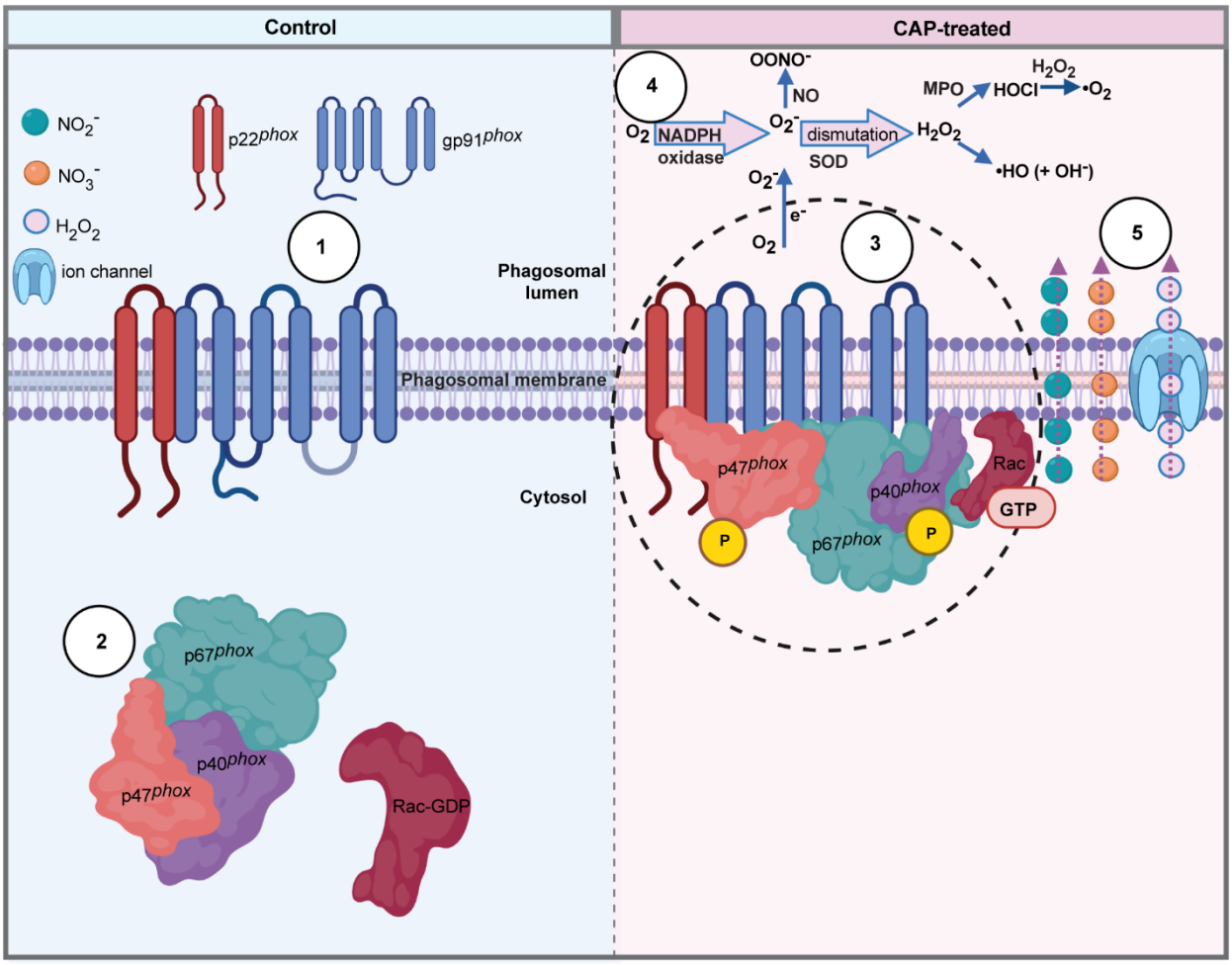

Supplementary Figure 5. Model depicting the effect of CAP on activation of NADPH oxidase NOX2 in macrophages. **(1)** Two membrane-bound components of NOX2 enzyme complex, gp91^{phox} and p22^{phox}, and **(2)** three cytosolic subunits p67^{phox}, p47^{phox} and p40^{phox} remain unassembled under unstimulated conditions. While inactive, guanosine diphosphate (GDP)-bound Rac exists in the cytosol.[19] **(3)** Association-dissociation of Rac with guanosine triphosphate (GTP) is regulated by a complex network of context-dependent interactions. We hypothesize that CAP induces conformational changes that stimulate increased binding affinity of Rac1 to GTP, thereby maintaining this catalytic NOX2 enzyme subunit in the active form. Upon activation, p47^{phox} and p40^{phox} become phosphorylated and along with p67^{phox} translocate to phagocytic cups on the endosome membrane followed by recruitment of activated GTP-bound Rac to p67^{phox}.[10,50] Our results demonstrate that CAP induces p47^{phox} and p40^{phox}

phosphorylation, which drives NOX2 enzyme complex activation and explains the increased ROS production in CAP-treated macrophages. We suggest, that the assembly and activation of NOX2 complex driven by CAP, catalyses the first step of ROS generation, i. e. single electron reduction of oxygen to superoxide. **(4)** Superoxide is metabolized to other through ROS, which are toxic to bacteria.[10] The predominant source of H_2O_2 is dismutation of O_2, which is facilitated by SOD.[28] Interaction between superoxide and nitric oxide leads to the formation of peroxinitrite. Hydrogen peroxide is metabolised to other downstream ROS, such as hypochloric acid. This reaction is catalyzed by myeloperoxidase. NO derivatives, such NO_2^- and NO_3^- have been detected in medium treated with CAP.[22,23,25] It is thought that in aqueous medium ROS and NO (derived from CAP) act in synergy to produce biological effects including enhanced wound healing and inactivation of bacteria.[21,51] **(5)** NO_2^- and NO_3^- are small molecules capable of diffusing through the cellular membrane, hence it is possible that these ions may also diffuse from the cytosol into phagosomal lumen where they may exert their antibacterial effects. H_2O_2 enter the cytosol through ion channels and hydrogen peroxide-transporting channel aquaporin-3 is thought to be an important regulator of H_2O_2 entry into the endosomal lumen.[52] Hence, it is reasonable to hypothesize that H_2O_2 generated by CAP is taken up by the endosomal peroxide channel, where it then mediates antibacterial effects. H_2O_2 hydrogen peroxide, NO_2^- nitrite, NO_3^- nitrate, $OONO^-$ peroxinitrite, SOD superoxide dismutase, NO nitric oxide, O_2 oxygen, O_2^- superoxide, HOCl hypochloric acid.

Supplementary Figure 6.

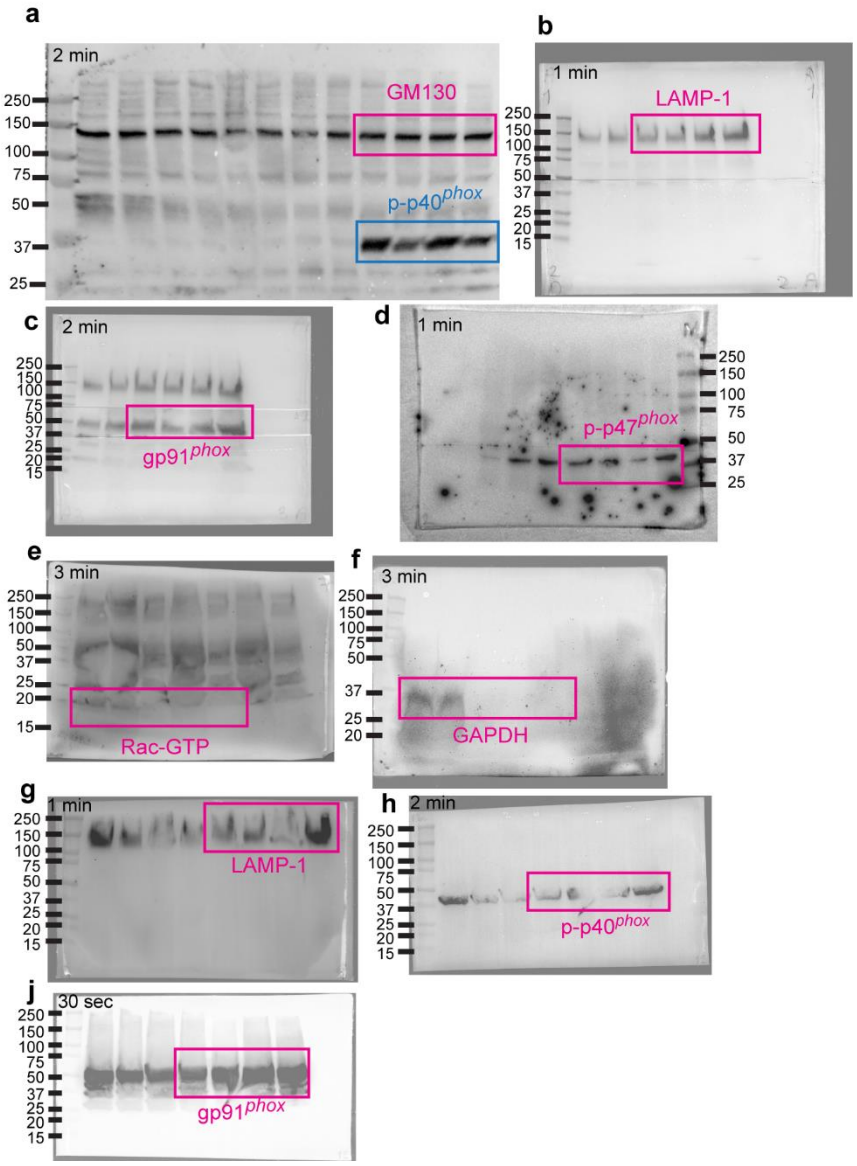

Supplementary Figure 6. Uncropped western blots displayed in **Figure 6f, Figure 6g**, and **Extended Data Figure 4e**. PVDF membranes were immunoblotted with indicated antibodies. Exposure times are provided (top left corner of each blot).

Supplementary Table 1. Primary antibodies, secondary antibodies and accessory reagents

Target protein	Manufacturer	Host	Catalogue Number /Clone	Dilution		
				IH	IF	WB
collagen I	Abcam	rabbit	ab270993	1:200		
collagen IV	Abcam	rabbit	ab19808	1:200		
fibronectin	Abcam	rabbit	ab23750	1:500		
laminin 5	Abcam	rabbit	ab11575	1:400		
collagen III	Abcam	rabbit	ab7778	1:200		
Isotype control (IgG)	Abcam	rabbit	ab171870	1:200		
S. aureus	Abcam	rabbit	ab20920	1:500		
keratin-14	Biolegend	chicken	906004/Poly9060		1:200 Mouse skin	
PCNA	Sigma	rabbit	PLA0079	1:2000		
Ki67	Abcam	rabbit	ab15580	1:500		
vimentin	Abcam	mouse	ab8978	1:200		
CD45	Abcam	rabbit	ab10558	1:600		
CD206/Mannose receptor	Abcam	rabbit	ab64693	1:500		
F4/80	Cell Signaling	rabbit	70076/ D2S9R	1:500		
myeloperoxidase	Abcam	rabbit	ab139748	1:100		
Ly6G	Bio X Cell	rat	BE0075-1/1A8	1:500		
keratin 14	Abcam	mouse	ab7800		1:200 3D skin	
keratin 1	Abcam	rabbit	ab111471	1:500		
involucrin	Biomedical Technologies	rabbit	BT-601		1:200	
laminin 5	Merck Millipore	mouse	MAB19562	1:400		
integrin β1	Abcam	mouse	ab3167/4B7R	1:100		
Lamp-1	BD Biosciences	mouse	611043			1:400
Lamp-1	Abcam	rat	ab25245/1D4B		1:400	
GAPDH	Proteintech	mouse	60004-1/1E6D9			1:1000
Rac1	BD Transduction Laboratories	mouse	610650/102/Rac1		1:200	1:200
phospho-p47^{phox}	Invitrogen	rabbit	PA5-36863/Ser370			1:200
Rac1/2/3	Cell Signaling	rabbit	2465T			1:200
phospho-p40^{phox}	Cell Signaling	rabbit	4311/Thr154			1:200

Cybb/NOX2	Novu Biologicals	rabbit	NBP2-41291			1:200
BODIPY™ FL Vancomycin	Thermo Fisher Scientific		V34850		1:1000	
$gp91^{phox}$	Santa Cruz Biotechnology	mouse	sc-130543/54.1		1:200	
Active Rac1	New East Biosciences	mouse	26903	1:200		
GM130	Abcam	rabbit	EP892Y			1:1000
Polyclonal Goat Anti-Rabbit Immunoglobulins/HRP	DAKO	goat	P0448			1:1000
TidyBlot HRP	Bio-Rad Laboratories		STAR209P			1:200
mouse anti-rabbit HRP	Santa Cruz Biotechnology	mouse	SC-2357			1:1000
goat anti-mouse IgG HRP	Santa Cruz Biotechnology	goat	SC-2005			1:1000
mouse anti-goat IgG HRP	Santa Cruz Biotechnology	mouse	SC-2354			1:1000
goat anti-Mouse IgG + IgM (H+L) HRP	Jackson ImmunoResearch	goat	115-035-044			1:1000
donkey anti-goat IgG (H+L) cross-adsorbed Alexa 488	Invitrogen Thermo Fisher Scientific	donkey	A-11055		1:200	
goat anti-rat IgG (H+L) cross-adsorbed Alexa 488	Invitrogen Thermo Fisher Scientific	goat	A110006		1:200	
goat anti-chicken IgY (H+L) cross-adsorbed Alexa Fluor Plus 488	Invitrogen Thermo Fisher Scientific	goat	A32931		1:200	
goat anti-rabbit IgG (H+L) highly cross-adsorbed Alexa 488	Invitrogen Thermo Fisher Scientific	goat	A-11034		1:200	
goat anti-rabbit IgG (H+L) cy3	Jackson Immunoresearch	goat	111-165-144		1:200	
goat anti-rabbit IgG (H+L) cy5	Jackson Immunoresearch	goat	111-175-144		1:200	
goat anti-mouse IgG (H+L) cy3	Jackson Immunoresearch	goat	115-165-003		1:200	
mouse IgG2b	Cell Signaling	mouse	53484/E7Q5L		1:200	
rat IgG2a	Abcam	rat	ab18450		1:200	
rabbit IgG	Cell Signaling	rabbit	3900/DA1E		1:200	

mouse IgM	Abcam	mouse	ab18401/MM-30		1:200	
mouse IgG1	Cell Signaling	mouse	G3A1		1:200	

IH immunohistochemistry**, IF** immunofluorescence**, WB** Western blotting

Supplementary Table 2. Primers used in this study

Primers	**Assay**	**Catalogue Number**	**Manufacturer**
Mm_Tgfbr1	QuantiTect Primer Assay #24900	QT00135828	Qiagen
Mm_Hprt	QuantiTect Primer Assay #249900	QT00166768	Qiagen
Mm_Gapdh	QuantiTect Primer Assay #249900	QT00199388	Qiagen
Mm_Cybb	QuantiTect Primer Assay #249900	QT00139797	Qiagen
Mm_Nos2	QuantiTect Primer Assay, #249900	QT00100275	Qiagen
Mm_Pdgfb	QuantiTect Primer Assay, #249900	QT00266910	Qiagen
Mm_Vegfa	QuantiTect Primer Assay, #249900	QT00160769	Qiagen
Mm_Tnf	QuantiTect Primer Assay, #249900	QT00104006	Qiagen
Mm_Il1b	Q QuantiTect Primer Assay, #249900	QT01048355	Qiagen

References

1 Moldovan, A. & Fraunholz, M. J. In or out: Phagosomal escape of Staphylococcus aureus. *Cell Microbiol* **21**, e12997, doi:10.1111/cmi.12997 (2019).

2 Lowy, F. D. Staphylococcus aureus infections. *N Engl J Med* **339**, 520-532, doi:10.1056/NEJM199808203390806 (1998).

3 Miller, L. S., Fowler, V. G., Shukla, S. K., Rose, W. E. & Proctor, R. A. Development of a vaccine against Staphylococcus aureus invasive infections: Evidence based on human immunity, genetics and bacterial evasion mechanisms. *FEMS Microbiol Rev* **44**, 123-153, doi:10.1093/femsre/fuz030 (2020).

4 Krismer, B., Weidenmaier, C., Zipperer, A. & Peschel, A. The commensal lifestyle of Staphylococcus aureus and its interactions with the nasal microbiota. *Nat Rev Microbiol* **15**, 675-687, doi:10.1038/nrmicro.2017.104 (2017).

5 Byrd, A. L., Belkaid, Y. & Segre, J. A. The human skin microbiome. *Nat Rev Microbiol* **16**, 143-155, doi:10.1038/nrmicro.2017.157 (2018).

6 Lee, A. S. *et al.* Methicillin-resistant Staphylococcus aureus. *Nat Rev Dis Primers* **4**, 18033, doi:10.1038/nrdp.2018.33 (2018).

7 Niec, R. E., Rudensky, A. Y. & Fuchs, E. Inflammatory adaptation in barrier tissues. *Cell* **184**, 3361-3375, doi:10.1016/j.cell.2021.05.036 (2021).

8 Okabe, Y. & Medzhitov, R. Tissue biology perspective on macrophages. *Nat Immunol* **17**, 9-17, doi:10.1038/ni.3320 (2016).

9 Mowat, A. M., Scott, C. L. & Bain, C. C. Barrier-tissue macrophages: functional adaptation to environmental challenges. *Nat Med* **23**, 1258-1270, doi:10.1038/nm.4430 (2017).

10 Buvelot, H., Posfay-Barbe, K. M., Linder, P., Schrenzel, J. & Krause, K. H. Staphylococcus aureus, phagocyte NADPH oxidase and chronic granulomatous disease. *FEMS Microbiol Rev* **41**, 139-157, doi:10.1093/femsre/fuw042 (2017).

11 Pidwill, G. R., Gibson, J. F., Cole, J., Renshaw, S. A. & Foster, S. J. The Role of Macrophages in Staphylococcus aureus Infection. *Front Immunol* **11**, 620339, doi:10.3389/fimmu.2020.620339 (2020).

12 Belambri, S. A. *et al.* NADPH oxidase activation in neutrophils: Role of the phosphorylation of its subunits. *Eur J Clin Invest* **48 Suppl 2**, e12951, doi:10.1111/eci.12951 (2018).

13 Baehner, R. L. & Nathan, D. G. Leukocyte oxidase: defective activity in chronic granulomatous disease. *Science* **155**, 835-836, doi:10.1126/science.155.3764.835 (1967).

14 Holmes, B., Page, A. R. & Good, R. A. Studies of the metabolic activity of leukocytes from patients with a genetic abnormality of phagocytic function. *J Clin Invest* **46**, 1422-1432, doi:10.1172/JCI105634 (1967).

15 Quie, P. G., White, J. G., Holmes, B. & Good, R. A. In vitro bactericidal capacity of human polymorphonuclear leukocytes: diminished activity in chronic granulomatous disease of childhood. *J Clin Invest* **46**, 668-679, doi:10.1172/JCI105568 (1967).

16 Antimicrobial Resistance, C. Global burden of bacterial antimicrobial resistance in 2019: a systematic analysis. *Lancet* **399**, 629-655, doi:10.1016/S0140-6736(21)02724-0 (2022).

17 Miethke, M. *et al.* Towards the sustainable discovery and development of new antibiotics. *Nat Rev Chem*, 1-24, doi:10.1038/s41570-021-00313-1 (2021).

18 Isbary, G. *et al.* Successful and safe use of 2 min cold atmospheric argon plasma in chronic wounds: results of a randomized controlled trial. *Br J Dermatol* **167**, 404-410, doi:10.1111/j.1365-2133.2012.10923.x (2012).

19 Bekeschus, S., von Woedtke, T., Emmert, S. & Schmidt, A. Medical gas plasma-stimulated wound healing: Evidence and mechanisms. *Redox Biol* **46**, 102116, doi:10.1016/j.redox.2021.102116 (2021).
20 Stratmann, B. *et al.* Effect of Cold Atmospheric Plasma Therapy vs Standard Therapy Placebo on Wound Healing in Patients With Diabetic Foot Ulcers: A Randomized Clinical Trial. *JAMA Netw Open* **3**, e2010411, doi:10.1001/jamanetworkopen.2020.10411 (2020).
21 Lunov, O. *et al.* The interplay between biological and physical scenarios of bacterial death induced by non-thermal plasma. *Biomaterials* **82**, 71-83, doi:10.1016/j.biomaterials.2015.12.027 (2016).
22 Duchesne, C. *et al.* Cold Atmospheric Plasma Promotes Killing of Staphylococcus aureus by Macrophages. *mSphere*, e0021721, doi:10.1128/mSphere.00217-21 (2021).
23 Tornin, J., Labay, C., Tampieri, F., Ginebra, M. P. & Canal, C. Evaluation of the effects of cold atmospheric plasma and plasma-treated liquids in cancer cell cultures. *Nat Protoc* **16**, 2826-2850, doi:10.1038/s41596-021-00521-5 (2021).
24 Park, S. *et al.* Stabilization of liquid instabilities with ionized gas jets. *Nature* **592**, 49-53, doi:10.1038/s41586-021-03359-9 (2021).
25 Duchesne, C., Banzet, S., Lataillade, J. J., Rousseau, A. & Frescaline, N. Cold atmospheric plasma modulates endothelial nitric oxide synthase signalling and enhances burn wound neovascularisation. *J Pathol* **249**, 368-380, doi:10.1002/path.5323 (2019).
26 Bruggeman, P. J. *et al.* Plasma-liquid interactions: a review and roadmap. *Plasma Sources Sci T* **25**, doi:10.1088/0963-0252/25/5/053002 (2016).
27 Frescaline, N. *et al.* Physical plasma therapy accelerates wound re-epithelialisation and enhances extracellular matrix formation in cutaneous skin grafts. *J Pathol* **252**, 451-464, doi:10.1002/path.5546 (2020).
28 Forman, H. J. & Zhang, H. Targeting oxidative stress in disease: promise and limitations of antioxidant therapy. *Nat Rev Drug Discov* **20**, 689-709, doi:10.1038/s41573-021-00233-1 (2021).
29 Blaise, O., Duchesne, C., Banzet, S., Rousseau, A. & Frescaline, N. A Murine Model of a Burn Wound Reconstructed with an Allogeneic Skin Graft. *J Vis Exp*, doi:10.3791/61339 (2020).
30 Joshi, N. *et al.* Comprehensive characterization of myeloid cells during wound healing in healthy and healing-impaired diabetic mice. *Eur J Immunol* **50**, 1335-1349, doi:10.1002/eji.201948438 (2020).
31 Matthews, D. C. *et al.* Radiolabeled anti-CD45 monoclonal antibodies target lymphohematopoietic tissue in the macaque. *Blood* **78**, 1864-1874 (1991).
32 Lin, H. H. *et al.* The macrophage F4/80 receptor is required for the induction of antigen-specific efferent regulatory T cells in peripheral tolerance. *J Exp Med* **201**, 1615-1625, doi:10.1084/jem.20042307 (2005).
33 Wu, J. J. *et al.* The ASIC3-M-CSF-M2 macrophage-positive feedback loop modulates fibroblast-to-myofibroblast differentiation in skin fibrosis pathogenesis. *Cell Death Dis* **13**, 527, doi:10.1038/s41419-022-04981-9 (2022).
34 Boivin, G. *et al.* Durable and controlled depletion of neutrophils in mice. *Nat Commun* **11**, 2762, doi:10.1038/s41467-020-16596-9 (2020).
35 Feuerstein, R., Kolter, J. & Henneke, P. Dynamic interactions between dermal macrophages and Staphylococcus aureus. *J Leukoc Biol* **101**, 99-106, doi:10.1189/jlb.3MR0316-097RR (2017).
36 Meuret, G., Bammert, J. & Hoffmann, G. Kinetics of human monocytopoiesis. *Blood* **44**, 801-816 (1974).

37 Greenhalgh, D. G. Management of Burns. *N Engl J Med* **380**, 2349-2359, doi:10.1056/NEJMra1807442 (2019).
38 Sun, B. K., Siprashvili, Z. & Khavari, P. A. Advances in skin grafting and treatment of cutaneous wounds. *Science* **346**, 941-945, doi:10.1126/science.1253836 (2014).
39 Watt, F. M. Mammalian skin cell biology: at the interface between laboratory and clinic. *Science* **346**, 937-940, doi:10.1126/science.1253734 (2014).
40 Wells, J. M. & Watt, F. M. Diverse mechanisms for endogenous regeneration and repair in mammalian organs. *Nature* **557**, 322-328, doi:10.1038/s41586-018-0073-7 (2018).
41 Yan, D. *et al.* A Physically Triggered Cell Death via Transbarrier Cold Atmospheric Plasma Cancer Treatment. *ACS Appl Mater Interfaces* **12**, 34548-34563, doi:10.1021/acsami.0c06500 (2020).
42 Zhao, M. *et al.* Electrical signals control wound healing through phosphatidylinositol-3-OH kinase-gamma and PTEN. *Nature* **442**, 457-460, doi:10.1038/nature04925 (2006).
43 Davies, L. C., Jenkins, S. J., Allen, J. E. & Taylor, P. R. Tissue-resident macrophages. *Nat Immunol* **14**, 986-995, doi:10.1038/ni.2705 (2013).
44 Pasparakis, M., Haase, I. & Nestle, F. O. Mechanisms regulating skin immunity and inflammation. *Nat Rev Immunol* **14**, 289-301, doi:10.1038/nri3646 (2014).
45 Reeves, E. P. *et al.* Killing activity of neutrophils is mediated through activation of proteases by K+ flux. *Nature* **416**, 291-297, doi:10.1038/416291a (2002).
46 Ruifrok, A. C. & Johnston, D. A. Quantification of histochemical staining by color deconvolution. *Anal Quant Cytol Histol* **23**, 291-299 (2001).
47 Ruzehaji, N. *et al.* Pan PPAR agonist IVA337 is effective in prevention and treatment of experimental skin fibrosis. *Ann Rheum Dis* **75**, 2175-2183, doi:10.1136/annrheumdis-2015-208029 (2016).
48 Stirling, D. R. *et al.* CellProfiler 4: improvements in speed, utility and usability. *BMC Bioinformatics* **22**, 433, doi:10.1186/s12859-021-04344-9 (2021).
49 de Castro Martin, I. F. *et al.* Influenza virus genome reaches the plasma membrane via a modified endoplasmic reticulum and Rab11-dependent vesicles. *Nat Commun* **8**, 1396, doi:10.1038/s41467-017-01557-6 (2017).
50 Woldu, S. L., Hutchinson, R. C., Krabbe, L. M., Sanli, O. & Margulis, V. The Rho GTPase signalling pathway in urothelial carcinoma. *Nat Rev Urol* **15**, 83-91, doi:10.1038/nrurol.2017.184 (2018).
51 Pai, K. *et al.* Investigation of the Roles of Plasma Species Generated by Surface Dielectric Barrier Discharge. *Sci Rep* **8**, 16674, doi:10.1038/s41598-018-35166-0 (2018).
52 Nalle, S. C. *et al.* Aquaporin-3 regulates endosome-to-cytosol transfer via lipid peroxidation for cross presentation. *PLoS One* **15**, e0238484, doi:10.1371/journal.pone.0238484 (2020).

1. Additional results to the study

In plasma medicine it is now well established that CAP has antibacterial properties or can modulate functions of cells. However, the precise mechanisms of action are still unclear especially as the devices used for plasma treatments are very diverse and lack standardization and that biological models used are not so complex as “normal” skin.

1. Transcriptomic analysis

In order to investigate potential mechanisms or mutations that are triggered by CAP we performed RNA extraction for transcriptomic analysis. The first set of experiments corresponded to five samples of macrophages infected with *S. aureus* Xen36 and treated by CAP or helium (2 min). Five hours after infection, RNA was extracted from macrophages infected with *S. aureus*. RNA sequencing (RNA-seq) was performed by next-generation sequencing (NGS). This technique allows to reveal gene expression profile and describes the continuous variations in the transcriptome.

First, we focused on macrophages results. In our previous work we noticed that CAP treatment does not change macrophage polarisation with no significant modification in CD80, CD86, CD163 or CD2O6 protein expression *in vivo* (markers of macrophage polarisation). Here we focused on RNA extracted from infected macrophages. The infection should induce modifications in pro-inflammatory pathway in helium and CAP group but specifically on NOX2 genes since this complex is highly involved in bacteria elimination. Analysis of the sequences revealed a good quality of the samples as shown in figure 21 A and B but interestingly no clusterisation or specific changes due to the different treatment emerged (figure 22). In addition, RTqPCR was performed based on the same RNA samples that were used in RNAseq. Thus, pro-inflammatory genes *Cybb*, *TNF* and *IL1b* genes were analysed and we expected to see an increase expression level due to *S. aureus* infection. Both RNAseq and RTqPCR analysis showed no significant difference in *Cybb, TNF* and *IL1b* gene expression in response to CAP compared to helium control.

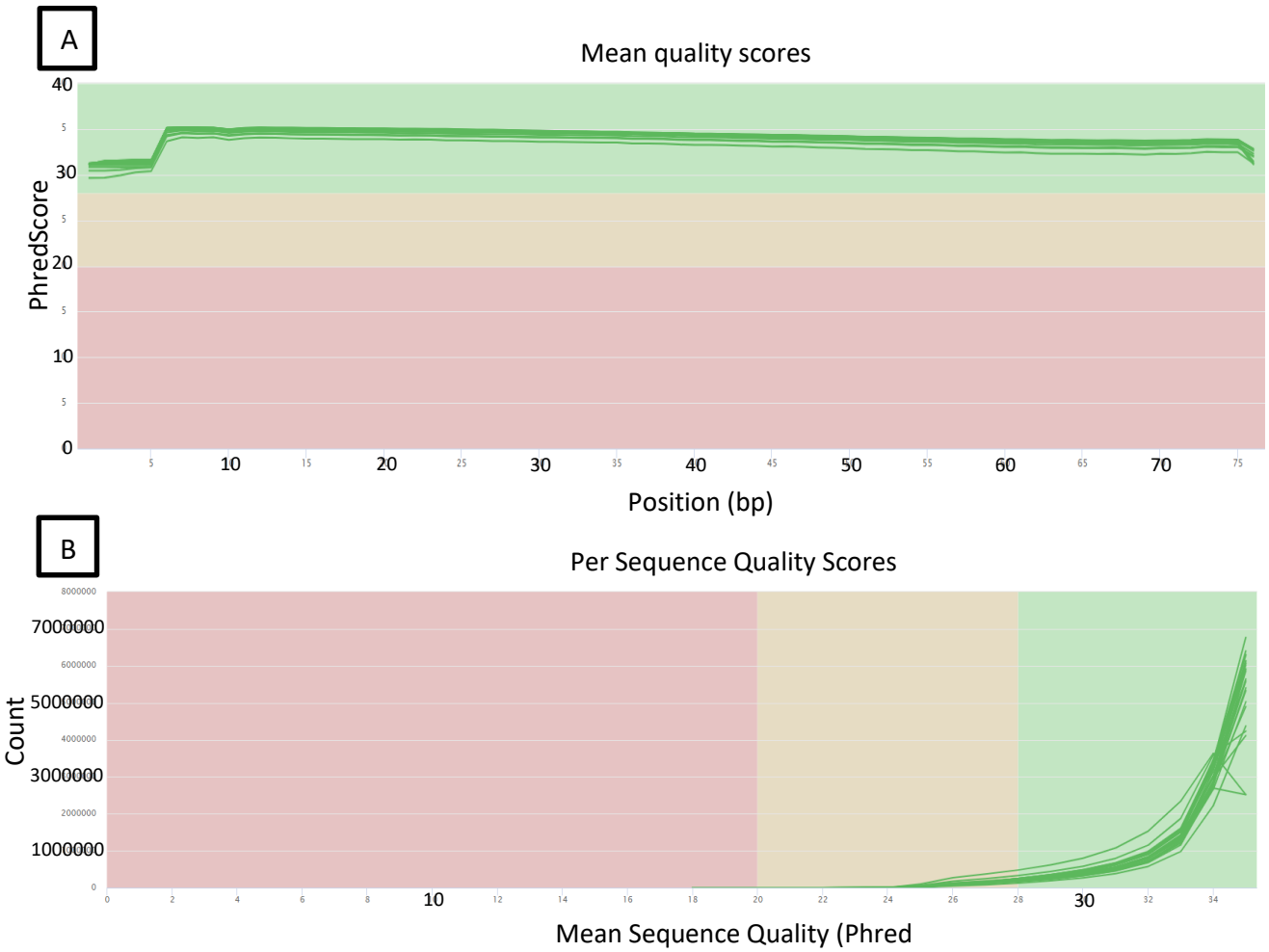

Figure 21: Assessment of the sequence quality scores of the raw FASTQC data for infected macrophages helium and CAP treated samples. The quality of the raw RNA-seq reads was evaluated using FASTQC and summarized with MultiQC. All data were assessed for mean per-base (A), and per-sequence (B) quality as measured by the Phred score. The background of the graphs divides the y-axis in very good quality calls (green), reasonable quality (orange) and poor quality (red). All the green curves represent data for 5 samples of infected helium-treated macrophages treated samples and 5 CAP-treated samples.

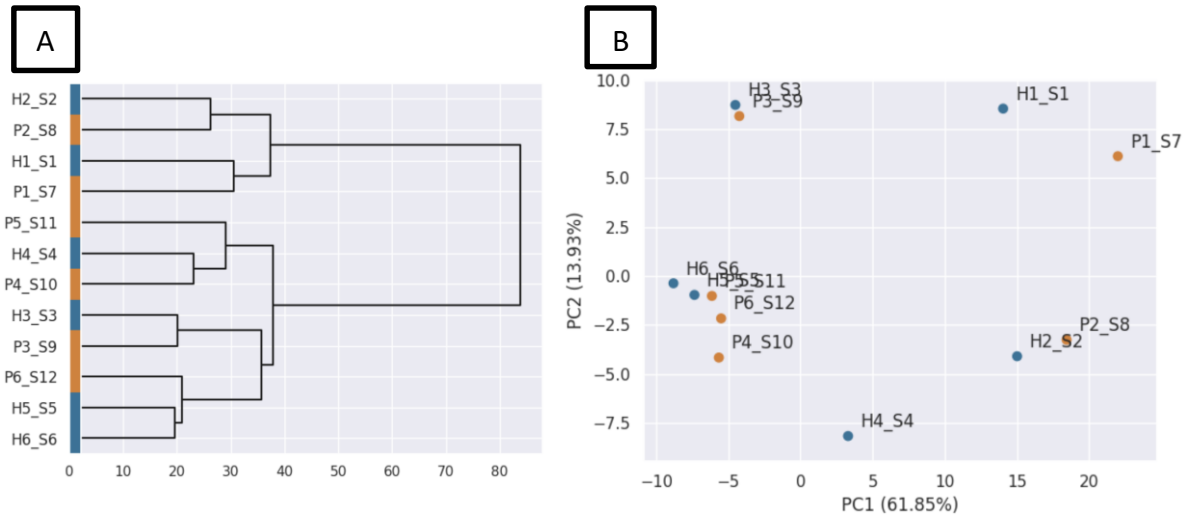

Figure 22: Summary of the Differential Gene Expression (DGE). The comparison is made between infected macrophages treated by CAP or helium. Hierarchical clusterisation of the whole sample set was done using Ward method (A), the experiment variability is represented by a principal component analysis. (B) Sample names beginning with H represent helium samples and with a P represent CAP samples.

As mentioned, we also performed RNA-seq on *S. aureus* Xen36 treated by helium or CAP but the same results as for macrophages were obtained (figure 23) with no significant differences.

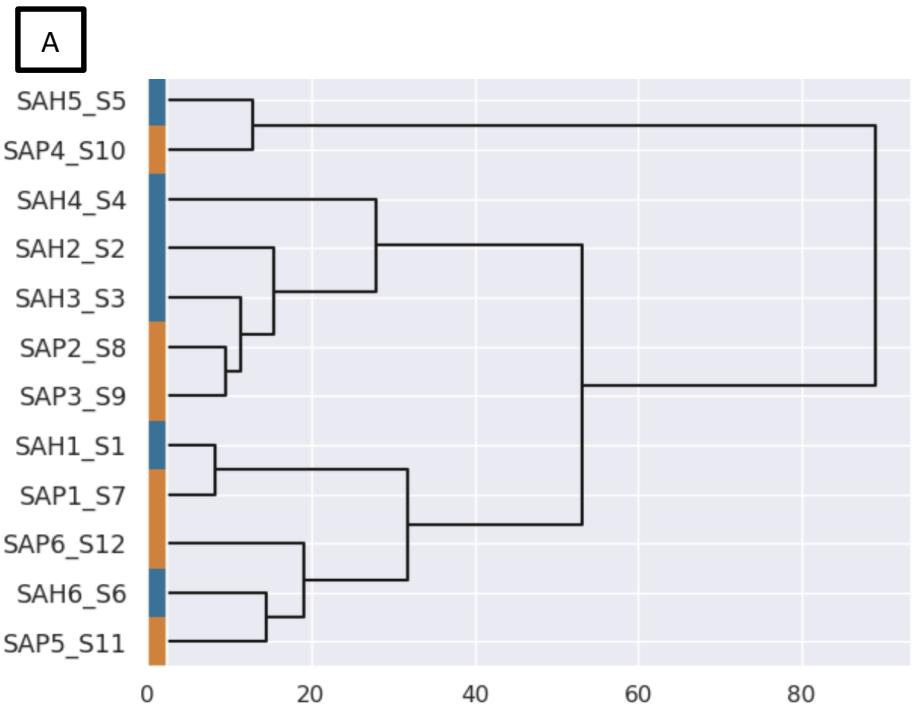

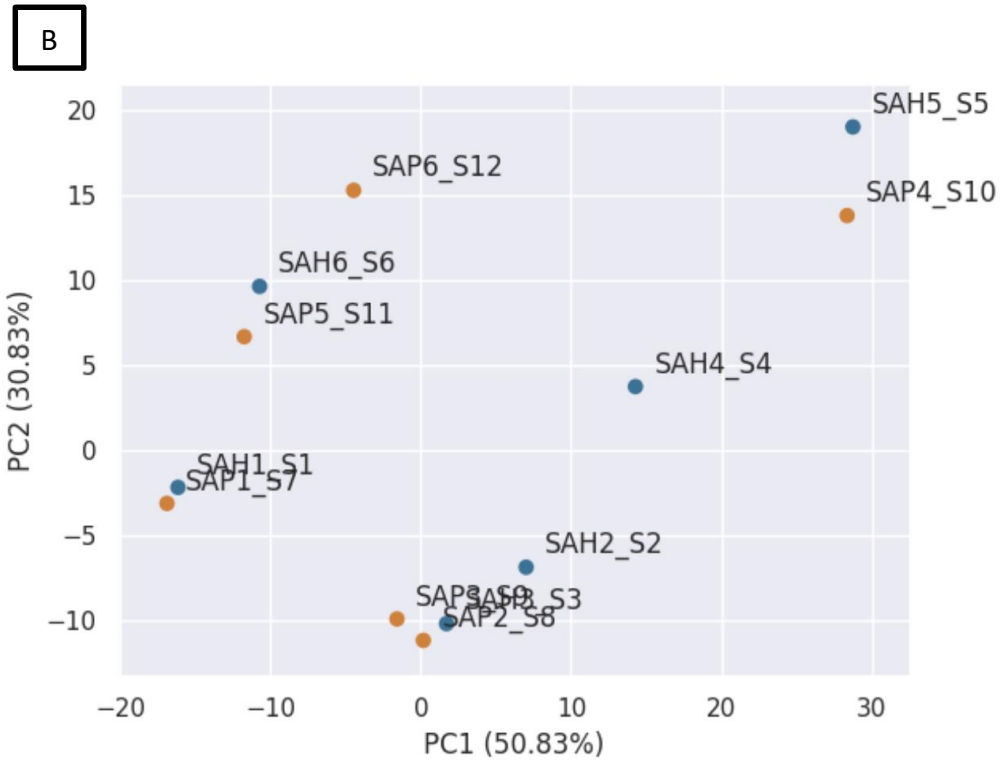

Figure 23: Summary of the Differential Gene Expression (DGE). Comparison is made between helium or CAP treated *S. aureus* Xen36 (2 min). Hierarchical clusterisation of the whole sample set was done using Ward method (A), the experiment variability is represented by a principal component analysis (B) Samples names beginning with SAH represent helium samples and with a SAP represent CAP samples.

To ensure that the absence of difference in the results were not due to protocol samples preparation issues, we decided to focus only on macrophages and to extract new RNA with a new control condition: non infected macrophages.

Uninfected macrophages treated by CAP or helium showed no significant differences for target genes *Cybb*, *Rac1* and *Rac2* (figure 24 A). Those genes give a general idea as they are some genes among the whole genome thus, the results are not surprising. We decided to do a comparison of control treatment (helium) with infected and non infected cells (figure 24 B). As expected, we obtained significant results when non infected cells are compared to the positive control: infected samples of RNA for *Cybb* gene. *Cybb* gene expression was higher in infected cells than in the non infected samples. As *Cybb* is involved in bacterial clearance by macrophages through the production of phagolysosomal ROS, the difference is coherent.

The second condition analysed with infected macrophages showed gene expression differences between helium and CAP treatment for *Cybb*, *Rac2* and *Ifn γ* (figure 25). Interferon-ɣ is a pro inflammatory protein and Rac1 is involved in diverse array of cellular events and is part of the NOX2 enzyme complex. Our expectations were to get higher levels of expression of those genes under CAP treatment in comparison to infected cells only, however we obtained the opposite result this can be explained by the choice of the time point that was chosen at 5 h post infection but it is possible that the pertinent time point is before of after the chosen one.

Even if the results are contradictory with our expectations we still see modifications in RNA expression levels between helium and CAP samples compared to transcriptomic analysis. Indeed, we expected to have higher level of inflammatory gene expression for the CAP treated condition as we supposed that they play a role in CAP bactericidal effect. These new results seem to highlight a problem in the first set of samples tested.

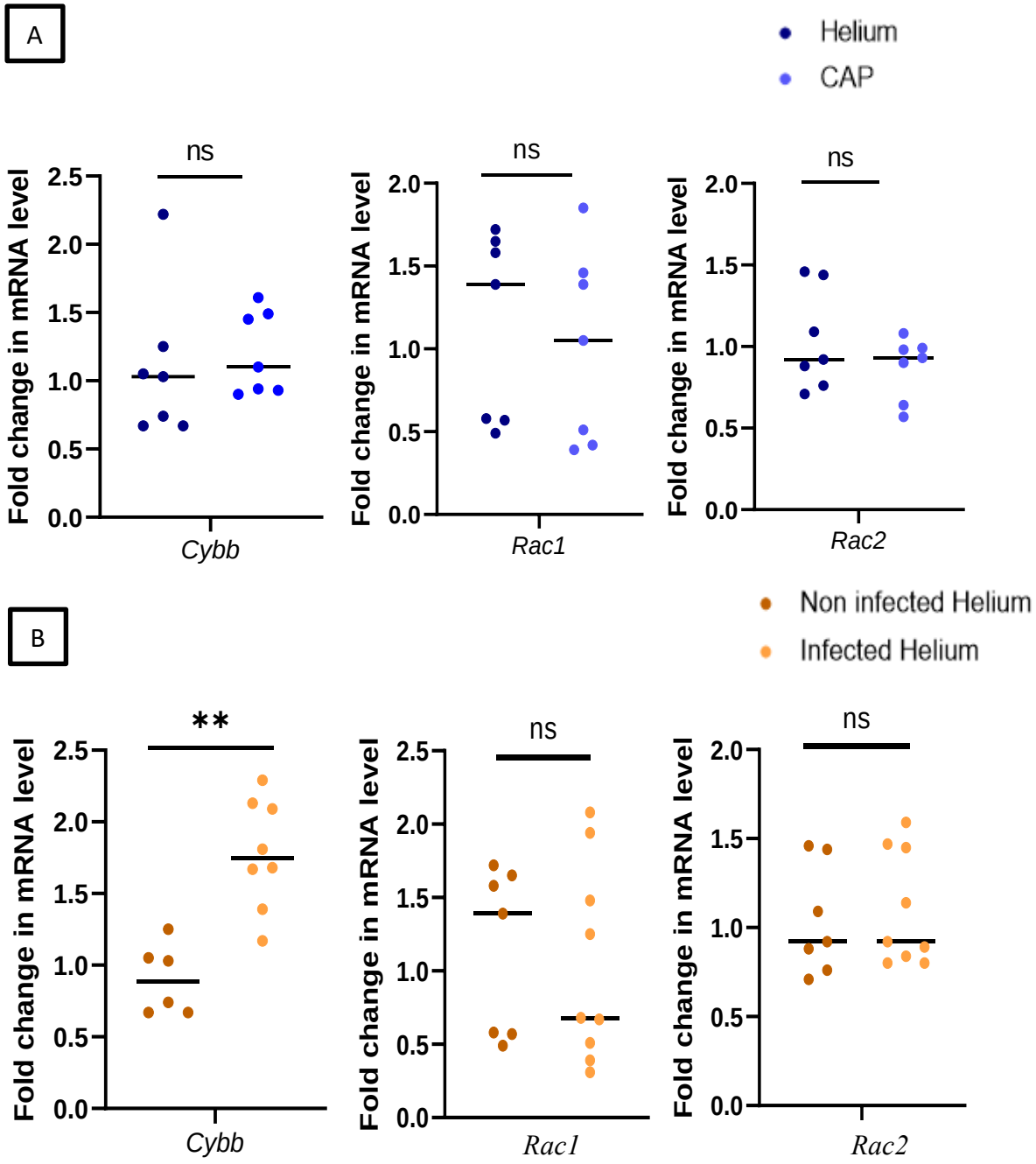

Figure 24: Relative mRNA levels of *Cybb, Rac1 and Rac2* in uninfected and infected macrophages. Relative mRNA levels were measured after CAP or helium treatment of uninfected macrophages and 5 h of incubation (A) or in uninfected macrophages compared to *S. aureus* Xen36 infected macrophages at 5 h post-infection after helium treatment for *Cybb*, *Rac1* and *Rac2* genes (B). (n>5)

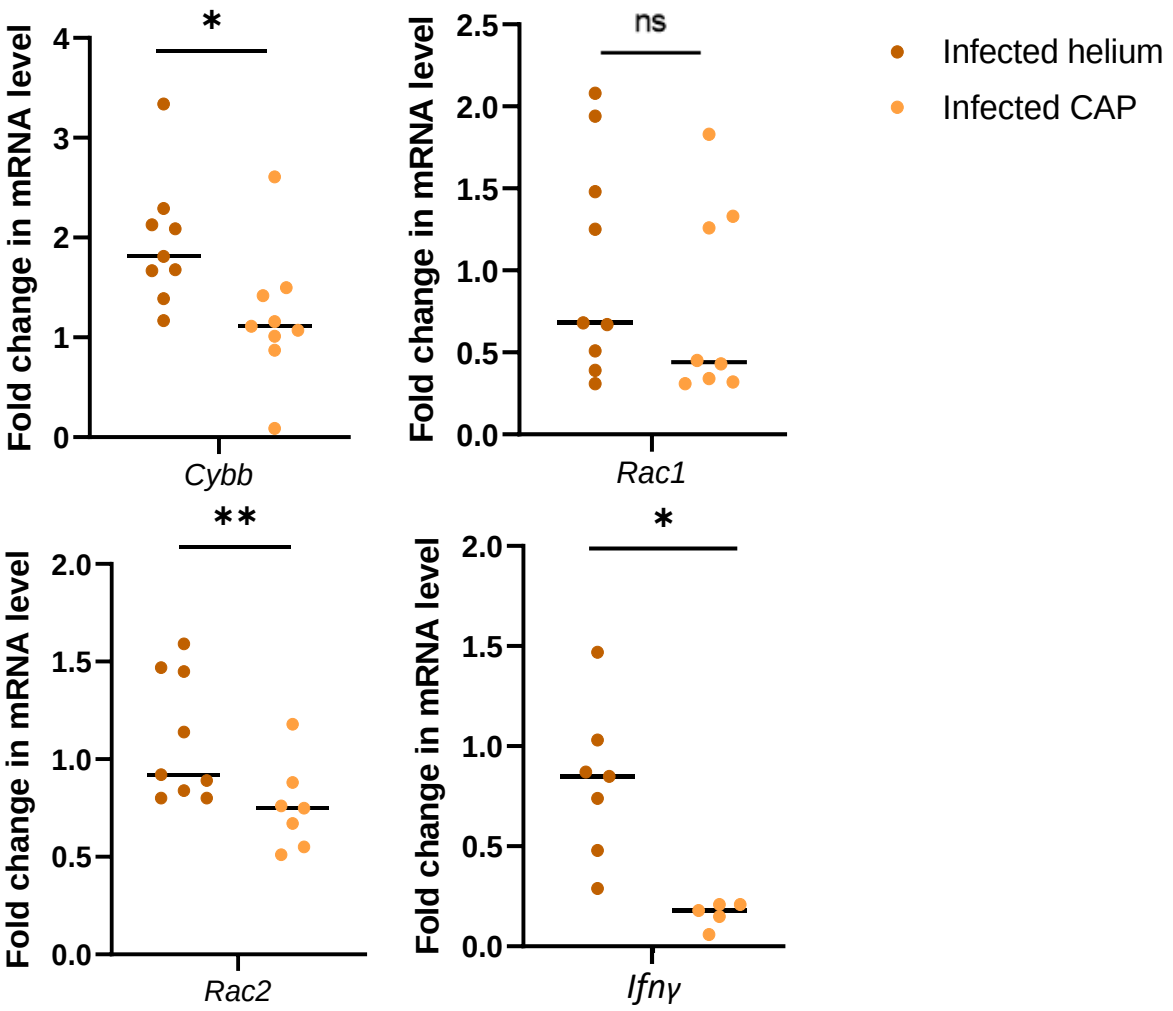

Figure 25: Relative mRNA levels of pro-inflammatory and NOX2 genes in *S. aureus* Xen36 infected macrophages. Relative mRNA levels were measured by RtqPCR after CAP or helium treatment of infected macrophages 5 h post-infection for *Cybb*, *Rac1*, *Rac2* and *Ifnγ* (n>5).

2. Mitochondria involvement in ROS production for *S. aureus* elimination

We demonstrated that gp91ds-tat (NOX2 inhibitor) inhibits the production of ROS. Here we investigated the role of superoxide anion ($O_2^{\cdot -}$) in the level of ROS induced by CAP treatment. In addition to our specific work on NOX2 we showed that superoxide plays a key role in the induced effect as its inhibition also induced a reduction of ROS level when macrophages are treated by CAP. It highlights the fact that reduction of bacterial load in macrophages is more due to an indirect effect of CAP. Indeed, $O_2^{\cdot -}$ is a highly reactive specie with a short life time and should disappear quickly after CAP treatment and not be so expressed at 5 h post-infection. Mitochondria are also responsible for ROS production and mROS acts within macrophages. Knowing this we studied changes in mROS with a fluorescent probe using necrox5, an inhibitor of mROS in RAW264.7 macrophages (figure 26 A). Mitochondria appear to play an important role in the effect observed. Indeed, when necrox5 is added the effect of CAP is inhibited in the

same way as gp91ds-tat at 2 and 5 hours post-infection. It may be interesting in the future experiment to combine necrox5 and gp91ds-tat to determine if there is an additional inhibition or not.

The same inhibitors (necrox5, gp91ds-tat) were used in 3D human bioprinted human skin (figure 26 B). Previously we demonstrated that CAP enhanced anti-bacterial activity of cells in a reproducible way in 3D bioprinted human skin. Here we investigated the effect of inhibitors on bacterial viability within complex model composed of a human primary cells organised as in the skin with fibroblasts mixed with macrophages in a specific matrix and keratinocytes on the upper layer. Interestingly we can see a tendency to an increase of bacteria viability for all the molecules but the effect is higher with the addition of SOD. Superoxide dismutase is an enzyme that allows the dismution $O_2^{\cdot -}$ into O_2 and H_2O_2 and is naturally present in cells; as $O_2^{\cdot -}$ is highly effective on bacteria its disappearance lead to bacteria increase. Interestingly effect of CAP is also inhibit with necrox5. In regards to those results, $O_2^{\cdot -}$ appears as a key player. However, this experiment was done only three times and helium condition could not be performed for this batch of models we can only see a tendency to CAP effect inhibition.

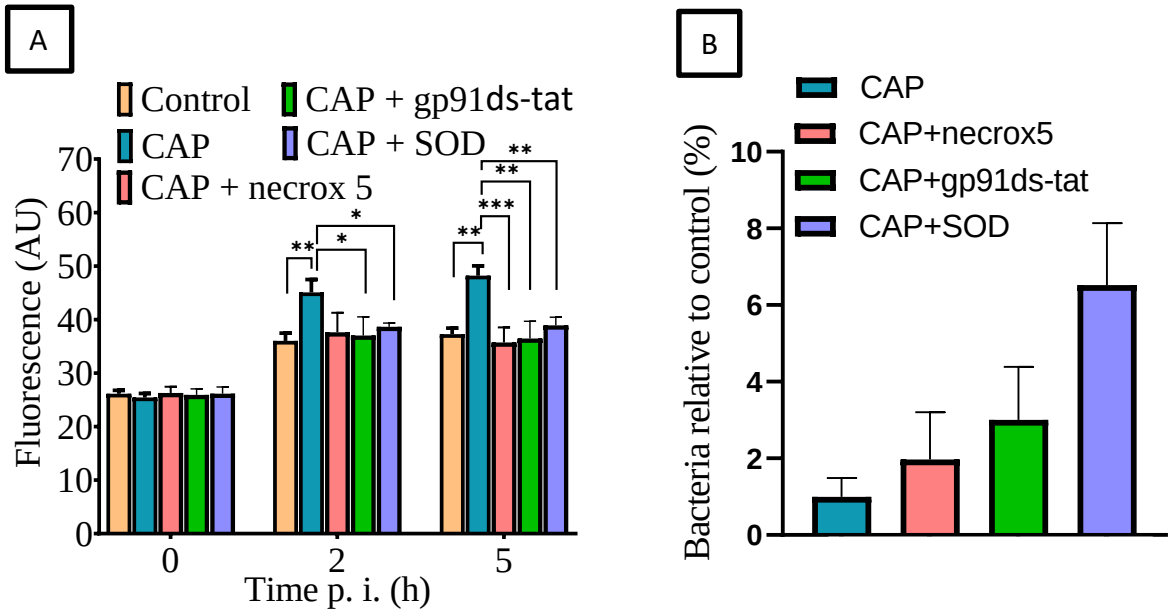

Figure 26: Effect of CAP on ROS production in RAW264.7 macrophages and in bactericidal activity in 3D bioprinted human skin.

(A) ROS production was measured using a fluorescent probe at 0, 2 and 5 post-infection of macrophages with *S. aureus* Xen36. Control (helium), CAP, CAP with inhibitor (necrox5, gp91ds-tat), CAP with enzyme (SOD) conditions were investigated. (B) Percentage of *S. aureus* Xen36 relative to control in 3D bioprinted human skin harvested 24h after the infection. Models were treated by CAP and necrox5, gp91ds-tat inhibitor and SOD enzyme were tested.

Discussion

Interest in CAP for tissue regenerating is rising over the last few years. *In vivo* experiments and clinical trials have been performed to improve wound healing and decrease the bacterial load of infected wounds. However, as many types of devices currently exist, an essential step was to develop plasma-generating device with defined parameters and test it on clinically relevant models.

We used a *S. aureus* Xen36 infected murine model to mimic bacterial infections in cutaneous wounds. Using this model, we validated the antimicrobial properties of our device that was previously seen *in vitro*. In addition, CAP induced a significant wound closure, an increase of re-epithelialisation and extracellular matrix formation. Here we succeed to show a positive impact of CAP on *S. aureus* infection and wound healing.
A majority of studies in plasma medicine for dermatology used rodent models *in vivo*[358]. However, they poorly mimic human system by their differences in healing process and the fact that have a superior immune system. Thus, new models are needed to get closer to the human anatomy and physiology.

An innovative model was used in our study to mimic infected human skin and which overcomes the limitations associated with previous rodent models as species-specific anatomical differences. 3D reproducible skin models have enabled us to design experiments that are more clinically relevant. It took us almost 2 years to developed and fine-tune a three-dimensional cutaneous model of infection which mimic the acute phase of staphylococcal skin infection in a reproducible manner. However, the process still needs optimization, multiple steps were undertaken to perfect the model. Nonetheless this allowed us to demonstrate the bactericidal activity of CAP in a multi-cellular model. In addition, the advantage of the 3D models used is that different cell populations (keratinocytes, fibroblasts and macrophages) are derived from the same donor. Peripheral blood-derived monocytes are polarized and differentiated *in situ* towards an M1 phenotype which allow to study specifically cells of interest.
In our case we are more interested in M1 macrophages due to their key functions in inflammation and bacterial clearance. Nevertheless, to go deeper in our investigation we have to optimize the maturation process of the 3D skin. Indeed, when models arrived to our laboratory they possess the dermis layer and a part of the epidermis which is not mature (the *stratum corneum* layer is not present). Thus, the maturation process is continued to have the full epidermis layer thanks to an air lift process, which mainly trigger the formation of the *stratum corneum*, but this step of differentiation is not yer under control. The epidermis is not firmly attached to the dermis and in some models the epidermis is even not visible. It seems that there is no or weaker dermal-epidermal junction. Various optimization points can be considered as the maturation time before the shipment to our laboratory or the maturation time once it arrived. In addition, more technical conditions are also problematic as the delivery. During the transfer between laboratories models undergo shock that can damage them. The main issue is that damage or shock are perceived as wound by the cells that will migrate to the site of injury, use matrix metalloproteinase to help recover and will “activate” cells as

fibroblasts or macrophages prior to our infection protocol. Another issue that is linked to the bioprinted process is the formation of bubbles in the dermis and epidermis due to the extrusion pressure of the 3D printer machine. Keratinocytes and other cells may migrate into it as if it is a wound and try to fill it, concentrating locally a cell type such as macrophages. This is a major issue in bioprinting.

Apart from the use of more complex models to study the effects of plasma on wound healing and disinfection, it is essential to understand the underlying mechanisms. CAP generates a plethora of reactive species and, redox signaling is often described as the basis of the plasma effects[359,360]. Nonetheless the molecular and functional roles of plasma on the skin and its barrier function remain unclear. In our study we focused on macrophages, key cells of inflammation and wound healing. Several studies reported the effect of CAP on macrophages essentially in the cancer field[361]. Results demonstrated an effect of CAP devices on macrophages polarization, inducing an elevation of both M1 and M2 phenotypes but with a higher expression of M1[362]. Other teams showed an anti-inflammatory profile[363], or an attraction of macrophages by CAP treated cells[364]. However, to our knowledge no specific mechanism has been described in macrophages.
As plasma generates ROS and macrophages are responsible for bacterial clearance through oxidative burst we decided to investigate CAP and macrophage phagosome maturation interactions.
Here we showed that plasma treatment after infection induces an increase in intracellular ROS at early and late time points post-infection. Knowing this we showed an activation of NOX2 enzymatic complex in RAW 264.7 macrophages in response to CAP treatment. NOX2 activation is mediated by several pathways. One of our hypothesis about upstream regulation is that ROS produced by CAP may trigger activation of kinases. Exposure of cells to hydrogen peroxide, for example, can trigger phosphorylation and activation of MAPKs (ERK1/2, JNK), themselves responsible for downstream phosphorylation for cell signaling[365]. ERK1/2 activation can for example induce phosphorylation of p40, p47 and p67 of NOX2 complex triggering its activation. Thus, in the future we would like to use an inhibitor of MAP kinase kinase (MAPKK or MEK1/2) that is responsible for ERK1/2 inhibition which can potentially lead to modifications on the NOX2 effect observed under CAP treatment. In addition, several *in vitro* studies demonstrated a correlation between CAP treatment time (20 s, 60 s, 180 s) and changes in gene expression in human skin cells highlighting an increase in expression and activity of targets of Nrf2 signaling or components of AP-1 (JUN) and MAPK pathways.

Global gene expression depends on many factors including cell type, environmental stimuli and developmental stages. Many genes are regulated by oxidation through superoxide, hydrogen peroxide and various nitrogen oxides[366]. Thus, transcriptomic analysis should give us interesting complementary data on NOX2 but also on macrophages polarization, mitochondrial pathways or even on potential mutations. If the new set of data do not show significant difference possible explanations are plausible as the need to optimize the time point of incubation after CAP treatment and RNA extraction or that modifications are at a proteomic and not a transcriptomic level. During our study we also noticed the potential role of mitochondria on the bactericidal effect of CAP through macrophages. Once again, little is

known about CAP and mitochondria interactions, a biochemical modelling and numerical simulation demonstrated that CAP affects the activity of the ATP synthesis machinery and the ROS regulation system in mitochondria[367] or dysfunction of mitochondria were shown in cancer field. However, to our knowledge nothing was demonstrated in wound healing. The interaction between CAP and mitochondria will be addressed in the general discussion of this manuscript. For instance, our transcriptomics results were obtained *in vitro* using macrophage murine cell line. It can thus be relevant to use 3D human bioprinted skin or *ex vivo* human skin and to extract RNA after helium or CAP treatment and infection to have clinically relevant information on more active cells as primary cells.

Conclusion

In our previous work we demonstrated that CAP increases intracellular ROS and NO leading to MSSA and MRSA oxidative killing[368]. Those results were obtained with macrophages that were treated with CAP 24 h before the infection. In this new set of results, the process was close to the reality with a CAP treatment performed one-hour post-infection *in vitro*.

Here we showed that CAP promotes bacterial clearance in a murine model of full-thickness burn wound infected with *S. aureus*. This model permitted the *in vivo* assessment of migration of the neoepidermis over the dermis.

We clearly demonstrated that CAP activates NOX2 enzymatic complex in RAW264.7 macrophages and human 3D skin model highlighting a more effective bacterial killing. We succeed to demonstrate for the first time in infected macrophages the activation of $p40^{phox}$ and $p47^{phox}$ correlated with anti-*S. aureus* activity of CAP. In addition, we shown an increase association level of two phagosomal membrane proteins LAMP-1 and $gp91^{phox}$ and an association of GTP-bound Rac (active form) with *S. aureus*-containing phagolysosomes in response in response to CAP.

The bactericidal effect was demonstrated with models of increasing complexity from the reductionist model to the 3D human skin model to finally *in vivo* studies with a positive effect of CAP treatment. The next step is to elucidate the activation path of NOX2 essentially through transcriptomic analysis to decipher the steps upstream of this activation.

Chapter IV.
Development of a homemade CAP device

Chapter IV-Development of a homemade CAP device

The jet used by our laboratory allowed significant advances in our *in vitro* and *in vivo* experiments[369] to understand interactions between CAP and the skin. The results are promising but ultimately will be limited in the future due to the small surface treatment which induces longer treatment time. The actual nozzle allows a treatment of around 1 cm^2 but severe burns can affect extensive part of the body and require a treatment that cover more than a dozen of cm^2. There is a challenge to develop sources that will cover larger surface while remaining practical and at a reasonable cost. The new device has been developed in the laboratory to allow a treatment of around 30 cm^2. However, characterization steps are needed to determine the treatment parameters and the safety of the device before using it *in vivo*.
The aims of this part of my PhD was to do the physico-chemical characterization of the new device *in vitro* to ensure its safety for the experimenter and for the target. Another point was to exchange with the expert of the different fields (biology, physic) for the design and ergonomics of the device for its clinical use with the future porcine model of burn wound in mind.
In this chapter the previous jet will be named jet I and the new device will be called jet II.

The section related to physical and chemical plasma caraceristics of the jet II as well as information about it cannot be detailed in this manuscript due to intellectual property.
The only element that can be mentioned is that the jet II produces higher amount of chemicals than the single jet. H_2O_2 and NO_2^- concentrations are higher than what was obtained with the previous jet but are still under deleterious concentrations and NO_3^- is not detectable under 3 min CAP which means that its production is not dominant.

1. Evaluation of the target temperature

Preliminary tests were performed to estimate the change of the temperature on a fixed surface. The initial temperature of the *ex vivo* skin was 24°C and reached 28°C after 1 min CAP treatment. Interestingly helium flow, heated by the massflow meter also induced an increase of the sample temperature to 28°C meaning that CAP treatment over 1 min does not significantly increase the sample temperature.
Tests were also performed with a scan of the target to mimic *in vivo* conditions. In that configuration the temperature went from 24°C to 26°C and cool down quickly after treatment.
A leather target was also used with a surface of 8 cm x 6.9 cm fixed on a device heated at 35°C. The treatment parameters were a helium flow rate of 2000 sccm, voltage of 14 kV and a gap of 20 mm. The temperature of the non treated area was 35°C, the temperature of the 2 min CAP treatment area was 36°C and the temperature in the center of the jet was 34°C.
A final test was performed on an *ex vivo* pig skin. In order to mimic a graft, a piece of pig skin measuring 8 cm x 8 cm was used *ex vivo*. Surgical staples were applied onto the skin and spaced at 3 mm appart. In a burn wound context surgical staples are used to fix the graft and promote the closing of the wound edges. Staples are easier to apply, stronger and faster to use to close

large wounds than suturing. As surgical staples are made of metal, it is necessary to ensure that they do not interfere with the treatment thus, we performed experiments.
All the plasma parameters were the same as previously mentioned but the treatment times varied: 10 s, 30 s, 1 min and 3 min. The CAP treatment was performed by scanning the surface. The temperature results are summarized in the table 6.

Table 6: Temperature of pig skin stapled with surgical staples treated with jet II measured with a digital infrared camera.

CAP treatment time	0 s	10 s	30 s	1 min	3 min
Temperature (°C)	21.6	21.9	22.6	23.8	24.3

The temperature deviations observed in fixed or by scanning do not exceed 2°C in fixed and are negligible in scanning for the different type of surface tested. The device appears to be safe in terms of target heating under those conditions.

2. Biological characterization

2.1. Hacat cells viability and proliferation

The first step to characterize the new device was to analyse its impact on cells viability for the chosen condition. For this set of experiment, we decided to use a human keratinocyte cell line as it is more sensitive than fibroblasts for preliminary tests. Hacat cells were cultured in 96 well plates and their mortality rate was assessed 48 h after treatment by cytometry and both necrotic and apoptotic cells were quantified (figure 27). There is no decrease in the percentage of cell viability and no increase in the number of necrotic or apoptotic cells following exposure to CAP for 30 s. Interestingly the percentage of living, apoptotic and necrotic cells follow the same tendency for helium and CAP treatment in comparison to non treated cells.

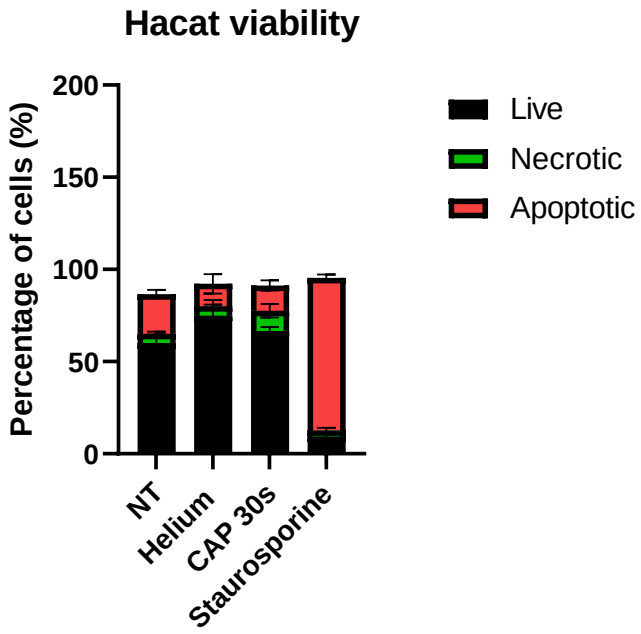

Figure 27: Influence of CAP on Hacat cell viability. Hacat cells were treated in suspension by CAP and viability was assessed at 48h after exposure to CAP using a two-colour annexin V/ propidium iodine (PI) fluorescence assay. Cell viability was determined by flow cytometry-based fluorescence detection. The graph represents the percentage of viable, necrotic and apoptotic cells after treatments. Staurosporine was used as a positive control for apoptotic cells (n=6).

Having established that the new device has no deleterious impact on cell viability, cell proliferation was then quantified 24 and 48 h after CAP treatment using WST-1 cellular proliferation assay. Direct treatment of CAP on cells shown no negative effect on cellular proliferation. There was no significant difference at 24 h but at 48 h an increase of cell proliferation was highlighted even with 30 s helium as shown in figure 28 (A) and (B). 30 s treatment was fixed in the experiments as it represents for us the timepoint for which we are not going to induce deleterious effect during the future pig trial in term of physical and chemical measurements.

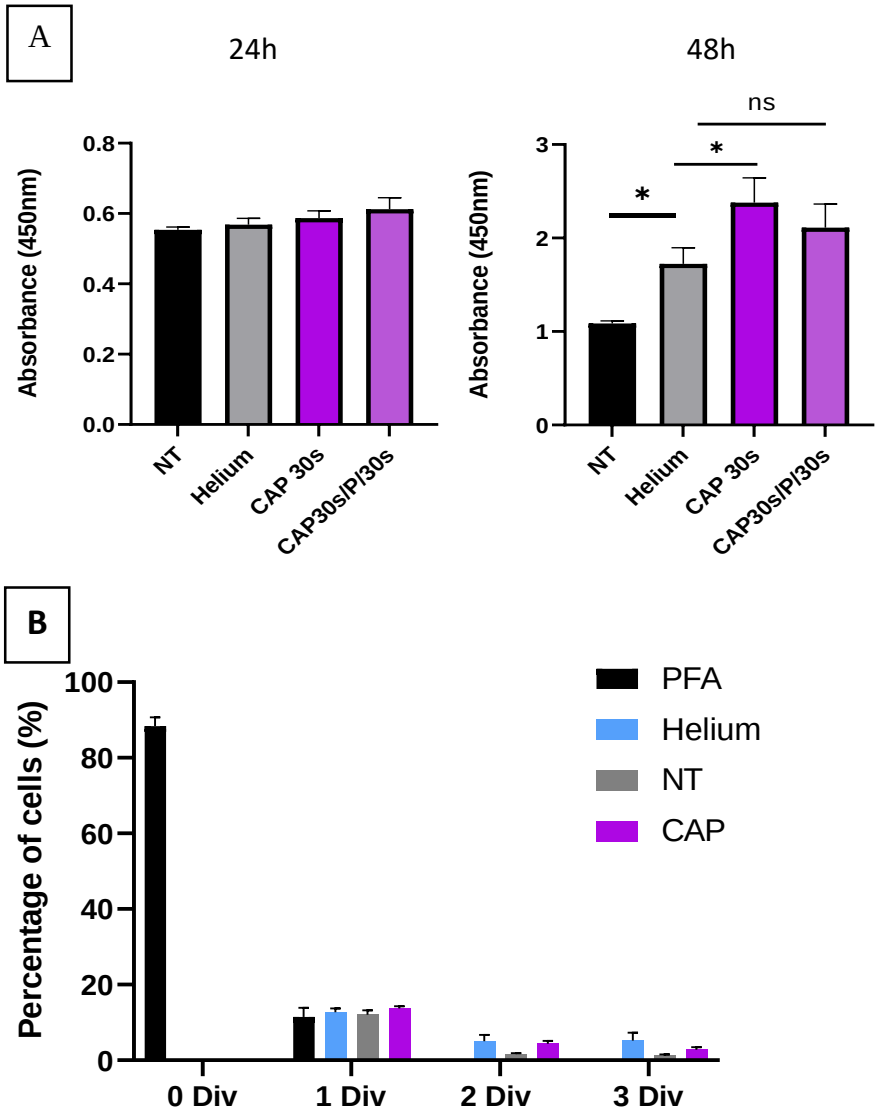

Figure 28: Effect of CAP on HaCat proliferation.

(A) Cellular monolayers were treated with CAP for 30 s, 30 s/pause/30 s with a gap of 20 mm. Proliferation was measured at 24 h and 48 h after CAP treatment using WST-1 assay. Data are mean of three independent experiments. Mean ±SEM (Mann-Whitney U test; n = 10; ns, not significant).

(B) Proliferation of Hacat cells was assessed using CFSE 4 days after treatment. 0 division condition was performed using cells fixed with PFA. The graph represents the percentage of cells which underwent 0, 1 or 2 divisions for NT (non treated), helium (30 s) and CAP (30 s).

2.2. Hacat migration

Migration of skin cells such as keratinocytes and fibroblasts into the wound bed is an important process for wound healing. The effect of CAP treatment on migration of Hacat cells was studied using a scratch assay and the percentage of wound scratch was calculated using a program developed in our laboratory. Hacat cells were cultured to sub-confluence and subjected to CAP for 30 s or 10 min. At day 2 a tendency to a faster wound closure is observed for helium and

CAP 30 s (figure 29) in comparison to their respective initial scratch. Non treated cells and cells treated with CAP for 10 min are associated with similar rate of wound closure. This effect is less pronounced at day 3, but is still present for CAP 30 s treatment. No delayed in wound healing was noted.

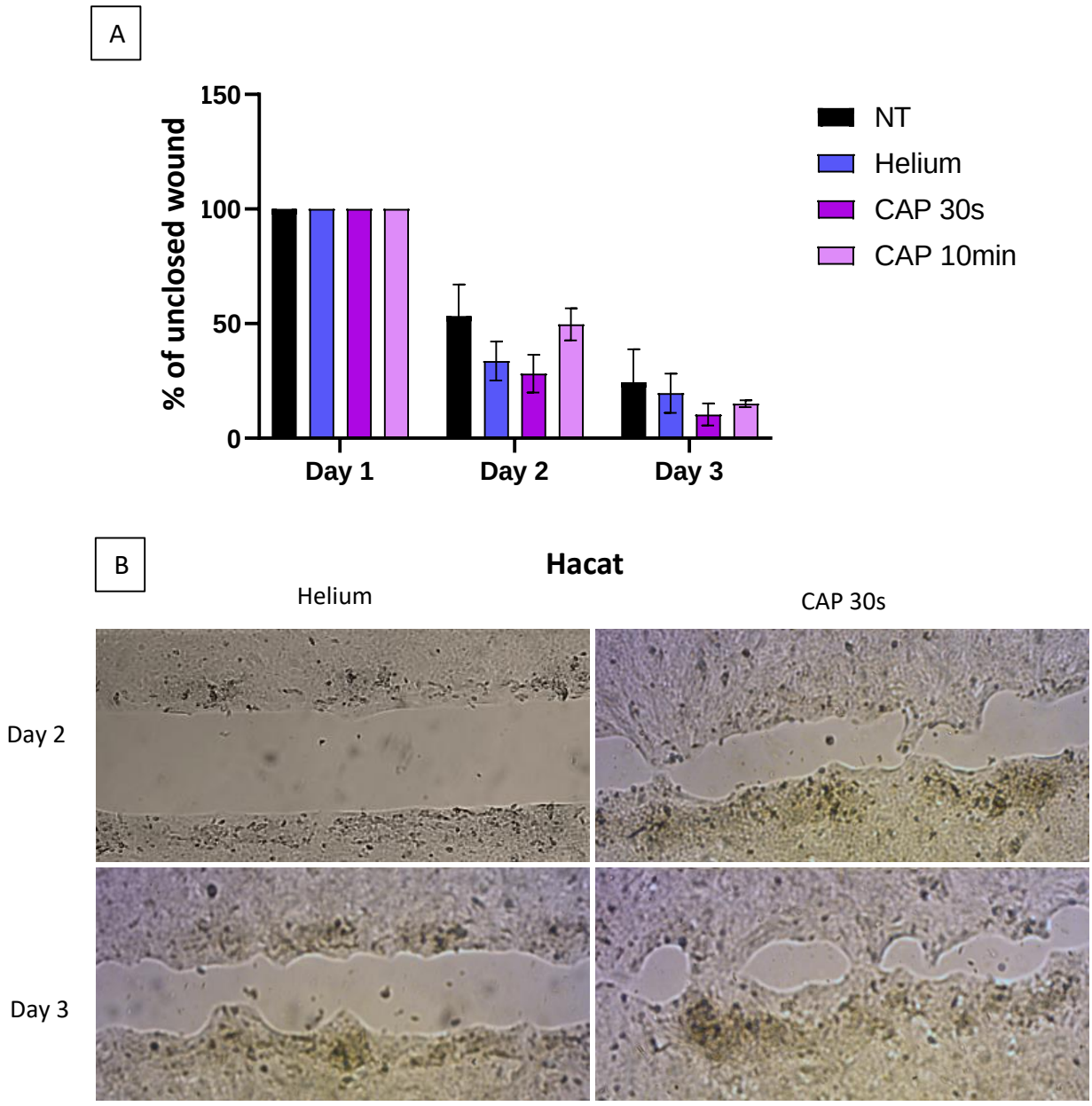

Figure 29: CAP treatment stimulated Hacat cells migration.

(A) Percentage of wound closure with non treated cells (NT), Helium, CAP 30 s and CAP 10 min at day 1, 2 and 3 after treatments (n=4). (B) Scratch wound made on confluent monolayer cells producing a wound of approximately 4 mm x 2cm. Photographs were taken at 24 h and 48 h after the scratch was made.

2.3. Conclusion on biological measurements

CAP treatment has no deleterious effect *in vitro* in Hacat human cells. It has no impact on cells viability, proliferation and migration for the selected plasma parameters. Interestingly helium alone seams to present an effect on cell proliferation. In comparison with the previous results obtained by Duchesne *et al.*[370] the new device may have also some beneficial effects on cell proliferation and migration as the previous jet. Even if plasma parameters are different between the two devices a beneficial effect is observed for wound closure and cell proliferation with no significant deleterious effect on cells.

Discussion

In plasma medicine in dermatology and wound healing field it is well established that CAP improves wound healing and reduces bacterial load. However, a panel of devices are used and make comparison difficult since plasma device energy and ROS production in liquid are not always published in the articles. Previously we developed a single jet that demonstrated beneficial effects on wound healing. In order to treat larger surfaces (burn wounds, extended chronic wounds) a jet II device is relevant and need to be safe and to have a homogenous spatial distribution. The aim of this section was to characterize the jet II device in order to have key information about its safety and its potential impact on cell viability for *in vivo* studies.

We demonstrated that H_2O_2 and NO_2^- production was respectively 10 or 6 times higher (~50 µM and ~13 µM) than the jet I (~8 µM and 1.2 µM) for 1 min. Strabenburg *et al.*, showed that CAP induced keratinocytes mortality but with H_2O_2 concentrations superiors to 100 µM[371]. Deleterious effect of H_2O_2 was also shown by Girard *et al.*, but with concentration more elevated (1mM)[372] than the ones produced by the jet II. The concentrations produced by our device is under the negative effect level. We can assume that in line with our *in vitro* results and the fact that for *in vivo* experiments the target will be treated by the device deplacement above the wound, that damages related to those species should not be obtained.

In wound healing and particularly during the proliferative phase, migration of cells as fibroblasts or keratinocytes are necessary for the wound closure. We studied the effect of CAP on keratinocytes cellular viability, proliferation and migration. The jet II is not detrimental for the cell viability and on the contrary, CAP increased cells proliferation and migration. Scratch wound close faster following 30 s CAP treatment. These preliminary results suggest that CAP could enhance wound closure for short treatment times. However, in the field of plasma medicine the effect of CAP on cell proliferation is still under debate since opposite results have been found. Studies demonstrated a lack of effect of CAP keratinocytes proliferation both *in vitro* and *in vivo*[341]. In contrast other groups showed a significant increase of keratinocytes after direct or indirect treatment[373,358].

Interestingly, we found that helium has a positive impact on cell migration and viability. Initially considered as an inert gas helium was then considered as biologically active since its use for respiratory diseases in 1934[374]. It is known to have protective function for certain organs as the heart, brain or lungs[375] and to induce cytoskeleton modifications in endothelial cells[376].

It has also been demonstrated that *ex vivo* it increases the collagen 1 and 3 ratio after laparotomy in rats leading to improved wound healing[377]. Until now our team never notified differences between helium and no treatment condition when using our first jet. It is likely that the gas injected will have biological effects on our models. It would be interesting to carry out these same experiments on other cell types and more complex models in order to verify its inocuity for the selected conditions.
Additional experiments have also to be done to investigate mutagenicity and genotoxicity of plasma device and its potential impact on DNA for clinical trials.

Conclusion

In conclusion, we demonstrated in this chapter that the new device was safe to use in terms of temperature, evaporation, or effects on cells. We have shown that CAP treatment has a time dependant effect on chemical production but also on cellular proliferation and migration. The treatment time of 30 s chosen for CAP treatment has beneficial effect *in vitro* on keratinocytes human cells. The positive impact on cell proliferation is coherent with the previous results obtained with the jet I despite the higher production of chemical species. The plasma treatment protocol did not increase cell mortality and improve cellular migration without negative effect while using longer treatment time as 10 min. Interestingly, the helium condition seams to increase cell viability, proliferation and present the same tendency for proliferation as CAP treatment.
Those results are relevant for wound healing and especially for the proposed pilot study on pig model. The plasma device and protocol for treatment is safe for *in vitro* tests and will be used *in vivo* in the next chapter.

Chapter V.

Development of a porcine model of full-thickness burn wound reconstructed with autologous skin graft

Chapter V - Development of porcine model of full-thickness burn wound reconstructed with autologous skin graft

Previously our team showed a beneficial effect of CAP on the closure of 2D models of wound healing using human keratinocytes and fibroblasts and skin healing after burning and grafting in the *in vivo* (murine) models[369]. CAP device used in our previously published work, functions on helium gas because it is an inert, stable, non-flammable gas and already used in various medical applications. Our work demonstrated that CAP treatment has improved grafting, stimulated proliferation and migration of skin cells, and stimulated angiogenesis and collagen production. However, the mouse model has limitations. For example, murine wounds heal primarily by contraction, and to a certain extent via re-epithelialisation. Human wounds, on the other hand, contract due to the presence of cytoskeletal α-smooth muscle actin, and heal primarily via -epithelialisation. Thus, we decided to set up a large mammal model closer to human in order to investigate the potential benefit of CAP treatment on burn wounds that were covered with a skin graft.
The realisation of this pilot study will provide initial indications on the safety of CAP device for the treatment of full-thickness burns and will help to optimize certain treatment conditions.

1. Development of the experimental procedure

Burn trauma is not a single pathophysiological event but a devastating injury causing structural and functional deficits in many organic systems. Due to its complexity and the involvement of several organs, *in vitro* experiments cannot reproduce this complexity or address the entire pathophysiology of the burn. In addition, our study proposes to study the effectiveness of a treatment by skin graft associated with CAP, making it necessary to use an animal model, not substitutable to other models. The animal model required extensive planning, and every step of the protocol development was the subject of many numerous exchanges between surgeons, nurses, veterinarians, animal technicians, and researchers.

1.1. Justification for the choice of mammalian species

Within this project a murine model was previously developed and demonstrated a positive effects of CAP. In the continuity of our studies a pig model was chosen to get closer to the clinical model. It has certain anatomical and physiological properties similar to human depending on the age, weight and type of pigs. Pig skin is characterized by a dermal and epidermal thickness close to that of the human. The pig epidermis ranges from 30 to 140 µm which is close to human one ranging from 50 to 120 µm. In addition, the pig has a firmly attached skin to the underlying tissues inducing a healing process in the same way as seen in humans[378]. The distribution of blood vessels in the dermis, the time of renewal of the epidermis or hair are also close to those of human. In the murine model the *panniculus carnosus* layer aids wound contraction. Generally scald burns in pigs heal by day 21[379] with a re-epithelialization

between day 7 and 14[380] post-wound infliction. Other similarities as epidermal enzyme patterns, keratinous protein, and the composition of the lipid film of the skin surface make the pig an ideal model for burn wound healing before clinical trials.

1.2. Experimental procedure

Two 15-20 kg, 8-10 weeks old Large White female pigs will be used in this procedure of 15 days reproducing the conventional management of severe burns. Only two pigs are involved in this pilot study thus, statistical analysis cannot be performed but qualitative results will be obtained.

Moreover, at this age pigs have a weight between 15 and 20 kg which facilitates the carrying out of the experimental process and the pigs will be prepubescent which makes it possible to free oneself from hormonal variations.

Animals will have a 7-day acclimation period before the start of the study to avoid additional stress that may impact the quality of the study and pig welfare. Under general anaesthesia and local subcutaneous anaesthesia, two burns will be carried on each side (about 13% of the total body surface) figure 30 (A) with a device containing water heated to 92°C figure 30 (B). The bottom of the 1L Schott bottle was removed and replaced by a thermoresistant tape. The removal of the base of the bottle has been chosen in order to better fit the body shapes and induce a burn that is as homogeneous as possible. The base of the bottle has a diameter of 8.5 cm, indicating that the wounds would have a surface area of approximately 57 cm^2 but due to the curvature of the flexible base the average size of the wound should be smaller around 43.0 ± 0.7 cm^2 as mentioned in Cuttle *et al.* study [381].

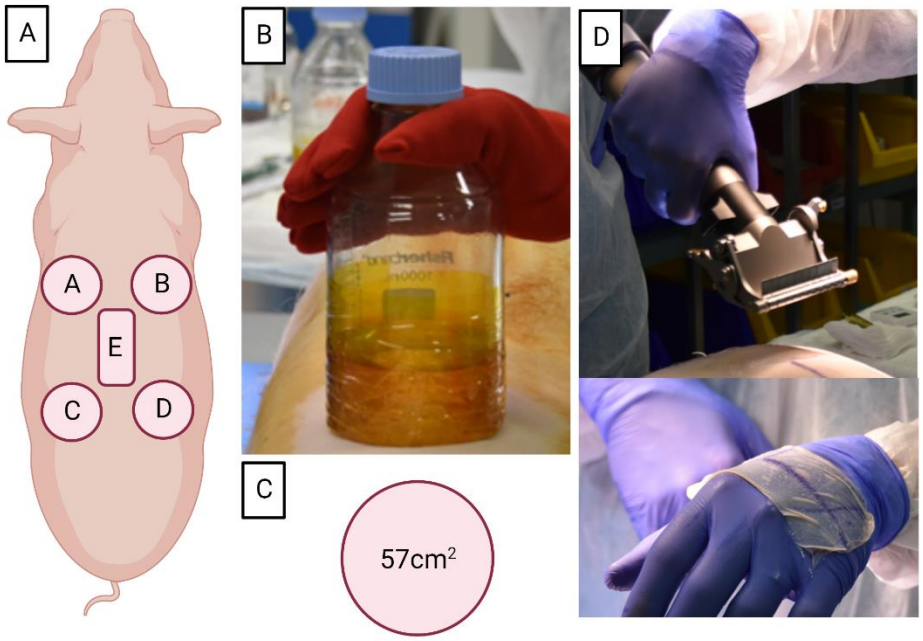

Figure 306: Burn induction and treatment of full-thickness burns.

(A) Anatomical position of donor sites E and recipient sites A, B, C, D. (B) Thermal injury device consisting of a Schott Duran bottle with the bottom removed and replaced with

thermoresistant wrap. The plastic wrap is secured to the bottle with tape. The bottle is filled with 300 mL of water heated to 92°C. The flexible base allows the device to fit the contours of the pig flank and to induce a uniform wound. (C) Size of the induced wound. (D) Dermatome used to proceed to the split thickness graft and the thickness of the skin graft will be equal to 300 µm. *This illustration was made using biorender.com.*

During the development stage of the protocol, we had an opportunity to test certain experimental parameters and re-use euthanized pigs that were previously used in other experimental procedures. These dead pigs came from an experiment conducted by other researchers on hemorrhagic shock which allowed us to use them without having to sacrifice other animals. They enabled us to check if the developed burn system is safe and allow the induction of a full-thickness burn (figure 31).

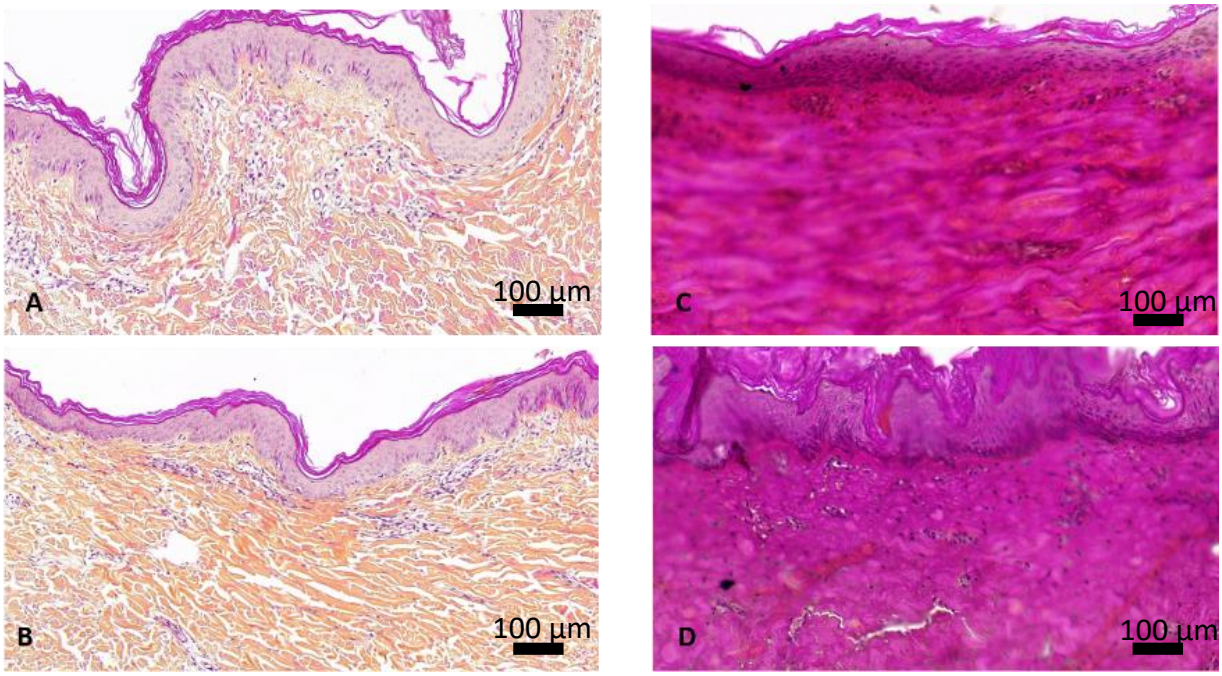

Figure 31: Microscopic images of porcine skin stained with H&E. (A) Normal unwounded porcine skin. (B) porcine skin exposed to water pre-heated to 85°C and applied over the skin for 60 sec. (C) 95°C for 90 sec. (D) 95°C for 150 sec. Original magnification 20 ×.

As the pig will be burned on each side when the animal is placed on the other side, the asepsis of zones A and C or B and D will be ensured by the use of sterile surgical drapes. Twenty-four hours after the induction of the burn, and during a new general anaesthesia, necrotic tissue of the burn wounds will be excised. A cutaneous sample will be taken using an electrical dermatome allowing to have 300 µm thick skin donor site E figure 30 (A). The donor site was chosen in an area where the animal will not have access and that is less prone to infection than the anterior part of the animal. The graft will then be expanded with a mesher (ratio 1:3) and attached to the recipient site with surgical staples. As surgical staples will be used, we performed some tests with the plasma device to ensure that there is no electric arc and no increase in temperature (chapter VI, II.d.). Grafts will be protected from mechanical damage by

using multi-layer wound dressings and a protective body jacket specially adapted to the animal and changed every two days figure 32.

Figure 32: Protective jacket. The protective jacket was specially designed for the morphology of the pig we used. It rises high enough in the neck and towards the back of the animal to optimize the protection of the areas of burning, grafting of any injury and risk of infection but also to protect the fentanyl patches to prevent them from falling off. The fabric was specially chosen to be washed. In addition, the weight of the animal on arrival is estimated at 20 kg but should reach 35 kg at the end of the procedure. Different jacket sizes were therefore anticipated to ensure the animal's well-being.

After the animal wakes up, it will be housed individually until day 2, then housed with other animals until the end of the study. This will allow the animal to recover from the procedure and prevent one of its companions from attacking the wounds which would increase the risk of infection and trauma. Post-operative pain will be managed on an ongoing basis by fentanyl transdermal patches (75 µg), placed 12-18 hours before the induction of burns and changed every 72 hours. The maintenance of the patches will be easier thanks to the protective vest but special monitoring will be put in place to prevent them from taking off. The place of the patches will be changed frequently to prevent overdose and irritation. From Day 2, wounds will be treated every two days with a transdermal application of CAP or treated with helium for the pig control. These treatments and daily dressing changes, will be systematically done under sedation. As repeated sedation can induce undesired side effects (e. g. hypothermia and weight loss) animals will be closely monitored. In case of too much weight loss, high calorific solution will be given by intravenous infusion known as Perikabiven (Fresenius Kabi, Uppsala, Sweden).
On Day 15, pigs will be sedated and euthanized.

1.3. Medication and wound management

1.3.1.1. Sedation

The day before the induction of the burn a fentanyl patch (75 µg) will be applied on the back of the neck. This drug is effective from 12 to 18 h and has an action time of 72 h, the patch will therefore be replaced every 72 h.
Before induction of general anesthesia an additional heat supply will be made to prevent hypothermia (heating mat). Ophthalmic ointment (Ocry-gel®) will be applied to the eyes to prevent corneal dryness and trauma. The animal's left ear will be disinfected with a 2% chlorhexidine solution and a cotton gauze. Venous catheterization in the lateral vein of the ear will be performed using a 22 G catheter that will be connected to an IV syringe pump. Catheterization will be performed on both ears in case of difficult installation.
The day of the burn procedure, premedication for anesthesia will be composed of 30mg/kg ketamine I.M and 1 mg/kg I.M xylazine. Frequent intubation increases the risk of unwanted laryngeal edema, mucosal lesions, inflammation of the trachea and paralysis of the vocal cords. Thus, we suggest intubation of the animal only on the day of skin grafting (the longer part of the total procedure) and when using hallogenic gas for anesthesia. For this part the larynx will be desensitized by spraying 0.1 ml of lidocaine 5% on the arytenoids. The animal will then be intubated using a standard laryngoscope (195 mm) with a tube of 5.5 mm fixed by means of an extensible band on the snout.
Our procedure requires a dressing change 6 times during the 15 days. Different anesthesia protocols will be alternated for these 6 times in order to determine if endotracheal intubation and inhalation anesthesia can be avoided. The first protocol involves propofol at 10 mg/ml, I.V., 2 mg/kg/h. The second one is ketamine at 20mg/ml, I.V, 6mg/mg/kg/h (will be adapted to the animal response). The last one is the protocol initially planned with endotracheal intubation with inhalation of isoflurane (1-2%).

1.3.1.2. Burn induction and skin grafting

In order to maintain surgical anesthesia during the burn induction and skin graft, midazolam (0.2 mg/kg/h, I. V.), and ketamine (2 mg/kg/h) will be given at low doses for the first hour and propofol will also be administred (10 mg/ml I.V). At the end of this hour the midazolam will be increased to 0.5 and 1.5 mg/kg/h, I.V. and the ketamine dose will increase to 2.5 mg/kg/h because of a risk of tolerance to drug substances. Analgesia will be managed by a sufentanil infusion (0.3 µg/kg/h). A 5 ml/kg/h Ringer solution will be given in IV to prevent dehydration.

After analgesia and anaesthesia, the animal will be placed on one of its flanks. Hair will be shaved and the skin will be disinfected with 2% chlorhexidine solution. Local pain management at the burn site will include infiltration of the surgical site with lidocaine and bupivacaine under the skin, the total volume will be 10 ml of lidocaine per wound (AGUETTANT 10 mg/ml) to 4 mg/kg and bupivacaine. Lidocaine is a short-acting local anesthetic (start 5-10 min, duration 30 min-1 h). Bupivacaine is a slow-acting, long-acting local anesthetic (beginning 15-30 min,

duration 4-8 h). The two anesthetics will be combined in the same syringe allowing a quick start with long duration local anesthesia (up to 7 hours).
The pig will have the same anesthesia process for necrotic tissue excision and skin graft. Dressing changes will then occur every two days.

1.3.1.3. Wound dressing

Prior to dressing changes, animals will be sedated with one of the three protocols mentioned in section (1.3.1.1). The thermotherapy will be used to counter hypothermia as previously mentioned and should not induce drying of the burned areas since they will be protected by over-fat dressings and protective films. If the wound treatment and dressing change take more than 30 minutes, inhalation agents (isoflurane administered via mask) will be used to maintain anesthesia.
Initially the protocol of anesthesia contained a step with an infusion of paracetamol at 15 mg/kg will be injected intravenously with a 15 min infusion to manage intraoperative and post-operative pain in multimodal analgesia without exceeding the daily dose of 60 mg/kg. Paracetamol is used in human medicine for mild to moderate pain and pyrexia. In pigs, however, paracetamol is associated with a limited analgesic effect[382], but with an effective antipyretic action[383,384]. Given that paracetamol has a limited analgesic effect in pigs, it was removed from the protocol.
Parenteral nutrition will be administered to optimise post-operative recovery and weight gain. Fasting before induction of general anesthesia reduces the risk of regurgitation. As part of this protocol, animals will be fasting 3 out of 7 afternoons. Repeated fasting and many medical interventions can hinder adequate food intake, delay weight gain, slow post-operative recovery and inhibit wound healing. Parenteral nutrition will be used intraoperative parental nutrition administered during each surgical procedure and dressing procedure. Artificial intravenous nutrition with appropriate energy, glucose, amino acids, lipids and electrolytes has been identified (PeriKabiven 1000 Fresenius Kabi).
On day 15 the animal will be sedated with 30 mg/kg of ketamine and 1 mg/kg xylazine I.M followed by 20 mL I.V. Dolethal injection®.
This experimental procedure can be subject to several complications which is why a series of emergency medication was considered.
In addition to the existing multimodal analgesia protocol (lidocaine, bupivacaine, transdermal fentanyl), we decided to add sufentanyl (0,1µg/kg). It will only be used if the current protocol is not effective enough to control intraoperative and post-operative pain. Sufentanyl (0,1µg/kg) will be used in an animal that shows significant signs of distress and abnormal behavioural parameters such as lameness, agitation, excessive vocalization and agitation.

1.3.1.4. Additional medication

Several opioid medications will be used repeatedly at high doses to provide sufficient intraoperative and post-operative analgesia. Opioids work by binding to the mu (µ), kappa (κ) and delta (δ) receptors as agonists. Naloxone is an antagonist of the opioid receptors, it

antagonises their effects: respiratory depression, drowsiness, myosis, bradycardia, hypotension and also analgesia. We decided to use naloxone (80 µg/kg, I.V.)[385] in cases of respiratory depression secondary to morphinomimetic overdose. Whenever possible, naloxone will be administered by I.V., but when this is not possible, it may be administered by I.M. or subcutaneously.
To treat post-operative complications such as bradycardia we decided to use atropine. It is an anticholinergic that works by reversing cholinergic-mediated decreases in heart rate, blood pressure and systemic vascular resistance. Atropine will be used at 0.1 mg/kg in IV dose[386].
Finally, in case of infection amoxicillin is envisaged. Skin bacterial infection is a common post-operative complication. The activity of amoxicillin is mainly in relation to Gram positive bacteria, but some Gram negative bacteria are also sensitive to the bactericidal effect of amoxicillin. If signs of wound infection appear, we suggest using amoxicillin (15 mg/kg, IM) 2 injections 48 hours apart.

1.3.1.5. Euthanasia

Animals will be euthanized 15 days after burn induction. On Day 15, pigs will be sedated with 30 mg/kg I.M ketamine and 1 mg/kg I.M xylazine and euthanized with 20 ml of pentobarbital I.V (Dolethal®).

1.4. Examinations and sampling during and after the procedure

During the daily clinical examination, digital photos will be taken. In the future it will also be interesting to do non-invasive measurements of trans-epidermal water loss (trans-epidermal water loss TEWL) using VapoMeter (Delfin Technologies), to assess the rate of water evaporation to determine the skin barrier function. As some studies demonstrated the impact of CAP devices on wettability this could allow us to determine if we observe the same phenomenon with our own device.
Wounds will be excised/collected for post-mortem histological analysis (day 15 after burn induction) in particular to compare engraftment in term of: collagen synthesis, neovascularisation, re-epithelialization rate or wound closure. Complementary tests will also be performed for soluble collagen, hydroxyproline and RtqPCR will be done for ColA1 and ColA3 analyses. The samples will also allow to analyze the safety of the device to be sure that it does not induce cellular mortality or local burn. The number of pigs will not be sufficient to perform statistical analysis. In the next trial RNA extraction and transcriptomic analysis should be done for mutagenicity and genotoxity of CAP on a larger pig number to allow statistical analysis.
Biopsies will be collected from the main organs as heart, lungs, kidney or liver for anatomopathological analysis. Blood will be collected at day 0 and 14 for blood gases and electrolytes studies using Abbott i-STAT test cartriges. Other samples will be frozen for other potential analysis table 7.

Table 7: Example of feasible tests on pig blood and organ samples.

	Toxicology	Markers
Systemic	Hematological	Complete blood count, haptoglobin, search for schizocytes, fibrinogen, Activated partial thromboplastin time (coagulation)
	Cardiac	Troponin and ultra-sensitive troponin, type B natriuretic peptide
	Renal	Creatininemie, uremie, natremie, kalemia, creatininurie,urinary urea, natriuria, kaliuria
	Hepatic	ASAT, ALAT, GGT, PAL, bilirubin free and conjugated
	Pancreatic	Glucose, lipase, amylase
	Adrenal	Blood cortisol
Organ lysate	Pulmonary	sRAGE
	Inflammatory markers	CRP, IL6, TNFα, IL1…
	Cell lysis syndrome	LDH, CPK, ionized Ca, phosphor

Some pig skin samples can also be taken to do RTqPCR to quantify the expression of genes that code for growth factors that play a role in wound healing. During wound closure a number of growth factors are released during the different phases of inflammation, proliferation and remodelling. Most important of these growth factors include vascular endothelial growth factor (VEGF), platelet-derived growth factor (PDGF-BB) and transforming factor β1 (TGF-β1)[387]. Studies with analysis of this specific proteins in pigs revealed a similar pattern of expression and concentration as in humans during wound healing[387]. Thus, those elements are of interest for our studies and translational relevance to humans. Markers of extracellular matrix formation will also be of interest as collagen I, III, IV, VII, laminin V, fibronectin and integrins to make comparison with our previous *in vivo* mouse results.
After euthanasia skin samples will be put into PBS to perform tensiometry tests (industrial tensiometer, Universal Instrument for Tests on Materials, SUN/500N, Biolab Aust). We expect to have a scar tissue in the dermis that appear thicker and stronger than the control as it is known to be more rigid and fragile[388]. Biometrical assessment of tissue strength and elasticity is a useful tool that several groups used to determine if particular treatments were effective at reducing scarring[389,390]. As the mechanical properties of the skin depend on the collagen fibres and architecture we will performed histological analysis and RTqPCR on this purpose particularly focused on collagen 1, 3,4 and 7 and on other specific protein important for tissue junction as laminin and fibronectin.

1.5. Animal welfare during the procedure

On their arrival the animals will be housed in a group during a pre-experimental acclimation period of 7 days then will be housed individually on day 0 and day 1 (day of graft). From day 2, if the animals show no signs of distress they will be housed in a group, socialization being

an important parameter for the welfare of the pigs. Enrichment objects will be placed in its enclosure with a sufficient quantity of materials for digging, research and handling activities (wood chip litter and bales). The arrangement of the enrichment objects will meet certain criteria: positioned on the ground or close to the ground so as to be accessible when the animal is lying down, outside the waste areas, in sufficient number and quantity permanently and renewed.

Animals will be housed collectively in an enriched environment and will be handled daily during and after the acclimation period (1 week prior to the procedure). In order to minimize any form of suffering, the anaesthetic and analgesic management proposed in this project, as well as wound care, are very similar to what is done for any act likely to cause pain will also be performed under anaesthesia and analgesia as described above. Care will be taken away from other congeners to avoid anguish, and reassignment will only occur once the animal is fully awake. Apart from these criteria, there will be a constant exchange between the animals, veterinarians, and the other members of the project to ensure that there is no suffering, pain or distress in the animal. Scoring grids will detect signs of ill-being early (figure 33). If a limit point (e. g. uncontrolled infection, high pain in the animal, important loss weight) is found before the theoretical end of the experiment, the procedure will be interrupted and the animal euthanized.

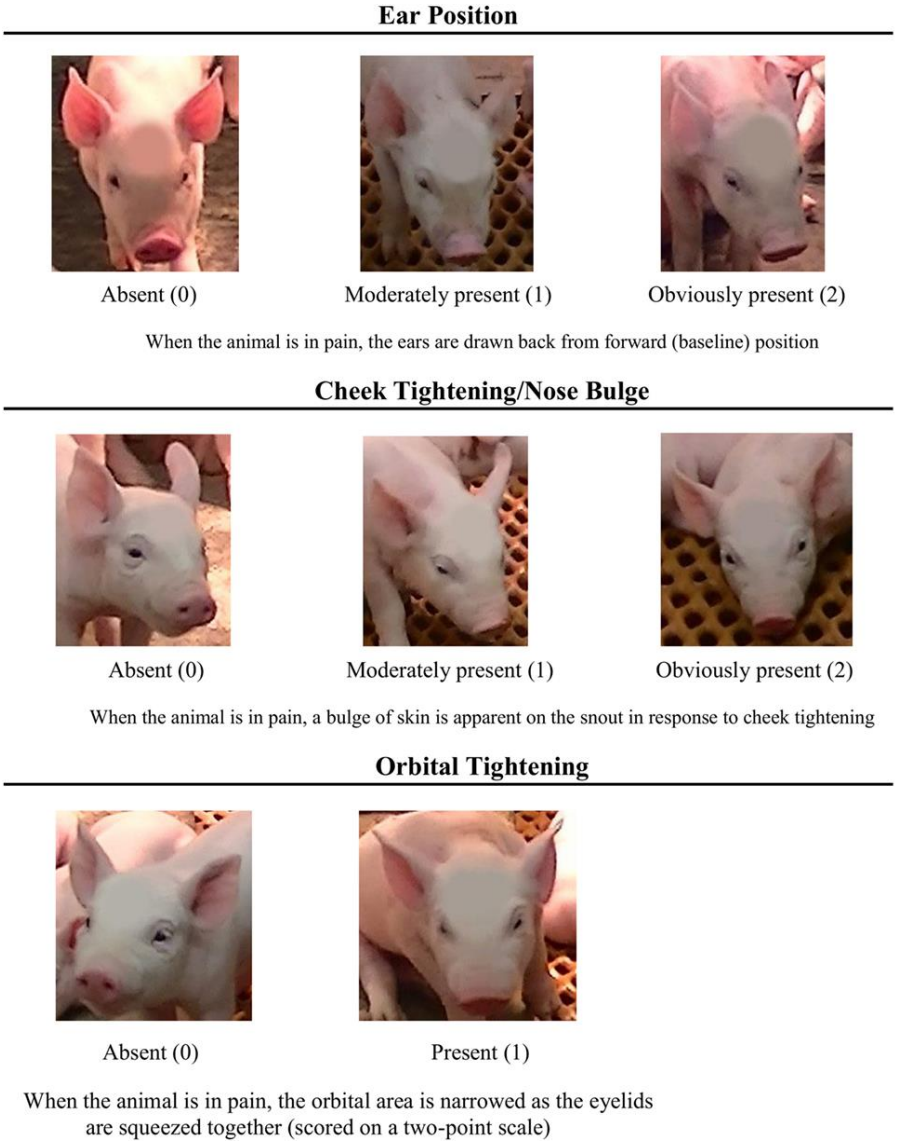

Figure 33: Example of pig grimace scale applied for the pilot study. Abbie V. Viscardi et *al.*, 2017[391].

Discussion

Burn injury is a severe form of trauma that is not a single pathophysiological event but a devastating injury that causes structural and functional dysfunctions in numerous organ. Due to its complexity and the involvement of multiple organs, *in vitro* studies cannot address this complexity in a pathophysiological way. In the last decade different animal burn models have been developed essentially to replicate the various aspects of burn injury or to explore potential treatment interventions.

In our pig model we decided to use a homemade device designed to induce large and deep burns in pigs[392]. However, in the future results we need to take into account that the burn may not be homogeneous and present variability between the different burnt areas. Clinically in order to have an idea of the depth of the burn induced researchers demonstrated that a pink/red color indicate a more superficial depth injury while a whiter burn indicates a much deeper damage[380]. Thus, the colour of the wound at the creation can help to determine the depths of the injury. Burn wounds will always show variabilities within the same individual independently of the burn device so, during the burn infliction we have to take into account variables that can increase them and if possible eliminate them.

Interestingly, Cuttle *et al.*, noticed that cleaning the skin surface with water or ethanol before burn infliction limits the depth of the burn potentially by increasing the local blood supply[381]. Maybe wiping the skin surface lightly before injury may have its importance. They also showed that the angle of the skin surface is important and they used a sandbag under the pig flank to create a better contact with the burning device. However, in our study this can only be done on one side since we induce two injuries on each flank. The use of a sandbag on the first burn side can modify the wound and move the dressings. These elements can help us to create a reproducible burn.

Animals should be housed individually however for their wellbeing they need a companion that why we decided to alternate between collective and individual accommodation. A major risk is the interaction between the pigs which may remove and/or eat dressings or the other pigs. As most of the wounds are pruritic, we choose specific dressings and a protection vest that should prevent dressing removal and self-mutilation of the healing wounds. Other objects of environment enrichment such as balls, ropes and other toys are also beneficial to keep animals occupying and less likely to eat or remove dressings. However, if the animal manages to move the dressings, the risk of infection will be even greater than with the protections. In our protocol we have not included prophylaxis (e. g. use of antibiotics to prevent infection), but we have planned to use amoxicillin in case of apparent infection during the process.

Another point that can be problematic for the proper conduct of the study is the frequency of anaesthesia of pigs that induces recurrent fasts. This procedure may interfere and lead to inadequate food intake, delay weight gain, slow post-operative recovery and inhibit wound healing.

If the anaesthesia procedure is too heavy, if an eventual infection persists which may interfere with the transplant and the health of the pig, the study will be stopped if previously defined experimental end points have been reached.

Another important point in our study concerns the plasma device. Its safety was shown *in vitro*, but it has never been used *in vivo* and let alone on a large animal. Theoretically we plan to use the device at 20 mm from the target but as the treatment surface is irregular and the head of the jet II is held by hand by the experimenter the distance will fluctuate which may move away or closer to the skin. This variable can either decrease the effectiveness of the treatment by moving too far from the target or increase the treatment with a potential risk of burning the already weakened skin. However, the preliminary tests carried out on the pig skin lead us to believe that the device will be safe for the selected parameters even in case of approximation. In addition, a device acting as a cleat is being designed to help the experimenter better visually estimate the distance. A risk of skin dryness and small erythema is expected but should be minimal. In studies using CAP from any sources, erythema tends to disappear after few minutes[338].

At the end of our study a question will persist on the safety of the plasma, we will have an idea of the systemic effect of CAP over a period of 15 days. In-hospital treatments for patients, whether for burns or chronic wounds, are more regular (two to three times a week) and continue for several weeks. Thus, questions of the effect of plasma from a systemic and mutagenic point of view will remain to be investigated.

Conclusion

We developed a full-thickness burn pig model reconstructed with an autologous graft treated by CAP or left untreated. The pilot study carried out in October 2022 will involve two pigs. Although the small sample size will not enable us to perform statistical analysis on measurements of various wound parameters, the protocol will provide valuable information for the development of our future studies. We will be able to see whether the device induces positive or negative effects on the skin, burn wound, skin engraftment and systemically. The feedback from this experience will enable to optimize protocol treatment and the engineering teams could optimize the ergonomics of the device which is at the prototype stage. Another study will statistically relevant sample size will be required to obtain meaningful results. This may provide an insight into effects of cold plasma in the treatment of extensive burns.

Discussion and perspectives

Discussion and perspectives

Burns are the fourth most common type of trauma worldwide. Despite significant progress in burn care in the last two decades, long lasting complications continue to challenge patient's quality of life. In full-thickness burns, wounds can remain open and pose a risk of microbial infections[347], over the last decade 42-65% of deaths in burn unit was attributed to infections[393]. Furthermore, some burn wounds produce high levels of exudates creating a moist and nourishing environment for bacterial growth which can lead to sepsis. Large surface areas of skin that remains open for an extensive period of time increase the risk of microbial colonization and spread from local wounds to the bloodstream causing sepsis. Numerousffective topical and systemic agents are available and used in the clinical setting to prevent and treat infections. However, some of these agents have been shown to be cytotoxic to skin grafts and granulation tissue. Several species of bacteria, in particular *Staphylococcus aureus*, have been associated with antimicrobial resistance. In addition, *S. aureus* is known to form a biofilm that envelops bacteria in a polymer-based matrix, decreasing its susceptibility to antimicrobials and immune defenses and making these infections more difficult to eradicate. It is therefore urgent to develop innovative treatments to tackle bacterial wound infections, which in turn, will help to reduce the morbidity and mortality associated with systemic complicaitons associated with bacterial infections.

This PhD work had two main objectives.

The first one was to analyse the ability of macrophages to eliminate *S. aureus* through phagocytosis and to understand the underlying mechanisms after CAP treatment. In the study, we were interested in investigating the phenomenon that proceeds the engulfment, i.e. intramacrophagic clearance of *S. aureus* enclosed within phagosome, digestion with hydrolytic enzymes and expression of marker of superoxide-generating machinery.

Previously, we developed an *in vivo* model of experimental full-thickness burn wound reconstructed with an allogeneic skin graft (Annex A). This method allows to induce a reproducible full-thickness burn as the depth of the burn is an important factor to consider. A limitation of the method we described in the article is that only full-thickness grafts (and notsplit-thickness grafts) were harvested from the tail of the mouse. This results from technical difficulty as the mouse skin is too thin to obtain split thickness graft. However, this reproducible model allows us to show that CAP has bactericidal properties *in vivo* and had an impact on both MSSA and MRSA strains.
These effects validated the direct impact of CAP observed *in vitro* on the inactivation of *S. aureus* in suspension. Nonetheless, the bactericidal effect of the device is compatible with further applications of CAP for skin treatments since the energy needed to inactivate bacteria is lower than the one needed to induce cellular damage in skin cells. Regarding the use of CAP for wound disinfection the main task would be to ensure that no development of resistance of microorganisms would follow CAP treatment. Bacteria are able to increase expression of ROS detoxification molecules and develop system to repair oxidative damage[394]. Thus, bacteria could develop strategies to overcome CAP effects. Few studies were done about resistance with contradictory results. In 2015 Mai-Prochnow *et al*. showed that CAP induced resistance of *P. aeruginosa* in biofilms, whereas Matthes *et al.* demonstrated that *S. aureus* biofilms do not develop resistance to repeated CAP treatment. Interestingly in 2016, Alsshraiedeh *et al.* showed the ability of bacteria (*Burkholderia cenocepacia*) to develop tolerance to CAP in a biofilm mode growth due to biomass and catalase production[395].

It is important to take into account the fact that bacteria can have a natural or an acquired resistance to antimicrobial agents through mutations or acquiring resistance genes. Zimmerman et *al.*, investigated if *E. coli* has natural and acquired resistance to CAP but none of this was observed. In the article published by Mai-Prochnow et *al.*, two hypotheses were done by authors: either colonies that grew up in the plasma treatment zone had favorable natural mutation before treatment or plasma exposure induced specific mutation.
Despite controversial studies CAP tolerance is a parameter that needs to be further studied. It would be interesting to test with our own conditions if resistant colonies appear after several treatments and if several treatment of the same liquid culture conduce to a complete tolerance.
To go further, we have clearly shown with our own jet that we induce bactericidal effect, but we still assume that it is due to oxidative species as H_2O_2 or $O_2^{\cdot -}$ produced without clear evidence. Thus, next investigations will be performed with mutants of *S. aureus* USA300 (highly virulent, clinically relevant strain isolated from bacteraemic patient) for which a knockout was performed for catalase or superoxide dismutase genes.

During our experiments we noticed that *S. aureus* formed clusters due to its ability to grow in biofilms. Biofilms represent a particular challenge in the healthcare setting since they present elevated tolerance to antimicrobial. Alkawareek *et al.* used a CAP treatment shorter than 4 min to fully eradicate Gram positive bacteria. However, certain Gram negative biofilms required longer treatment time as 10 min to obtain an eradication of bacteria[396]. During my PhD, a preliminary experiment (assessment of biofilm formation using crystal violet assay) showed a decrease in *S. aureus* biofilm formation after the treatment with CAP, but this effect was observed only for MSSA strain and not MRSA (USA300). Those results on biofilm have prompted a new project currently underway, which will follow up the question of the effect of CAP on *S. aureus* biofilm on the *in vitro* and *in vivo* models of wound infection.

As macrophages are key cells involved in wound clearance and healing in a burn wound context, we investigated deeper the effect of CAP on these innate immune cells. We demonstrated that CAP bactericidal effects were also indirect since CAP-treated murine macrophages showed an enhanced ability to kill bacteria. We showed that CAP induced an increase of intracellular RONS, which is correlated with a decrease of the bacterial load when macrophages are CAP-treated 24 h before the infection[368]. Microscopy and pull-down immunoprecipitation experiments also demonstrated that this effect was correlated with an advanced maturation of phagosome into degradative and acidic vesicles with an increased level of phagolysosome membrane-bound LAMP-1 and intraphagosomal cathepsin-D. Studies have demonstrated that CAP can induce macrophage polarisation to a M1 or M2 phenotype[362,363]. However, in our studies no significant difference of macrophages polarisation was observed between CAP and control. This absence of changes in cell polarisation is certainly due to the characteristics of the plasma device (gap, gas flow, voltage, frequency) and the treatment conditions (type of the target, time of exposure, type of gas). Those plastic cells assume certain phenotypes in response to context.

In order to get closer to reality the infection model was then modified to induce the infection before CAP treatment. We obtained the same bactericidal effect as in the previous model that lasts 5 hours after CAP application and the same intracellular ROS increase was obtained. We know that CAP can act on phagosome maturation when macrophages are treated 24 h before infection but in this new procedure the effect is confirmed again to be reproduce.

The major finding of this PhD concerned the identification of activation of the NOX2 complex in response to CAP. In macrophages the phagocytosis process induces an oxidative burst mainly through the NADPH oxidase (NOX2). Knockdown macrophages for NOX2 and pharmacological inhibitor molecules were used in the infectious model. NOX2 inhibition abrogated the antibacterial effect of CAP in 2D models of infection. Macrophages transfected with *Cybb* coding for NOX2/gp91^{phox} followed by CAP treatment resulted in a reduction of intramacrophagic ROS and increase the number of living bacteria compared to the control. To go deeper in the mechanistic involved, our microscopy and pull-down immunoprecipitation analysis revealed a higher level of colocalisation of Rac-GTP and gp91^{phox} with *S. aureus*-containing vacuoles. This observation is correlated with a significant increased rate of phosphorylation of cytosolic components of NADPH oxidase complex (p40^{phox} and p47^{phox}) at 5h p.i. Our results demonstrated that CAP induces the switch between GDP-bound and GTP-bound forms of Rac1, key component of NOX2 activation.
In addition to the 2D model of infection we developed an infected three-dimensional model of macrophage-laden human skin equivalents. The intradermal inoculation of *S. aureus* resulted in reproducible results showing that *S. aureus* was present in clusters in the model due to its preference to exist in biofilms. Using this complex 3D model we demonstrated that NOX2 inhibitors also increase the bacterial load within the model highlighting the importance of the complex for the clearance. The 3D model is promising however the infectious protocol still need to be optimized in order to get standardized results independently of the experimenter.

The strength of this work is that we used several models from *in vitro* to *in vivo* and we succeed to demonstrate a bactericidal effect that is in part due to the activation of NOX2 phagosome complex after CAP treatment. Recruitment of cytosolic components of NOX2 complex to phagolysosomal membrane, post-translational modification characterized by phosphorylation of p47^{phox}, p40^{phox}, and induction of Rac-GTP demonstrate the strong activation of NOX2 by CAP. The next step will be to go upstream in the mechanistic to understand how NOX2 is activated. It was previously shown that H_2O_2 activates NOX2 or p22^{phox} subunit to produce $O_2^{\cdot -}$ in fibroblasts and smooth muscle[397] but to our knowledge nothing is known for CAP-NOX2 activation. CAP device produces H_2O_2, thus it is reasonable to hypothesize that there is an activation of MAPKs (ERK1/2, JNK). Next investigation will focus on the use of ERK1/2 inhibitors in macrophages. Activation can induce the phosphorylation of p40^{phox}, p47^{phox} and p67^{phox} of NOX2.

Interestingly, during our experimentations the use of mitochondrial inhibitor molecules induced a similar level of intracellular ROS and bacteria survival as with the use of NOX2 inhibitors. Researchers demonstrated that ROS produced by mitochondria act within macrophages. The stress induced by the infection by *S. aureus* triggers the production of mROS which are delivered to the bacterial-containing phagosome by mitochondria-derived vesicles[197]. This additional element is particularly of interest as it can be related to the increase of intracellular ROS levels we observed in macrophages. However, mitochondria have pleiotropic functions in cells so we cannot produce knockdown for mitochondrial genes that may impair cell viability and produce non-specific results. It could be relevant to follow mROS using specific probe as MitoSOX™ which specifically target mitochondria and their superoxide production.

The therapeutic efficacy of plasma has been observed in various diseases but the fundamental consequences of plasma-derived ROS on cells remain elusive. Transcriptomic analysis is thus, an

important tool to understand the mechanistic pathways triggered in CAP-treated macrophages. Using our infectious protocol of macrophages, we performed RNA extraction of treated and non-treated cells, samples are under analysis. Those results will allow us to determine the genes that are up or down regulated and highlight new mechanistic pathways triggered by CAP treatment. However, the preliminary results obtain with RT-qPCR suggest heterogeneity in the results. Thus, different time points in addition of the 5 h post infection need to be done and it is also of interest to perform proteomic analysis to determine the level of action for each point.
Plasma for biomedical applications is known to have beneficial properties on disinfection (surfaces and wounds), healing of acute and chronic wounds, and solid tumours but little is known about the underlaying mechanisms responsible for these effects. *In vitro* CAP was demonstrated to have an impact on proteins and enzymes (denaturation, oxidation), lipids and fatty acids ($O_2^{\cdot -}$, H_2O_2 inducing membrane lipid peroxidation), and to induce DNA and RNA damages on cells and bacteria. On the cell wall and membrane researchers demonstrated that CAP can produce an erosion due to bombardments by radicals, breaking of chemical bounds and membrane disruption. However, transposition of those results are still difficult due to the diversity of physical and chemical properties of the plasma resulting from the multitude of devices.

In wound injury apart from macrophages, neutrophils are also key cells and are even the first cells to join the site of injury. Neutrophils are sometimes described as detrimental cells in pathological wound healing[398] and cancer[399] but literature also demonstrates the opposite[400,401] . They possess important qualities for wound clearance with a fast oxidative burst and the formation of extracellular traps (NET). Bekeschus team demonstrated that neutrophils exposed to CAP induce a low level of apoptosis, a strong release of IL8, robust release of NETs and interestingly a decrease of the NADPH oxidase activity[402]. NETs formation are known to have negatives effects on diabetic wounds however senescent neutrophils and their removal via NETs formation is a way of wound healing. Proteomic analysis of neutrophils after CAP exposure showed several changes as in the redox regulating proteins as annexins, myeloperoxidases, collagenases, superoxide dismutases and thioredoxin[403]. Most of the cold plasma-modified proteins in this study are important in acute wound healing[404]. Thus, as neutrophils proteomics profile of neutrophils changes after the treatment with CAP, it could be interesting to study the interaction of bacteria, neutrophils and macrophages after CAP treatment or to integrate these innate immune cells into 3D models.

The second axis of my PhD work concerns the characterization of a new plasma device for the treatment of wounds with larger surface area for clinical applications.

Until now our results were obtained with a jet allowing a 1 cm^2 surface treatment. The main drawback of the device for clinical applications is the size of the generated plasma and the lack of flexibility limited to vertical application. The objective of this axis was to produce a prototype of an extended cold plasma for cutaneous wound healing for use in preclinical tests on pigs planned in October 2022. Rodent models used previously poorly mimic human systems in a burn injury context[91]. They differ in their healing process and above all they possess a superior immune system. Pig model is classically used to study tissue regeneration and scar reduction in burn wound. Wu et *al.*, studied the toxicity of CAP in pig model,[405] but its effect on healing process has not yet been studied in this complex model. Our pilot study will allow to have better anatomic and physiological similarities with humans.

The cold plasma is created by electric discharge in a noble gas in jet to increase the treatment surface and reduce application times. Coming out of capillary, the noble ionized gas generates reactive species of oxygen and nitrogen in contact with the ambient air that interact with the skin wounds to stimulate their healing.

Preliminary chemical and biological tests were done to set parameters that can be used safely for the pig trial. Biological tests were performed on human keratinocytes only so the impact on cellular viability, proliferation and migration may be subject to changes during the pilot study of a more complex model. As expected the H_2O_2 and NO_2 concentrations were 10 times higher than the one obtain with the jet I. However, those concentrations are under the one needed to induce deleterious effect on human skin cells. Studies investigating the impact of CAP on macrophages/monocytes showed that they are highly robust against plasma-derived oxidant cell death. According to authors cells use their redox signalling pathway to modulate the inflammatory response and migration as well as their phenotype.
In addition, in our porcine *in vivo* models a surface of around 57 cm^2 will be treated under movement so reactive species should not be concentrated in a single zone allowing a larger diffusion and decreasing potential deleterious effects. Interestingly the gas flow difference between the jet I and the jet II triggered an increase in cellular viability and proliferation. The difference is lower than the one induced by CAP but the phenomenon was not observed with the jet I. We are using helium which has low solubility, is rather inert and is an easy to use gas. It has been demonstrated that it can favour wound healing and has cellular effect leading to cardio- and neuroprotection that help to fight against organ ischemia[375]. Thus it is plausible that its activity can favour burn wound healing and have a protective impact.

The "dose" to be applied is the most difficult element to predict despite the *in vitro* upstream tests performed with the jet II. A major limitation in plasma medicine is the lack of standardisation of the plasma device. The design, the parameters as the working gas and flow patterns vary. All those parameters are important for biological effect thus, comparison and translation of results from one study to another are difficult. In dermatology, *in vivo* CAP application can be performed daily and even twice a day depending on the team[406]. The duration time is also very diverse and depend on the plasma device (as seen in section 4.6.4.1). For the same device the parameters such as the frequency and the duration can change according to the target; in our study *in vitro* treatment were generally 1-2 min and *in vivo* 30 s.

To be able to do comparison between studies researchers should perform standard analyses of energy of application, the temperature, the UV spectrum and the quantification of the long-lived species produced as nitrite/nitrate and H_2O_2. Short-lived species quantification is still challenging. For example, the chemical half-life of $NO^{\cdot}$ is shorter than one second and $OH^{\cdot}$ is in the nanosecond range. The electric field produced is known to induce migration of cells, but higher electric field can lead to burns and irritations in addition RONS can be toxic if they exceed a certain threshold. UV light is also a parameter to consider due to DNA mutation that it can trigger inducing cell death and mutagenesis. Different measurement of UV emission and chemical generation need to be done to ensure the safety of the device. CAP device differs in term of plasma device and experimental procedure thus it is difficult to quantify all the actives species that are generate. In comparison, drugs can be precisely defined but it is more difficult for CAP that can also change through environmental parameters as the humidity of the ambient air.

The pilot study on pig model is set with 30 s CAP treatment with several points of treatment per wound and specific plasma parameters that are not detailed in this manuscript. Due to the versatility of biological systems those preliminary parameters will certainly have to be modified particularly the distance to the target and the duration.
In addition, we must take into account that we are not treating a healthy skin. Indeed, normal skin is protected by the *stratum corneum* known for its mechanical and chemical resilience but is not present in the case of full-thickness burn. In the pilot study, the wounded area will be covered with an autologous split-thickness graft that is fragile and can be easily damaged. The potential presence of pathogen can also impair the graft intake. It is wise to extend the treatment time and to shorten the frequency to control eventual infection but specially to ensure the taking of the graft. A risk of the study is the presence of infection; the experimental process does not incorporate prophylaxis so in case of infection antibiotic can be used but difficulties to control infection can lead to the loss of the graft.

The homogeneity of the graft can also be a challenge. When the burn is induced, the necrotic tissue is removed providing a heterogeneous area and the graft is performed on this surface. *In vitro* and theoretically we planned to treat the target at 20 mm with the jet II. Nonetheless the heterogeneity of the surface and the variations induced by the experimenter who manually move the device above the wound will induce a heterogeneous treatment. To avoid inter and intra experimental variation, each wound should be treated at several points pre-marked at 12, 3, 6, 9 o'clock and center of the wound for 30 s each time. An expansion spacer placed on the head of the device will help the experimenter to visually respect the distance and limit bias. According to the treatment of the area the inside and the edges of the wound will be CAP-treated. We assumed that peripheral healthy cells also participate in the healing process as they migrate to the injured site and secrete proteins important for healing.
Another critical point related to the graft is the repeated anaesthesia induced to the pig. Their frequency can lead to weight loss, a feeling of discomfort in the throat, fatigue and a general condition that may lead to animal's illness. Poor psychological and psysical conditions of the animal can induce bias in the results independently of the experimental procedure.

At the end of the pilot study different types of analysis will be performed and especially toxicological analysis. Samples will be collected for RNA analysis even if there is only one pig per condition in order to have a global view of potential changes. We also plan in the future to settle *ex vivo* model using pig skin or human skin from plastic surgery to tests different parameters of the jet II on the skin. These tests will allow to optimize treatment conditions for the next pig trial and potentially to develop a burn model or an infected burn wound model. In case of an infected model this will also allow us to analyse the impact of CAP on biofilms since clinically relevant infection often involves the formation of biofilm in the wound bed. The disadvantages of these models are that the skin is not readily available and donor's variability exists requiring several donors and multiple experiments.

Plasma devices are developed for clinical use but to date the question of CAP as drug or medical device for indirect treatment still persit. The complexity of the question is increased by different legislation. In Europe and the US drugs or medical device are under separate laws and cannot be used together. Medical drugs are distinguished by their pharmacological, metabolic and immunologic impacts and the medical device is essentially based on physical parameters and depending on their potential risk they are classified in other subclasses. Categorisation of CAP is done according to their

mode of action, for example CAP devices used for cutting or coagulation were approved as medical devices. However, MEDDEV-Bordelines defines a pharmacological effect as the interaction between molecules and cellular components of the target. The European directive 2004/27/EG and the European Court support the definition of pharmacological effect as an interaction with any cellular components of the body including foreign targets as bacteria or viruses. The classification of CAP device depends on its use if its act physically or pharmacologically. All results reported are based on the effect of reactive species that are produced and are associated with biological effects. However, in wound healing, and in our case burn wound healing therapeutic effects cannot be explained by only physical effects. Even if biological mechanisms are not fully understood the effects on mitogen-activated protein kinase, growth factors, integrins and other proteins or molecules let indicate pharmacological and immunological effects of CAP. In comparison to classic medical drugs some elements are lacking: it cannot be prepared and stored in vials, cannot have precise concentrations and dosages. The role of the electric field, which may play a role as electroporation is also not understood.
Several additional parameters need to be quantified as the energy application (J/m^2), UV spectrum, gas uses and the associated radicals for example. Due to technical limitations the quantification of radicals is not possible and it is challenging to maintain the energy application constant for plasma sources. Comparatively to drugs, CAP and its biologically active compounds are generated during the application of the medical device. Regardless to classical definition CAP is associated to a drug, but legislation makes more complex the categorisation thus the question is still under debates.

In the last two decades the spectrum of different plasma sources with various names as plasma needle, plasma brush, atmospheric pressure glow discharge torch or atmospheric plasma jet appeared on the market and are dedicated to biomedical applications. Researchers try a classification with three plasma sources used for biomedical applications organised as barrier discharges, plasma jets, and corona discharges. However, in order to establish general requirements for plasma sources in medicine Mann *et al.* published in 2014 a technical standard DIN SPEC 91315 in order to establish general requirements for plasma sources in medicine. The objective is to give the basic physical and technical performance parameters of plasma sources for biomedical applications. This document does not define new standard values concerning UV irradiance, formation of toxic gases but they refer to already existing standards and guidelines (DIN EN ISO 12100, DIN EN 60601-1, DIN EN 60601-1-6, and DIN EN 60601-2-57). This document needs to be adapted to every plasma sources but will give suitable information on effectiveness and safety but also on basic physical and chemical datas. In addition to the standardization for comparability a risk for adverse effects such as genotoxicity and mutagenicity are highly important. Few studies indicated that CAP does not impact both parameters in cultured cells[340,407]. Those preliminary data are promising however further studies need to be done to investigate the potential risk of CAP under different conditions specifically on repeated treatment and long time after exposition. Both preclinical and clinical investigations need to be performed and complemented with tests of clinical effectiveness with the exclusion of chronically toxic, mutagenic and carcinogenic risks.

Conclusion

Despite the evolution of clinical practices, the management of severe burns remains complex and difficult especially in case of infection. Within the framework of my thesis we continued the work of Dr Duchesne[369] focusing on the molecular mechanisms responsible for antibacterial effects in the skin obtained with the plasma device. Current PhD project consisted of two work packages. The first package was designated to investigate of host-derived mechanisms responsible for antibacterial effect of CAP using two and three dimensional experimental models of infection. The second package was dedicated to the development of a new plasma-generating device, its physico-chemical characterisation, and its use in a porcine model of burn wound healing.

This PhD work, on a completely new issue, highlights the indirect effect of CAP on the bactericidal properties of macrophages. RONS production are increased not only under the influence of direct CAP treatment, but also through the activation of specific mechanisms as the NOX2 complex, known for its key role in the oxidative burst. Future studies of the transcriptomic profile of infected macrophages will provide crucial information on the influence of CAP on host gene expression and its potential mutagenic and genotoxic effects.
In the larger context of the project related to burn wounds the jet II developed will bring us closer to clinical trials. Work needs to be done on more complex models to ensure its safety for both experimentators and patients and to improve its engineering for a better control of plasma parameters for future trial in surgery room.

These results highlight the interest of CAP treatment for infected full-thickness burns raising up new interrogations but also open up perspectives for the treatment of chronic wounds. Additional work needs to be done to further understand the mechanisms involves in improved CAP infected wound healing as its complexity still makes its mode of action elusive in all plasma medicine fields. Despite the great progress in plasma wound healing, a lack of standardization of plasma parameters slows the understanding of underlying mechanisms and needs to be improved between research teams.

Significant milestones were reached in the course of this doctoral degree. In the first year of my PhD project, I published my first article as the first author in the *Journal of Visualized Experimentation* in 2020. In the second year of my PhD, I published an article as the second author. I took an active role in the process of data collection and preparation of this manuscript, which was accepted for publication in a journal of the American Society for Microbiology *mSphere* in 2021. In 2022, we prepared a new manuscript. This first-author article is now ready for submission into a journal with a very high impact factor. Another first-author manuscript is ready for submission. This article will be submitted to an open-access journal and will highlight the results of the genome sequencing performed on two different strains of *S. aureus* (Xen31 and Xen36). Together with other members of our group, I am working on preparing a review article. Apart from the academic output associated with the doctoral studies, I actively participated in the development of porcine model of burn wound healing, and assisted in characterisation of a new plasma-generating device. In conclusion, this PhD study has been very productive. It provided essential baseline knowledge, which will be applied in the next steps of the project.

Materials and method

This section describes the materials and methods used in experiments that have not been published and are part of further studies.

1. Materials and method of chapter III

1.1. Raw264.7 culture conditions

Macrophage murine cell line RAW264.7 (ATCC®, Molsheim, France) were grown in DMEM (1X) + GlutaMAX™ (Gibco Paisley, PA, USA) supplemented with 1mM Na pyruvate (Thermofisher Scientific, Waltham, MA, USA) and 10% FBS (BioWest, Nuaillé, France). No antibiotics were used. Cells were passed when reaching 80% of confluence with a scraper and were seeded at a concentration of 5000 cells/cm^2 and media changed every two days. The number of passage did not exceed 20.

1.2. Bacteria culture and preparation

Two bioluminescent *Staphylococcus aureus* strains were used: Xen36 (PerkinElmer) and USA300 (ATCC reference BAA-1717) respectively methicillin sensitive and methicillin resistant. Bacteria were grown on BHI agar plates at 37°C, 5% CO_2. A colony was isolated and grown overnight in liquid BHI at 37°C, 5% CO_2 and 200 rpm. 100 µl of this culture was transferred into 10ml of fresh BHI and grown at 37°C, 5% CO_2 and 200 rpm. When bacteria reached the exponential growth with a DO=2 corresponding to 1x10^9 bacteria/ml they were harvested by centrifugation (10 000 g, 5 min) and suspended in PBS or media depending on the experiment.

1.3. RNA isolation

RNA isolation from RAW 264.7 cells was carried out using TRIzol Reagent (Thermofisher Scientific, Waltham, MA, USA) and RNeasy Mini Extraction Kit (Qiagen, Courtaboeuf, France) as described by the manufacturer. DNA elimination was performed using Invitrogen™Ambion™ TURBO DNA-free kit (Invitrogen Life Technologies Corporation, Oregon, USA). Total RNA concentration was quantified using Nanodrop 2000 (ThermoScientific, Waltham, MA, USA). The RNA quality was determined by analysing the proportion between 28S to 18S ribosomal RNA electropherogram peak using an Agilent RNA 6000 Nano Kit and Agilent 2100 Bioanalyzer (Agilent Technologies, Waldbronn, Germany). Samples with a RNA integrity number >8 were used for cDNA synthesis.

1.4. Quantitative reverse-transcription–PCR

cDNA was synthesized from 1 µg of RNA using reverse Transcriptase Core Kit (Eurogentec, Seraing, Belgium). Quantitative reverse-transcription–PCR (qRT–PCR) was performed using a QuantiTect SYBR Green PCR Kit (Qiagen, Courtaboeuf, France) and C1000 CFX384 Touch Real-Time PCR System (Bio-Rad Laboratories, Hercules, California, USA). Housekeeping control gene was used to normalize the amounts of cDNA within each sample. Differences were calculated using the Ct and comparative Ct methods for relative quantification. The relative level of gene expression was normalized with a housekeeping gene and used as a reference to calculate the relative level of gene

expression according to the following formula: 2-ΔΔCt, where-ΔΔCt=Δ Ct gene - Δ Ct Average where Δ Ct gene = Ct gene - Ct Hprt1 and Δ Ct Average = Average Δ Ct control. For all biological replicates, 2 technical replicates were performed. All samples were evaluated in at least three independent experiments.

Primers used for the study.

Mm_Cybb	QuantiTect Primer Assay #249900	QT00139797	Qiagen
Mm_Tnf	QuantiTect Primer Assay, #249900	QT00104006	Qiagen
Mm_Il1b	Q QuantiTect Primer Assay, #249900	QT01048355	Qiagen
Mm_Rac1	QuantiTect Primer Assay #249900	QT01070146	Qiagen
Mm_Rac2	QuantiTect Primer Assay #249900	QT00104062	Qiagen

1.5. Pharmacological inhibition of ROS activity

RAW 264.7 cells were pre-incubated with a mitochondrial ROS inhibitor Necrox-5 methanesulfonate (Bertin Bioreagent, Montigny-le-Bretonneux, France) at 1 µM. Following a 30-min incubation with Necrox5, samples were treated either with placebo control (helium) or CAP.

2. Material and methods plasma device characterization

2.1. Physical characteristics

2.1.1. Plasma jet I

2.1.1.1. Design

The plasma jet used has been made in Laboratoire de Physique des Plasmas (LPP, Ecole Polytechnique). It is composed of a tube surrounded by an electrode powered by AC high voltage. A noble gas, helium, flows into it and when the electric potential between the high voltage electrode and the target is high enough the discharge is ignited. The jet consists of a 3D-printed (Makershop, Le Mans, France) capillary in ethylene polyterephtalate (PET) with a needle electrode inside. The capillary has a high of 60 mm and a diameter of 3 mm. The electrode was printed in a conductive plastic; plastics are excellent insulators which become conductive when they contain graphite or graphene fibers. Thus, two conductive plastics were used: PLA-Graphite (resistivity $\rho = 44\ m\Omega.m$ from Proto-Pasta) and PLA-Graphene ($\rho = 6\ m\Omega.m$, BLACKMAGIC3D). The electrical resistance of the part printed in PLA-Graphene is of the order of a few ohms from one side to another. The insulating ring placed between the high voltage electrode and the gas tube is made of PLA.

The helium flow is controlled by a mass flow controller Brooks 0254 (Serv'instrumentation, Irigny, France) and set to 500 sccm. A sinusoidal current is provided by a 50 Hz generator. A maximum peak to peak voltage of 32 kV is used during *in vitro* experiments. Mechanical supports for CAP enable to choose the vertical position of the plasma-jet. For *in vitro* experiments the height of the plasma source above the liquid was fixed to 5 mm.

2.1.1.2. Power measurement

Voltage measurement was acquired with an oscilloscope RTE1024 (Rohde&Schwarz, Munich, Germany) characterized by 4 channels, band-pass = 200 MHz, sampling rate 5 GSa/s. The voltage of the generator was measured with a probe connected to the oscilloscope (PPE20kV, 1/1000 attenuation).
A capacitor **Cm** (100 nF) is connected in series with the target of the plasma jet. The voltage **Um** was measured at the terminal of the capacitor with the relation *Q = Cm x Um*. The current flowing through the measuring capacitor is known through the expression $I = Cm\frac{dUm}{dt}$.
With approximation Um<<Valim, the amount of energy **E** consumed from 0 to τ is:

$$E = \int_0^{\tau} Valim\ I\ dt = \int_0^{\tau} Valim\ Cm\ \frac{dUm}{dt}\ dt$$

Which gives a period τ of electrical signal:

$$E = \int_0^{\tau} Valim\ dQ(t) = \int_{Qmin}^{Qmax} Valim\ dQ$$

When Lissajou curve is plotted, i.e. the curve with following parametric equation

(t→ (x = Um(t), y = Valim (t)),

E is also the internal area delimited by the parametric curve multiplied by Cm.

Power consumption is calculated in real time with a software option which perform calculations thanks to a code written by Dr. Honnorat[408]. A temporal gate located at the end of the acquisition window enabled to record the energy consumption during one acquisition. The acquisition time was 20 ms corresponding to one period of the 50 Hz generator and the acquisition rate was 2.5 MS/s. Calculation of the power was done by accumulation of at least 1000 points. The variation of the power *in vitro* was studied according to different parameters as the voltage, the helium flow and the gap between the plasma and the target.

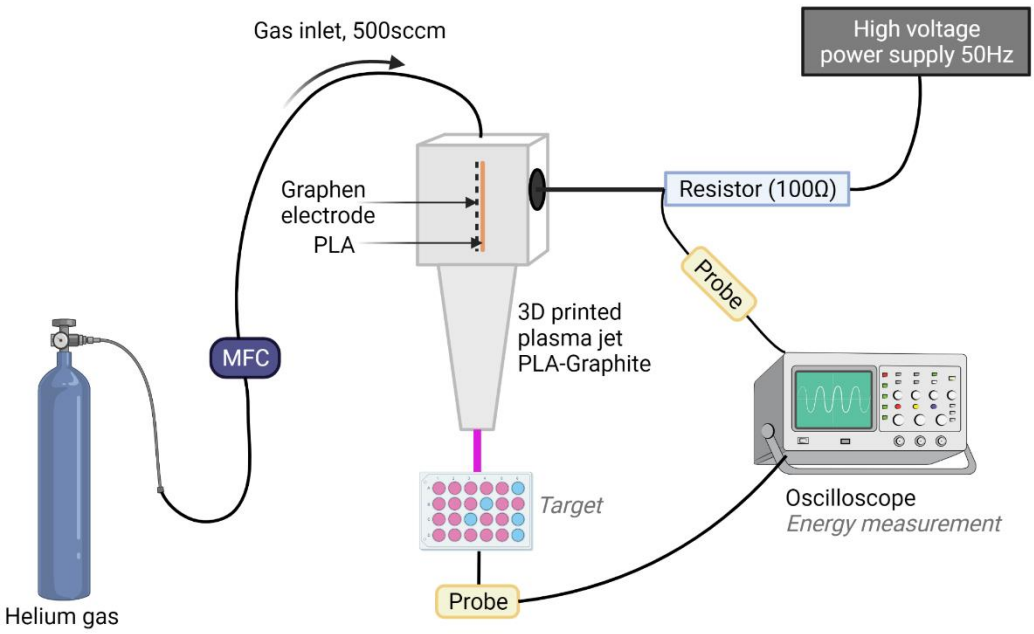

Figure 34: Schematic representation of the plasma device used *in vitro*. The device is composed of a 50 Hz generator, a 3D printed source and a helium bottle providing helium through a mass-flow controller (MFC). *This illustration was made using biorender.com.*

2.1.2. Jet II plasma device

Information cannot be provided in this manuscript.

2.1.2.1. Temperature measurement

In order to see if the jet II treatment induced an increase of the target temperature different samples were treated with several conditions. Temperature was measured with a digital camera TESTO 868 (Lenzkirch, Germany) before, during and after plasma application.

2.2. Chemical characteristics

2.2.1. H_2O_2 quantification

Hydrogen peroxide quantification was performed with a colorimetric reaction using Amplex® Red (10-Acetyl-3,7-dihydroxyphenoxazine) from Sigma-Aldrich (Saint-Louis, MO, USA) to detect hydrogen peroxide or peroxidase activity. In the presence of peroxidase the Amplex® Red reacts with H_2O_2 to create a fluorescent red oxidation product the resorufin. Experiments were performed in the dark and quantification of H_2O_2 was performed by the addition of 50 µl of HRP (0.5 U/ml, dilution in DPBS), 50 µl of Amplex® Red (100µM, dilution in DPBS), and 50 µl of media. Sample was quickly added to avoid reaction between HRP and Amplex® Red. The plates were agitated and incubated at room temperature in the dark during 15min. Absorbance was read with a microplate reader (Labsystems iEMS Reader MF, Vantaa, Finland) at 540 nm.

Another colorimetric kit was used to detect H_2O_2 for jet II: Spectroquant® hydrogen peroxide test. In the presence of a phenanthroline derivative hydrogen peroxide induces a reduction of copper (II) to copper (I) ions. The reduction leads to the formation of an orange-coloured complex. To induce the reaction 100 µl of each reactant were added to 200 µl of samples. The cuvettes (Brand®) were agitated and placed in the dark at room temperature for 15 min. The absorbance was read at 445 nm with the spectrophotometer Secomam UVILINE 9100.
For each kit the calibration curve was made at the same time as the sample using H_2O_2 3% (Sigma-Aldrich, Saint-Louis, MO, USA) in a range of concentration between 0 and 100 µM.

2.2.2. Measure of NO_x^-

Nitrite quantification was performed using griess reagents (Sigma-Aldrich, Saint Louis, MO, USA). The Griess test involve two reactions. First nitrite will react with sulphanilamide to form a diazonium salt then, it reacts with N-(1-naphthyl) ethylenediamine to form a purple azo product absorbance of which is measured at 546 nm. CAP treated water were mixed with 10% (v./v.) of Griess reagent in disposable cuvettes of 2.5 ml (900 µl of samples and 100 µl of Giress reactant). After 20 min of incubation at room temperature in dark absorbance was read using a spectrophotometer Secomam UVILINE 9100 at 546 nm. In parallel a calibration curve was made using $NaNO_2$ solution (Sigma-Aldrich, Saint-Luis, MO, USA) in concentration between 0 and 150 µM.
Nitrate and nitrites were quantified using Nitrite/Nitrate assay kit (Sigma-Aldrch, Saint Louis, MO, USA). Nitrate reductase and a co-factor enzyme reduced nitrates in nitrite. Nitrites were then quantified using the Griess reagent previously mentioned. For nitrite and nitration quantification 800 µl of treated water was mixed with 100 µl of each enzyme. For nitrite, 800 µl of sample was used and incubated during 1 hour. Then 100 µl of Griess reagent I is added and after 5 min of incubation reagent II is added to the mix. After 20 min of incubation at room temperature in the dark the measurement is performed with the spectrophotometer. The difference of the total nitrite and nitrate concentration to the separate measure of nitrite concentration gives the nitrate concentration.

2.3. *In vitro* analysis using human cells

2.3.1. Hacat culture conditions

Hacat immortal keratinocytes cell line (ATCC®, Molsheim, France) were grown in DMEM high glucose, supplemented with 1% antibiotic-antimycotic 1x (Gibco, Paisley, PA, USA) and 10% HyClone FetalClone II serum (GE Healthcare Life Sciences, Tewksbury, MA, USA). Media were changed every 2 to 3 days and cells passed or harvested with trypsine at 80%.

2.3.2. WST-1 cell proliferation assay

The effect of CAP on adherent cells was assessed with the WST-1 proliferation assay. The tetrazolium salt WST-1 is cleaved by the activity of mitochondrial dehydrogenases and produce a yellow formazon dye. The amount of formazan dye is directly proportional to the number of viable cells.
Adherent cells were suspended at 2000 cells/ well in 100 µL of complete medium (DMEM high glucose, supplemented with 1% antibiotic-antimycotic 1x, 10% HyClone FetalClone II serum) in a 96 well plate. At 24 or 48 h after treatment 10 µL of Cell Proliferation Reagent WST-1 (Sigma-Aldrich, St Louis, MO, USA) was added per well and incubated 1hour at 37°C. The absorbance of

the samples was read at 450 nm with 600 nm reference using a microplate reader (Labsystems iEMS Reader MF, Vantaa, Finland).

2.3.3. CFSE proliferation assay

Hacat cell proliferation was also assessed with carboxyfluorescein diacetate succinimidyl ester (CFSE). The CellTrace™ diffuse into cells and bind covalently to intracellular amines inducing a well-retained fluorescent staining. Excess of unconjugated reagent passively diffuses to the extracellular medium and can be washed away. When CFSE-labeled cell divides, its progeny is endowed with half the number of carboxyfluorescein-tagged molecules. Thus, each cell division can be assessed by measuring the corresponding decrease in cell fluorescence using flow cytometry. Hacat cells were suspended in growing media at a concentration of 10^6 cells/ml and treated. According to the CellTrace™ CFSE Cell Proliferation Kit Protocol (Thermofisher Scientific, Waltham, MA, USA) CFSE was added to a final concentration of 1.5 µM in the suspension. After an incubation of 10 min at room temperature, cells were centrifuged at 800G during 5 min and re-suspended in fresh media without CFSE. Some non-treated cells were fixed in 0.2 µm filtered 4% paraformaldehyde (Electron Microscopy Sciences, Hatfield, USA) and served as a reference (no division).

2.3.4. Scratch wound assay

The effect of the jet II on cellular migration was assessed using a scratch wound assay. Hacat cells were seeded in 6 well plate. When they reach confluent, cells were scratch with P200 pipette tip producing a wound around 2 mm x1 cm. Wells were washed with fresh media to remove detached cells and treated by CAP. The cells were photographed after the scratch wound, at 24, 48 and 72 h with an inverted light microscope (Axiovert 200M, Zeiss) equipped with an AxioCamera ERcS1. Using the software Axovision the photos were acquired automatically.

Bibliography

1. Sandby-Møller, J., Poulsen, T. & Wulf, H. C. Epidermal thickness at different body sites: relationship to age, gender, pigmentation, blood content, skin type and smoking habits. *Acta Derm. Venereol.* **83**, 410–413 (2003).
2. Tobin, D. J. Biochemistry of human skin--our brain on the outside. *Chem. Soc. Rev.* **35**, 52–67 (2006).
3. Moll, I. Merkel cell distribution in human hair follicles of the fetal and adult scalp. *Cell Tissue Res.* **277**, 131–138 (1994).
4. Van Agtmael, T. & Bruckner-Tuderman, L. Basement membranes and human disease. *Cell Tissue Res.* **339**, 167–188 (2010).
5. Has, C. & Nyström, A. Epidermal Basement Membrane in Health and Disease. *Curr. Top. Membr.* **76**, 117–170 (2015).
6. Fagrell, B., Hermansson, I. L., Karlander, S. G. & Ostergren, J. Vital capillary microscopy for assessment of skin viability and microangiopathy in patients with diabetes mellitus. *Acta Med. Scand. Suppl.* **687**, 25–28 (1984).
7. Tracy, L. E., Minasian, R. A. & Caterson, E. J. Extracellular Matrix and Dermal Fibroblast Function in the Healing Wound. *Adv. Wound Care* **5**, 119–136 (2016).
8. Sorrell, J. M. & Caplan, A. I. Fibroblasts-a diverse population at the center of it all. *Int. Rev. Cell Mol. Biol.* **276**, 161–214 (2009).
9. Watanabe, M. *et al.* Type XVII collagen coordinates proliferation in the interfollicular epidermis. *eLife* **6**, e26635.
10. Anatomy and Physiology of the Skin: Erratum. *J. Dermatol. Nurses Assoc.* **3**, 366 (2011).
11. Serhan, C. N., Chiang, N., Dalli, J. & Levy, B. D. Lipid mediators in the resolution of inflammation. *Cold Spring Harb. Perspect. Biol.* **7**, a016311 (2014).
12. Pfalzgraff, A., Brandenburg, K. & Weindl, G. Antimicrobial Peptides and Their Therapeutic Potential for Bacterial Skin Infections and Wounds. *Front. Pharmacol.* **9**, 281 (2018).
13. Niyonsaba, F., Kiatsurayanon, C., Chieosilapatham, P. & Ogawa, H. Friends or Foes? Host defense (antimicrobial) peptides and proteins in human skin diseases. *Exp. Dermatol.* **26**, 989–998 (2017).

14. Ryu, S., Song, P. I., Seo, C. H., Cheong, H. & Park, Y. Colonization and infection of the skin by S. aureus: immune system evasion and the response to cationic antimicrobial peptides. *Int. J. Mol. Sci.* **15**, 8753–8772 (2014).

15. Dominguez-Bello, M. G. *et al.* Delivery mode shapes the acquisition and structure of the initial microbiota across multiple body habitats in newborns. *Proc. Natl. Acad. Sci. U. S. A.* **107**, 11971–11975 (2010).

16. Mueller, N. T., Bakacs, E., Combellick, J., Grigoryan, Z. & Dominguez-Bello, M. G. The infant microbiome development: mom matters. *Trends Mol. Med.* **21**, 109–117 (2015).

17. Sender, R., Fuchs, S. & Milo, R. Revised Estimates for the Number of Human and Bacteria Cells in the Body. *PLoS Biol.* **14**, e1002533 (2016).

18. Grice, E. A. *et al.* A diversity profile of the human skin microbiota. *Genome Res.* **18**, 1043–1050 (2008).

19. Naik, S. *et al.* Compartmentalized control of skin immunity by resident commensals. *Science* **337**, 1115–1119 (2012).

20. Chehoud, C. *et al.* Complement modulates the cutaneous microbiome and inflammatory milieu. *Proc. Natl. Acad. Sci. U. S. A.* **110**, 15061–15066 (2013).

21. Constantinides, M. G. *et al.* MAIT cells are imprinted by the microbiota in early life and promote tissue repair. *Science* **366**, eaax6624 (2019).

22. Harris-Tryon, T. A. & Grice, E. A. Microbiota and maintenance of skin barrier function. *Science* **376**, 940–945 (2022).

23. Scharschmidt, T. C. & Fischbach, M. A. What Lives On Our Skin: Ecology, Genomics and Therapeutic Opportunities Of the Skin Microbiome. *Drug Discov. Today Dis. Mech.* **10**, e83–e89 (2013).

24. Belkaid, Y. & Segre, J. A. Dialogue between skin microbiota and immunity. *Science* **346**, 954–959 (2014).

25. Costello, E. K. *et al.* Bacterial Community Variation in Human Body Habitats Across Space and Time. *Science* **326**, 1694–1697 (2009).

26. Belkaid, Y. & Tamoutounour, S. The influence of skin microorganisms on cutaneous immunity. *Nat. Rev. Immunol.* **16**, 353–366 (2016).

27. Naik, S. *et al.* Compartmentalized control of skin immunity by resident commensals. *Science* **337**, 1115–1119 (2012).

28. Nagy, I. *et al.* Distinct strains of Propionibacterium acnes induce selective human beta-defensin-2 and interleukin-8 expression in human keratinocytes through toll-like receptors. *J. Invest. Dermatol.* **124**, 931–938 (2005).

29. Iwasaki, A. & Medzhitov, R. Control of adaptive immunity by the innate immune system. *Nat. Immunol.* **16**, 343–353 (2015).

30. Scharschmidt, T. C. *et al.* A Wave of Regulatory T Cells into Neonatal Skin Mediates Tolerance to Commensal Microbes. *Immunity* **43**, 1011–1021 (2015).

31. Naik, S. *et al.* Commensal-dendritic-cell interaction specifies a unique protective skin immune signature. *Nature* **520**, 104–108 (2015).

32. Werner, S. & Grose, R. Regulation of wound healing by growth factors and cytokines. *Physiol. Rev.* **83**, 835–870 (2003).

33. Eming, S. A., Krieg, T. & Davidson, J. M. Inflammation in Wound Repair: Molecular and Cellular Mechanisms. *J. Invest. Dermatol.* **127**, 514–525 (2007).

34. Cañedo-Dorantes, L. & Cañedo-Ayala, M. Skin Acute Wound Healing: A Comprehensive Review. *Int. J. Inflamm.* **2019**, 3706315 (2019).

35. Martin, P. & Leibovich, S. J. Inflammatory cells during wound repair: the good, the bad and the ugly. *Trends Cell Biol.* **15**, 599–607 (2005).

36. Koh, T. J. & DiPietro, L. A. Inflammation and wound healing: the role of the macrophage. *Expert Rev. Mol. Med.* **13**, e23 (2011).

37. Martin, P. Wound healing--aiming for perfect skin regeneration. *Science* **276**, 75–81 (1997).

38. DiPietro, L. A. Wound healing: the role of the macrophage and other immune cells. *Shock Augusta Ga* **4**, 233–240 (1995).

39. Sica, A. & Mantovani, A. Macrophage plasticity and polarization: in vivo veritas. *J. Clin. Invest.* **122**, 787–795 (2012).

40. Murray, P. J. Macrophage Polarization. *Annu. Rev. Physiol.* **79**, 541–566 (2017).

41. Pesce, J. T. *et al.* Arginase-1–Expressing Macrophages Suppress Th2 Cytokine–Driven Inflammation and Fibrosis. *PLoS Pathog.* **5**, (2009).

42. Fantin, A. *et al.* Tissue macrophages act as cellular chaperones for vascular anastomosis downstream of VEGF-mediated endothelial tip cell induction. *Blood* **116**, 829–840 (2010).

43. Ogle, M. E., Segar, C. E., Sridhar, S. & Botchwey, E. A. Monocytes and macrophages in tissue repair: Implications for immunoregenerative biomaterial design. *Exp. Biol. Med. Maywood NJ* **241**, 1084–1097 (2016).

44. Hesketh, M., Sahin, K. B., West, Z. E. & Murray, R. Z. Macrophage Phenotypes Regulate Scar Formation and Chronic Wound Healing. *Int. J. Mol. Sci.* **18**, E1545 (2017).

45. Kim, S. Y. & Nair, M. G. Macrophages in wound healing: activation and plasticity. *Immunol. Cell Biol.* **97**, 258–267 (2019).

46. Lucas, T. *et al.* Differential roles of macrophages in diverse phases of skin repair. *J. Immunol. Baltim. Md 1950* **184**, 3964–3977 (2010).

47. Mirza, R., DiPietro, L. A. & Koh, T. J. Selective and specific macrophage ablation is detrimental to wound healing in mice. *Am. J. Pathol.* **175**, 2454–2462 (2009).

48. Endrich, B. & Menger, M. D. [Regeneration of the microcirculation during wound healing?]. *Unfallchirurg* **103**, 1006–1008 (2000).

49. Wynn, T. A. & Barron, L. Macrophages: master regulators of inflammation and fibrosis. *Semin. Liver Dis.* **30**, 245–257 (2010).

50. Nauta, A., Gurtner, G. C. & Longaker, M. T. Wound healing and regenerative strategies. *Oral Dis.* **17**, 541–549 (2011).

51. Hinz, B. Formation and function of the myofibroblast during tissue repair. *J. Invest. Dermatol.* **127**, 526–537 (2007).

52. Yannas, I. V., Tzeranis, D. S. & So, P. T. C. Regeneration of injured skin and peripheral nerves requires control of wound contraction, not scar formation. *Wound Repair Regen. Off. Publ. Wound Heal. Soc. Eur. Tissue Repair Soc.* **25**, 177–191 (2017).

53. Greenhalgh, D. G. Management of Burns. *N. Engl. J. Med.* **380**, 2349–2359 (2019).

54. Peck, M. D. Epidemiology of burns throughout the world. Part I: Distribution and risk factors. *Burns J. Int. Soc. Burn Inj.* **37**, 1087–1100 (2011).

55. World Health Organization. *The injury chart book : a graphical overview of the global burden of injuries*. https://apps.who.int/iris/handle/10665/42566 (2002).

56. Hettiaratchy, S. & Dziewulski, P. ABC of burns: pathophysiology and types of burns. *BMJ* **328**, 1427–1429 (2004).

57. Wassermann, D. Critères de gravité des brûlures. Épidémiologie, prévention, organisation de la prise en charge. *Pathol. Biol.* **50**, 65–73 (2002).

58. Brusselaers, N., Monstrey, S., Vogelaers, D., Hoste, E. & Blot, S. Severe burn injury in Europe: a systematic review of the incidence, etiology, morbidity, and mortality. *Crit. Care Lond. Engl.* **14**, R188 (2010).

59. Médecine & Armées tome 43 n° 2. *calameo.com* https://www.calameo.com/books/000354785ec3e1f909acb.

60. Tolles, J. Emergency department management of patients with thermal burns. *Emerg. Med. Pract.* **20**, 1–24 (2018).

61. Bohr, S. *et al.* Alternative erythropoietin-mediated signaling prevents secondary microvascular thrombosis and inflammation within cutaneous burns. *Proc. Natl. Acad. Sci. U. S. A.* **110**, 3513–3518 (2013).

62. Rani, M., Nicholson, S. E., Zhang, Q. & Schwacha, M. G. Damage-associated molecular patterns (DAMPs) released after burn are associated with inflammation and monocyte activation. *Burns J. Int. Soc. Burn Inj.* **43**, 297–303 (2017).

63. Schwacha, M. G. Macrophages and post-burn immune dysfunction. *Burns* **29**, 1–14 (2003).

64. Rawlingson, A. Nitric oxide, inflammation and acute burn injury. *Burns J. Int. Soc. Burn Inj.* **29**, 631–640 (2003).

65. Horton, J. W. Free radicals and lipid peroxidation mediated injury in burn trauma: the role of antioxidant therapy. *Toxicology* **189**, 75–88 (2003).

66. Di Meo, S., Reed, T. T., Venditti, P. & Victor, V. M. Role of ROS and RNS Sources in Physiological and Pathological Conditions. *Oxid. Med. Cell. Longev.* **2016**, 1245049 (2016).

67. Parihar, A., Parihar, M. S., Milner, S. & Bhat, S. Oxidative stress and anti-oxidative mobilization in burn injury. *Burns J. Int. Soc. Burn Inj.* **34**, 6–17 (2008).

68. Muzio, G., Maggiora, M., Paiuzzi, E., Oraldi, M. & Canuto, R. A. Aldehyde dehydrogenases and cell proliferation. *Free Radic. Biol. Med.* **52**, 735–746 (2012).

69. Mehrabani, D. *et al.* The healing effect of curcumin on burn wounds in rat. *World J. Plast. Surg.* **4**, 29–35 (2015).

70. Loo, A. E. K. *et al.* Effects of hydrogen peroxide on wound healing in mice in relation to oxidative damage. *PloS One* **7**, e49215 (2012).

71. Sparkes, B. G. Immunological responses to thermal injury. *Burns J. Int. Soc. Burn Inj.* **23**, 106–113 (1997).

72. Leclerc, T. *et al.* Transport aérien longue distance des brûlés graves: revue de la littérature et application pratique. *Ann. Burns Fire Disasters* **28**, 57–66 (2015).

73. Garner, J. P. & Heppell, P. S. J. Cerium nitrate in the management of burns. *Burns J. Int. Soc. Burn Inj.* **31**, 539–547 (2005).

74. Pereira, C. T. *et al.* Age-dependent differences in survival after severe burns: a unicentric review of 1,674 patients and 179 autopsies over 15 years. *J. Am. Coll. Surg.* **202**, 536–548 (2006).

75. Williams, F. N. *et al.* Modulation of the hypermetabolic response to trauma: temperature, nutrition, and drugs. *J. Am. Coll. Surg.* **208**, 489–502 (2009).

76. James, S. E., Booth, S., Gilbert, P., Jones, I. & Shevchenko, R. Clinical approaches to skin regeneration. in *Strategies in regenerative medicine: integrating biology with materials design* (ed. Santin, M.) 1–34 (Springer, 2009).

77. Chua, A. W. C. *et al.* Skin tissue engineering advances in severe burns: review and therapeutic applications. *Burns Trauma* **4**, 3 (2016).

78. Hakimi, N. *et al.* Handheld Skin Printer: In-Situ Formation of Planar Biomaterials and Tissues. *Lab. Chip* **18**, 1440–1451 (2018).

79. Kym, D. *et al.* The application of cultured epithelial autografts improves survival in burns. *Wound Repair Regen. Off. Publ. Wound Heal. Soc. Eur. Tissue Repair Soc.* **23**, 340–344 (2015).

80. Domaszewska-Szostek, A. P., Krzyżanowska, M. O., Czarnecka, A. M. & Siemionow, M. Local Treatment of Burns with Cell-Based Therapies Tested in Clinical Studies. *J. Clin. Med.* **10**, 396 (2021).

81. Kirsner, R. S. *et al.* Spray-applied cell therapy with human allogeneic fibroblasts and keratinocytes for the treatment of chronic venous leg ulcers: a phase 2, multicentre, double-blind, randomised, placebo-controlled trial. *Lancet Lond. Engl.* **380**, 977–985 (2012).

82. Price, R. D., Das-Gupta, V., Leigh, I. M. & Navsaria, H. A. A comparison of tissue-engineered hyaluronic acid dermal matrices in a human wound model. *Tissue Eng.* **12**, 2985–2995 (2006).

83. Amani, H., Dougherty, W. R. & Blome-Eberwein, S. Use of Transcyte and dermabrasion to treat burns reduces length of stay in burns of all size and etiology. *Burns J. Int. Soc. Burn Inj.* **32**, 828–832 (2006).

84. Ayaz, M., Najafi, A. & Karami, M. Y. Thin Split Thickness Skin Grafting on Human Acellular Dermal Matrix Scaffold for the Treatment of Deep Burn Wounds. *Int. J. Organ Transplant. Med.* **12**, 44–51 (2021).

85. Hansbrough, J. Dermagraft-TC for partial-thickness burns: a clinical evaluation. *J. Burn Care Rehabil.* **18**, S25-28 (1997).

86. Lohana, P., Hassan, S. & Watson, S. B. Integra™ in burns reconstruction: Our experience and report of an unusual immunological reaction. *Ann. Burns Fire Disasters* **27**, 17–21 (2014).

87. Kolokythas, P., Aust, M. C., Vogt, P. M. & Paulsen, F. [Dermal subsitute with the collagen-elastin matrix Matriderm in burn injuries: a comprehensive review]. *Handchir. Mikrochir. Plast. Chir. Organ Deutschsprachigen Arbeitsgemeinschaft Handchir. Organ Deutschsprachigen Arbeitsgemeinschaft Mikrochir. Peripher. Nerven Gefasse Organ V* **40**, 367–371 (2008).

88. Still, J., Glat, P., Silverstein, P., Griswold, J. & Mozingo, D. The use of a collagen sponge/living cell composite material to treat donor sites in burn patients. *Burns J. Int. Soc. Burn Inj.* **29**, 837–841 (2003).

89. Kirsner, R. S. The use of Apligraf in acute wounds. *J. Dermatol.* **25**, 805–811 (1998).

90. Peck, M. D. Epidemiology of burns throughout the world. Part I: Distribution and risk factors. *Burns J. Int. Soc. Burn Inj.* **37**, 1087–1100 (2011).

91. Qu, M. & Nourbakhsh, M. Current Experimental Models of Burns. *Discov. Med.* **23**, 95–103 (2017).

92. Parnell, L. K. S. & Volk, S. W. The Evolution of Animal Models in Wound Healing Research: 1993-2017. *Adv. Wound Care* **8**, 692–702 (2019).

93. O'Brien, K. *et al.* Identification of the critical therapeutic entity in secreted Hsp90α that promotes wound healing in newly re-standardized healthy and diabetic pig models. *PloS One* **9**, e113956 (2014).

94. Wong, V. W., Sorkin, M., Glotzbach, J. P., Longaker, M. T. & Gurtner, G. C. Surgical approaches to create murine models of human wound healing. *J. Biomed. Biotechnol.* **2011**, 969618 (2011).

95. Mestas, J. & Hughes, C. C. W. Of mice and not men: differences between mouse and human immunology. *J. Immunol. Baltim. Md 1950* **172**, 2731–2738 (2004).

96. Branski, L. K. *et al.* Emerging infections in burns. *Surg. Infect.* **10**, 389–397 (2009).

97. Groll, J. *et al.* Biofabrication: reappraising the definition of an evolving field. *Biofabrication* **8**, 013001 (2016).

98. Vig, K. *et al.* Advances in Skin Regeneration Using Tissue Engineering. *Int. J. Mol. Sci.* **18**, E789 (2017).

99. Dixit, S. *et al.* Immunological challenges associated with artificial skin grafts: available solutions and stem cells in future design of synthetic skin. *J. Biol. Eng.* **11**, 49 (2017).

100. Coalson, E. *et al.* Stem cell therapy for chronic skin wounds in the era of personalized medicine: From bench to bedside. *Genes Dis.* **6**, 342–358 (2019).

101. Przekora, A. A Concise Review on Tissue Engineered Artificial Skin Grafts for Chronic Wound Treatment: Can We Reconstruct Functional Skin Tissue In Vitro? *Cells* **9**, E1622 (2020).

102. Frykberg, R. G. & Banks, J. Challenges in the Treatment of Chronic Wounds. *Adv. Wound Care* **4**, 560–582 (2015).

103. Magne, B., Lataillade, J.-J. & Trouillas, M. Mesenchymal Stromal Cell Preconditioning: The Next Step Toward a Customized Treatment For Severe Burn. *Stem Cells Dev.* **27**, 1385–1405 (2018).

104. Williams, F. N. *et al.* The leading causes of death after burn injury in a single pediatric burn center. *Crit. Care Lond. Engl.* **13**, R183 (2009).

105. Greenhalgh, D. G. *et al.* American Burn Association consensus conference to define sepsis and infection in burns. *J. Burn Care Res. Off. Publ. Am. Burn Assoc.* **28**, 776–790 (2007).

106. Rafla, K. & Tredget, E. E. Infection control in the burn unit. *Burns J. Int. Soc. Burn Inj.* **37**, 5–15 (2011).

107. Greenhalgh, D. G. *et al.* American burn association consensus conference to define sepsis and infection in burns. *J. Burn Care Res.* **28**, 776–790 (2007).

108. Fitzwater, J., Purdue, G. F., Hunt, J. L. & O'Keefe, G. E. The risk factors and time course of sepsis and organ dysfunction after burn trauma. *J. Trauma* **54**, 959–966 (2003).

109. Tredget, E. E., Shankowsky, H. A., Rennie, R., Burrell, R. E. & Logsetty, S. Pseudomonas infections in the thermally injured patient. *Burns J. Int. Soc. Burn Inj.* **30**, 3–26 (2004).

110. Keen, E. F. *et al.* Prevalence of multidrug-resistant organisms recovered at a military burn center. *Burns* **36**, 819–825 (2010).

111. Horn, J., Stelzner, K., Rudel, T. & Fraunholz, M. Inside job: Staphylococcus aureus host-pathogen interactions. *Int. J. Med. Microbiol. IJMM* **308**, 607–624 (2018).

112. Zhou, J., Tan, J., Gong, Y., Li, N. & Luo, G. Candidemia in major burn patients and its possible risk factors: A 6-year period retrospective study at a burn ICU. *Burns J. Int. Soc. Burn Inj.* **45**, 1164–1171 (2019).

113. Ballard, J. *et al.* Positive fungal cultures in burn patients: a multicenter review. *J. Burn Care Res. Off. Publ. Am. Burn Assoc.* **29**, 213–221 (2008).

114. Norbury, W., Herndon, D. N., Tanksley, J., Jeschke, M. G. & Finnerty, C. C. Infection in Burns. *Surg. Infect.* **17**, 250–255 (2016).

115. Chen, Z., Turxun, N. & Ning, F. Meta-analysis of the diagnostic value of procalcitonin in adult burn sepsis. *Adv. Clin. Exp. Med. Off. Organ Wroclaw Med. Univ.* **30**, 455–463 (2021).

116. Girard, D. *et al.* Biotechnological Management of Skin Burn Injuries: Challenges and Perspectives in Wound Healing and Sensory Recovery. *Tissue Eng. Part B Rev.* **23**, 59–82 (2017).

117. Fox, C. L. Silver sulfadiazine--a new topical therapy for Pseudomonas in burns. Therapy of Pseudomonas infection in burns. *Arch. Surg. Chic. Ill 1960* **96**, 184–188 (1968).

118. Atiyeh, B. S., Costagliola, M., Hayek, S. N. & Dibo, S. A. Effect of silver on burn wound infection control and healing: review of the literature. *Burns J. Int. Soc. Burn Inj.* **33**, 139–148 (2007).

119. Yoshino, Y. *et al.* The wound/burn guidelines - 6: Guidelines for the management of burns. *J. Dermatol.* **43**, 989–1010 (2016).

120. Finley, P. J. *et al.* Unprecedented Silver Resistance in Clinically Isolated Enterobacteriaceae: Major Implications for Burn and Wound Management. *Antimicrob. Agents Chemother.* **59**, 4734–4741 (2015).

121. Silva, J. P. *et al.* Improved burn wound healing by the antimicrobial peptide LLKKK18 released from conjugates with dextrin embedded in a carbopol gel. *Acta Biomater.* **26**, 249–262 (2015).

122. Diederen, B. M. W., Wardle, C. L. W., Krijnen, P., Tuinebreijer, W. E. & Breederveld, R. S. Epidemiology of clinically relevant bacterial pathogens in a burn center in the Netherlands between 2005 and 2011. *J. Burn Care Res. Off. Publ. Am. Burn Assoc.* **36**, 446–453 (2015).

123. Azzopardi, E. A., Boyce, D. E., Thomas, D. W. & Dickson, W. A. Colistin in burn intensive care: back to the future? *Burns J. Int. Soc. Burn Inj.* **39**, 7–15 (2013).

124. Balaban, N. Q. *et al.* Definitions and guidelines for research on antibiotic persistence. *Nat. Rev. Microbiol.* **17**, 441–448 (2019).

125. Roberts, J. A. *et al.* Individualised antibiotic dosing for patients who are critically ill: challenges and potential solutions. *Lancet Infect. Dis.* **14**, 498–509 (2014).

126. Ravat, F. *et al.* Antibiotics and the burn patient. *Burns* **37**, 16–26 (2011).

127. Yali, G. *et al.* Comparison of pathogens and antibiotic resistance of burn patients in the burn ICU or in the common burn ward. *Burns J. Int. Soc. Burn Inj.* **40**, 402–407 (2014).

128. Prestinaci, F., Pezzotti, P. & Pantosti, A. Antimicrobial resistance: a global multifaceted phenomenon. *Pathog. Glob. Health* **109**, 309–318 (2015).

129. Otto, M. Staphylococcus aureus toxins. *Curr. Opin. Microbiol.* **17**, 32–37 (2014).

130. Fowler, V. G. *et al.* Clinical identifiers of complicated Staphylococcus aureus bacteremia. *Arch. Intern. Med.* **163**, 2066–2072 (2003).

131. Cosgrove, S. E. *et al.* Comparison of mortality associated with methicillin-resistant and methicillin-susceptible Staphylococcus aureus bacteremia: a meta-analysis. *Clin. Infect. Dis. Off. Publ. Infect. Dis. Soc. Am.* **36**, 53–59 (2003).

132. CDC. The biggest antibiotic-resistant threats in the U.S. *Centers for Disease Control and Prevention* https://www.cdc.gov/drugresistance/biggest-threats.html (2022).

133. Jevons, M. P. “Celbenin” - resistant Staphylococci. *Br. Med. J.* **1**, 124–125 (1961).

134. Lakhundi, S. & Zhang, K. Methicillin-Resistant Staphylococcus aureus: Molecular Characterization, Evolution, and Epidemiology. *Clin. Microbiol. Rev.* **31**, e00020-18 (2018).

135. Lee, A. S. *et al.* Methicillin-resistant Staphylococcus aureus. *Nat. Rev. Dis. Primer* **4**, 1–23 (2018).

136. Chambers, H. F. & Deleo, F. R. Waves of resistance: Staphylococcus aureus in the antibiotic era. *Nat. Rev. Microbiol.* **7**, 629–641 (2009).

137. L'OMS publie une liste de bactéries contre lesquelles il est urgent d'avoir de nouveaux antibiotiques. https://www.who.int/fr/news/item/27-02-2017-who-publishes-list-of-bacteria-for-which-new-antibiotics-are-urgently-needed.

138. Holland, T. L., Arnold, C. & Fowler, V. G. Clinical management of Staphylococcus aureus bacteremia: a review. *JAMA* **312**, 1330–1341 (2014).

139. Kullar, R., Davis, S. L., Levine, D. P. & Rybak, M. J. Impact of vancomycin exposure on outcomes in patients with methicillin-resistant Staphylococcus aureus bacteremia: support for consensus guidelines suggested targets. *Clin. Infect. Dis. Off. Publ. Infect. Dis. Soc. Am.* **52**, 975–981 (2011).

140. Barlam, T. F. *et al.* Implementing an Antibiotic Stewardship Program: Guidelines by the Infectious Diseases Society of America and the Society for Healthcare Epidemiology of America. *Clin. Infect. Dis. Off. Publ. Infect. Dis. Soc. Am.* **62**, e51-77 (2016).

141. Wagner, B. *et al.* Antimicrobial stewardship programs in inpatient hospital settings: a systematic review. *Infect. Control Hosp. Epidemiol.* **35**, 1209–1228 (2014).

142. Brown, A. F., Leech, J. M., Rogers, T. R. & McLoughlin, R. M. Staphylococcus aureus Colonization: Modulation of Host Immune Response and Impact on Human Vaccine Design. *Front. Immunol.* **4**, 507 (2014).

143. Theuretzbacher, U., Outterson, K., Engel, A. & Karlén, A. The global preclinical antibacterial pipeline. *Nat. Rev. Microbiol.* **18**, 275–285 (2020).

144. Pillay, C. S., Elliott, E. & Dennison, C. Endolysosomal proteolysis and its regulation. *Biochem. J.* **363**, 417–429 (2002).

145. Jabado, N. *et al.* Natural resistance to intracellular infections: natural resistance-associated macrophage protein 1 (Nramp1) functions as a pH-dependent manganese transporter at the phagosomal membrane. *J. Exp. Med.* **192**, 1237–1248 (2000).

146. Christoforidis, S., McBride, H. M., Burgoyne, R. D. & Zerial, M. The Rab5 effector EEA1 is a core component of endosome docking. *Nature* **397**, 621–625 (1999).

147. Kinchen, J. M. & Ravichandran, K. S. Phagosome maturation: going through the acid test. *Nat. Rev. Mol. Cell Biol.* **9**, 781–795 (2008).

148. Storrie, B. & Desjardins, M. The biogenesis of lysosomes: is it a kiss and run, continuous fusion and fission process? *BioEssays News Rev. Mol. Cell. Dev. Biol.* **18**, 895–903 (1996).

149. Harrison, R. E., Bucci, C., Vieira, O. V., Schroer, T. A. & Grinstein, S. Phagosomes fuse with late endosomes and/or lysosomes by extension of membrane protrusions along microtubules: role of Rab7 and RILP. *Mol. Cell. Biol.* **23**, 6494–6506 (2003).

150. Buvelot, H., Jaquet, V. & Krause, K.-H. Mammalian NADPH Oxidases. *Methods Mol. Biol. Clifton NJ* **1982**, 17–36 (2019).

151. Bedard, K. & Krause, K.-H. The NOX family of ROS-generating NADPH oxidases: physiology and pathophysiology. *Physiol. Rev.* **87**, 245–313 (2007).

152. Sumimoto, H. Structure, regulation and evolution of Nox-family NADPH oxidases that produce reactive oxygen species. *FEBS J.* **275**, 3249–3277 (2008).

153. Abo, A., Webb, M. R., Grogan, A. & Segal, A. W. Activation of NADPH oxidase involves the dissociation of p21rac from its inhibitory GDP/GTP exchange protein (rhoGDI) followed by its translocation to the plasma membrane. *Biochem. J.* **298 Pt 3**, 585–591 (1994).

154. Lapouge, K. *et al.* Structure of the TPR domain of p67phox in complex with Rac.GTP. *Mol. Cell* **6**, 899–907 (2000).

155. Slauch, J. M. How does the oxidative burst of macrophages kill bacteria? Still an open question. *Mol. Microbiol.* **80**, 580–583 (2011).

156. Winterbourn, C. C., Hampton, M. B., Livesey, J. H. & Kettle, A. J. Modeling the reactions of superoxide and myeloperoxidase in the neutrophil phagosome: implications for microbial killing. *J. Biol. Chem.* **281**, 39860–39869 (2006).

157. Javeshghani, D. *et al.* Molecular characterization of a superoxide-generating NAD(P)H oxidase in the ventilatory muscles. *Am. J. Respir. Crit. Care Med.* **165**, 412–418 (2002).

158. Nayernia, Z. *et al.* Decreased neural precursor cell pool in NADPH oxidase 2-deficiency: From mouse brain to neural differentiation of patient derived iPSC. *Redox Biol.* **13**, 82–93 (2017).

159. Görlach, A. *et al.* A gp91phox containing NADPH oxidase selectively expressed in endothelial cells is a major source of oxygen radical generation in the arterial wall. *Circ. Res.* **87**, 26–32 (2000).

160. Ezraty, B., Gennaris, A., Barras, F. & Collet, J.-F. Oxidative stress, protein damage and repair in bacteria. *Nat. Rev. Microbiol.* **15**, 385–396 (2017).

161. Bandyopadhyay, U., Das, D. & Banerjee, R. K. Reactive oxygen species: Oxidative damage and pathogenesis. *Curr. Sci.* **77**, 658–666 (1999).

162. Fontecave, M. & Ollagnier-de-Choudens, S. Iron–sulfur cluster biosynthesis in bacteria: Mechanisms of cluster assembly and transfer. *Arch. Biochem. Biophys.* **474**, 226–237 (2008).

163. Cachat, J., Deffert, C., Hugues, S. & Krause, K.-H. Phagocyte NADPH oxidase and specific immunity. *Clin. Sci. Lond. Engl. 1979* **128**, 635–648 (2015).

164. de Luca, A. *et al.* IL-1 receptor blockade restores autophagy and reduces inflammation in chronic granulomatous disease in mice and in humans. *Proc. Natl. Acad. Sci. U. S. A.* **111**, 3526–3531 (2014).

165. Vignais, P. V. The superoxide-generating NADPH oxidase: structural aspects and activation mechanism. *Cell. Mol. Life Sci. CMLS* **59**, 1428–1459 (2002).

166. Yang, Y., Bazhin, A. V., Werner, J. & Karakhanova, S. Reactive oxygen species in the immune system. *Int. Rev. Immunol.* **32**, 249–270 (2013).

167. Valavanidis, A., Vlachogianni, T., Fiotakis, K. & Loridas, S. Pulmonary oxidative stress, inflammation and cancer: respirable particulate matter, fibrous dusts and ozone as major causes of lung carcinogenesis through reactive oxygen species mechanisms. *Int. J. Environ. Res. Public. Health* **10**, 3886–3907 (2013).

168. Davies, M. J. The oxidative environment and protein damage. *Biochim. Biophys. Acta* **1703**, 93–109 (2005).

169. Sakr, A., Brégeon, F., Mège, J.-L., Rolain, J.-M. & Blin, O. Staphylococcus aureus Nasal Colonization: An Update on Mechanisms, Epidemiology, Risk Factors, and Subsequent Infections. *Front. Microbiol.* **9**, 2419 (2018).

170. SKINNER, D. & KEEFER, C. S. SIGNIFICANCE OF BACTEREMIA CAUSED BY STAPHYLOCOCCUS AUREUS: A STUDY OF ONE HUNDRED AND TWENTY-TWO CASES AND A REVIEW OF THE LITERATURE CONCERNED WITH EXPERIMENTAL INFECTION IN ANIMALS. *Arch. Intern. Med.* **68**, 851–875 (1941).

171. van Hal, S. J. *et al.* Predictors of mortality in Staphylococcus aureus Bacteremia. *Clin. Microbiol. Rev.* **25**, 362–386 (2012).

172. Gillet, Y., Henry, T. & Vandenesch, F. Fulminant Staphylococcal Infections. *Microbiol. Spectr.* **6**, (2018).

173. Xue, L. *et al.* Staphyloxanthin: a potential target for antivirulence therapy. *Infect. Drug Resist.* **12**, 2151–2160 (2019).

174. Cosgrove, K. *et al.* Catalase (KatA) and alkyl hydroperoxide reductase (AhpC) have compensatory roles in peroxide stress resistance and are required for survival, persistence, and nasal colonization in Staphylococcus aureus. *J. Bacteriol.* **189**, 1025–1035 (2007).

175. Watanabe, I., Ichiki, M., Shiratsuchi, A. & Nakanishi, Y. TLR2-mediated survival of Staphylococcus aureus in macrophages: a novel bacterial strategy against host innate immunity. *J. Immunol. Baltim. Md 1950* **178**, 4917–4925 (2007).

176. Grayczyk, J. P., Harvey, C. J., Laczkovich, I. & Alonzo, F. A Lipoylated Metabolic Protein Released by Staphylococcus aureus Suppresses Macrophage Activation. *Cell Host Microbe* **22**, 678-687.e9 (2017).

177. Pollitt, E. J. G., Szkuta, P. T., Burns, N. & Foster, S. J. Staphylococcus aureus infection dynamics. *PLoS Pathog.* **14**, e1007112 (2018).

178. Surewaard, B. G. J. *et al.* Identification and treatment of the Staphylococcus aureus reservoir in vivo. *J. Exp. Med.* **213**, 1141–1151 (2016).

179. Prajsnar, T. K., Cunliffe, V. T., Foster, S. J. & Renshaw, S. A. A novel vertebrate model of Staphylococcus aureus infection reveals phagocyte-dependent resistance of zebrafish to non-host specialized pathogens. *Cell. Microbiol.* **10**, 2312–2325 (2008).

180. Fournier, B. & Philpott, D. J. Recognition of Staphylococcus aureus by the innate immune system. *Clin. Microbiol. Rev.* **18**, 521–540 (2005).

181. Kumar, A., Zhang, J. & Yu, F.-S. X. Innate immune response of corneal epithelial cells to Staphylococcus aureus infection: role of peptidoglycan in stimulating proinflammatory cytokine secretion. *Invest. Ophthalmol. Vis. Sci.* **45**, 3513–3522 (2004).

182. Rot, A., Henderson, L. E. & Leonard, E. J. Staphylococcus aureus-derived chemoattractant activity for human monocytes. *J. Leukoc. Biol.* **40**, 43–53 (1986).

183. Wilkinson, B. J., Kim, Y., Peterson, P. K., Quie, P. G. & Michael, A. F. Activation of complement by cell surface components of Staphylococcus aureus. *Infect. Immun.* **20**, 388–392 (1978).

184. Thurlow, L. R. *et al.* Staphylococcus aureus biofilms prevent macrophage phagocytosis and attenuate inflammation in vivo. *J. Immunol. Baltim. Md 1950* **186**, 6585–6596 (2011).

185. Asai, A. *et al.* Pathogenic role of macrophages in intradermal infection of methicillin-resistant Staphylococcus aureus in thermally injured mice. *Infect. Immun.* **78**, 4311–4319 (2010).

186. Secor, P. R. *et al.* Staphylococcus aureus Biofilm and Planktonic cultures differentially impact gene expression, mapk phosphorylation, and cytokine production in human keratinocytes. *BMC Microbiol.* **11**, 143 (2011).

187. Werz, O. *et al.* Human macrophages differentially produce specific resolvin or leukotriene signals that depend on bacterial pathogenicity. *Nat. Commun.* **9**, 59 (2018).

188. Winterbourn, C. C., Hampton, M. B., Livesey, J. H. & Kettle, A. J. Modeling the Reactions of Superoxide and Myeloperoxidase in the Neutrophil Phagosome: IMPLICATIONS FOR MICROBIAL KILLING*. *J. Biol. Chem.* **281**, 39860–39869 (2006).

189. Fang, F. C. Antimicrobial actions of reactive oxygen species. *mBio* **2**, e00141-11 (2011).

190. Cassat, J. E. & Skaar, E. P. Iron in infection and immunity. *Cell Host Microbe* **13**, 509–519 (2013).

191. Halliwell, B. & Gutteridge, J. M. C. *Free Radicals in Biology and Medicine*. (Oxford University Press, 2015). doi:10.1093/acprof:oso/9780198717478.001.0001.

192. Klebanoff, S. J., Kettle, A. J., Rosen, H., Winterbourn, C. C. & Nauseef, W. M. Myeloperoxidase: a front-line defender against phagocytosed microorganisms. *J. Leukoc. Biol.* **93**, 185–198 (2013).

193. Bogdan, C., Röllinghoff, M. & Diefenbach, A. The role of nitric oxide in innate immunity. *Immunol. Rev.* **173**, 17–26 (2000).

194. Pizzolla, A. *et al.* Reactive oxygen species produced by the NADPH oxidase 2 complex in monocytes protect mice from bacterial infections. *J. Immunol. Baltim. Md 1950* **188**, 5003–5011 (2012).

195. Surewaard, B. G. J. *et al.* Identification and treatment of the Staphylococcus aureus reservoir in vivo. *J. Exp. Med.* **213**, 1141–1151 (2016).

196. Ariffin, J. K. *et al.* Histone Deacetylase Inhibitors Promote Mitochondrial Reactive Oxygen Species Production and Bacterial Clearance by Human Macrophages. *Antimicrob. Agents Chemother.* **60**, 1521–1529 (2015).

197. Abuaita, B. H., Schultz, T. L. & O'Riordan, M. X. Mitochondria-Derived Vesicles Deliver Antimicrobial Reactive Oxygen Species to Control Phagosome-Localized Staphylococcus aureus. *Cell Host Microbe* **24**, 625-636.e5 (2018).

198. Cohen, T. S. *et al.* S. aureus Evades Macrophage Killing through NLRP3-Dependent Effects on Mitochondrial Trafficking. *Cell Rep.* **22**, 2431–2441 (2018).

199. Krause, K. *et al.* Caspase-11 counteracts mitochondrial ROS-mediated clearance of Staphylococcus aureus in macrophages. *EMBO Rep.* **20**, e48109 (2019).

200. Gordon, S. Phagocytosis: An Immunobiologic Process. *Immunity* **44**, 463–475 (2016).

201. Maxson, M. E. & Grinstein, S. The vacuolar-type H^+-ATPase at a glance - more than a proton pump. *J. Cell Sci.* **127**, 4987–4993 (2014).

202. Lukacs, G. L., Rotstein, O. D. & Grinstein, S. Determinants of the phagosomal pH in macrophages. In situ assessment of vacuolar H(+)-ATPase activity, counterion conductance, and H+ 'leak'. *J. Biol. Chem.* **266**, 24540–24548 (1991).

203. Flannagan, R. S., Kuiack, R. C., McGavin, M. J. & Heinrichs, D. E. Staphylococcus aureus Uses the GraXRS Regulatory System To Sense and Adapt to the Acidified Phagolysosome in Macrophages. *mBio* **9**, e01143-18 (2018).

204. Lukacs, G. L., Rotstein, O. D. & Grinstein, S. Phagosomal acidification is mediated by a vacuolar-type H(+)-ATPase in murine macrophages. *J. Biol. Chem.* **265**, 21099–21107 (1990).

205. Flannagan, R. S., Heit, B. & Heinrichs, D. E. Intracellular replication of Staphylococcus aureus in mature phagolysosomes in macrophages precedes host cell death, and bacterial escape and dissemination. *Cell. Microbiol.* **18**, 514–535 (2016).

206. Jubrail, J. *et al.* Inability to sustain intraphagolysosomal killing of Staphylococcus aureus predisposes to bacterial persistence in macrophages. *Cell. Microbiol.* **18**, 80–96 (2016).

207. Pidwill, G. R., Gibson, J. F., Cole, J., Renshaw, S. A. & Foster, S. J. The Role of Macrophages in Staphylococcus aureus Infection. *Front. Immunol.* **11**, 620339 (2021).

208. Müller, S. *et al.* The endolysosomal cysteine cathepsins L and K are involved in macrophage-mediated clearance of Staphylococcus aureus and the concomitant cytokine induction. *FASEB J. Off. Publ. Fed. Am. Soc. Exp. Biol.* **28**, 162–175 (2014).

209. Damo, S. M. *et al.* Molecular basis for manganese sequestration by calprotectin and roles in the innate immune response to invading bacterial pathogens. *Proc. Natl. Acad. Sci. U. S. A.* **110**, 3841–3846 (2013).

210. Lishko, V. K., Moreno, B., Podolnikova, N. P. & Ugarova, T. P. Identification of Human Cathelicidin Peptide LL-37 as a Ligand for Macrophage Integrin αMβ2 (Mac-1, CD11b/CD18) that Promotes Phagocytosis by Opsonizing Bacteria. *Res. Rep. Biochem.* **2016**, 39–55 (2016).

211. Tang, X., Basavarajappa, D., Haeggström, J. Z. & Wan, M. P2X7 Receptor Regulates Internalization of Antimicrobial Peptide LL-37 by Human Macrophages That Promotes Intracellular Pathogen Clearance. *J. Immunol. Baltim. Md 1950* **195**, 1191–1201 (2015).

212. Watson, K. *et al.* Developing Novel Host-Based Therapies Targeting Microbicidal Responses in Macrophages and Neutrophils to Combat Bacterial Antimicrobial Resistance. *Front. Immunol.* **11**, 786 (2020).

213. Xiong, M.-H. *et al.* Bacteria-responsive multifunctional nanogel for targeted antibiotic delivery. *Adv. Mater. Deerfield Beach Fla* **24**, 6175–6180 (2012).

214. Cai, Q. *et al.* Macrophage-Instructed Intracellular Staphylococcus aureus Killing by Targeting Photodynamic Dimers. *ACS Appl. Mater. Interfaces* **10**, 9197–9202 (2018).

215. Miethke, M. *et al.* Towards the sustainable discovery and development of new antibiotics. *Nat. Rev. Chem.* **5**, 726–749 (2021).

216. von Woedtke, Th., Reuter, S., Masur, K. & Weltmann, K.-D. Plasmas for medicine. *Phys. Rep.* **530**, 291–320 (2013).

217. Ermolaeva, S. A. *et al.* Bactericidal effects of non-thermal argon plasma in vitro, in biofilms and in the animal model of infected wounds. *J. Med. Microbiol.* **60**, 75–83 (2011).

218. Laroussi, M. Sterilization of contaminated matter with an atmospheric pressure plasma. *IEEE Trans. Plasma Sci.* **24**, 1188–1191 (1996).

219. Laroussi, M., Fridman, A. & Satava, R. M. Editorial. *Plasma Process. Polym.* **5**, 501–502 (2008).

220. Keidar, M. Plasma for cancer treatment. *Plasma Sources Sci. Technol.* **24**, 033001 (2015).

221. Zhou, Y. *et al.* Plasma Sterilization of Root Canal Abscess. *Plasma Med.* **8**, (2018).

222. Lloyd, G. *et al.* Gas Plasma: Medical Uses and Developments in Wound Care. *Plasma Process. Polym.* **7**, 194–211 (2010).

223. Bernhardt, T. *et al.* Plasma Medicine: Applications of Cold Atmospheric Pressure Plasma in Dermatology. *Oxid. Med. Cell. Longev.* **2019**, 3873928 (2019).

224. Leduc, M., Guay, D., Leask, R. L. & Coulombe, S. Cell permeabilization using a non-thermal plasma. *New J. Phys.* **11**, 115021 (2009).

225. Xiong, Z. *et al.* Selective neuronal differentiation of neural stem cells induced by nanosecond microplasma agitation. *Stem Cell Res.* **12**, 387–399 (2014).

226. Steinbeck, M. J. *et al.* Skeletal Cell Differentiation Is Enhanced by Atmospheric Dielectric Barrier Discharge Plasma Treatment. *PLOS ONE* **8**, e82143 (2013).

227. Tanaka, H. *et al.* State of the art in medical applications using non-thermal atmospheric pressure plasma. *Rev. Mod. Plasma Phys.* **1**, 3 (2017).

228. Heinlin, J. *et al.* Plasma applications in medicine with a special focus on dermatology. *J. Eur. Acad. Dermatol. Venereol.* **25**, 1–11 (2011).

229. Heinlin, J. *et al.* A randomized two-sided placebo-controlled study on the efficacy and safety of atmospheric non-thermal argon plasma for pruritus. *J. Eur. Acad. Dermatol. Venereol. JEADV* **27**, 324–331 (2013).

230. Chutsirimongkol, C., Boonyawan, D., Polnikorn, N., Techawatthanawisan, W. & Kundilokchai, T. Non-Thermal Plasma for Acne and Aesthetic Skin Improvement. *Plasma Med.* **4**, (2014).

231. Roots, R. & Okada, S. Estimation of Life Times and Diffusion Distances of Radicals Involved in X-Ray-Induced DNA Strand Breaks or Killing of Mammalian Cells. *Radiat. Res.* **64**, 306–320 (1975).

232. Wende, K. *et al.* Identification of the biologically active liquid chemistry induced by a nonthermal atmospheric pressure plasma jet. *Biointerphases* **10**, 029518 (2015).

233. Wu, H. *et al.* Reactive Oxygen Species in a Non-thermal Plasma Microjet and Water System: Generation, Conversion, and Contributions to Bacteria Inactivation-An Analysis by Electron Spin Resonance Spectroscopy. *Plasma Process. Polym.* **9**, 417 (2012).

234. Samukawa, S. *et al.* The 2012 Plasma Roadmap (Invited Review Article). *J. Phys. Appl. Phys.* **45**, 253001 (2012).

235. Kaushik, N. *et al.* Biological and medical application of plasma-activated media, water and solutions. *Biol. Chem.* **400**, (2018).

236. Harman, D. Aging: a theory based on free radical and radiation chemistry. *J. Gerontol.* **11**, 298–300 (1956).

237. Rhee, S. G. H2O2, a Necessary Evil for Cell Signaling. *Science* **312**, 1882–1883 (2006).

238. Winterbourn, C. C. Reconciling the chemistry and biology of reactive oxygen species. *Nat. Chem. Biol.* **4**, 278–286 (2008).

239. Laroussi, M., Mendis, D. A. & Rosenberg, M. Plasma interaction with microbes. *New J. Phys.* **5**, 41–41 (2003).

240. Lebeer, S., Vanderleyden, J. & De Keersmaecker, S. C. J. Host interactions of probiotic bacterial surface molecules: comparison with commensals and pathogens. *Nat. Rev. Microbiol.* **8**, 171–184 (2010).

241. Lunov, O. *et al.* The interplay between biological and physical scenarios of bacterial death induced by non-thermal plasma. *Biomaterials* **82**, 71–83 (2016).

242. Han, L. *et al.* Mechanisms of Inactivation by High-Voltage Atmospheric Cold Plasma Differ for Escherichia coli and Staphylococcus aureus. *Appl. Environ. Microbiol.* **82**, 450–458 (2016).

243. Liao, X. *et al.* Combating Staphylococcus aureus and its methicillin resistance gene (mecA) with cold plasma. *Sci. Total Environ.* **645**, 1287–1295 (2018).

244. Liao, X. *et al.* Inactivation mechanisms of non-thermal plasma on microbes: A review. *Food Control* **75**, 83–91 (2017).

245. Takamatsu, T. *et al.* Imaging of the Staphylococcus aureus Inactivation Process Induced by a Multigas Plasma Jet. *Curr. Microbiol.* **73**, 1–7 (2016).

246. Delben, J. A., Zago, C. E., Tyhovych, N., Duarte, S. & Vergani, C. E. Effect of Atmospheric-Pressure Cold Plasma on Pathogenic Oral Biofilms and In Vitro Reconstituted Oral Epithelium. *PloS One* **11**, e0155427 (2016).

247. Gouarderes, S. *et al.* Electroporation does not affect human dermal fibroblast proliferation and migration properties directly but indirectly via the secretome. *Bioelectrochemistry* **134**, 107531 (2020).

248. Liao, X. *et al.* Combating Staphylococcus aureus and its methicillin resistance gene (mecA) with cold plasma. *Sci. Total Environ.* **645**, 1287–1295 (2018).

249. Brun, P. *et al.* Antibacterial efficacy and mechanisms of action of low power atmospheric pressure cold plasma: membrane permeability, biofilm penetration and antimicrobial sensitization. *J. Appl. Microbiol.* **125**, 398–408 (2018).

250. Coutinho, N. M. *et al.* Cold plasma processing of milk and dairy products. *Trends Food Sci. Technol.* (2018).

251. Guo, L. *et al.* Cold atmospheric-pressure plasma induces DNA-protein crosslinks through protein oxidation. *Free Radic. Res.* **52**, 783–798 (2018).

252. Hosseinzadeh Colagar, A., Memariani, H., Sohbatzadeh, F. & Valinataj Omran, A. Nonthermal Atmospheric Argon Plasma Jet Effects on Escherichia coli Biomacromolecules. *Appl. Biochem. Biotechnol.* **171**, 1617–1629 (2013).

253. Mai-Prochnow, A., Murphy, A. B., McLean, K. M., Kong, M. G. & Ostrikov, K. (Ken). Atmospheric pressure plasmas: Infection control and bacterial responses. *Int. J. Antimicrob. Agents* **43**, 508–517 (2014).

254. Dolezalova, E. & Lukes, P. Membrane damage and active but nonculturable state in liquid cultures of Escherichia coli treated with an atmospheric pressure plasma jet. *Bioelectrochemistry Amst. Neth.* **103**, 7–14 (2015).

255. Deng, X., Shi, J. & Kong, M. G. Physical Mechanisms of Inactivation of Bacillus subtilis Spores Using Cold Atmospheric Plasmas. *IEEE Trans. Plasma Sci.* **34**, 1310–1316 (2006).

256. Flynn, P. B. *et al.* Bactericidal efficacy of atmospheric pressure non-thermal plasma (APNTP) against the ESKAPE pathogens. *Int. J. Antimicrob. Agents* **46**, 101–107 (2015).

257. Mai-Prochnow, A., Clauson, M., Hong, J. & Murphy, A. B. Gram positive and Gram negative bacteria differ in their sensitivity to cold plasma. *Sci. Rep.* **6**, 38610 (2016).

258. Chen, Z., Garcia, G., Arumugaswami, V. & Wirz, R. E. Cold atmospheric plasma for SARS-CoV-2 inactivation. *Phys. Fluids Woodbury N 1994* **32**, 111702 (2020).

259. Vitorino, C., Sousa, J. & Pais, A. Overcoming the skin permeation barrier: challenges and opportunities. *Curr. Pharm. Des.* **21**, 2698–2712 (2015).

260. Oh, J.-S. *et al.* How to assess the plasma delivery of RONS into tissue fluid and tissue. *J. Phys. Appl. Phys.* **49**, 304005 (2016).

261. Borchardt, T. *et al.* Effect of direct cold atmospheric plasma (diCAP) on microcirculation of intact skin in a controlled mechanical environment. *Microcirc. N. Y. N 1994* **24**, e12399 (2017).

262. Hong, S.-H., Szili, E. J., Jenkins, A. T. A. & Short, R. D. Ionized gas (plasma) delivery of reactive oxygen species (ROS) into artificial cells. *J. Phys. Appl. Phys.* **47**, 362001 (2014).

263. Szili, E. J., Bradley, J. W. & Short, R. D. A `tissue model' to study the plasma delivery of reactive oxygen species. *J. Phys. Appl. Phys.* **47**, 152002 (2014).

264. Duan, J., Lu, X. & He, G. On the penetration depth of reactive oxygen and nitrogen species generated by a plasma jet through real biological tissue. *Phys. Plasmas* **24**, 073506 (2017).

265. Duan, J. *et al.* On the penetration of reactive oxygen and nitrogen species generated by a plasma jet into and through mice skin with/without stratum corneum. *Phys. Plasmas* **26**, 043504 (2019).

266. Nie, L. *et al.* Effect of tissue thickness and liquid composition on the penetration of long-lifetime reactive oxygen and nitrogen species (RONS) generated by a plasma jet. *J. Phys. Appl. Phys.* **51**, 345204 (2018).

267. Boury-Jamot, M. *et al.* Skin aquaporins: function in hydration, wound healing, and skin epidermis homeostasis. *Handb. Exp. Pharmacol.* 205–217 (2009) doi:10.1007/978-3-540-79885-9_10.

268. Patel, R., Kevin Heard, L., Chen, X. & Bollag, W. B. Aquaporins in the Skin. *Adv. Exp. Med. Biol.* **969**, 173–191 (2017).

269. Yan, D. *et al.* The role of aquaporins in the anti-glioblastoma capacity of the cold plasma-stimulated medium. *J. Phys. Appl. Phys.* **50**, 055401 (2017).

270. Yusupov, M., Razzokov, J., Cordeiro, R. & Bogaerts, A. Transport of Reactive Oxygen and Nitrogen Species across Aquaporin: A Molecular Level Picture. *Oxid. Med. Cell. Longev.* **2019**, 1–11 (2019).

271. Yusupov, M., Van der Paal, J., Neyts, E. C. & Bogaerts, A. Synergistic effect of electric field and lipid oxidation on the permeability of cell membranes. *Biochim. Biophys. Acta Gen. Subj.* **1861**, 839–847 (2017).

272. Vijayarangan, V. *et al.* Cold Atmospheric Plasma Parameters Investigation for Efficient Drug Delivery in HeLa Cells. *IEEE Trans. Radiat. Plasma Med. Sci.* **2**, 109–115 (2018).

273. Campbell, J. J. *et al.* A 3-D in vitro co-culture model of mammary gland involution. *Integr. Biol. U. K.* **6**, 618–626 (2014).

274. Malcor, J.-D. *et al.* The synthesis and coupling of photoreactive collagen-based peptides to restore integrin reactivity to an inert substrate, chemically-crosslinked collagen. *Biomaterials* **85**, 65–77 (2016).

275. Davidenko, N. *et al.* Evaluation of cell binding to collagen and gelatin: a study of the effect of 2D and 3D architecture and surface chemistry. *J. Mater. Sci. Mater. Med.* **27**, (2016).

276. BASF and CTIBiotech to develop first 3D bioprinted human reconstructed skin including immune macrophages. https://www.basf.com/global/en/media/news-releases/2019/09/p-19-318.html.

277. Busco, G. *et al.* Cold atmospheric plasma-induced acidification of tissue surface: visualization and quantification using agarose gel models. *J. Phys. Appl. Phys.* **52**, 24LT01 (2019).

278. Brisset, J.-L., Benstaali, B., Moussa, D., Fanmoe, J. & Njoyim-Tamungang, E. Acidity control of plasma-chemical oxidation: Applications to dye removal, urban waste abatement and microbial inactivation. *Plasma Sources Sci. Technol.* **20**, 034021 (2011).

279. Helmke, A. *et al.* The acidification of lipid film surfaces by non-thermal DBD at atmospheric pressure in air. *New J. Phys.* **11**, 115025 (2009).

280. Borchardt, T. *et al.* Effect of direct cold atmospheric plasma (diCAP) on microcirculation of intact skin in a controlled mechanical environment. *Microcirc. N. Y. N 1994* **24**, (2017).

281. Heuer, K. *et al.* The topical use of non-thermal dielectric barrier discharge (DBD): Nitric oxide related effects on human skin. *Nitric Oxide* **44**, 52–60 (2015).

282. Schneider, L. A., Korber, A., Grabbe, S. & Dissemond, J. Influence of pH on wound-healing: a new perspective for wound-therapy? *Arch. Dermatol. Res.* **298**, 413–420 (2007).

283. Fluhr, J. W. *et al.* In vivo skin treatment with tissue-tolerable plasma influences skin physiology and antioxidant profile in human stratum corneum. *Exp. Dermatol.* **21**, 130–134 (2012).

284. Athanasopoulos, D. K., Svarnas, P. & Gerakis, A. Cold plasma bullet influence on the water contact angle of human skin surface. *J. Electrost.* **102**, 103378 (2019).

285. Dzimitrowicz, A. *et al.* Activation of the Normal Human Skin Cells by a Portable Dielectric Barrier Discharge-Based Reaction-Discharge System of a Defined Gas Temperature. *Plasma Chem. Plasma Process.* **40**, (2020).

286. Choi, J. H. *et al.* Skin renewal activity of non-thermal plasma through the activation of β-catenin in keratinocytes. *Sci. Rep.* **7**, 6146 (2017).

287. Chowdhury, M. K. H. *et al.* Glucagon phosphorylates serine 552 of β-catenin leading to increased expression of cyclin D1 and c-Myc in the isolated rat liver. *Arch. Physiol. Biochem.* **121**, 88–96 (2015).

288. Haertel, B., Wende, K., von Woedtke, T., Weltmann, K. D. & Lindequist, U. Non-thermal atmospheric-pressure plasma can influence cell adhesion molecules on HaCaT-keratinocytes. *Exp. Dermatol.* **20**, 282–284 (2011).

289. Schmidt, A., von Woedtke, T. & Bekeschus, S. Periodic Exposure of Keratinocytes to Cold Physical Plasma: An In Vitro Model for Redox-Related Diseases of the Skin. *Oxid. Med. Cell. Longev.* **2016**, 9816072 (2016).

290. Schmidt, A. *et al.* Cold Physical Plasma Modulates p53 and Mitogen-Activated Protein Kinase Signaling in Keratinocytes. *Oxid. Med. Cell. Longev.* **2019**, 7017363 (2019).

291. Shome, D., von Woedtke, T., Riedel, K. & Masur, K. The HIPPO Transducer YAP and Its Targets CTGF and Cyr61 Drive a Paracrine Signalling in Cold Atmospheric Plasma-Mediated Wound Healing. *Oxid. Med. Cell. Longev.* **2020**, 4910280 (2020).

292. Yu, F.-X. & Guan, K.-L. The Hippo pathway: regulators and regulations. *Genes Dev.* **27**, 355–371 (2013).

293. Schmidt, A. *et al.* Non-thermal plasma activates human keratinocytes by stimulation of antioxidant and phase II pathways. *J. Biol. Chem.* **290**, 6731–6750 (2015).

294. Shi, X. *et al.* Effect of Cold Plasma on Cell Viability and Collagen Synthesis in Cultured Murine Fibroblasts. *Plasma Sci. Technol.* **18**, 353–359 (2016).

295. Bourdens, M. *et al.* Short exposure to cold atmospheric plasma induces senescence in human skin fibroblasts and adipose mesenchymal stromal cells. *Sci. Rep.* **9**, 8671 (2019).

296. Oh, J.-S. *et al.* How plasma induced oxidation, oxygenation, and de-oxygenation influences viability of skin cells. *Appl. Phys. Lett.* **109**, 203701 (2016).

297. Kisch, T. *et al.* Improvement of cutaneous microcirculation by cold atmospheric plasma (CAP): Results of a controlled, prospective cohort study. *Microvasc. Res.* **104**, 55–62 (2016).

298. Kalghatgi, S., Friedman, G., Fridman, A. & Clyne, A. Endothelial Cell Proliferation is Enhanced by Low Dose Non-Thermal Plasma Through Fibroblast Growth Factor-2 Release. *Ann. Biomed. Eng.* **38**, 748–57 (2009).

299. Arndt, S., Unger, P., Berneburg, M., Bosserhoff, A.-K. & Karrer, S. Cold atmospheric plasma (CAP) activates angiogenesis-related molecules in skin keratinocytes, fibroblasts and endothelial cells and improves wound angiogenesis in an autocrine and paracrine mode. *J. Dermatol. Sci.* **89**, 181–190 (2018).

300. Arjunan, K. P., Friedman, G., Fridman, A. & Clyne, A. M. Non-thermal dielectric barrier discharge plasma induces angiogenesis through reactive oxygen species. *J. R. Soc. Interface* **9**, 147–157 (2012).

301. Arjunan, K. P. & Clyne, A. Hydroxyl Radical and Hydrogen Peroxide are Primarily Responsible for Dielectric Barrier Discharge Plasma-Induced Angiogenesis. *Plasma Process. Polym.* **8**, (2011).

302. Haertel, B. *et al.* Differential effect of non-thermal atmospheric-pressure plasma on angiogenesis. *Lett Appl NanoBioSci* **3**, 159–166 (2014).

303. Ziche, M. & Morbidelli, L. Nitric oxide and angiogenesis. *J. Neurooncol.* **50**, 139–148 (2000).

304. Babaei, S. *et al.* Angiogenic Actions of Angiopoietin-1 Require Endothelium-Derived Nitric Oxide. *Am. J. Pathol.* **162**, 1927–1936 (2003).

305. Polytarchou, C. & Papadimitriou, E. Antioxidants inhibit angiogenesis in vivo through down-regulation of nitric oxide synthase expression and activity. *Free Radic. Res.* **38**, 501–508 (2004).

306. Gweon, B. *et al.* Suppression of angiogenesis by atmospheric pressure plasma in human aortic endothelial cells. *Appl. Phys. Lett.* **104**, 133701 (2014).

307. Barchowsky, A., Munro, S. R., Morana, S. J., Vincenti, M. P. & Treadwell, M. Oxidant-sensitive and phosphorylation-dependent activation of NF-kappa B and AP-1 in endothelial cells. *Am. J. Physiol.* **269**, L829-836 (1995).

308. Blaise, O., Duchesne, C., Banzet, S., Rousseau, A. & Frescaline, N. A Murine Model of a Burn Wound Reconstructed with an Allogeneic Skin Graft. *JoVE J. Vis. Exp.* e61339 (2020) doi:10.3791/61339.

309. Duchesne, C., Banzet, S., Lataillade, J.-J., Rousseau, A. & Frescaline, N. Cold atmospheric plasma modulates endothelial nitric oxide synthase signalling and enhances burn wound neovascularisation. *J. Pathol.* **249**, 368–380 (2019).

310. Cui, H. S. *et al.* Wound Healing Potential of Low Temperature Plasma in Human Primary Epidermal Keratinocytes. *Tissue Eng. Regen. Med.* **16**, 585–593 (2019).

311. Miller, V., Lin, A., Fridman, G., Dobrynin, D. & Fridman, A. Plasma Stimulation of Migration of Macrophages. *Plasma Process. Polym.* **11**, 1193–1197 (2014).

312. Maikho, T., Patwardhan, R. S., Das, T. N., Sharma, D. & Sandur, S. K. Cold atmospheric plasma-modulated phorbol 12-myristate 13-acetate-induced differentiation of U937 cells to macrophage-like cells. *Free Radic. Res.* **52**, 212–222 (2018).

313. Lin, A. *et al.* Uniform Nanosecond Pulsed Dielectric Barrier Discharge Plasma Enhances Anti-Tumor Effects by Induction of Immunogenic Cell Death in Tumors and Stimulation of Macrophages. *Plasma Process. Polym.* **12**, 1392–1399 (2015).

314. Lin, A. *et al.* Nanosecond-Pulsed DBD Plasma-Generated Reactive Oxygen Species Trigger Immunogenic Cell Death in A549 Lung Carcinoma Cells through Intracellular Oxidative Stress. *Int. J. Mol. Sci.* **18**, 966 (2017).

315. Kupke, L. S. *et al.* Cold Atmospheric Plasma Promotes the Immunoreactivity of Granulocytes In Vitro. *Biomolecules* **11**, 902 (2021).

316. Bekeschus, S. *et al.* Redox Stimulation of Human THP-1 Monocytes in Response to Cold Physical Plasma. *Oxid. Med. Cell. Longev.* **2016**, 5910695 (2016).

317. Kilmer, S., Semchyshyn, N., Shah, G. & Fitzpatrick, R. A pilot study on the use of a plasma skin regeneration device (Portrait PSR3) in full facial rejuvenation procedures. *Lasers Med. Sci.* **22**, 101–109 (2007).

318. Bernhardt, T. *et al.* Plasma Medicine: Applications of Cold Atmospheric Pressure Plasma in Dermatology. *Oxid. Med. Cell. Longev.* **2019**, 3873928 (2019).
319. Isbary, G. *et al.* A first prospective randomized controlled trial to decrease bacterial load using cold atmospheric argon plasma on chronic wounds in patients. *Br. J. Dermatol.* **163**, 78–82 (2010).
320. Isbary, G. *et al.* Successful and safe use of 2 min cold atmospheric argon plasma in chronic wounds: results of a randomized controlled trial. *Br. J. Dermatol.* **167**, 404–410 (2012).
321. Bevis, P. & Earnshaw, J. Venous ulcer review. *Clin. Cosmet. Investig. Dermatol.* **4**, 7–14 (2011).
322. Scotton, M. F., Miot, H. A. & Abbade, L. P. F. Factors that influence healing of chronic venous leg ulcers: a retrospective cohort. *An. Bras. Dermatol.* **89**, 414–422 (2014).
323. Rit, K., Nag, F., Sarkar, A. & Maiti, P. K. Chronic venous leg ulcer with multidrug resistant bacterial infection in a tertiary care hospital of Eastern India. *J. Sci. Soc.* **40**, 116 (2013).
324. Isbary, G. *et al.* Successful and safe use of 2 min cold atmospheric argon plasma in chronic wounds: results of a randomized controlled trial. *Br. J. Dermatol.* **167**, 404–410 (2012).
325. Brehmer, F. *et al.* Alleviation of chronic venous leg ulcers with a hand-held dielectric barrier discharge plasma generator (PlasmaDerm(®) VU-2010): results of a monocentric, two-armed, open, prospective, randomized and controlled trial (NCT01415622). *J. Eur. Acad. Dermatol. Venereol. JEADV* **29**, 148–155 (2015).
326. Gao, J. *et al.* Cold atmospheric plasma promotes different types of superficial skin erosion wounds healing. *Int. Wound J.* **16**, 1103–1111 (2019).
327. Isbary, G. *et al.* Cold atmospheric argon plasma treatment may accelerate wound healing in chronic wounds: Results of an open retrospective randomized controlled study in vivo. *Clin. Plasma Med.* **1**, 25–30 (2013).
328. Stratmann, B. *et al.* Effect of Cold Atmospheric Plasma Therapy vs Standard Therapy Placebo on Wound Healing in Patients With Diabetic Foot Ulcers. *JAMA Netw. Open* **3**, e2010411 (2020).
329. Mirpour, S. *et al.* Cold atmospheric plasma as an effective method to treat diabetic foot ulcers: A randomized clinical trial. *Sci. Rep.* **10**, 10440 (2020).
330. Xiong, Z. Cold Atmospheric Pressure Plasmas (CAPs) for Skin Wound Healing. in (2018). doi:10.5772/intechopen.76093.

331. von Woedtke, Th., Reuter, S., Masur, K. & Weltmann, K.-D. Plasmas for medicine. *Phys. Rep.* **530**, 291–320 (2013).

332. Heinlin, J. *et al.* Randomized placebo-controlled human pilot study of cold atmospheric argon plasma on skin graft donor sites. *Wound Repair Regen. Off. Publ. Wound Heal. Soc. Eur. Tissue Repair Soc.* **21**, 800–807 (2013).

333. Gao, J. *et al.* Cold atmospheric plasma promotes different types of superficial skin erosion wounds healing. *Int. Wound J.* **16**, 1103–1111 (2019).

334. Betancourt-Ángeles, M. *et al.* Treatment in the healing of burns with a cold plasma source. *Int. J. Burns Trauma* **7**, 142–146 (2017).

335. Metelmann, H.-R. *et al.* Scar formation of laser skin lesions after cold atmospheric pressure plasma (CAP) treatment: A clinical long term observation. *Clin. Plasma Med.* **1**, 30–35 (2013).

336. Winter, S., Meyer-Lindenberg, A., Wolf, G., Reese, S. & Nolff, M. C. In vitro evaluation of the decontamination effect of cold atmospheric argon plasma on selected bacteria frequently encountered in small animal bite injuries. *J. Microbiol. Methods* **169**, 105728 (2020).

337. Xu, Y. *et al.* Systematic Safety Evaluation of Cold Plasma-Activated Liquid in Rabbits. *Front. Phys.* **9**, (2021).

338. Dobrynin, D. *et al.* Live Pig Skin Tissue and Wound Toxicity of Cold Plasma Treatment. *Plasma Med.* **1**, (2011).

339. Boxhammer, V. *et al.* Investigation of the mutagenic potential of cold atmospheric plasma at bactericidal dosages. *Mutat. Res.* **753**, 23–28 (2013).

340. Maisch, T. *et al.* Investigation of toxicity and mutagenicity of cold atmospheric argon plasma. *Environ. Mol. Mutagen.* **58**, 172–177 (2017).

341. Arndt, S. *et al.* Effects of cold atmospheric plasma (CAP) on ß-defensins, inflammatory cytokines, and apoptosis-related molecules in keratinocytes in vitro and in vivo. *PloS One* **10**, e0120041 (2015).

342. Schmidt, A. *et al.* One Year Follow-Up Risk Assessment in SKH-1 Mice and Wounds Treated with an Argon Plasma Jet. *Int. J. Mol. Sci.* **18**, E868 (2017).

343. Fluhr, J. W. *et al.* In vivo skin treatment with tissue-tolerable plasma influences skin physiology and antioxidant profile in human stratum corneum. *Exp. Dermatol.* **21**, 130–134 (2012).

344. Lademann, O. *et al.* Drug delivery through the skin barrier enhanced by treatment with tissue-tolerable plasma. *Exp. Dermatol.* **20**, 488–490 (2011).

345. Metelmann, H.-R. *et al.* Scar formation of laser skin lesions after cold atmospheric pressure plasma (CAP) treatment: A clinical long term observation. *Clin. Plasma Med.* **1**, 30–35 (2013).

346. Assadian, O. *et al.* Effects and safety of atmospheric low-temperature plasma on bacterial reduction in chronic wounds and wound size reduction: A systematic review and meta-analysis. *Int. Wound J.* **16**, 103–111 (2019).

347. Church, D., Elsayed, S., Reid, O., Winston, B. & Lindsay, R. Burn wound infections. *Clin. Microbiol. Rev.* **19**, 403–434 (2006).

348. Rennie, R. P., Jones, R. N., Mutnick, A. H., & SENTRY Program Study Group (North America). Occurrence and antimicrobial susceptibility patterns of pathogens isolated from skin and soft tissue infections: report from the SENTRY Antimicrobial Surveillance Program (United States and Canada, 2000). *Diagn. Microbiol. Infect. Dis.* **45**, 287–293 (2003).

349. Rao, Y., Shang, W., Yang, Y., Zhou, R. & Rao, X. Fighting Mixed-Species Microbial Biofilms With Cold Atmospheric Plasma. *Front. Microbiol.* **11**, 1000 (2020).

350. Nguyen, L. *et al.* Cold atmospheric plasma is a viable solution for treating orthopedic infection: a review. *Biol. Chem.* **400**, 77–86 (2018).

351. Haertel, B., von Woedtke, T., Weltmann, K.-D. & Lindequist, U. Non-thermal atmospheric-pressure plasma possible application in wound healing. *Biomol. Ther.* **22**, 477–490 (2014).

352. Stratmann, B. *et al.* Effect of Cold Atmospheric Plasma Therapy vs Standard Therapy Placebo on Wound Healing in Patients With Diabetic Foot Ulcers. *JAMA Netw. Open* **3**, e2010411 (2020).

353. Kisch, T. *et al.* Improvement of cutaneous microcirculation by cold atmospheric plasma (CAP): Results of a controlled, prospective cohort study. *Microvasc. Res.* **104**, 55–62 (2016).

354. Miller, V., Lin, A., Fridman, G., Dobrynin, D. & Fridman, A. Plasma Stimulation of Migration of Macrophages. *Plasma Process. Polym.* **11**, 1193–1197 (2014).

355. Kaushik, N. K. *et al.* Cytotoxic macrophage-released tumour necrosis factor-alpha (TNF-$\less$i$\greater$$\upalpha$$\less$/i$\greater$) as a killing mechanism for cancer cell death after cold plasma activation. *J. Phys. Appl. Phys.* **49**, 084001 (2016).

356. Kaushik, N. K. *et al.* Biological and medical applications of plasma-activated media, water and solutions. *Biol. Chem.* **400**, 39–62 (2018).

357. Vilhardt, F., Haslund-Vinding, J., Jaquet, V. & McBean, G. Microglia antioxidant systems and redox signalling. *Br. J. Pharmacol.* **174**, 1719–1732 (2017).

358. Arndt, S., Schmidt, A., Karrer, S. & von Woedtke, T. Comparing two different plasma devices kINPen and Adtec SteriPlas regarding their molecular and cellular effects on wound healing. *Clin. Plasma Med.* **9**, 24–33 (2018).

359. VON Woedtke, T., Schmidt, A., Bekeschus, S., Wende, K. & Weltmann, K.-D. Plasma Medicine: A Field of Applied Redox Biology. *Vivo Athens Greece* **33**, 1011–1026 (2019).

360. Graves, D. B. The emerging role of reactive oxygen and nitrogen species in redox biology and some implications for plasma applications to medicine and biology. *J. Phys. Appl. Phys.* **45**, 263001 (2012).

361. Kaushik, N. K. *et al.* Cytotoxic macrophage-released tumour necrosis factor-alpha (TNF-$\less$i$\greater$$\upalpha$$\less$/i$\greater$) as a killing mechanism for cancer cell death after cold plasma activation. *J. Phys. Appl. Phys.* **49**, 084001 (2016).

362. Kaushik, N. K. *et al.* Preventing the Solid Cancer Progression via Release of Anticancer-Cytokines in Co-Culture with Cold Plasma-Stimulated Macrophages. *Cancers* **11**, E842 (2019).

363. Crestale, L. *et al.* Cold Atmospheric Pressure Plasma Treatment Modulates Human Monocytes/Macrophages Responsiveness. *Plasma* **1**, 261–276 (2018).

364. Khabipov, A. *et al.* Murine Macrophages Modulate Their Inflammatory Profile in Response to Gas Plasma-Inactivated Pancreatic Cancer Cells. *Cancers* **13**, 2525 (2021).

365. Bedard, K. & Krause, K.-H. The NOX family of ROS-generating NADPH oxidases: physiology and pathophysiology. *Physiol. Rev.* **87**, 245–313 (2007).

366. Sen, C. K. & Packer, L. Antioxidant and redox regulation of gene transcription. *FASEB J. Off. Publ. Fed. Am. Soc. Exp. Biol.* **10**, 709–720 (1996).

367. Murakami, T. Numerical modelling of the effects of cold atmospheric plasma on mitochondrial redox homeostasis and energy metabolism. *Sci. Rep.* **9**, 17138 (2019).

368. Duchesne, C. *et al.* Cold Atmospheric Plasma Promotes Killing of Staphylococcus aureus by Macrophages. *mSphere* **6**, e00217-21.

369. Duchesne, C., Banzet, S., Lataillade, J.-J., Rousseau, A. & Frescaline, N. Cold atmospheric plasma modulates endothelial nitric oxide synthase signalling and enhances burn wound neovascularisation. *J. Pathol.* **249**, 368–380 (2019).

370. Duchesne, C. Cold-atmospheric plasma improves burn injury repair via modulation of angiogenesis, extracellular matrix formation and antibacterial effect. (Université Paris-Saclay, 2019).

371. Straßenburg, S. *et al.* Comparison of Biological Effects on Human Keratinocytes Using Different Plasma Treatment Regimes. *Plasma Med.* **3**, 57–69 (2013).

372. Girard, P.-M. *et al.* Synergistic Effect of H2O2 and NO2 in Cell Death Induced by Cold Atmospheric He Plasma. *Sci. Rep.* **6**, 29098 (2016).

373. Schmidt, A. *et al.* Non-thermal plasma activates human keratinocytes by stimulation of antioxidant and phase II pathways. *J. Biol. Chem.* **290**, 6731–6750 (2015).

374. Hashemian, S. M. & Fallahian, F. The use of heliox in critical care. *Int. J. Crit. Illn. Inj. Sci.* **4**, 138–142 (2014).

375. Oei, G. T. M. L., Weber, N. C., Hollmann, M. W. & Preckel, B. Cellular effects of helium in different organs. *Anesthesiology* **112**, 1503–1510 (2010).

376. Smit, K. F. *et al.* Helium alters the cytoskeleton and decreases permeability in endothelial cells cultured in vitro through a pathway involving Caveolin-1. *Sci. Rep.* **8**, 4768 (2018).

377. Rosch, R. *et al.* Improved abdominal wall wound healing by helium pneumoperitoneum. *Surg. Endosc.* **20**, 1892–1896 (2006).

378. Sullivan, T. P., Eaglstein, W. H., Davis, S. C. & Mertz, P. The pig as a model for human wound healing. *Wound Repair Regen. Off. Publ. Wound Heal. Soc. Eur. Tissue Repair Soc.* **9**, 66–76 (2001).

379. Byl, N. N. *et al.* Pulsed microamperage stimulation: a controlled study of healing of surgically induced wounds in Yucatan pigs. *Phys. Ther.* **74**, 201–213; discussion 213-218 (1994).

380. Papp, A. *et al.* The progression of burn depth in experimental burns: a histological and methodological study. *Burns J. Int. Soc. Burn Inj.* **30**, 684–690 (2004).

381. Cuttle, L. *et al.* A porcine deep dermal partial thickness burn model with hypertrophic scarring. *Burns J. Int. Soc. Burn Inj.* **32**, 806–820 (2006).

382. Schoos, A., Devreese, M. & Maes, D. G. Use of non-steroidal anti-inflammatory drugs in porcine health management. *Vet. Rec.* **185**, 172 (2019).

383. Salichs, M., Sabaté, D., Ciervo, O. & Homedes, J. Comparison of the antipyretic efficacy of ketoprofen, acetylsalicylic acid, and paracetamol, orally administered to swine. *J. Vet. Pharmacol. Ther.* **35**, 198–201 (2012).

384. Reyes, L., Tinworth, K. D., Li, K. M., Yau, D. F. & Waters, K. A. Observer-blinded comparison of two nonopioid analgesics for postoperative pain in piglets. *Pharmacol. Biochem. Behav.* **73**, 521–528 (2002).

385. Boyd, J. J. *et al.* Cardiovascular changes after naloxone administration in propofol-sedated piglets during opioid overdose. *Acta Anaesthesiol. Scand.* **50**, 1271–1276 (2006).

386. Poletto, R. *et al.* Identification of low and high frequency ranges for heart rate variability and blood pressure variability analyses using pharmacological autonomic blockade with atropine and propranolol in swine. *Physiol. Behav.* **103**, 188–196 (2011).

387. Yao, F. *et al.* Age and growth factors in porcine full-thickness wound healing. *Wound Repair Regen. Off. Publ. Wound Heal. Soc. Eur. Tissue Repair Soc.* **9**, 371–377 (2001).

388. Dunn, M. G., Silver, F. H. & Swann, D. A. Mechanical analysis of hypertrophic scar tissue: structural basis for apparent increased rigidity. *J. Invest. Dermatol.* **84**, 9–13 (1985).

389. Dunaiski, V. & Belford, D. A. Contribution of circulating IGF-I to wound repair in GH-treated rats. *Growth Horm. IGF Res. Off. J. Growth Horm. Res. Soc. Int. IGF Res. Soc.* **12**, 381–387 (2002).

390. Ferguson, M. W. J. & O'Kane, S. Scar-free healing: from embryonic mechanisms to adult therapeutic intervention. *Philos. Trans. R. Soc. Lond. B. Biol. Sci.* **359**, 839–850 (2004).

391. Viscardi, A. V., Hunniford, M., Lawlis, P., Leach, M. & Turner, P. V. Development of a Piglet Grimace Scale to Evaluate Piglet Pain Using Facial Expressions Following Castration and Tail Docking: A Pilot Study. *Front. Vet. Sci.* **4**, (2017).

392. Dahiya, P. Burns as a model of SIRS. *Front. Biosci. Landmark Ed.* **14**, 4962–4967 (2009).

393. Lachiewicz, A. M., Hauck, C. G., Weber, D. J., Cairns, B. A. & van Duin, D. Bacterial Infections After Burn Injuries: Impact of Multidrug Resistance. *Clin. Infect. Dis. Off. Publ. Infect. Dis. Soc. Am.* **65**, 2130–2136 (2017).

394. Pomposiello, P. J. & Demple, B. Global adjustment of microbial physiology during free radical stress. *Adv. Microb. Physiol.* **46**, 319–341 (2002).

395. Bourke, P., Ziuzina, D., Han, L., Cullen, P. J. & Gilmore, B. F. Microbiological interactions with cold plasma. *J. Appl. Microbiol.* **123**, 308–324 (2017).

396. Alkawareek, M. Y. *et al.* Application of atmospheric pressure nonthermal plasma for the in vitro eradication of bacterial biofilms. *FEMS Immunol. Med. Microbiol.* **65**, 381–384 (2012).

397. Li, W. G. *et al.* H(2)O(2)-induced O(2) production by a non-phagocytic NAD(P)H oxidase causes oxidant injury. *J. Biol. Chem.* **276**, 29251–29256 (2001).

398. McDaniel, J. C., Roy, S. & Wilgus, T. A. Neutrophil activity in chronic venous leg ulcers--a target for therapy? *Wound Repair Regen. Off. Publ. Wound Heal. Soc. Eur. Tissue Repair Soc.* **21**, 339–351 (2013).

399. Tüting, T. & Visser, K. E. de. How neutrophils promote metastasis. *Science* **352**, 145–146 (2016).

400. Costa, A. C., Santos, J. M. O., Gil da Costa, R. M. & Medeiros, R. Impact of immune cells on the hallmarks of cancer: A literature review. *Crit. Rev. Oncol. Hematol.* **168**, 103541 (2021).

401. Yan, J. *et al.* Human polymorphonuclear neutrophils specifically recognize and kill cancerous cells. *Oncoimmunology* **3**, e950163 (2014).

402. Bekeschus, S. *et al.* Neutrophil extracellular trap formation is elicited in response to cold physical plasma. *J. Leukoc. Biol.* **100**, 791–799 (2016).

403. Bekeschus, S., Moritz, J., Schmidt, A. & Wende, K. Redox regulation of leukocyte-derived microparticle release and protein content in response to cold physical plasma-derived oxidants. *Clin. Plasma Med.* **7–8**, 24–35 (2017).

404. Bekeschus, S., Favia, P., Robert, E. & von Woedtke, T. White paper on plasma for medicine and hygiene: Future in plasma health sciences. *Plasma Process. Polym.* **16**, 1800033 (2019).

405. Wu, A. S. *et al.* Porcine intact and wounded skin responses to atmospheric nonthermal plasma. *J. Surg. Res.* **179**, e1–e12 (2013).

406. Schmidt, A., Bekeschus, S., Wende, K., Vollmar, B. & von Woedtke, T. A cold plasma jet accelerates wound healing in a murine model of full-thickness skin wounds. *Exp. Dermatol.* **26**, 156–162 (2017).

407. Wende, K. *et al.* Risk assessment of a cold argon plasma jet in respect to its mutagenicity. *Mutat. Res. Genet. Toxicol. Environ. Mutagen.* **798–799**, 48–54 (2016).

408. Honnorat, B. Application of cold plasma in oncology, multidisciplinary experiments, physical, chemical and biological modeling. (Sorbonne Université, 2018).

409. Hołub, M. On the measurement of plasma power in atmospheric pressure DBD plasma reactors. *Int. J. Appl. Electromagn. Mech.* **39**, 81–87 (2012).

410. Davis, M. F. *et al.* Household transmission of meticillin-resistant Staphylococcus aureus and other staphylococci. *Lancet Infect. Dis.* **12**, 703–716 (2012).

411. Kozajda, A., Jeżak, K. & Kapsa, A. Airborne Staphylococcus aureus in different environments—a review. *Environ. Sci. Pollut. Res.* **26**, 34741–34753 (2019).

412. Wertheim, H. F. *et al.* The role of nasal carriage in Staphylococcus aureus infections. *Lancet Infect. Dis.* **5**, 751–762 (2005).

413. Krismer, B., Weidenmaier, C., Zipperer, A. & Peschel, A. The commensal lifestyle of Staphylococcus aureus and its interactions with the nasal microbiota. *Nat. Rev. Microbiol.* **15**, 675–687 (2017).

414. Abdullahi, I. N. *et al.* Wild Animals Are Reservoirs and Sentinels of Staphylococcus aureus and MRSA Clones: A Problem with "One Health" Concern. *Antibiotics* **10**, 1556 (2021).

415. Tong, S. Y. C., Davis, J. S., Eichenberger, E., Holland, T. L. & Fowler, V. G. Staphylococcus aureus Infections: Epidemiology, Pathophysiology, Clinical Manifestations, and Management. *Clin. Microbiol. Rev.* **28**, 603–661 (2015).

416. Ahmad-Mansour, N. *et al.* Staphylococcus aureus Toxins: An Update on Their Pathogenic Properties and Potential Treatments. *Toxins* **13**, 677 (2021).

417. Thomer, L., Schneewind, O. & Missiakas, D. Pathogenesis of Staphylococcus aureus Bloodstream Infections. 24 (2016).

418. Cheung, G. Y. C., Bae, J. S. & Otto, M. Pathogenicity and virulence of *Staphylococcus aureus*. *Virulence* **12**, 547–569 (2021).

419. Foster, T. J. Immune evasion by staphylococci. *Nat. Rev. Microbiol.* **3**, 948–958 (2005).

420. Foster, T. J., Geoghegan, J. A., Ganesh, V. K. & Höök, M. Adhesion, invasion and evasion: the many functions of the surface proteins of Staphylococcus aureus. *Nat. Rev. Microbiol.* **12**, 49–62 (2014).

421. Murray, C. J. *et al.* Global burden of bacterial antimicrobial resistance in 2019: a systematic analysis. *The Lancet* S0140673621027240 (2022) doi:10.1016/S0140-6736(21)02724-0.

422. Avci, P. *et al. In-vivo* monitoring of infectious diseases in living animals using bioluminescence imaging. *Virulence* **9**, 28–63 (2018).

423. Syed, A. J. & Anderson, J. C. Applications of bioluminescence in biotechnology and beyond. *Chem. Soc. Rev.* **50**, 5668–5705 (2021).

424. Guo, Y. *et al. In Vivo* Bioluminescence Imaging To Evaluate Systemic and Topical Antibiotics against Community-Acquired Methicillin-Resistant Staphylococcus aureus-Infected Skin Wounds in Mice. *Antimicrob. Agents Chemother.* **57**, 855–863 (2013).

425. Francis, K. P. *et al.* Monitoring bioluminescent Staphylococcus aureus infections in living mice using a novel luxABCDE construct. *Infect. Immun.* **68**, 3594–3600 (2000).

426. Tenhami, M., Hakkila, K. & Karp, M. Measurement of Effects of Antibiotics in Bioluminescent *Staphylococcus aureus* RN4220. *Antimicrob. Agents Chemother.* **45**, 3456–3461 (2001).

427. Xiong, Y. Q. *et al.* Real-Time In Vivo Bioluminescent Imaging for Evaluating the Efficacy of Antibiotics in a Rat *Staphylococcus aureus* Endocarditis Model. *Antimicrob. Agents Chemother.* **49**, 380–387 (2005).

428. Lambrechts, S. A. G., Demidova, T. N., Aalders, M. C. G., Hasan, T. & Hamblin, M. R. Photodynamic therapy for Staphylococcus aureus infected burn wounds in mice. *Photochem. Photobiol. Sci.* **4**, 503 (2005).

429. Mortin, L. I. *et al.* Rapid Bactericidal Activity of Daptomycin against Methicillin-Resistant and Methicillin-Susceptible Staphylococcus aureus Peritonitis in Mice as Measured with Bioluminescent Bacteria. *Antimicrob. Agents Chemother.* **51**, 1787–1794 (2007).

430. Zhang, H., Kalkeri, G., Mani, N. & Grossman, T. H. Development and Validation of a Multi-dose Neutropenic Rat Thigh Infection Model Using Real-time Monitoring of Staphylococcus aureus Growth In Vivo. *In Vivo* 6 (2008).

431. Munro, P. *et al.* The Staphylococcus aureus epidermal cell differentiation inhibitor toxin promotes formation of infection foci in a mouse model of bacteremia. *Infect. Immun.* **78**, 3404–3411 (2010).

432. Lorenz, U. *et al.* In Vivo Detection of Staphylococcus aureus in Biofilm on Vascular Prostheses Using Non-invasive Biophotonic Imaging. *Eur. J. Vasc. Endovasc. Surg.* **41**, 68–75 (2011).

433. Cho, J. S. *et al.* Noninvasive In Vivo Imaging to Evaluate Immune Responses and Antimicrobial Therapy against Staphylococcus aureus and USA300 MRSA Skin Infections. *J. Invest. Dermatol.* **131**, 907–915 (2011).

434. Plaut, R. D., Mocca, C. P., Prabhakara, R., Merkel, T. J. & Stibitz, S. Stably Luminescent Staphylococcus aureus Clinical Strains for Use in Bioluminescent Imaging. *PLoS ONE* **8**, e59232 (2013).

435. van Staden, A. D. P., Heunis, T., Smith, C., Deane, S. & Dicks, L. M. T. Efficacy of Lantibiotic Treatment of Staphylococcus aureus-Induced Skin Infections, Monitored by *In Vivo* Bioluminescent Imaging. *Antimicrob. Agents Chemother.* **60**, 3948–3955 (2016).

436. Bostian, P. A. *et al.* Novel rat tail discitis model using bioluminescent *Staphylococcus aur* e *us*: RAT TAIL DISCITIS MODEL. *J. Orthop. Res.* **35**, 2075–2081 (2017).

437. Rozenbaum, R. T. *et al.* Antimicrobial synergy of monolaurin lipid nanocapsules with adsorbed antimicrobial peptides against Staphylococcus aureus biofilms in vitro is absent in vivo. *J. Controlled Release* **293**, 73–83 (2019).

438. Miller, R. J. *et al.* Development of a Staphylococcus aureus reporter strain with click beetle red luciferase for enhanced in vivo imaging of experimental bacteremia and mixed infections. *Sci. Rep.* **9**, 16663 (2019).

439. Kobayashi, H. *et al.* Differential effects of anti-RANKL monoclonal antibody and zoledronic acid on necrotic bone in a murine model of *Staphylococcus aureus* -induced osteomyelitis. *J. Orthop. Res.* **40**, 614–623 (2022).

440. Benjamin, A. B. *et al.* Efficacy of Cathelicidin-Mimetic Antimicrobial Peptoids against Staphylococcus aureus. *Microbiol. Spectr.* **10**, e00534-22 (2022).

441. Schaefler, S., Perry, W. & Jones, D. Methicillin-Resistant Strains of *Staphylococcus aureus* Phage Type 92. *Antimicrob. Agents Chemother.* **15**, 74–80 (1979).

442. Lebeaux, D. *et al.* pH-Mediated Potentiation of Aminoglycosides Kills Bacterial Persisters and Eradicates In Vivo Biofilms. *J. Infect. Dis.* **210**, 1357–1366 (2014).

443. Chauhan, A., Ghigo, J.-M. & Beloin, C. Study of in vivo catheter biofilm infections using pediatric central venous catheter implanted in rat. *Nat. Protoc.* **11**, 525–541 (2016).

444. Gelin, M. *et al.* From Substrate to Fragments to Inhibitor Active In Vivo against Staphylococcus aureus. *ACS Infect. Dis.* 1–14 (2020) doi:10.1021/acsinfecdis.9b00368.

445. Visperas, A. *et al.* Standardized quantification of biofilm in a novel rabbit model of periprosthetic joint infection. *J. Bone Jt. Infect.* **7**, 91–99 (2022).

446. Trikha, R. *et al.* Active rheumatoid arthritis in a mouse model is not an independent risk factor for periprosthetic joint infection. *PLOS ONE* **16**, e0250910 (2021).

447. Quan, K. *et al.* Influence of interaction between surface-modified magnetic nanoparticles with infectious biofilm components in artificial channel digging and biofilm eradication by antibiotics *in vitro* and *in vivo*. *Nanoscale* **13**, 4644–4653 (2021).

448. Trikha, R. *et al.* Inhibition of Angiotensin Converting Enzyme Impairs Anti-staphylococcal Immune Function in a Preclinical Model of Implant Infection. *Front. Immunol.* **11**, 1919 (2020).

449. Jørgensen, N. P., Meyer, R., Dagnæs-Hansen, F., Fuursted, K. & Petersen, E. A Modified Chronic Infection Model for Testing Treatment of Staphylococcus aureus Biofilms on Implants. *PLoS ONE* **9**, e103688 (2014).

450. Ovchinnikov, K. V., Kranjec, C., Thorstensen, T., Carlsen, H. & Diep, D. B. Successful Development of Bacteriocins into Therapeutic Formulation for Treatment of MRSA Skin Infection in a Murine Model. *Antimicrob. Agents Chemother.* **64**, e00829-20 (2020).

451. Grønseth, T. *et al.* Lugol's solution and Gentian violet eradicate methicillin-resistant *Staphylococcus aureus* biofilm in skin wound infections. *Int. Wound J.* iwj.13846 (2022) doi:10.1111/iwj.13846.

452. Arndt, D. *et al.* PHASTER: a better, faster version of the PHAST phage search tool. *Nucleic Acids Res.* **44**, W16–W21 (2016).

453. Bortolaia, V. *et al.* ResFinder 4.0 for predictions of phenotypes from genotypes. *J. Antimicrob. Chemother.* **75**, 3491–3500 (2020).

Annex A: Method article on full-thickness burn mouse model reconstructed with an allogenic skin graft.

jove

A Murine Model of a Burn Wound Reconstructed with an Allogeneic Skin Graft

Océane Blaise[*,1,2], **Constance Duchesne**[*,1,2], **Sébastien Banzet**[2], **Antoine Rousseau**[1], **Nadira Frescaline**[1,2]

[1] Laboratoire de Physique des Plasmas, École Polytechnique, Sorbonne Université, CNRS [2] Institut de Recherche Biomédicale des Armées, Clamart, INSERM UMRS-MD

[*] These authors contributed equally

Corresponding Author

Nadira Frescaline
nadira.frescaline@lpp.polytechnique.fr

Citation

Blaise, O., Duchesne, C., Banzet, S., Rousseau, A., Frescaline, N. A Murine Model of a Burn Wound Reconstructed with an Allogeneic Skin Graft. *J. Vis. Exp.* (162), e61339, doi:10.3791/61339 (2020).

Date Published

August 8, 2020

DOI

10.3791/61339

URL

jove.com/video/61339

Abstract

Trivial superficial wounds heal without complications by primary intention. Deep wounds, such as full thickness burns, heal by secondary intention and require surgical debridement and skin grafting. Successful integration of the donor graft into a recipient wound bed depends on timely recruitment of immune cells, robust angiogenic response and new extracellular matrix formation. The development of novel therapeutic agents, which target some key processes involved in wound healing, are hindered by the lack of reliable preclinical models with optimized objective assessment of wound closure. Here, we describe an inexpensive and reproducible model of experimental full thickness burn wound reconstructed with an allogeneic skin graft. The wound is induced on the dorsum surface of anaesthetized inbred wild type mice from the BALB/C and SKH1-Hrhr backgrounds. The burn is produced using a brass template measuring 10 mm in diameter, which is preheated to 80 °C and delivered at a constant pressure for 20 s. Burn eschar is excised 24 hours after the injury and replaced with a full thickness graft harvested from the tail of a genetically similar donor mouse. No specialized equipment is required for the procedure and surgical techniques are straightforward to follow. The method may be effortlessly implemented and reproduced in most research settings. Certain limitations are associated with the model. Due to technical difficulties, the harvest of thinner split thickness skin grafts is not possible. The surgical method we describe here allows for the reconstruction of burn wounds using full thickness skin grafts. It may be used to carry out preclinical therapeutic testing.

Introduction

Surgical debridement and skin grafting are common clinical practices used in the management of chronic wounds[1], burn wounds[2], and acute wounds such as traumatic wounds[3]. Skin grafting refers to the surgical procedure, which involves

Copyright © 2020 JoVE Creative Commons Attribution-NonCommercial-NoDerivs 3.0 Unported License

the removal of healthy skin from one part of the body and transferring it to another. Donor grafts replace the lost tissue and provide a structural scaffold for cellular migration and growth. Following integration into the recipient site, skin grafts replace the lost skin barrier by providing protection from microbial invasion, harmful effects of the external environment and excessive loss of moisture[4]. Successful skin graft integration depends on several factors. These include adequate immune responses in the presence of microbial infections and timely resolution of inflammation, robust angiogenesis at the wound site and establishment of vascular anastomoses between the recipient bed and the donor graft[5]. As the graft begins to degrade, resident dermal cells must be replaced by cells capable of producing new extracellular matrix. At the same time, the epidermal keratinocytes must crawl over the newly produced matrix to form the neo-epidermis and re-epithelialize the wound. It is, therefore, evident that efficient migration of cells from the recipient bed into the donor graft is another determining factor that influences successful graft incorporation. Given the vast number of factors involved in wound healing[6], which may be impossible to control in the human trials due to ethical limitations, models of pre-clinical experimental skin grafting are necessary. Development of pre-clinical models of burn wound healing and associated skin grafting will be important for understanding of complex mechanisms involved in cutaneous tissue repair and essential for the testing of new therapeutic agents. The in vitro models of wound healing are unable to accurately mimic the complexity of the cutaneous tissue. The in vivo animal models are an indispensable investigative tool in understanding the mechanisms involved in tissue repair.

Several methods of skin grafting technique were developed in rodents to mimic surgical excision and burn wound reconstruction[7,8,9]. However, most of the previously described procedures failed to induce a thermal burn injury prior to skin grafting. Instead of the burn wound, a full thickness excisional wound was induced, which was then reconstructed with a full thickness skin allograft[7]. Various anatomical landmarks such as the ear, tail and back have been used for harvesting of the donor skin in rodents[7,8]. Different graft fixation and stabilization techniques were reported, including a “no suture technique”[9], sutures[7] and surgical glue[10,11,12].

The purpose of this study was to develop a murine model of a full thickness burn wound that would recapitulate the current gold standard approach in burn treatment, which involves nonviable tissue excision and skin grafting. A thermal burn was induced on the dorsum surface of a mouse using a preheated brass template. Burn eschar was excised and replaced with a full thickness graft harvested from the tail of a donor mouse. There are three key advantages to this experimental model. First, more than one burn wound may be induced on the back of the recipient mouse, and four donor skin grafts may be harvested from a single tail of the donor mouse. This means that several experimental and control treatments may potentially be compared using the same recipient and donor animals. Depending on the desired route of administration, the control treatment may include local or systemic administration of the vehicle or placebo control (e.g., topical application of ointment, subcutaneous, intraperitoneal or intravenous injection of solution). Second, timing of the treatment and the endpoint of the experiment may be controlled. Third, this model depends on the reconstruction of wounds using full thickness grafts harvested from the tail, which are known to have a higher probability for successful incorporation into the donor site compared to the skin harvested from the back[13]. This may be due to the lower

Copyright © 2020 JoVE Creative Commons Attribution-NonCommercial-NoDerivs 3.0 Unported License

number of epidermal Langerhans cells, which play a key role in cutaneous immunobiology, and are associated with the skin graft rejection[14].

The proposed model of wound healing and graft integration may well be applied to transgenic and knockout mice. The use of genetically modified mice will assist in elucidating the roles that certain genes may play during wound repair. Exogenous application of topical wound preparations or subcutaneous administration of therapeutic antibodies at the site of the injury may also be considered.

Due to technical difficulties, split thickness skin grafts consisting of the epidermis and part of the dermis are difficult to obtain in mice. Full thickness skin grafts consisting of the epidermis and full thickness dermis are known to require a well-vascularized wound bed for successful integration. The inability to harvest split thickness skin grafts in mice may be regarded as a limitation of this model. The fixation of the skin graft to the recipient wound bed was achieved via the application of the surgical adhesive glue, which is associated with less trauma and rapid degradation compared to other means of tissue fixation[15]. Previous studies have shown that suturing is associated with stronger tissue fixation than the surgical glue at 24 h after the surgical procedure[15], which may be considered as a disadvantage of the procedure. However, at later timepoints, the biomechanical strength of wounds treated with a surgical adhesive becomes comparable to sutures[15] and better than staple fixation[16]. Following tissue fixation with the surgical glue, wounds must be covered with a wound dressing. Although wounds on the dorsal surface of the mouse are difficult for the animal to reach, the wound dressing, on the other hand, is easy for the animal to manipulate and remove. Frequent wound dressing changes may be warranted.

Anesthesia-induced hypothermia in small rodents is a well-documented phenomenon[17]. Hypothermia is a side effect of this procedure, which causes complications, and potentially compromises both animal health and data quality. Therefore, this method warrants the implementation of temperature management strategies, especially if hairless SKH1-Hrhr are used.

The most significant limitation of using mice to mimic human wound closure is the difference between the skin anatomy and physiology. Mouse wounds heal mostly via contraction, whereas human wounds heal through granulation tissue formation and re-epithelialization[18]. To account for this discrepancy, the current model may be modified and used in combination with a splinting ring tightly adhered around the wound to prevent skin contraction[19]. Given some advantages and disadvantages of this in vivo protocol, this model could serve as a tool to study certain processes involved in wound healing that are impossible to study in vitro.

Protocol

All experiments were approved by the French Department of Higher Education and Research (Study Number: 12216201711161651767 0v2 and DAP180012). All mice were single-housed upon arrival in plastic cages and were allowed a 7-day acclimatization period prior to the study. The animal room was maintained at a 12/12 h light/dark cycle (lights on at 07:00). Food and tap water were provided ad libitum. BALB/c and SKH1-Hrhr mice were fed traditional wheat/soy-based diet. Sawdust bedding was provided along with nesting material.

Copyright © 2020 JoVE Creative Commons Attribution-NonCommercial-NoDerivs 3.0 Unported License

1. Equipment preparation

1. Prepare a burning device for the procedure and set it to 80 °C using the temperature controller (**Figure 1A**). Verify the temperature of the brass template (**Figure 1B,C**) using the infrared thermal imaging camera.
2. Ensure that the digital manometer is operating correctly.
3. Cover the stage with a surgical drape and adjust the height of the table (**Figure 1A**).

2. Pre-operative and intra-operative animal care

1. Acquire BALB/c and SKH1-Hrhr mice, 6-8 weeks of age.
2. Add paracetamol suspension at 3 mg/mL to drinking water and supply 12 hours before and up to 72 hours after the procedure.
3. Using a 1 mL syringe and a 26 G needle, administer buprenorphine subcutaneously at 0.05 µg/g 30 min before the procedure and every 6 hours for the first 72 hours after the procedure.
4. Using a 1 mL syringe and a 26 G needle, administer lidocaine to the dorsum of the mouse and 2-3 mm distal to the area of the burn wound. Inject lidocaine at 0.05 µg/g subcutaneously 15 min before the induction of the burn wound.
5. Anesthetize mice using an intraperitoneal injection of xylazine at 10 mg/kg and ketamine 100 mg/kg. Use a 1 mL syringe and a 26 G needle to administer the injection.
6. Critical step: Place the anaesthetized mouse on a heated pad and keep the mouse warm to prevent hypothermia for the first 30 minutes after the induction of anesthesia and for at least 15 minutes after the recovery from anesthesia. In addition to the heated pad, other modalities including *heat lamps*, circulating *warm* liquids or air, and pre-warmed *heat* reservoirs may be used to regulate the body temperature.
7. Apply lubrication gel on the eyes of the mouse to prevent dehydration of the cornea.
8. Use the toe pinch withdrawal reflex to assess the depth of anesthesia.
9. Using a 1 mL syringe and a 26 G needle administer 200 µL of Lactated Ringer's Solution supplemented with 5% dextrose. Administer fluid replacement subcutaneously immediately after the induction of anesthesia and 6 hours after the procedure to prevent dehydration.

3. Full thickness burn wound induction

1. Shave the anaesthetized mouse with the hair clippers.
2. Apply depilating cream on the dorsum surface of the mouse for 1 minute. Wipe off the cream using some sterile gauze and clean the area with a piece of damp gauze. Blot the skin with some gauze until dry.
3. Place the mouse on the stage covered with a surgical drape and move the stage upward closer to the preheated brass template.
4. Apply the circular brass template on the back of the mouse (80 °C for 20 s) using constant pressure of 0.15 N (**Figure 2**).
5. **Critical step:** Immediately after the burn induction, place the anaesthetized animal on the heated pad to prevent hypothermia and keep the mouse warm during and after the procedure. Once recovered from anesthesia, return the mouse back to the cage.
6. **Critical step:** Provide a mashed diet on the cage floor for the first 72 hours after the surgical procedure. Mice are

Copyright © 2020 JoVE Creative Commons Attribution-NonCommercial-NoDerivs 3.0 Unported License

sometimes reluctant to reach up to a sipper tube to drink water after a burn wound injury.

4. Harvesting of the donor graft

1. Make a longitudinal incision with a scalpel in the upper part of the tail of the donor mouse and gently remove the skin using surgical forceps.
2. Place the tail skin into a sterile Petri dish filled with 10 mL of sterile 0.9% saline solution. Use a ruler to measure out individual grafts and cut the tail skin into pieces, each measuring 15 mm, using a scalpel.
3. Once prepared, keep the skin grafts in 0.9% saline solution at 4 °C for up to 2 hours.

5. Surgical excision and skin grafting

1. Twenty-four hours after the burn induction, prepare the mouse for anesthesia by inhalation of isoflurane. Place the mouse into the induction chamber and induce anesthesia using 5% isoflurane in 100% oxygen at a flow rate of 4 L/min. To maintain anesthesia during surgery, use 2% isoflurane at 2 L/min.
2. Place a surgical drape on the mouse and cut out a window to expose the surgical field. Using the aseptic technique, swab the wound first with povidone-iodine and then with 70% alcohol.
3. Gently pick up the burned tissue with a pair of surgical tweezers and excise all necrotic and nonviable tissue with sterile surgical scissors and tweezers. Remove the panniculus carnosus layer of the hypodermis to create a stable recipient bed.
4. Place the skin graft on the freshly prepared wound bed. Gently pull the surrounding skin toward the skin graft using surgical tweezers. Apply some surgical adhesive to attach the graft to the wound bed and gently press to align the skin edges. Critical step: The size of the wound bed must be slight larger than the size of the skin graft to ensure successful engraftment.
5. Allow the mouse to recover from anesthesia. **Critical step**: Place the mouse on a heated pad. Keep the mouse warm during and after the procedure to prevent hypothermia.
6. Apply inert paraffin gauze dressing and adhesive secondary dressing over the grafted wound.
7. Place the mouse into an individual cage. Critical step: Provide some mashed diet on the cage floor for the first 72 hours after the surgical procedure and monitor daily.
8. Provide toys and enrich the environment.

6. Digital imaging and post-mortem wound collection

1. Photograph wounds with a digital camera by placing a ruler next to the wound (**Figure 3**).
2. At the end point of the experiment, euthanize animals by exposure to carbon dioxide and cervical dislocation. **Critical step**: Excessive pulling action of the skin during the cervical dislocation may damage the graft.
3. At post-mortem, surgically excise the dorsal burn wounds to the fascia using scissors. Bisect wounds. Fix half in 10% buffered formalin and process for histology and immunohistochemistry. Fast freeze the other half in liquid nitrogen for RNA extraction and protein quantitation and keep at -80 °C.

Copyright © 2020 JoVE Creative Commons Attribution-NonCommercial-NoDerivs 3.0 Unported License

7. Skin histology, immunohistochemistry and collagen visualization

1. Embed samples of skin into paraffin, cut to 4 µm sections and place onto positively charged slides.
2. Use slides stained with hematoxylin and eosin to evaluate the rate of re-epithelialization (% of the original wound). The area of the wound that is covered with neo-epidermis may be expressed as a percentage of the entire wound (**Figure 4**). Use a digital microscope application and ImageJ software to perform the microscopic analysis of the sections.
3. Use histological sections (4 µm thickness) prepared from formalin-fixed and paraffin-embedded tissue and subject them to immunohistochemistry.
4. To assess collagen I and fibronectin expression in wounds, apply primary antibodies and incubate for 1 h. Detection may be performed by species-specific horseradish peroxidase (HRP) or alkaline phosphatase (AP)-conjugated secondary antibodies.
5. React sections with either: (i) HRP,3,3'-diaminobenzidine (DAB) or (ii) AP, Bond Polymer Refine Red (Table of Materials), which yields a bright red color (**Figure 5**). Scan the sections using an instrument and analyze with the digital microscope application and ImageJ.
6. To enable histological assessment of collagen deposition, perform trichrome staining on histological sections using a commercial kit.
7. For collagen fiber visualization, use multiphoton microscopy and second harmonic generation technique (**Figure 5**). Use a multiphoton microscope for tissue imaging as previously described[20]. Use a Ti:Sapphire laser with a center wavelength at 810 nm as the laser source for generating second harmonic and two-photon excited fluorescence signals (TPEF).
8. Use a laser beam equipped with a 25x/0.95 W objective to collect and excite second harmonic generation (SHG) and TPEF. Detect signals as described previously[21] by NDD PMT detectors. Use software for laser scanning control and image acquisition.

Representative Results

The results demonstrate that the protocol developed is a straightforward method, which permits the induction of a full thickness burn wound in mice. Burns are induced using a preheated brass template (**Figure 1A-C**). The burned area appears as a circular wound with a white eschar and a hyperemic zone. The size of the burn wound is slightly larger at 24 hours after the burn injury as a result of the well-described phenomenon known as the burn injury progression, which is possibly due to acute inflammation[22]. After excision, burn wounds are reconstructed using allogeneic skin graft (**Figure 3**). On day 7 after the burn injury, wounds become vascularized[5], which is an indication of successful engraftment. Epidermal keratinocytes migrate from the adjacent recipient skin in the effort to close the wound and bridge the gap between the two edges of the wounds. Microscopic analysis of H and E stained section of wounds revealed that the length of the neo-epidermis becomes significantly longer on day 7 after burn injury compared to day 3 after burn injury (**Figure 4B**). Prior to performing a large study, it is highly recommended that researchers complete a pilot study, which enables the exploration of a novel intervention, assessment of feasibility, identification of modifications to the method to ensure reproducibility. Statistically significant effects are difficult to detect in smaller samples, whereas increasing the sample size is one way to

Copyright © 2020 JoVE Creative Commons Attribution-NonCommercial-NoDerivs 3.0 Unported License

boost the statistical power of a test. For example, to detect a statistically significant difference ($p < 0.05$) in the rate of wound re-epithelialization (**Figure 4**) between groups, the sample size should be between six and eight mice per group. All experiments should be repeated at least twice. As matrix producing cells, such as fibroblasts, migrate from the recipient tissue into the graft, key components of the extracellular matrix, including collagen I and fibronectin become highly expressed in the newly formed matrix (**Figure 5**).

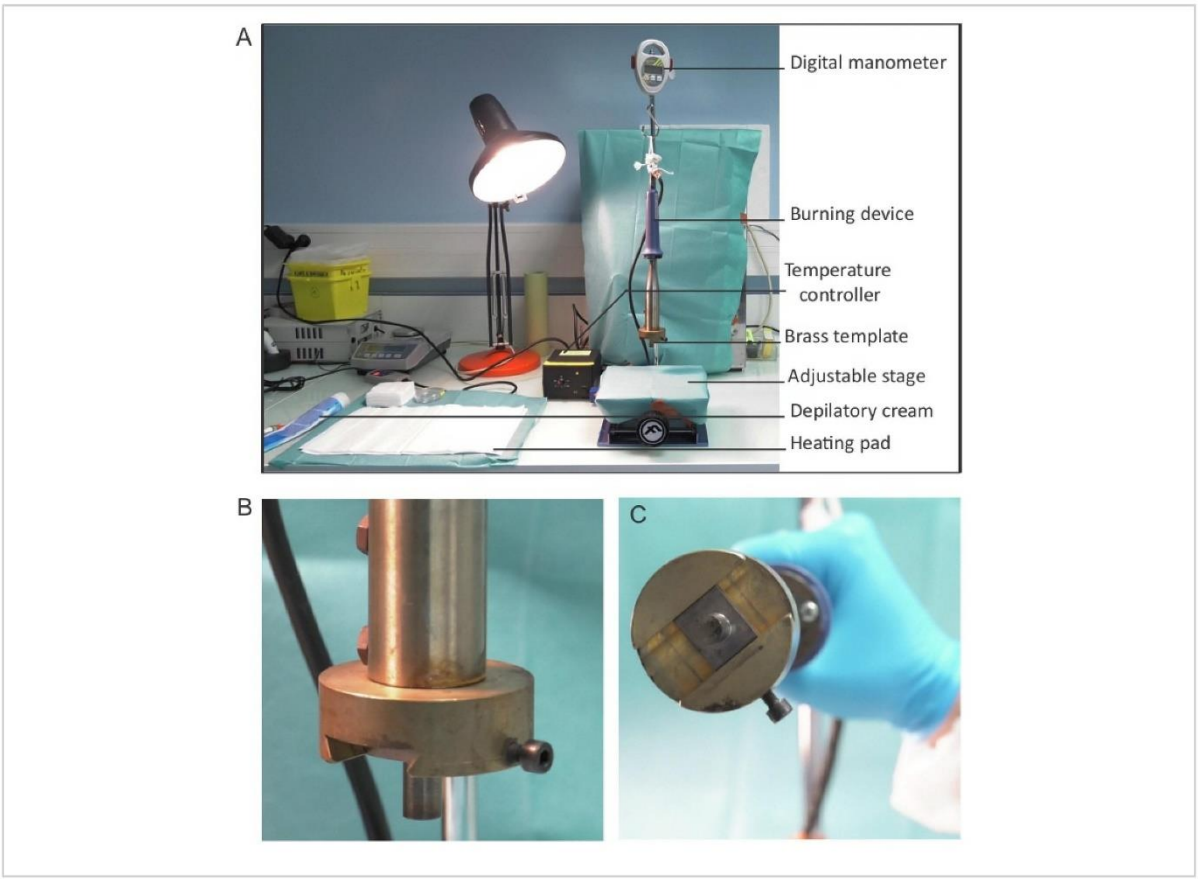

Figure 1: Burning device setup. (**A**) Placement and set-up of the burning device. The burning device is connected to the temperature controller and is attached to the digital monometer to enable the monitoring of pressure. The burning device is suspended above an adjustable stage – flat surface onto which mice are placed for the induction of burn. (**B-C**) A close up image of the brass template used to induce wound burns. (**C**) The diameter of the brass template is 1 cm. Please click here to view a larger version of this figure.

Copyright © 2020 JoVE Creative Commons Attribution-NonCommercial-NoDerivs 3.0 Unported License

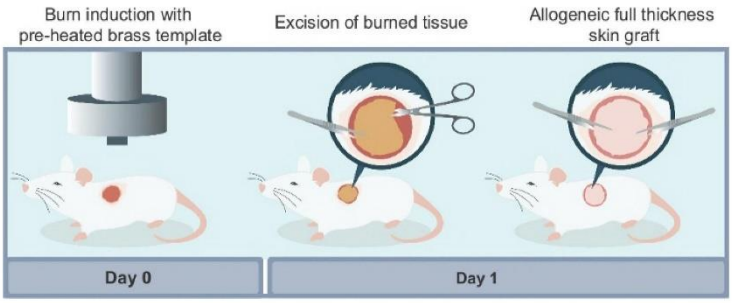

Figure 2: Schematic illustration of the different steps required to reproduce the experimental model described in this article. There are three main steps to the procedure: (i) induction of the burn wound using a preheated brass template; (ii) surgical excision of the non-viable necrotic tissue at 24 hours after the burn injury; (iii) surgical wound reconstruction using a full thickness allogeneic skin graft harvested from a donor mouse. Please click here to view a larger version of this figure.

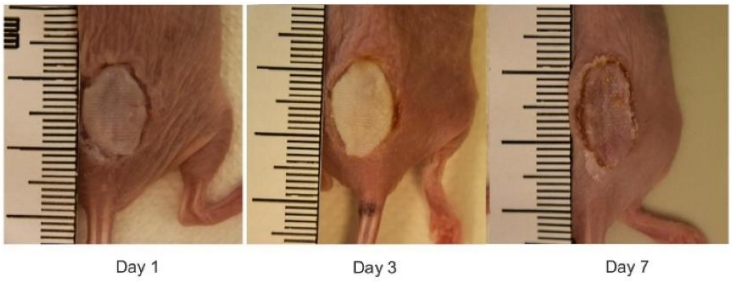

Figure 3: The macroscopic view of reconstructed mouse burn wounds. Representative digital images of burn wounds reconstructed with allogeneic skin grafts on days 0, 1, 3 and 7 after burn injury. The ruler on images is in millimeters. Please click here to view a larger version of this figure.

Copyright © 2020 JoVE Creative Commons Attribution-NonCommercial-NoDerivs 3.0 Unported License

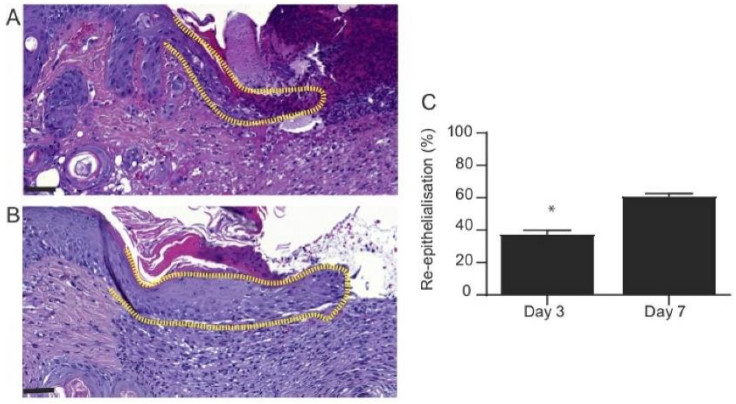

Figure 4: Microscopic appearance of wounds at 3 and 7 days after burn injury. H&E-stained sections of wounds 3 and 7 days after burn injury. The length of neo-epidermis (dotted line) is significantly increased in (**A**) day 3 wounds compared to (**B**) day 7 wounds. In (**A**) and (**B**), the scale bar is 100 µm. (**C**) Graphical representation of the percentage of wound re-epithelialization. This was evaluated by measuring the length of neo-epidermis at day 3 and 7 post-burn injury and expressed as a percentage of the whole wound length. Results represent mean ± S.E.M. (n = 6 mice in day 3 group; n = 6 mice in day 7 group, *p < 0.05; Student's t-test). Please click here to view a larger version of this figure.

Copyright © 2020 JoVE Creative Commons Attribution-NonCommercial-NoDerivs 3.0 Unported License

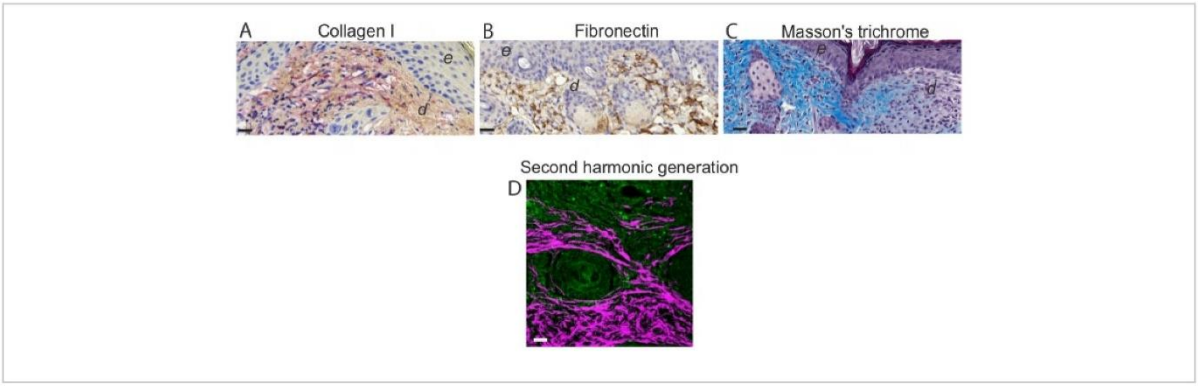

Figure 5: Assessment of the extracellular matrix and collagen I visualization. Representative images of immunohistochemistry analysis on day 7 mouse wounds stained for (**A**) collagen and (**B**) fibronectin. Note intense red staining in elongated spindle-shaped collagen I-positive cells. Note brown staining in fibronectin-positive cells in the dermis of day 7 wounds. Scale bar = 50 µm in all images. In (**A**) and (**B**), e denotes epidermis and d denotes dermis. (**C**) Visualization of collagen fibers and histological assessment of collagen deposition. (**D**) Representative TPEF/SHG collagen image of day 7 mouse wounds. Simultaneous TPEF/SHG acquisition using circular polarization and SHG signals were selectively processed to obtain a binary distribution of SHG after applying a threshold. TPEF images (green) and SHG images (white) were pseudo-colored and overlaid. Scale bar = 50 µm. Please click here to view a larger version of this figure.

Discussion

According to the thickness classification of burn injury[23], full thickness burns are characterized by evident involvement of the whole thickness of the skin and certain portion of the subcutaneous tissue. This type of wound can heal only by contraction or with skin grafting[2]. An inherent limitation of the method described in this article is that only full thickness grafts, as opposed to the split thickness grafts, which are often used in the clinical setting, were harvested from the tail of a mouse. This was due to the technical difficulty, as the mouse skin is too thin to obtain split thickness grafts. It must be pointed out that full thickness grafts require a well vascularized wound bed, whereas split thickness skin grafts are able to survive at donor sites with less vascularity[24]. Previous studies showed that a burn wound induced on the back of the mouse was associated with a robust formation of new vasculature[5]. This suggests that a well vascularized area, such as the dorsum of the mouse, could be considered as the anatomical landmark for the induction of burn wounds.

Burn wound depth is an important factor to consider. The depth of the burn wound must be consistent between individual mice. The reproducibility of the burn wound depth depends on the temperature of the brass template, pressure and duration of the heat exposure. The burn wound depth must be verified histologically. It is important to keep in mind that excessive pressure or prolonged exposure of the skin to the preheated brass template may injure the underlying tissue. The tissue surrounding the vertebral column, including the components of the central and peripheral nervous system,

Copyright © 2020 JoVE Creative Commons Attribution-NonCommercial-NoDerivs 3.0 Unported License

are sensitive to heat, and if damaged may result in hind leg paralysis.

Although no postoperative mortality was directly associated with the surgical procedure, a small number of hairless SKH1-Hrhr mice, which are especially sensitive to cold, developed hypothermia and failed to recover after the general anaesthesia. Therefore, supplementary heat must be provided during all aesthetic events and constant surveillance is required while the mouse is anaesthetized.

The method described in this study was not associated with the surgical site infection. However, aseptic technique must be used to prevent the transfer of microorganisms into the surgical wound during the perioperative period. Inoculation of the wound with bioluminescent or fluorescent microorganisms may be incorporated into the procedure. This technique may be useful in studying infectious organisms and their pathogenesis[25]. For example, exogenous addition or injection of bioluminescent bacteria, may permit the monitoring of the microbial burden using the in vivo whole animal imaging[25]. Given that mouse hair is known to interfere with the in vivo whole animal fluorescence and bioluminescence imaging, hairless SKH1-Hrhr mice are ideal hosts for the studies involving fluorescent or bioluminescent reporters.

Wound tissue samples may be collected at different time points and processed for histological and immunohistochemical analysis. Protein and RNA may be isolated from the skin biopsy and molecular biology techniques may be used to assess the expression of key molecules involved in wound healing.

In the present study, we described an experimental model of burn wound healing and allogeneic skin engraftment. This procedure can be modified and serve as a model for preclinical studies.

Disclosures

The authors declare that they have no competing financial interests.

Acknowledgments

This work was supported by La Direction Générale de L'Armement, l'Agence de l'Innovation de Défense and École Polytechnique. We thank our colleague Mr Yann Plantier from École Polytechnique who provided insight and expertise that greatly assisted the production of the video file. The authors thank Mr Benoit Peuteman and Ms Charlotte Auriau from INSERM Lavoisier (SEIVIL) US 33, Hôpital Paul Brousse, Villejuif for their animal well-being and care expertise provided during the course of this project.

References

1. Shakir, S. et al. Indications and Limitations of Bilayer Wound Matrix-Based Lower Extremity Reconstruction: A Multidisciplinary Case-Control Study of 191 Wounds. *Plastic and Reconstructive Surgery.* (2019).
2. Greenhalgh, D. G. Management of Burns. *New England Journal of Medicine.* **380** (24), 2349-2359 (2019).
3. Bosse, M. J. et al. An analysis of outcomes of reconstruction or amputation after leg-threatening injuries. *New England Journal of Medicine.* **347** (24), 1924-1931 (2002).
4. Braza, M. E., Fahrenkopf, M. P. in *StatPearls.* (2019).
5. Duchesne, C., Banzet, S., Lataillade, J. J., Rousseau, A., Frescaline, N. Cold atmospheric plasma modulates endothelial nitric oxide synthase signalling and enhances

Copyright © 2020 JoVE Creative Commons Attribution-NonCommercial-NoDerivs 3.0 Unported License

burn wound neovascularisation. *Journal of Pathology.* **249** (3), 368-380 (2019).

6. Eming, S. A., Martin, P., Tomic-Canic, M. Wound repair and regeneration: mechanisms, signaling, and translation. *Science Translational Medicine.* **6** (265), 265sr266 (2014).
7. Pakyari, M. et al. Local Expression of Indoleamine 2,3, Dioxygenase Prolongs Allogenic Skin Graft Take in a Mouse Model. *Advances in Wound Care (New Rochelle).* **8** (2), 58-70 (2019).
8. Pakyari, M. et al. A new method for skin grafting in murine model. *Wound Repair and Regeneration.* **24** (4), 695-704 (2016).
9. McFarland, H. I., Rosenberg, A. S. Skin allograft rejection. *Current Protocols in Immunology.* **Chapter 4**, Unit 4 4 (2009).
10. Cristobal, L. et al. Local Growth Hormone Therapy for Pressure Ulcer Healing on a Human Skin Mouse Model. *International Journal of Molecular Sciences.* **20** (17) (2019).
11. Melican, K., Aubey, F., Dumenil, G. Humanized mouse model to study bacterial infections targeting the microvasculature. *Journal of Visualized Experiments.* (86) (2014).
12. Racki, W. J. et al. NOD-scid IL2rgamma(null) mouse model of human skin transplantation and allograft rejection. *Transplantation.* **89** (5), 527-536 (2010).
13. Larsen, C. P. et al. Migration and maturation of Langerhans cells in skin transplants and explants. *Journal of Experimental Medicine.* **172** (5), 1483-1493 (1990).
14. Leonard, D. A., Kurtz, J. M., Cetrulo, C. L., Jr. Vascularized composite allotransplantation: towards tolerance and the importance of skin-specific immunobiology. *Current Opinion in Organ Transplantationt.* **18** (6), 645-651 (2013).
15. Stoikes, N. et al. Biomechanical evaluation of fixation properties of fibrin glue for ventral incisional hernia repair. *Hernia: The Journal of Hernias and Abdominal Wall Surgery.* **19** (1), 161-166 (2015).
16. Foster, K. et al. Efficacy and safety of a fibrin sealant for adherence of autologous skin grafts to burn wounds: results of a phase 3 clinical study. *Journal of Burn Care & Research.* **29** (2), 293-303 (2008).
17. Caro, A. C., Hankenson, F. C., Marx, J. O. Comparison of thermoregulatory devices used during anesthesia of C57BL/6 mice and correlations between body temperature and physiologic parameters. *Journal of the American Association for Laboratory Animal Science.* **52** (5), 577-583 (2013).
18. Grada, A., Mervis, J., Falanga, V. Research Techniques Made Simple: Animal Models of Wound Healing. *Journal of Investigative Dermatology.* **138** (10), 2095-2105 e2091 (2018).
19. Wang, X., Ge, J., Tredget, E. E., Wu, Y. The mouse excisional wound splinting model, including applications for stem cell transplantation. *Nature Protocols.* **8** (2), 302-309 (2013).
20. Ruzehaji, N. et al. Pan PPAR agonist IVA337 is effective in prevention and treatment of experimental skin fibrosis. *Annals of the Rheumatic Diseases.* **75** (12), 2175-2183 (2016).
21. Ruzehaji, N. et al. Combined effect of genetic background and gender in a mouse model of bleomycin-induced skin fibrosis. *Arthritis Research & Therapy.* **17** 145 (2015).

Copyright © 2020 JoVE Creative Commons Attribution-NonCommercial-NoDerivs 3.0 Unported License

22. Singer, A. J., Boyce, S. T. Burn Wound Healing and Tissue Engineering. *Journal of Burn Care & Research.* **38** (3), e605-e613 (2017).

23. Shakespeare, P. Burn wound healing and skin substitutes. *Burns.* **27** (5), 517-522 (2001).

24. Sun, B. K., Siprashvili, Z., Khavari, P. A. Advances in skin grafting and treatment of cutaneous wounds. *Science.* **346** (6212), 941-945 (2014).

25. Miller, R. J. et al. Development of a Staphylococcus aureus reporter strain with click beetle red luciferase for enhanced in vivo imaging of experimental bacteremia and mixed infections. *Scientific Reports.* **9** (1), 16663 (2019).

Copyright © 2020 JoVE Creative Commons Attribution-NonCommercial-NoDerivs 3.0 Unported License

Annex B: Xen36 and Xen31 *Staphylococcus aureus* genomes.

Staphylococcus aureus is a ubiquitous saprophytic bacterium found in a wide variety of environments, such as soil, water, air, food, household appliances, medical devices, and hospital equipment [410,411]. It also colonizes the skin and mucosa of birds and mammals, including humans in which it frequently associates with nasal mucosa [412–414]. When host immunity is defective or cellular barriers are breached, *S. aureus* can cause a wide array of diseases ranging from benign skin and soft tissue infections to fatal endocarditis [415]. Pathogenesis relies on finely regulated secretion of a plethora of toxins, production of immune evasion factors and tissue invasion determinants, and formation of biofilms [416–420]. There is growing concern about healthcare- and community-associated infections caused by methicillin-resistant S. *aureus* (MRSA). MRSA infections led to more than 100 000 deaths due to antimicrobial resistance in 2019 worldwide [421]. Identification of new drug targets and development of innovative therapeutics is an urgent priority to reduce the global burden of *S. aureus* antimicrobial resistance. Bioluminescent microorganisms are powerful tools to investigate pathogenesis, screen antimicrobial drugs *in vitro* and evaluate drug efficacy *in vivo* [422–424]. Bioluminescent *S. aureus* strains have proved useful for noninvasive real-time monitoring of infection, measurement of antibiotics sensitivity and assessment of therapies [424–440]. Here, we report genome sequences of the two bioluminescent *S. aureus* strains Xen31 and Xen36, obtained from PerkinElmer (#119242 and #119243, respectively). Xen31 was derived from the parental MRSA strain ATCC33591, a clinical strain isolated at Elmhurst Hospital in New York City [441]. Xen36 was derived from parental strain ATCC 49525, a clinical isolate from a bacteremic patient [425]. A copy of the modified *luxABCDE* operon from *Photorhadbus luminescens* is integrated in the chromosome of Xen31 and in a native plasmid of Xen36. Full genomic characterization of these strains is of interest as they are commonly used in infection models and preclinical studies [431,436,437,440,442–451].

Bacteria were grown in brain heart infusion (BHI) broth (BD) with shaking at 200 rpm at 37°C overnight. Bacterial suspensions were diluted in BHI broth and bacteria grown to OD_{600nm}=2 with shaking at 200 rpm at 37°C. Genomic DNA was isolated from bacteria using the PureLink DNeasy

kit (Invitrogen) with the addition of 5 mg/mL lysozyme and 0.05 mg/mL lysostaphin to the lysis buffer. Whole genome sequencing was performed using Illumina and Pacific Biosciences (PacBio) sequencing technologies (libraries, sequencing, quality filtering, trimming, reads quality check, assembly, assembly quality check, circularization and adjustment of the origin of replication, genome completeness, annotation, other softwares, important parameters…).

Four contigs were assembled for the MRSA Xen31 strain, covering X sequenced bases, with an N_{50} value of X bp. The assembled genome sequence was covered 63 times. Xen31 genome size consists of 3,067,763 bp with a GC content of X%. In total, X raw reads were obtained for the Xen36 strain. Three/six ? contigs were assembled, with an N_{50} value of 2,749,617 bp, covering the genome 62 times. The genome size was determined to be 2,927,090 bp and the GC content 32,86%. Xen36 contains the RepUS5 replicon plasmid. Phages ϕNM3 and ϕJB were detected in Xen31, and PT1028 in both strains using PHASTER [452]. Using ResFinder-4.1 [453] and GenBank, we identified several antimicrobial resistance genes in the Xen31 genome including *aac(6')-aph(2")*, *aadD*, *ant*(9)-Ia, *bla*TEM-1A, *bleO*, *cat*(pC194), *erm*(A), *erm*(B), *fosB*, *tet*(M) and, expectedly, the methicillin resistance gene *mecA*. The Xen36 genome contained the *aph*(3')-III and *blaZ* genes. A search in Virulence Factor of Pathogenic Bacteria Database (VFDB) and Genbank revealed many virulence genes common to Xen31 and Xen36 strains. Both genomes encode multiple factors responsible for subversion of host immunity, *e.g.* capsule, staphylococcal protein A SpA, staphyloxanthine (check crtMNPQO), staphylococcal superantigen-like proteins, AdsA, chemotaxis-inhibitory protein of *Staphylococcus* CHIPS, staphopain protease, Geh lipase, staphylococcal complement inhibitor SCIN, extracellular fibrinogen-binding protein Efb, staphylocoagulase, staphylokinase, staphylococcal serine V8 protease SspA, cysteine protease SspB, aureolysin Aur, catalase KatA, alkyl hydroperoxidase AhpCF, superoxide dismutases SodA and SodM, α-hemolysin Hla, δ-hemolysin Hld, leukocidins LukDE, HlgAB, HlgCB, enterotoxin A, and type VII secretion system. Other genes common to the two strains encode determinants required for tissue and cell invasion (*e.g.* fibronectin-binding protein A FnBPA), biofilm formation (*e.g. icaABCD* encoded polysaccharide intercellular adhesin PIA) and virulence gene regulation (e.g. AgrABCD, RNAIII, SarR, SarV, SarX, SigB, Rot,

SaeRS, ArlRS, SrrAB, CodY, LytRS (Xen31 only ?), MgrA (Xen31 only ?) and Fur. Xen31 virulence genes absent from Xen36 included clumping factor B ClfB, fibronectin-binding protein B FnBPB, SdrC, Serine protease-like SplABCDEF, leukotoxin D, SarA, SarS, SarT, SarU SarZ (check). Inversely, collagen adhesin Cna, von Willebrand factor-binding protein, SdrE, SspC, enterotoxins B and G, and SarY encoding genes were found only in Xen36. The *lukS-PV* and *lukF-PV* genes encoding the Panton-Valentine leucocidin, the toxic shock syndrome toxin-1 gene, clumping factor A ClfA, exfoliative toxins, FLIPr, extracellular complement-binding protein Ecb, staphylococcal peroxide inhibitor SPIN, D-alanyl-lipoteichoic acid DltABCD, multiple peptide resistance factor MprF, GraRSX, O-acetyl transferase OatA (doublecheck, they must be present), LukAB/GH, phenol-soluble modulins (check, they must be present too), extracellular adherence protein Eap, Rsr were not found in Xen31 nor Xen36.

TABLE 1 General features of the *Staphylococcus aureus* strains Xen31 and Xen36

Features	**Xen31**	**Xen36**
Strain origin	Clinical isolate	Clinical isolate (bacteremia)
Resistance type	MRSA	MSSA
Genome size (bp)	3,067,763	2,927,090
G+C content (%)	X	32.86
Contigs	4	6
Number of protein coding genes	2,889	2,697
Number of rRNAs	19	19
Number of tRNAs	62	60
Number of tmRNAs	1	1
Number of CRISR regions	10	5
Prophages	3	1
Plasmids	1	1

DATA AVAILABILITY

Sequences were deposited in DDBJ/ENA/GenBank under the accession number…

ACKNOWLEDGMENTS

We thank PerkinElmer for providing *S. aureus* strains Xen31 and Xen36. Biomics, URY... This work was supported by the Institut Pasteur, Université Paris Cité, CNRS, … O.B. is a fellow from the, E.C. is a fellow from…

REFERENCES

1. Davis MF, Iverson SA, Baron P, Vasse A, Silbergeld EK, Lautenbach E, et al. Household transmission of meticillin-resistant Staphylococcus aureus and other staphylococci. Lancet Infect Dis. 2012 Sep;12(9):703–16.

2. Kozajda A, Jeżak K, Kapsa A. Airborne Staphylococcus aureus in different environments—a review. Environ Sci Pollut Res. 2019 Dec;26(34):34741–53.

3. Wertheim HF, Melles DC, Vos MC, van Leeuwen W, van Belkum A, Verbrugh HA, et al. The role of nasal carriage in Staphylococcus aureus infections. Lancet Infect Dis. 2005 Dec;5(12):751–62.

4. Krismer B, Weidenmaier C, Zipperer A, Peschel A. The commensal lifestyle of Staphylococcus aureus and its interactions with the nasal microbiota. Nat Rev Microbiol. 2017 Nov 1;15(11):675–87.

5. Abdullahi IN, Fernández-Fernández R, Juárez-Fernández G, Martínez-Álvarez S, Eguizábal P, Zarazaga M, et al. Wild Animals Are Reservoirs and Sentinels of Staphylococcus aureus and MRSA Clones: A Problem with "One Health" Concern. Antibiotics. 2021 Dec 20;10(12):1556.

6. Tong SYC, Davis JS, Eichenberger E, Holland TL, Fowler VG. Staphylococcus aureus Infections: Epidemiology, Pathophysiology, Clinical Manifestations, and Management. Clin Microbiol Rev. 2015 Jul;28(3):603–61.

7. Ahmad-Mansour N, Loubet P, Pouget C, Dunyach-Remy C, Sotto A, Lavigne JP, et al. Staphylococcus aureus Toxins: An Update on Their Pathogenic Properties and Potential Treatments. Toxins. 2021 Sep 23;13(10):677.

8. Thomer L, Schneewind O, Missiakas D. Pathogenesis of Staphylococcus aureus Bloodstream Infections. 2016;24.

9. Cheung GYC, Bae JS, Otto M. Pathogenicity and virulence of Staphylococcus aureus. Virulence. 2021 Jan 1;12(1):547–69.

10. Foster TJ. Immune evasion by staphylococci. Nat Rev Microbiol. 2005 Dec 1;3(12):948–58.

11. Foster TJ, Geoghegan JA, Ganesh VK, Höök M. Adhesion, invasion and evasion: the many functions of the surface proteins of Staphylococcus aureus. Nat Rev Microbiol. 2014 Jan;12(1):49–62.

12. Murray CJ, Ikuta KS, Sharara F, Swetschinski L, Robles Aguilar G, Gray A, et al. Global burden of bacterial antimicrobial resistance in 2019: a systematic analysis. The Lancet. 2022 Jan;S0140673621027240.

13. Avci P, Karimi M, Sadasivam M, Antunes-Melo WC, Carrasco E, Hamblin MR. In-vivo monitoring of infectious diseases in living animals using bioluminescence imaging. Virulence. 2018 Dec 31;9(1):28–63.

14. Syed AJ, Anderson JC. Applications of bioluminescence in biotechnology and beyond. Chem Soc Rev. 2021;50(9):5668–705.

15. Guo Y, Ramos RI, Cho JS, Donegan NP, Cheung AL, Miller LS. In Vivo Bioluminescence Imaging To Evaluate Systemic and Topical Antibiotics against Community-Acquired Methicillin-Resistant Staphylococcus aureus-Infected Skin Wounds in Mice. Antimicrob Agents Chemother. 2013 Feb;57(2):855–63.

16. Francis KP, Joh D, Bellinger-Kawahara C, Hawkinson MJ, Purchio TF, Contag PR. Monitoring bioluminescent Staphylococcus aureus infections in living mice using a novel luxABCDE construct. Infect Immun. 2000 Jun 1;68(6):3594–600.

17. Tenhami M, Hakkila K, Karp M. Measurement of Effects of Antibiotics in Bioluminescent Staphylococcus aureus RN4220. Antimicrob Agents Chemother. 2001 Dec;45(12):3456–61.

18. Xiong YQ, Willard J, Kadurugamuwa JL, Yu J, Francis KP, Bayer AS. Real-Time In Vivo Bioluminescent Imaging for Evaluating the Efficacy of Antibiotics in a Rat Staphylococcus aureus Endocarditis Model. Antimicrob Agents Chemother. 2005 Jan;49(1):380–7.

19. Lambrechts SAG, Demidova TN, Aalders MCG, Hasan T, Hamblin MR. Photodynamic therapy for Staphylococcus aureus infected burn wounds in mice. Photochem Photobiol Sci. 2005;4(7):503.

20. Mortin LI, Li T, Van Praagh ADG, Zhang S, Zhang XX, Alder JD. Rapid Bactericidal Activity of Daptomycin against Methicillin-Resistant and Methicillin-Susceptible Staphylococcus aureus Peritonitis in Mice as Measured with Bioluminescent Bacteria. Antimicrob Agents Chemother. 2007 Feb 26;51(5):1787–94.

21. Zhang H, Kalkeri G, Mani N, Grossman TH. Development and Validation of a Multi-dose Neutropenic Rat Thigh Infection Model Using Real-time Monitoring of Staphylococcus aureus Growth In Vivo. In Vivo. 2008;6.

22. Munro P, Benchetrit M, Nahori MA, Stefani C, Clément R, Michiels JF, et al. The Staphylococcus aureus epidermal cell differentiation inhibitor toxin promotes formation of infection foci in a mouse model of bacteremia. Infect Immun. 2010 Aug 1;78(8):3404–11.

23. Lorenz U, Schäfer T, Ohlsen K, Tiurbe GC, Bühler C, Germer CT, et al. In Vivo Detection of Staphylococcus aureus in Biofilm on Vascular Prostheses Using Non-invasive Biophotonic Imaging. Eur J Vasc Endovasc Surg. 2011 Jan;41(1):68–75.

24. Cho JS, Zussman J, Donegan NP, Ramos RI, Garcia NC, Uslan DZ, et al. Noninvasive In Vivo Imaging to Evaluate Immune Responses and Antimicrobial Therapy against Staphylococcus aureus and USA300 MRSA Skin Infections. J Invest Dermatol. 2011 Apr;131(4):907–15.

25. Plaut RD, Mocca CP, Prabhakara R, Merkel TJ, Stibitz S. Stably Luminescent Staphylococcus aureus Clinical Strains for Use in Bioluminescent Imaging. Rohde H, editor. PLoS ONE. 2013 Mar 12;8(3):e59232.

26. van Staden ADP, Heunis T, Smith C, Deane S, Dicks LMT. Efficacy of Lantibiotic Treatment of Staphylococcus aureus-Induced Skin Infections, Monitored by In Vivo Bioluminescent Imaging. Antimicrob Agents Chemother. 2016 Jul;60(7):3948–55.

27. Bostian PA, Karnes JM, Cui S, Robinson LJ, Daffner SD, Witt MR, et al. Novel rat tail discitis model using bioluminescent Staphylococcus aur e us: RAT TAIL DISCITIS MODEL. J Orthop Res. 2017 Sep;35(9):2075–81.

28. Rozenbaum RT, Su L, Umerska A, Eveillard M, Håkansson J, Mahlapuu M, et al. Antimicrobial synergy of monolaurin lipid nanocapsules with adsorbed antimicrobial peptides against Staphylococcus aureus biofilms in vitro is absent in vivo. J Controlled Release. 2019 Jan;293:73–83.

29. Miller RJ, Crosby HA, Schilcher K, Wang Y, Ortines RV, Mazhar M, et al. Development of a Staphylococcus aureus reporter strain with click beetle red luciferase for enhanced in vivo imaging of experimental bacteremia and mixed infections. Sci Rep. 2019 Dec;9(1):16663.

30. Kobayashi H, Fujita R, Hiratsuka S, Shimizu T, Sato D, Hamano H, et al. Differential effects of anti-RANKL monoclonal antibody and zoledronic acid on necrotic bone in a murine model of Staphylococcus aureus -induced osteomyelitis. J Orthop Res. 2022 Mar;40(3):614–23.

31. Benjamin AB, Moule MG, Didwania MK, Hardy J, Saenkham-Huntsinger P, Sule P, et al. Efficacy of Cathelicidin-Mimetic Antimicrobial Peptoids against Staphylococcus aureus. Zhang K, editor. Microbiol Spectr. 2022 Jun 29;10(3):e00534-22.

32. Schaefler S, Perry W, Jones D. Methicillin-Resistant Strains of Staphylococcus aureus Phage Type 92. Antimicrob Agents Chemother. 1979 Jan;15(1):74–80.

33. Lebeaux D, Chauhan A, Létoffé S, Fischer F, de Reuse H, Beloin C, et al. pH-Mediated Potentiation of Aminoglycosides Kills Bacterial Persisters and Eradicates In Vivo Biofilms. J Infect Dis. 2014 Nov 1;210(9):1357–66.

34. Chauhan A, Ghigo JM, Beloin C. Study of in vivo catheter biofilm infections using pediatric central venous catheter implanted in rat. Nat Protoc. 2016 Mar 1;11(3):525–41.

35. Gelin M, Paoletti J, Nahori MA, Huteau V, Leseigneur C, Jouvion G, et al. From Substrate to Fragments to Inhibitor Active In Vivo against Staphylococcus aureus. ACS Infect Dis. 2020 Feb 4;1–14.

36. Visperas A, Santana D, Ju M, Milbrandt NB, Tsai YH, Wickramasinghe S, et al. Standardized quantification of biofilm in a novel rabbit model of periprosthetic joint infection. J Bone Jt Infect. 2022 Apr 20;7(2):91–9.

37. Trikha R, Greig D, Sekimura T, Cevallos N, Kelley B, Mamouei Z, et al. Active rheumatoid arthritis in a mouse model is not an independent risk factor for periprosthetic joint infection. Di Paola R, editor. PLOS ONE. 2021 Aug 16;16(8):e0250910.

38. Quan K, Jiang G, Liu J, Zhang Z, Ren Y, Busscher HJ, et al. Influence of interaction between surface-modified magnetic nanoparticles with infectious biofilm components in artificial channel digging and biofilm eradication by antibiotics in vitro and in vivo. Nanoscale. 2021;13(8):4644–53.

39. Trikha R, Greig D, Kelley BV, Mamouei Z, Sekimura T, Cevallos N, et al. Inhibition of Angiotensin Converting Enzyme Impairs Anti-staphylococcal Immune Function in a Preclinical Model of Implant Infection. Front Immunol. 2020 Sep 11;11:1919.

40. Jørgensen NP, Meyer R, Dagnæs-Hansen F, Fuursted K, Petersen E. A Modified Chronic Infection Model for Testing Treatment of Staphylococcus aureus Biofilms on Implants. de Lencastre H, editor. PLoS ONE. 2014 Oct 3;9(10):e103688.

41. Ovchinnikov KV, Kranjec C, Thorstensen T, Carlsen H, Diep DB. Successful Development of Bacteriocins into Therapeutic Formulation for Treatment of MRSA Skin Infection in a Murine Model. Antimicrob Agents Chemother. 2020 Nov 17;64(12):e00829-20.

42. Grønseth T, Ovchinnikov KV, Carlsen H, Benth JŠ, Diep DB, von Unge M, et al. Lugol's solution and Gentian violet eradicate methicillin-resistant Staphylococcus aureus biofilm in skin wound infections. Int Wound J. 2022 May 28;iwj.13846.

43. Arndt D, Grant JR, Marcu A, Sajed T, Pon A, Liang Y, et al. PHASTER: a better, faster version of the PHAST phage search tool. Nucleic Acids Res. 2016 Jul 8;44(W1):W16–21.

44. Bortolaia V, Kaas RS, Ruppe E, Roberts MC, Schwarz S, Cattoir V, et al. ResFinder 4.0 for predictions of phenotypes from genotypes. J Antimicrob Chemother. 2020 Dec 1;75(12):3491–500.

Titre : Le plasma atmosphérique froid stimule l'élimination de bactéries pathogènes par les macrophages.

Mots clés : Plasmas froids, infections, *S. aureus*, macrophages, NOX2, modèles 3D, étude pilote sur modèle porcin.

La prise en charge des patients souffrant de brûlures thermiques est un domaine complexe pour les unités de soins avec des millions d'adultes et d'enfants concernés dans le monde entier. Des progrès importants ont été réalisés au cours de la dernière décennie en matière de réanimation, de traitement des plaies ou de reconstruction. Cependant, les patients souffrant de brûlures graves font toujours face à des conséquences invalidantes comme des cicatrices hypertrophiques et surtout un risque élevé d'infections et de septicémie mortelle. Les plasmas froids (CAP) sont des gaz partiellement ionisés qui favorisent la cicatrisation des plaies et ont des propriétés antimicrobiennes. L'objectif de cette thèse vise à comprendre les mécanismes sous-jacents responsables des effets bénéfiques lors des infections des plaies avec un intérêt particulier pour les macrophages.
Premièrement nous avons démontré *in vitro* que le traitement par CAP engendrait une diminution significative de la charge bactérienne pour deux types de souches de *Staphylococcus aureus* (sensible et résistante à la méthicilline : MSSA, MRSA) lors de leur internalisation par les macrophages. Nous avons ensuite montré que l'amélioration de la destruction de *S. aureus* par les macrophages est médiée par des mécanismes oxydatifs et que CAP favorise la maturation des phagosomes en vésicules de dégradation. Deuxièmement, nous avons montré une corrélation positive entre l'action antibactérienne de CAP et l'activation du complexe NADPH oxydase (NOX2), dans des modèles cellulaires et tridimensionnels d'infection cutanée.
CAP est également un régulateur positif de la cicatrisation cutanée, comme le montre les résultats obtenus avec notre modèle murin infecté par *S. aureus*.
Enfin, le but ultime du projet est de traiter des modèles de plaies de brûlure infectées plus complexes tels que des porcs pour les études précliniques permettant de se rapprocher de l'Homme. Ainsi, un nouvel appareil à plasma a été développé pour traiter de plus grandes surfaces et sera utilisé pour la première fois *in vivo* pour une étude pilote sur modèle porcin en octobre 2022.
Cette étude a démontré le potentiel thérapeutique de CAP sur la réparation des tissus infectés. Les résultats dans le domaine de la cicatrisation cutanée sont prometteurs mais d'autres études sont nécessaires, en particulier en ce qui concerne les effets mutagènes ou génotoxiques liés à l'utilisation de CAP sur des modèles animaux présentant une plus grande similarité avec l'Homme.

Title: Cold atmospheric plasma stimulates macrophage killing of bacterial pathogens.

Keywords: Cold atmospheric plasma, infection, *S. aureus*, macrophages, NOX2, three-dimensional models, pig trial.

Management of thermal burn-injured patients is a challenging field for care units with millions of adults and children concerned worldwide. Significant advances over the past decade have occurred in resuscitation, burn wound management and reconstruction. However, patients with severe burns still face disabling consequences such as hypertrophic scars, high risk of infections and sepsis. Cold atmospheric plasma (CAP) is a partially ionised gas delivering a mixture of reactive oxygen and nitrogen species which favour wound healing and have antimicrobial properties.
This PhD study aimed to understand the underlying mechanisms that are responsible for beneficial effects during wound infections specifically on macrophages immune cells. First, we demonstrated *in vitro* that CAP treatment resulted in a significant decrease in bacterial load for two strains of *Staphylococcus aureus* (methicillin-resistant and sensitive: MSSA, MRSA) during their internalization by macrophages. Then, we showed that the enhancement killing of *S. aureus* by macrophages is mediated by oxidative mechanisms and that CAP promotes phagosome maturation into acidic degradative vesicle. Second, we reported a positive correlation between antibacterial action of CAP and activation of phagocyte NADPH oxidase (NOX2) machinery in two and three-dimensional models of cutaneous infection.
In addition, to its antimicrobial effects, CAP is a positive regulator of cutaneous wound healing as shown in an *in vivo* murine mouse model infected with *S. aureus*. Finally, the ultimate goal of the project is to treat either uninfected or infected full-thickness burn wounds. Thus, a new plasma device has been developed to treat wounds with large surface area. For the first time, this new prototype will be used in porcine model of full-thickness burn wound reconstructed with partial-thickness allografts. This study demonstrated the therapeutic potential of CAP on infected tissue repair. Investigation on tissue repair are promising, however further investigations are needed especially on the mutagenicity and genotoxicity of CAP use on animal models with greater similarity to human.

Institut Polytechnique de Paris
91120 Palaiseau, France